Biogeochemical cycling of gold:

Exploring the links between gold transformation, microbial communities, biogeochemical processes and mineralisation style

Maria Angelica Rea
MSc. Biological Sciences
BSc. Biology, LPT

Submitted for the degree of Doctor of Philosophy
Department of Molecular and Cellular Biology
School of Biological Sciences
The University of Adelaide
Adelaide, South Australia, Australia

October 2018

Table of Contents

Publications from this Thesis

Published Peer-Reviewed Journal Articles

Rea MA, Zammit CM, Reith F* (2016) Bacterial biofilms on gold grains – Implications for geomicrobial transformations of gold. *FEMS Microbiol. Ecol*., 92. fiw082

Rea MA*, Standish CD, Shuster J, Bissett A, Reith F* (2018) Progressive biogeochemical transformation of placer gold particles drives compositional changes in associated biofilm communities. *FEMS Microbiol. Ecol.* fiy080

Journal Articles in preparation
Rea MA, Brugger J, Etschmann B, Shuster J, Reith F* (under review). Effect of physical and biogeochemical factors on placer gold transformation in mountainous landscapes of Switzerland. *Gondwana Research.*

Rea MA, Shuster J, Reith F* (in preparation) Does placer gold from epi- and hydrothermal sources behave differently during transformation in the weathering environment? *Science of the Total Environment.*

Rea MA, Brugger J, Etschmann B, Shuster J, Reith F* (in preparation) Microbial-mediated mobility of gold: Assessing the mode of transport of Au from natural gold particles. *Nature Communications.*

Publications and Abstracts in Conference Proceedings:
Rea MA*, Reith F (2016) Microbial-mediated transformation of gold in temperate European environments. In: Australian Earth Science Convention 2016. Geological Society of Australia Abstract No 118, Adelaide Convention Centre, Adelaide, South Australia, pp. 369.

Reith F, **Rea MA***, Bissett A (2016) Using microbial indicators in mineral exploration: New lessons from Australia. In: Australian Earth Sciences Convention 2016. Geological Society of Australia Abstract No 118, Adelaide Convention Centre, Adelaide, South Australia, pp. 370.

Sanyal SK, **Rea MA***, Shuster J, Reith (2017) Cultured Bacterial Communities from Australian and African Gold Grains. In: Goldschmidt 2017. European Association of Geochemistry, Le Palais des Congrès de Paris, Paris, France.

Rea MA, Bissett A, Reith F (2017) Microbial Gold (Trans)formation: Examples from Europe and Asia. In: Goldschmidt 2017. European Association of Geochemistry, Le Palais des Congrès de Paris, Paris, France.

Abstract

The biogeochemical cycle of gold (Au), wherein biofilms contribute to the transformation of Au particles, has been demonstrated from various ecological and environmental settings. In this study, we explore the links between Au particle transformation and (bio)geochemical processes including deposit style/regional mineralisation, microbial community composition, position in landscape and physical weathering. A total of 114 placer Au particles were characterised using scanning electron microscopy collected from the UK (eight sites), Switzerland (eight sites) and Germany (14 sites). These placer Au particles demonstrated different degrees of alteration as shown by a range of morphology and surface textures. Collectively, these Au particles represented a continuum of Au particle transformation mediated by microorganisms and geochemical and physical processes. Additional evidence of Au biogeochemical cycling at the interface of the Au particle surface was demonstrated by the abundance of polymorphic layers containing clay minerals in which microbial cells, extracellular polymeric substances (EPS) and Au nano- and micro-particles were closely associated. A total of 260 placer Au particles were assessed for resident biofilm community composition using nested 16S rRNA polymerase chain reaction (PCR) combined with next generation sequencing (NGS) using the Illumina MiSeq platform. Findings from UK Au particles demonstrated that the biofilm community assemblages evolved to a more similar composition of metal-resistant members as Au particles progressively became more transformed. Analysis of 36 placer Au particles from Switzerland suggested that transformation stages of Au were highly influenced by the landscape setting leading to the recruitment of diverse members of the biofilm community with increased distance of Au particle transport. A total of 198 placer Au particles from Germany were quantitatively mapped using the Cameca™ SXFive Electron Microprobe. The analysis demonstrated that the conditions of epithermal and hydrothermal deposits produce the difference in Au:Ag ratios that ultimately dictate how the microbial communities sense the difference in the Au-Ag 'fabric' and therefore direct Au transformation differently. Proteobacteria dominated the community assemblage from all sites in UK, Switzerland and Germany (>30 % of total OTUs and sequencing reads) suggesting that highly-specialised biofilm communities adapted to Au-toxicity perform key roles in the transformation of Au particles. These include the genera *Pseudomonas, Leptothrix* and *Acinetobacter* detected in Germany placer Au in addition to putative exoelectrogenic genera *Rhodoferax* and *Geobacter* that were highly abundant on Au particles from the UK. This study also reports the

contribution of biofilm communities to the mobility of Au in iron (Fe)-, organic matter (OM)- and calcium (Ca)-rich soil. Soil columns with Au particles placed in pouches and inoculated with active Au mobilisers *Chromobacterium violaceum* and *Corynebacterium glutamicum*, and precipitating organism *Cupriavidus metallidurans* demonstrated that Au was mobilised either as a complex (up to 320 mg/L Au) or natural Au nanoparticles (AuNPs) (~27–38 nm), respectively. These suggest amino acid- and cyanide-complexation or reductive precipitation in the periplasm leading to Au mobility. The results of this study will improve the use of (bio)geochemical models to predict Au transport for applications in Au exploration and to advance the understanding of the biogeochemical cycle of Au in other environmental and climatic regions across the globe.

Declaration

I certify that this work only contains original materials which have not been accepted for the award of any other degree or diploma in my name, in any university or other tertiary institutions and, to the best of my knowledge and belief, not previously published or written by another person, except where due reference has been made. In addition, I certify that no part of this work will be used in any future submissions in my name, for any other degree or diploma in any university or other tertiary institutions without the prior approval of the University of Adelaide and where applicable, any partner institution responsible for the joint-award of this degree.

I acknowledge that the copyright of published works contained within this thesis resides with the copyright holder(s) of those works.

I give consent to make available the copy of my thesis when deposited in the University Library for loan and photocopying, subject to the provisions of the Copyright Act 1968.

I permit the digital version of my thesis to be made available on the web, via the University's digital research repository, the Library Search, and also through web search engines, unless permission has been granted by the University to restrict access for a certain period.

Maria Angelica Rea
October 2018

Acknowledgments

Another great year, another great milestone… this achievement will not be possible without the great minds guiding me through this PhD journey.

Firstly, to my supervisor, mentor and lab-parent A/Prof. Frank Reith. I was able to adapt easily to Australia because of your welcoming and encouraging spirit. Your supervision technique has trained me to become an independent researcher. The challenging environment and your high expectations motivated me to aim for more, not only to accomplish this PhD but also to be involved in various side-projects. Thank you also to the heaps of valuable life lessons and skills. Your non-attachment to cellular phones improved my skills to compose email replies quickly, and most importantly, your attachment to whisky, wine, beer, and liquor introduced me to the wonderful world of drinking.

To my supervisors and dear friends Dr. Jeremiah Shuster, Dr. Carla Zammit and Dr. Florian Weiland. Jer, thank you for keeping the MHM group functioning in these trying times. Your regular WhatsApp™ messages and emails kept me going. Thank you for the adventure time in Paris. To Carla, for being supportive along the way and patiently answering my emails too. And Florian, for attending my Uni research updates even on last-minute notices.

To Prof. Joël Brugger and Dr. Barbara Etschmann, the dynamic duo of synchrotron. Joël and Barb, your visits and our encounters in Melbourne and Adelaide for experiments, research, and more importantly, for raclette and pizza nights are valuable fun experience during my PhD. And of course, I will never forget the basics of wine tasting (and not forgetting to breathe—haha!)

To Dr. Donna Falconer, our long sessions doing SEM, FIB-SEM and TEM is undoubtedly an incredible learning experience for me. Donna, the memorable IKEA bonding trip will surely happen every time you visit Adelaide.

To the staff of Adelaide Microscopy for their untiring assistance, especially Dr. Animesh Basak, Dr. Benjamin Wade, Aoife McFadden, Ken Neubauer, Dr. Sarah Gilbert and Angus Netting. Animesh for your advice not only on the FIB but also in what to expect after PhD. Ben for the microprobe assistance and pieces of advice via email and Sarah for the wonderful lasering experience.

To Flinders University and Flinders Analytical staff Dr. Claire Lenehan, Dr. Christine Ta, Jennie Bartle, Dr. Daniel Jardine, Jason Young for the use of instrumentation and advice. Thank you, Daniel and Jason, for being patient with assisting us on the SP-ICP-MS.

To CSIRO and Uni of Adelaide staff Dr. Anu Kumar, Adrienne Gregg, Deborah Gonzago-Carter, Hai Doan, Dr. Peter Bain, Dr. Paul Harvey, Dr. Belinda Strummer, Bhanu Nidumolu, Dr. Jing Zhao and Dr. Divina Navarro and other CSIRO staff that I met. I greatly appreciate the greetings and short chats with all of you. I may have been a pain in the lab during my first year, but I hope I did great after.

To the generous people who granted excellent field support and to the landowners at the sampling sites for site access.

To my fellow PhD student Santonu Sanyal, my bus buddy Shermeen Tahir and fellow Filipino PhDs in an entirely different department of Uni of Adelaide. Thank you for being a reminder that I am not alone in my career choice.

To our Filipino friends in Adelaide for the non-stop "chibog" (eating) sessions on weekends and holidays. And Mignonette Tudara, the closest non-bias friend that became my sounding board when I badly needed someone to hear me out.

To Tina Reith for the support, patience, love and care that you have extended to me and Marlon. And most importantly, thank you, to you and Frank for giving us a safe and comfy home.

To my parents and sisters, though far away, for keeping me part of the family line despite taking a non-typical career path that you have envisioned for me. Receiving your chat messages every day made me feel that you were just around the corner.

And lastly, to my best friend, hubby and exercise buddy, Marlon, for your words of encouragement when I randomly cry whenever I ask, "Why am I doing this?", for believing in me, and for all of our random trips to take my mind off from doing this 24/7. You have kept me sane and 'normal' through these years.

"… A grain of gold will gild a great surface,
but not so much as a grain of wisdom."
— Henry David Thoreau

List of Figures

List of Tables

List of Abbreviations

AuNPs	Gold nanoparticles
BSE	Backscattered Electron
CAP	Canonical analysis of principal coordinates
CV	Coefficient of variation
DC	Dissolved carbon
DGGE	Denaturing gradient gel electrophoresis
DOC	Dissolved organic carbon
EDX	Energy dispersive X-ray
EMPA	Electron Microprobe analysis
EPS	Extracellular polymeric substances
FIB	Focused ion beam
HPLC	High performance liquid chromatography
ICP-OES	Inductively coupled plasma – optical emission spectrometry
ICP-MS	Inductively coupled plasma – mass spectrometry
KEGG	Kyoto Encyclopaedia of Genes and Genomes
MME	Minimal media
NCBI	National Centre for Biotechnology Information
NGS	Next generation sequencing
nMDS	Non-metrical multidimensional scaling
OTU	Operational taxonomic units
PBS	Phosphate buffered saline
PCR	Polymerase chain reaction
PHB	Polyhydroxybutyrate
PICRUSt	Phylogenetic Investigation of Communities by Reconstruction of Unobserved States
QPC	Quartz pebble conglomerates
rRNA	Ribosomal ribonucleic acid
SE	Secondary Electron
SIMPER	Similarity Percentages
sp.	Specific epithet with only one type of OTU
spp.	Specific epithet with more than one type of OTU
SP-ICP-MS	Single Particle Inductively Coupled Plasma Mass Spectrometry
SRB	Sulphate reducing bacteria
SXRF	Synchrotron micro X-ray fluorescence
v:v	Ratio of volume to volume
wt. %	Weight percent
XANES	X-Ray Absorption Near Edge Structure
XFM	X-ray fluorescence microscopy

Chapter I

General Introduction*

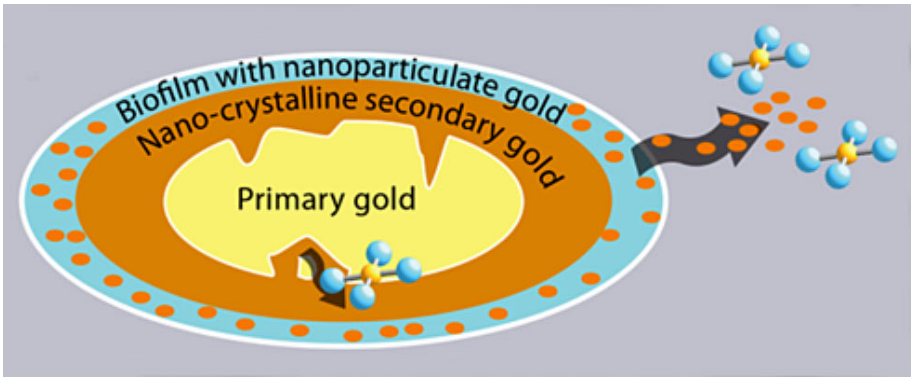

*The content of this chapter is an extended version of: **Rea MA**, Zammit CM, Reith F (2016) Bacterial biofilms on Au grains – Implications for geomicrobial transformations of Au. *FEMS Microbiol. Ecol.*, fiw082

Statement of Authorship

Title of Paper	Bacterial biofilms on gold grains – implications for geomicrobial transformations of gold
Publication Status	☑ Published ☐ Accepted for Publication ☐ Submitted for Publication ☐ Unpublished and Unsubmitted work written in manuscript style
Publication Details	**Rea MA**, Zammit CM, Reith F (2016) Bacterial biofilms on gold grains – implications for geomicrobial transformations of gold. FEMS Microbiol. Ecol., 92.

Principal Author

Name of Principal Author (Candidate)	Rea, Maria Angelica
Contribution to the Paper	Performed data processing, phylogenetic analysis. Interpreted results. Wrote the manuscript and created the figures.
Overall percentage (%)	50
Certification:	This paper reports on original research I conducted during the period of my Higher Degree by Research candidature and is not subject to any obligations or contractual agreements with a third party that would constrain its inclusion in this thesis. I am the primary author of this paper.
Signature	Date 15.05.18

Co-Author Contributions

By signing the Statement of Authorship, each author certifies that:

i. the candidate's stated contribution to the publication is accurate (as detailed above);

ii. permission is granted for the candidate in include the publication in the thesis; and

iii. the sum of all co-author contributions is equal to 100% less the candidate's stated contribution.

Name of Co-Author	Dr. Carla Zammit
Contribution to the Paper	Performed DNA extractions and PCR amplifications for DGGE-Sanger Sequencing, edited the manuscript.
Signature	Date 10/5/18

Name of Co-Author	A/Prof. Frank Reith
Contribution to the Paper	Conceived manuscript theme. Constructed figures. Manuscript evaluation and editing. Acting corresponding author.
Signature	Date 17/05/2018

Chapter 1: General Introduction

1.1. Rationale

Gold (Au) is a rare noble metal. Its high malleability, ductility, lustre and conductivity make it ideal for value storage, ornamentation, and more recently, technological applications (Corti and Holliday 2004). Throughout history, ~150,000 tonnes of Au has been mined, with over 50 % having been mined since the 1950s (World Gold Council 2018). The US geological survey estimates that around 52,000 metric tonnes of Au reserves are yet to be mined and will be discovered in the future (George 2013). Although the production of Au has been steadily increasing with demand, production has been slowing down in recent years, making it increasingly expensive for technological and scientific applications (Hall-Stoodley et al. 2004; World Gold Council 2018). The discovery of world-class Au and base metal deposits is becoming progressively rarer, many un(der)explored regions are covered by thick layers of *in situ* and/or transported regolith and easily accessible deposits have already been discovered and exploited. Discovery of metal deposits under regolith is difficult and expensive, in many cases making exploration unfeasible. Therefore, new methods for detecting Au in brownfield studies would be highly valuable to the mining industry. Gold is highly mobile in the regolith which can lead to the formation of secondary enrichment zones (so-called exploration halos) around buried Au deposits. Microbial weathering further contributes to the mobility of Au by releasing Au trapped within minerals and solubilising it via oxidation-promoting complexation from Au particles and nuggets (Southam et al. 2009; Reith et al. 2013). As these microorganisms both directly and indirectly interact with Au-complexes, the prospect of using microbial signatures to ascertain the presence of Au through regolith cover is a promising technological development for the mining industry.

To develop a Au detection technology based on the interactions between Au and microorganisms, there is a need to increase the fundamental knowledge of Au biogeochemical cycling and transport in Earth surface environments. Secondary enrichment zones formed by mobile Au, either as Au nanoparticles and/or the transport of Au-complexes is unknown, and so is the environmental 'kinetics' of Au mobility determining their formation. Thus, this PhD thesis aims to link Au transformation and microbial community composition to biogeochemical influence, physical factors, and mineralisation style and quantify Au transport and sorption

associated with soils and regolith materials including the effect of microbiota on Au mobility.

1.2. Biogeochemical cycling of gold

Primary Au deposits are commonly formed by precipitation of Au and other metals, especially silver (Ag), from hydrothermal solutions under high pressure/temperature conditions deep within the Earth's crust (Southam et al. 2009; Reith et al. 2013). Hydrothermal fluid permeates rocks and forms primary Au deposits in skarn- and vein-type deposits, igneous, volcanic and sedimentary rock as well as quartz (conglomerates and quartzite). A number of other metals such as copper (Cu), iron (Fe), bismuth (Bi), lead (Pb), zinc (Zn), palladium (Pd) and platinum (Pt) are incorporated but the most common minerals of Au are the native Au, *i.e.*, electrum and rhodite as well as Au tellurides (Boyle 1979). Under Earth surface conditions primary Au is progressively transformed by mechanical and (bio)geochemical processes ultimately resulting in secondary Au particles and nuggets, which commonly occur in eluvial and alluvial deposits, so-called placers (Fig. 1.1; Southam et al. 2009; Reith et al. 2013). Secondary Au is highly pure (>99 wt. % Au), finely crystalline (0.01 to 5 μm), and occurs as nanoparticulate, bacteriomorphic, sheet-like and wire Au, as well as euhedral, hexagonal, octahedral and pseudo-trigonal microcrystals, which can aggregate to form mm-sized Au particles (Falconer and Craw 2009; Southam et al. 2009; Hough et al. 2011; Fairbrother et al. 2012; Reith et al. 2012a; Shuster and Southam 2015).

Theories describing their origins were established to explain their formation; however, some formations cannot be explained by any one theory alone. The detrital theory involves physical movement of primary Au by weathering of source rocks and dealloying process (Boyle 1979). Detrital Au particles often exhibit a rim depleted in silver (Hough et al. 2007) with indicators of physical movement from striations and rounding (Knight et al. 1999). Chemical accretion theory which extends to the biogeochemical transformation involves solubilisation of primary Au, transport through the environment as Au-complexes and eventual precipitation. Secondary Au formed by this pathway has little Ag or other metal content and exhibits minimal mechanical abrasion (Boyle 1987). Episodes of deformation and metamorphosis remobilise the materials either by physical or (bio)chemical processes. Physical modification of Au particles may occur by hydrodynamic shear force and mechanical weathering leading to a (de)formed Au particle; as such it can be used as an indicator

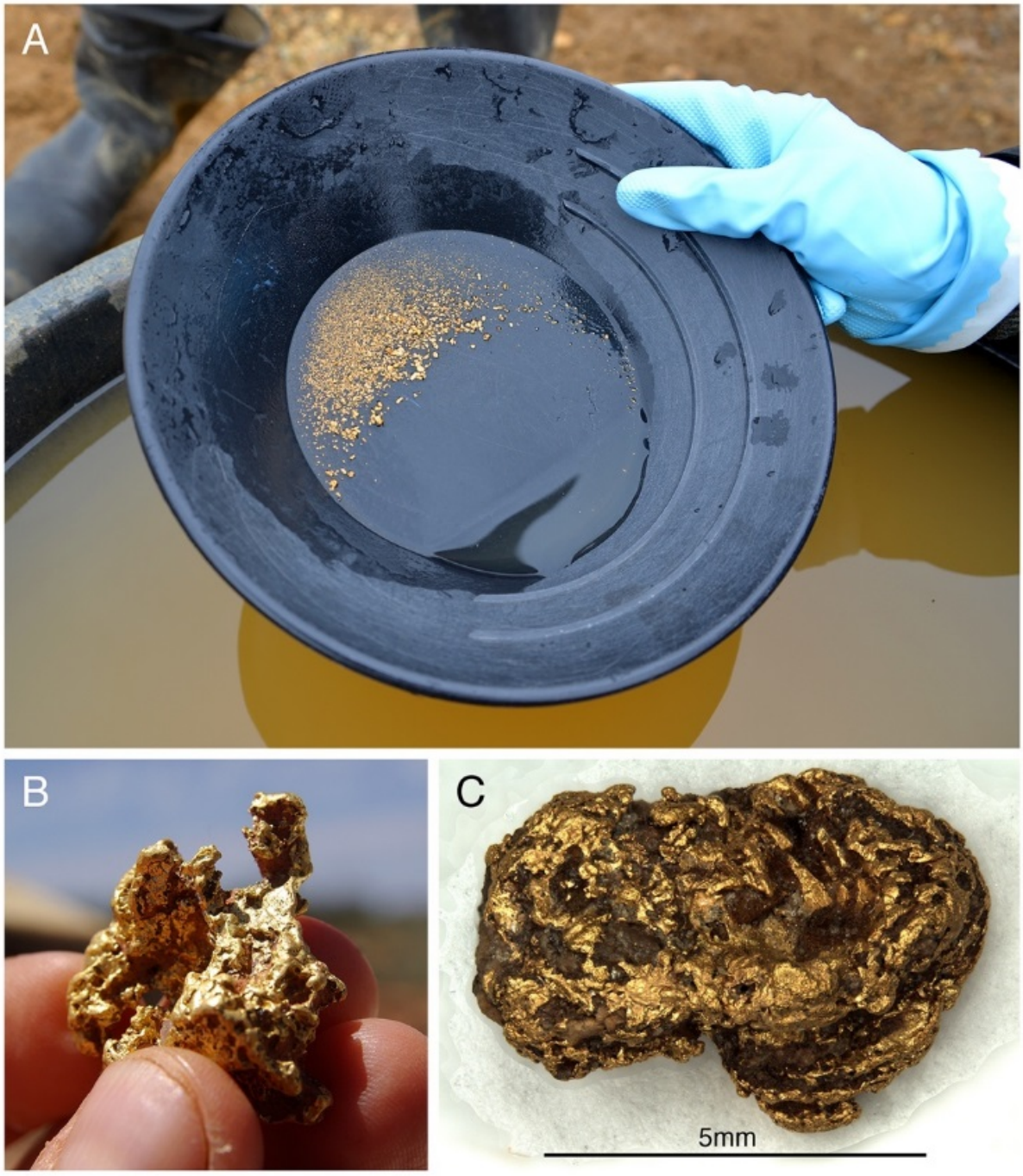

Figure 1.1 Gold from Earth surface environment; **(A)** Au particles sampling with a pan; **(B)** a Au nugget from arid Australia, and **(C)** a Au particle from Arrowtown (New Zealand) coated with layers Fe- and Mn-biominerals and secondary Au. Adapted from "Bacterial biofilms on gold grains – Implications for geomicrobial transformations of gold," by MA. Rea, C. Zammit and F. Reith, 2014, *FEMS Microbiol. Ecol.*, fiw082.

of travelled distance and potentially for the detection of unknown deposits (Knight et al. 1999; Townley et al. 2003; Hough et al. 2007). Indicators of primary physical modifications include the presence of primary cavities, growth hillocks, microlaminations and deformation textures, *e.g.*, striated surfaces and rare pulled filaments (Kinnunen 1996). Eventual formation of secondary surface features occurs

when in contact with mineral and rock edges such as corners of quartz fragments and pebbles or soft minerals forming mechanical markings such as shaving scratches, rimmed pits, rippled grooves and impact pits. These morphological transformations serve as a proxy for transport distance and are easily abraded and destroyed during sedimentological and erosional processes (DiLabio 1991; Kinnunen 1996). Some placer Au particles transformed by the biogeochemical process also undergo physical recrystallisation at particle boundaries (Stewart et al. 2017). Overgrowths can form and reform on Au particles over a span of <1 Ma and changes the surface texture by forming a near-complete coating of Au on the outside of detrital particles (Craw and Lilly 2016; Craw et al. 2017). The rims are formed by recrystallisation in the highly deformed margins of Au particles *in situ* after deposition. The recycled Au particles mix with freshly liberated Au particles resulting in the presence of Au with varying degrees of transformation within the same placer setting (Craw et al. 2017; Stewart et al. 2017).

Gold in surface conditions is found either as metallic Au (0) or aurous (I) and auric (III) Au-complexes (Boyle 1979). Free Au ions rarely exist as it is thermodynamically unfavourable due to the fact that the standard redox potential of Au(I) and Au(III) exceeds that of water (Boyle 1979; Vlassopoulos et al. 1990). Gold(I/III) often form complexes with thiosulphate, cyanides and halides, particularly chlorides, and are present in waters that contain little dissolved organic matter based on thermodynamic calculations and natural abundances (Boyle 1979; Mann 1984; Ta et al. 2014, 2015). Au(I)-thiosulphate is stable from highly acidic to highly alkaline pH under moderately oxidising/reducing conditions (Mineyev 1976; Webster 1986). Thiosulphate likely dominates groundwater systems surrounding Au-bearing sulphide deposits during the oxidation of sulphide minerals (Stoffregen 1987). High dissolved chloride contents in groundwater systems, common in arid and semi-arid zones across Australia, may solubilise Au leading to the formation of Au(I/III) complexes. In the presence of the metastable ligand cyanide, the formation of the $[Au(CN)_2]^-$ complex dominates. A manganese (Mn) pathway is also possible in the oxidation of Au to Au(III) with Mn-oxides under acidic conditions resulting in surface-bound Au(III)-complexes. Soils with high concentration of organic matter may also play a role in Au-complexation, organic acids such as humic, fulvic and carboxylic acids strongly bind to organic matter thus promoting solubilisation (Freise 1931; Boyle 1979; Vlassopoulus et al. 1990; Gray et al. 1998).

Microorganisms are involved in every step of the geochemical cycle of Au, from the formation of primary Au deposits to its solubilisation, dispersion and re-

concentration as secondary Au (Fig. 1.2; Reith et al. 2007; Southam et al. 2009; Kamenov et al. 2013; Reith et al. 2013; Yesares et al. 2015). In turn, microbial communities in soils/sediments overlying buried Au deposits are affected by the presence of elevated Au and pathfinder-element concentrations (Reith and Rogers 2008; Reith et al. 2012b, 2015). Soils overlying Au-deposits have been shown to be

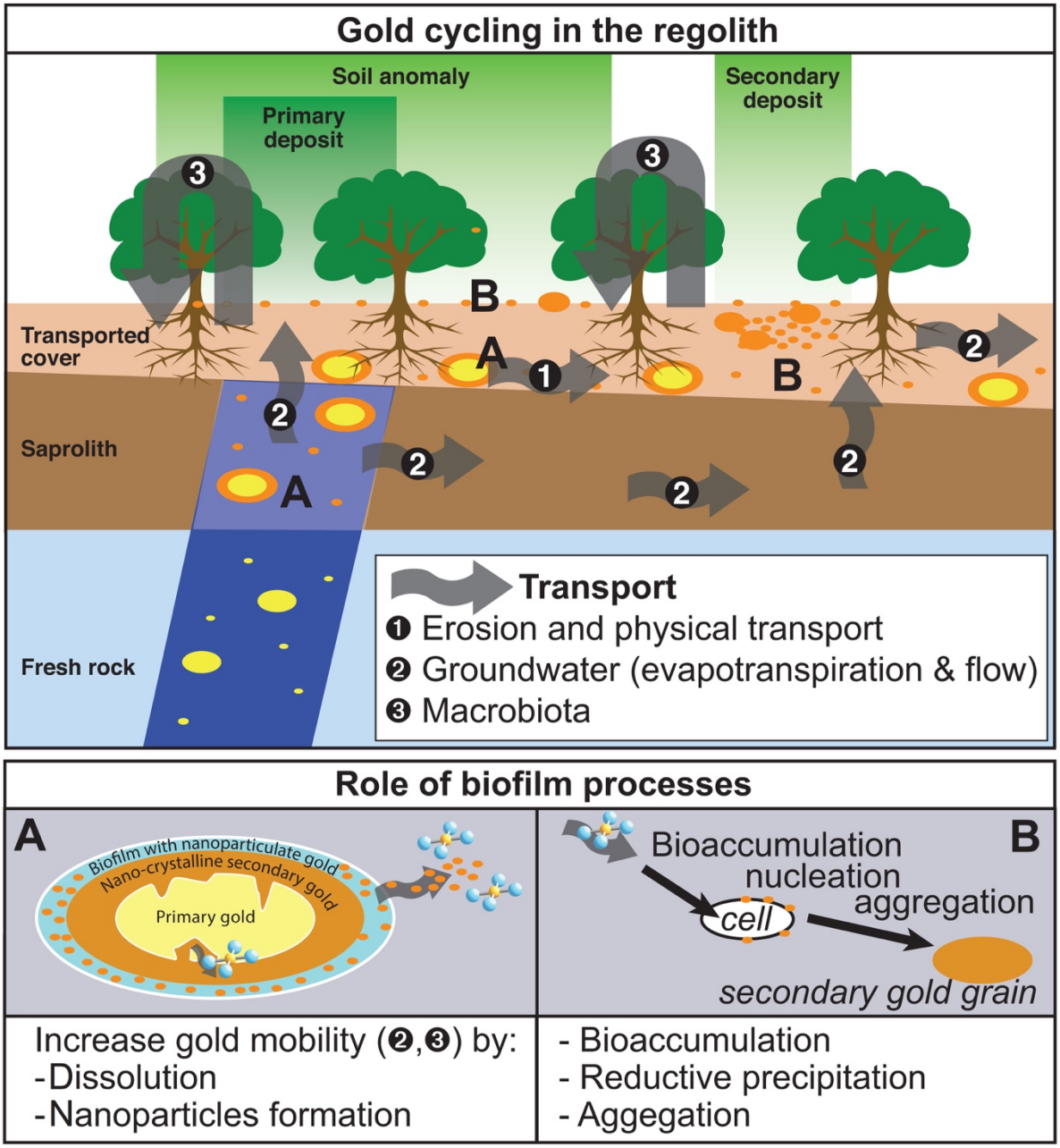

Figure 1.2 The geobiological cycle of Au comprises the solubilisation of primary Au (yellow; **A**), biomediated and abiogenic transport (1, 2, 3), bioaccumulation/reductive biomineralisation **(B)** and secondary Au (trans)formation in microbial biofilms (orange; **A, B**). Adapted from "Bacterial biofilms on gold grains – Implications for geomicrobial transformations of gold," by MA. Rea, C. Zammit and F. Reith, 2014, *FEMS Microbiol. Ecol.*, fiw082.

significantly enriched in Class Acidobacteria, Bacilli, β- and ε-Proteobacteria along with a range of genes involved in metal transport and resistance, *e.g.*, *copA*, *chrA* and *czcA* (Reith et al. 2012b; Reith et al. 2015).

Tomkins (2013a) suggested that microbial processes had a major influence on the formation of primary Au deposits throughout the Earth's history. His study indicated that interactions between the Earth's evolving tectonic processes and the biosphere might have driven changes in global geochemistry to conditions more suitable for uptake of Au into sedimentary pyrite. Indeed, the presence of dispersed Au in framboidal/biogenic sulphides suggests biogenic pathways for the incorporation of Au into sulphide minerals (Orberger et al. 2003; Tomkins 2013b). Sulphate-reducing bacteria (SRB) may drive the formation of the Au-bearing sedimentary pyrite (Reith et al. 2007). Sulphate-reducing bacteria can metabolically degrade thiosulphate as well as Au-thiosulphate complexes resulting in the formation of hydrogen sulphide. This ultimately leads to the formation of pyrite (Kaji and McElroy 1959). Destabilised Au-thiosulphate complexes can be directly incorporated into the pyrite lattices as well as be ab/adsorbed by microbial cells (Lengke and Southam 2006). Upon cell lysis, sorbed precipitated Au can aggregate into octahedral or spherical μm-sized Au, which is dispersed in the pyritic sediments (Southam and Beveridge 1996). In addition, reductive precipitation of mobile Au(III)-chloride and Au(I)-sulphide complexes on pyrite surfaces is an important abiogenic mechanism that leads to the formation of Au(0) (Mycroft et al. 1995; Widler and Seward 2002). These processes allow the formation of Au-enriched sedimentary sequences, which are ideal source rocks for hydrothermal, *i.e.*, primary Au deposits.

Under acidic conditions, iron- and/or sulphur-oxidising bacteria (*e.g.*, *Acidithiobacillus ferrooxidans* and *At. thiooxidans*) are known to break down Au-hosting sulphide minerals and release associated Au (Hutchins 1986; Gadd 2004). Gold-hosting minerals are 'broken down' following two pathways: pyrite (FeS_2), molybdenite (MoS_2) and tungstenite (WS_2) are decomposed via a thiosulphate mechanism, with sphalerite (ZnS), chalcopyrite ($CuFeS_2$), galena (PbS), hauerite (MnS_2), orpiment (As_2S_3) and realgar (As_4S_4) being 'broken down' via a polysulphide mechanism (Schippers and Sand 1999). Both pathways can lead to the formation of ligands known to contribute to Au mobility by forming stable, water-soluble S-bearing complexes with Au (Etschmann et al. 2011). Iron-oxidising microorganisms will also oxidise Fe in the pyrite. Other microbial processes, such as the excretion of organic acids, *e.g.*, acetate, citrate and oxalate, as well as peptides, proteins and cyanide, may drive Au solubilisation in Au-containing soils (Reith and McPhail 2006,

2007). *Corynebacterium glutamicum*, an aerobic, gram-positive soil bacterium, can form large-scale production of amino acids such as glutamate (Kalinowski et al. 2003). Glutamate is an acidic anion that can cap the Au nanoparticle thereby inducing electrostatic repulsion among the nanoparticles, keeping them from agglomerating. Bacteria with the ability to produce cyanide contribute to Au mobilisation through Au complexation with cyanide. The ability to form cyanide is widely distributed in environmental bacteria and fungi as well as in some plants (Michaels and Corpe 1965). Some other known cyanide-producing bacteria (*e.g.*, *Pseudomonas fluorescens* and *P. plecoglossicida*), algae (*e.g., Chlorella vulgaris*) and fungi (*e.g., Marasmius oreades, Stemphylium loti* and *Gloeocercospora sorghi*), have shown to solubilise Au by releasing cyanide (Brandl et al. 2008; Fairbrother et al. 2009). Cyanide may play an important role in the transformation of primary to secondary Au particles by providing mobile Au-complexes in the biofilm environment. Indeed, *Chromobacterium violaceum* has been shown to mediate Au solubilisation when growing as a single-species biofilm on ultra-flat Au foils (Fairbrother et al. 2009; Brugger et al. 2013). Humic and fulvic acids contribute to the mobilisation of Au by forming complexes with Au(I/III)-ions, reduction of Au-complexes and the formation of stabilised Au nanoparticles (Freise 1931; Ong and Swanson 1969; Boyle 1979). The mobilised Au is eventually released and transported as dissolved mobile Au-complexes and/or nanoparticles in surface, soils and groundwater systems. The presence of other metals/minerals can also affect Au solubilisation. For example, mobile Cu/Zn, Fe and Mg are known to stimulate cyanide formation in fungi, and gram-negative and gram-positive bacteria, respectively (Faramarzi et al. 2004). Two recent studies have shown that reactive Mn-oxide minerals, *e.g.*, microbially produced birnesitte, are important catalysts of Au solubilisation in low carbon environments (Ta et al. 2014, 2015).

Mobile Au(I/III)-complexes are highly cytotoxic, in the multi-metal resistant bacteria *Cupriavidus metallidurans*, the minimal inhibitory concentration (MIC) of Au(I)-thiosulphate is 0.5 μM and Au(III)-chloride is 0.9 μM which is in a similar range of tolerance as silver (Ag) and mercury (Hg) (Brugger et al. 2013; Wiesemann et al. 2013; Nies 2016). A number of bacteria and archaea are capable of active precipitation of mobile Au(I/III)-complexes (Reith et al. 2007). Reductive precipitation of Au-complexes may improve survival rates of bacterial populations that are capable of (i) gaining metabolic energy by utilising Au-complexing ligands (*e.g.*, thiosulphate by *At. ferrooxidans*) and (ii) detoxifying the immediate cell environment by detecting, excreting and reducing Au-complexes in aerobic (*e.g.*, *D. acidovorans*, *C. metallidurans*

CH34, *Plectonema boryanum*; Lengke et al. 2006; Lengke and Southam 2006; Reith et al. 2009) and anaerobic conditions (*Salmonella typhimurium*; Checa et al. 2007).

Cupriavidus metallidurans and *D. acidovorans* were detected in biofilm communities on Au particles from moderate and tropical climates in Australia (Reith et al. 2006; Reith et al. 2010). *Cupriavidus metallidurans*, a non-spore forming aerobic β-Proteobacterium, is able to tolerate high levels of heavy metals and in particular the oxidative/metal stress induced by toxic Au-complexes (Nies 1999; Reith et al. 2009; Wiesemann et al. 2013). *Delftia acidovorans*, another non-spore-forming, aerobic β-Proteobacterium, produces/excretes a metabolite, delftibactin, to detoxify Au extracellularly (Johnston et al. 2013). Both species actively contribute to the formation of secondary Au-biominerals (Fairbrother et al. 2013; Johnston et al. 2013).

In a recent study, biogenic secondary Au formed from the reduction of soluble Au(I/III)-complexes by Fe-oxidising bacteria, cyanobacteria and SRB were combined in an experimental tumbler system representing a model for a fluvial environment in which placer Au could occur (Shuster and Southam 2015). Results showed that biofilms combined with physical aggregation were critical for the accumulation of nm- to μm-sized Au particles of up to five millimetres in diameter. Secondary Au is also common in quartz pebble conglomerates (QPC), *e.g.*, the Witwatersrand QPC, which is the world's largest Au deposit (Mossman and Dyer 1985; Frimmel et al. 1993). Here Au is commonly associated with bituminous organic matter of putative microbial origin. Falconer et al. (2006) and Falconer and Craw (2009) provided evidence that geobiological processes play an important role in the formation of QPC-deposits by showing that carbonaceous mudstones within a QPC sequence in New Zealand contained Au particles displaying abundant bacteriomorphic and sheet-like secondary Au morphologies.

1.3. Biofilms in extreme environments

Biofilm communities are present in many natural and anthropogenic environments (Costerton et al. 1995; Hall-Stoodley et al. 2004). Biofilms play an important role in biogeochemical cycles; therefore, they are considered primary drivers of metal mobility in Earth surface environments (Gadd 2004). Commonly, microorganisms exist as part of a biofilm community rather than as free-living planktonic cells, which may be attributable to the natural protection conferred in biofilms (Costerton et al. 1995; Donlan 2002). Higher survival rates (compared to planktonic cells) are observed by biofilm-associated microorganisms in challenging environments, *e.g.*, biofilms adjacent to hydrothermal systems (Costerton et al. 1995;

Hall-Stoodley et al. 2004). Therefore, biofilm formation is now considered an innate part of the bacterial life cycle (Stoodley et al. 2002; Hall-Stoodley et al. 2004). In particular, biofilm consortia are less susceptible to metal toxicity than planktonic cells (Costerton et al. 1995). For example, single-species biofilms of *Burkholderia cepacia, C. metallidurans* and *Escherichia coli* were able to survive five times higher concentrations of Ag nanoparticles, Au(I)-complexes and Ga(III), respectively, than when cells were planktonic (Geslin et al. 2001; Harrison et al. 2007; Fairbrother et al. 2013). Biofilms can form complexes with metals and protect the microbial community from excessive metal stress by nucleation (Gillan 2016). The increased resistance of biofilm communities to metal toxicity is the result of complex interactions between chemical, physical, physiological and biochemical factors that govern biofilm activities (Harrison et al. 2007). For instance, cells in a biofilm community communicate with other cells via quorum sensing. These are signalling molecules used by cells to communicate with one another, thereby controlling the development of a biofilm through attachment, maturation and aggregation (Parsek and Greenberg 2005). Quorum sensing also improves the response of biofilms to oxidative stress caused by metals (Geslin et al. 2001). Cells in biofilms are commonly embedded in extracellular polymeric substance (EPS), which provides structural cohesion of biofilm communities, regulates the availability of water and nutrients, provides a protective barrier against toxic compounds and acts as a carrier of genetic information for horizontal gene transfer among biofilm-associated cells (Hall-Stoodley et al. 2004; Pal and Paul 2008).

Due to the toxicity of mobile Au-complexes, environmental Au cycling has been linked to the activity of microbial biofilms (Reith et al. 2006, 2013). The elevated toxicity of Au(III) in natural waters is very important as this likely drives the formation of Au-detoxifying biofilms that catalyse the biomineralisation of spheroidal nanoparticulate Au, hence, accelerating the biogeochemical cycling of Au. The presence of EPS, as observed on biofilms in column experiments and on natural Au particles, leads to the immobilisation of Au-complexes thereby decreasing the amount of toxic mobile Au-complexes reaching the cells (Harrison et al. 2007; Fairbrother et al. 2013). The amount of toxic Au-complexes reaching viable cells is also reduced through the reactivity of dead cells contained in the biofilms, which are rapidly fossilised by transition metals (Peeters et al. 2008).

Microbial community data is available from Au particles collected at ten sites across Australia, New Zealand and South America and Finland. The majority of bacteria detected belonged to operational taxonomic units (OTUs) from α-, β- and γ-

Proteobacteria and Actinobacteria. A range of organisms appears to contribute predominantly to biofilm establishment and nutrient cycling, some affect the mobilisation of Au via excretion of Au-complexing ligands, *e.g.*, organic acids, thiosulphate and cyanide, while a range of resident Proteobacteria, especially *C. metallidurans* and *D. acidovorans,* have developed Au-specific biochemical responses to deal with Au-toxicity and reductively precipitate mobile Au-complexes. This leads to the biomineralisation of secondary Au and drives the environmental cycle of Au.

1.4. Composition and functional associations of biofilms on placer gold

Biofilms have been detected on Au particles from ten sites in Australia, New Zealand and South America (examples shown in Fig. 1.3A–B, Table 1.1 provides site information). Commonly associated with these biofilms was abundant secondary and bacterioform Au (Fig. 1.3C and D). Across all sites, biofilms were mostly composed of Actinobacteria, Firmicutes and Proteobacteria, with α-, β- and γ-Proteobacteria being most abundant (Fig. 1.4A). Canonical analysis of principal coordinates (CAP) using the PRIMER-6 software (Clarke and Warwick 2001; Anderson et al. 2008), showed a significant link ($p < 0.05$) between community composition and the origin of the Au particles, *i.e.*, Australia, New Zealand or Brazil (Fig. 1.4B). However, no significant link to climatic settings could be detected suggesting that other physicochemical or geological factors drive regional differences in community composition. SIMPER analyses showed that a range of OTUs was highly differentiative for communities on Australian, New Zealand and Brazilian Au particles (Fig. 1.4B; Reith et al. 2015). Bacteria detected on Au particles belong to a range of phyla with wide-ranging metabolic capabilities.

A range of species may have the ability to directly or indirectly affect Au mobilisation, with one or more key-microorganisms present in the consortium having described or putative Au detoxifying/precipitation abilities. The aurophilic bacterium *C. metallidurans*, which was detected on Au particles is one of the key-species involved in Au cycling. It reduces toxic Au(I/III)-complexes in the periplasm, which leads to the formation of Au nanoparticles (Reith et al. 2009; Wiesemann et al. 2013, 2017). These contribute to the formation of secondary Au, and hence the biological (trans)formation of Au particles (Fig. 1.3D, 1.5).

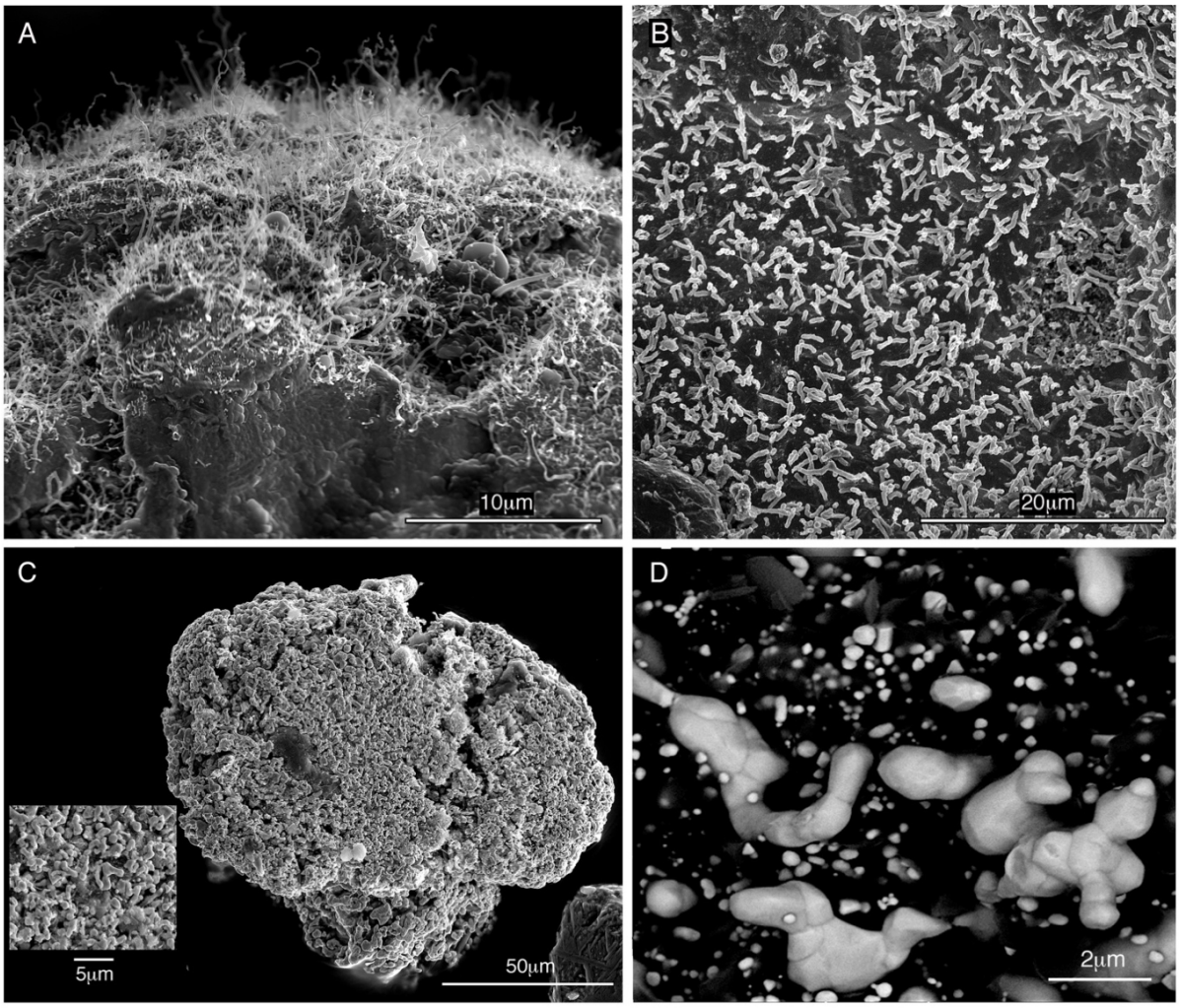

Figure 1.3 Electron micrographs of biofilms on Au particle surface at **(A)** Lively's Find (Australia), **(B)** Corrego Bom Sucesso (Brazil) as well as **(C)** nano- and micro-phase Au and **(D)** a transformed secondary particle from the Prophet Mine (Australia). Adapted from "Bacterial biofilms on gold grains – Implications for geomicrobial transformations of gold," by MA. Rea, C. Zammit and F. Reith, 2014, *FEMS Microbiol. Ecol*., fiw082.

During the initial stages of biofilm formation, gram-positive bacteria can initiate attachment to Au particle surfaces (Fig. 1.6). Gram-positive bacteria have a thicker peptidoglycan layer, which can withstand electrostatic disruptions on the cell membrane caused by surface charge (Gottenbos et al. 2001; Sbordone and Bortolaia 2003). Thus, it is likely that gram-positive organisms detected in the biofilms, *e.g.*, *Arthrobacter* spp., *Corynebacterium* sp., *Deinococcus* sp., *Kocuria* sp., *Microbacterium* spp., *Micrococcus* spp., *Propionibacterium* spp. *and Staphylococcus* spp. (Table 1.2), mediate initial colonisation on the Au particles. In addition, gram-positive bacteria produce EPS, which further conditions the Au particle surfaces and forms the backbone of the biofilm. Because colonisation with gram-positive bacteria negates the potential electrostatic disruption to bacterial cell membranes, gram-negative bacteria can begin to settle in the biofilm (Fig. 1.6).

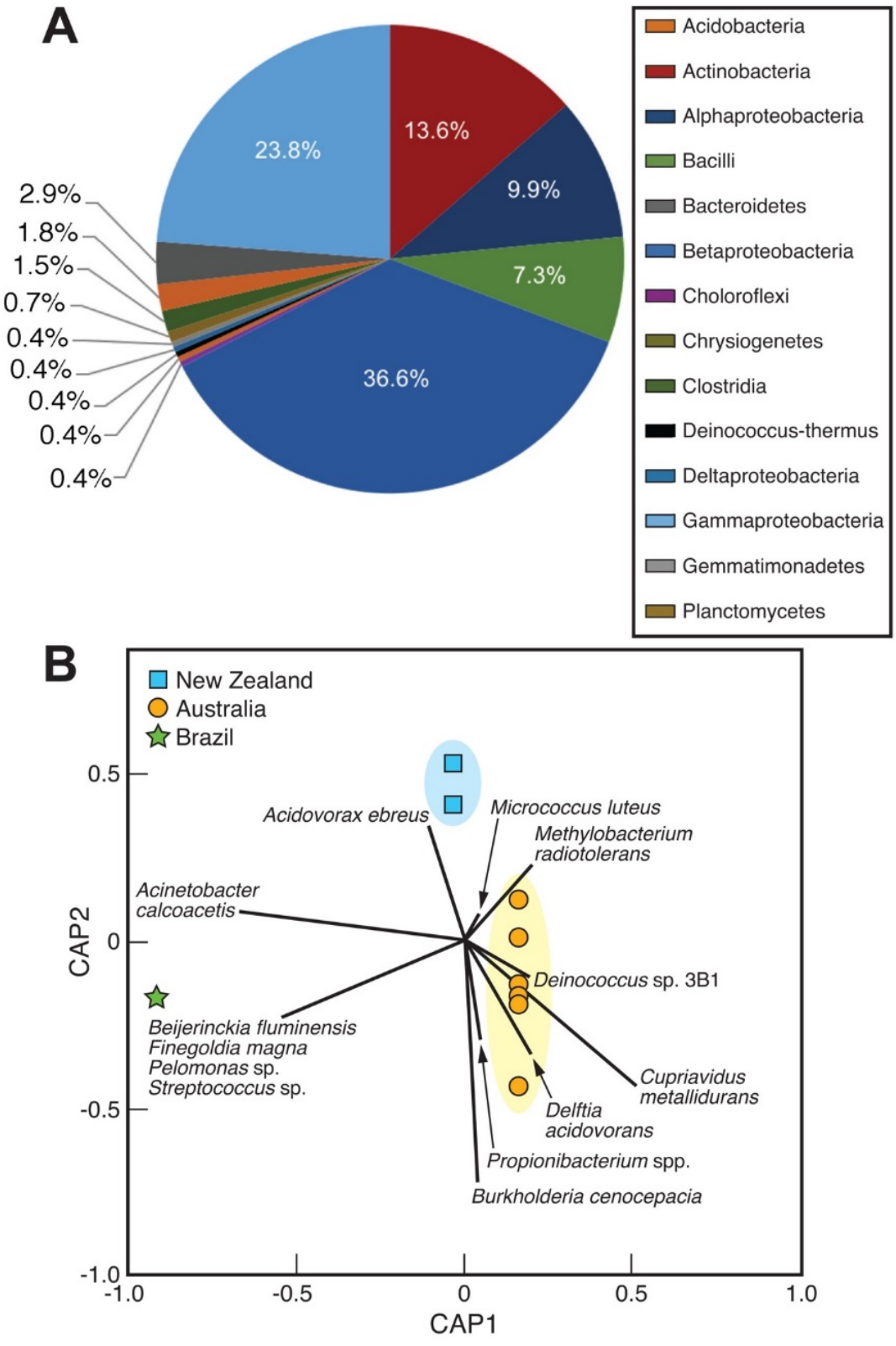

Figure 1.4 **(A)** Distribution of dominant prokaryotic phyla/classes; note: classes are shown for Proteobacteria and Firmicutes, and **(B)** canonical analysis of principal coordinates (CAP) of community data, based on individual taxa. Adapted from "Bacterial biofilms on gold grains – Implications for geomicrobial transformations of gold," by MA. Rea, C. Zammit and F. Reith, 2014, *FEMS Microbiol. Ecol.*, fiw082.

Table 1.1 – Site information concerning the gold particle collection localities in Australia, New Zealand and South America.

Locality (abbreviation)	State/region and country	GPS coordinates	Number of Au particles with biofilm consortia assessed	Reference or accession number
Prophet Mine (Pr)	Queensland, Australia	S 26°06′51.98″, E 152°17′0.94″	14	Reith et al. 2010; KX078227–KX078244
Hit or Miss Mine (H)	Queensland, Australia	S 16°03′32″, E 144°19′09″	5	Reith et al. 2006
Corrego Bom Successo (CBS)	Minas Gerais, Brazil	near Serro, Minas Gerais, Brazil[a]	9	KX033861–3864; KX033871–3878; KX033880; KX033882–3884; KX033887–3889; KX033894–3895; KX033898–3901; KX033905–3906; KX033910; KX033912–3914; KX033948–3961; KX033963–3964; KX033970–3976; KX033987; KX033994–3997; KX033999–4002
Rio Saldana (R)	Tolima, Colombia	N 3°56′26.07″, W 74° 58′ 10.09″	4	Shuster et al. 2015
Tomakin Park (T)	New South Wales, Australia	S 35°48′ 51.90″, E 150°100′26.40″	8	Reith et al. 2006
Shantytown (S)	South Island, New Zealand	S 42°32′13.50″, E171°10′37.79″	3	KX033892–KX033925; KX034003–KX034005
Arrowtown (Ar)	South Island, New Zealand	S44°59′25.61″, E168°51′14.37″	23	KX033886; KX033926; KX033928–3930; KX033935–3937; KX033962; KX033991
Lively's Find (L)	South Australia, Australia	S30°17′12.97″, E139°20′23.31″	21	KX033865–3870; KX033885; KX033904; KX033921; KX033927; KX033931–3932; KX033938; KX033941; KX033977; KX033986; KX033993; KX034006
Platina Deep Lead System (F)	New South Wales, Australia	S32°50′34.05″, E147°28′6.02″	11	KX033879; KX033881; KX033890–3891; KX033911; KX033915–3916; KX033918; KX033939–3940; KX033965–3969; KX033978; KX033980–3983; KX033985; KX033990; KX033992; KX033998
Adelaide Hills (Ad)	South Australia, Australia	S 34°39′3.63″, E138°49′59.14″ S 34°40′49.75″, E138°50′51.36″ S 34°43′30.04″, E 138°56′1.25″	6	KX033907; KX033919; KX033933–3934

Note: Reprinted from "Bacterial biofilms on gold grains – Implications for geomicrobial transformations of gold," by MA. Rea, C. Zammit and F. Reith, 2014, *FEMS Microbiol. Ecol.*, fiw082.

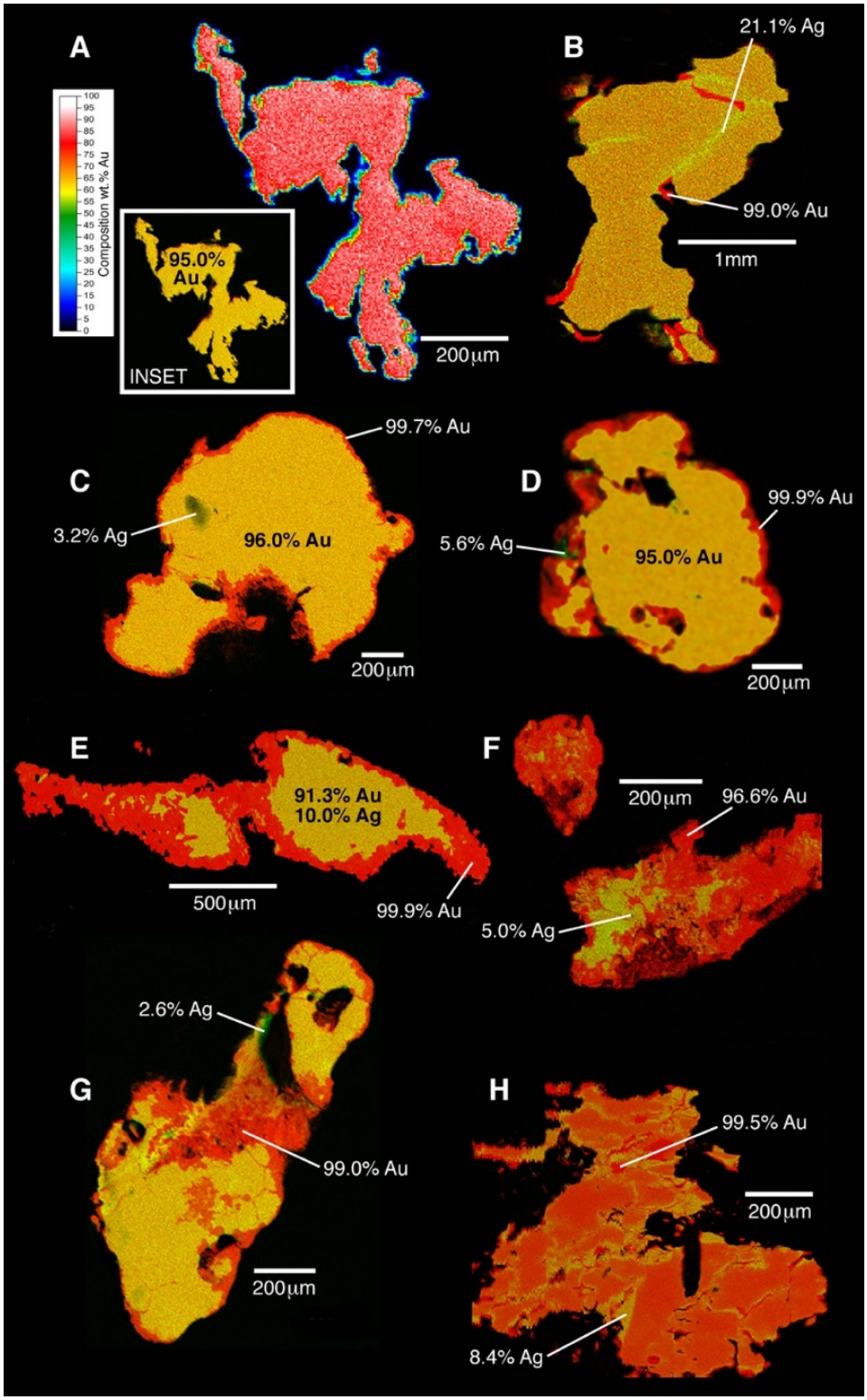

Figure 1.5 Electron microprobe maps, Au (red) and Ag (green) showing the progressive transformation of Au particles. **(A)** Adelaide Hills' primary Au particles composed of a homogenous Au-Ag alloy (inset); **(B)** Au particle from Old Pirate deposit showing initial signs of secondary Au formation (*i.e.*, rims of >99 % Au). Increasingly transformed Au particles from **(C)** the Hit and Miss Mine, **(D)** Arrowtown, **(E)** Fifield, **(F)** the Prophet Mine, **(G)** the Tomakin Park Mine and **(H)** Lively's Find. Adapted from "Bacterial biofilms on gold grains – Implications for geomicrobial transformations of gold," by MA. Rea, C. Zammit and F. Reith, 2014, *FEMS Microbiol. Ecol*., fiw082.

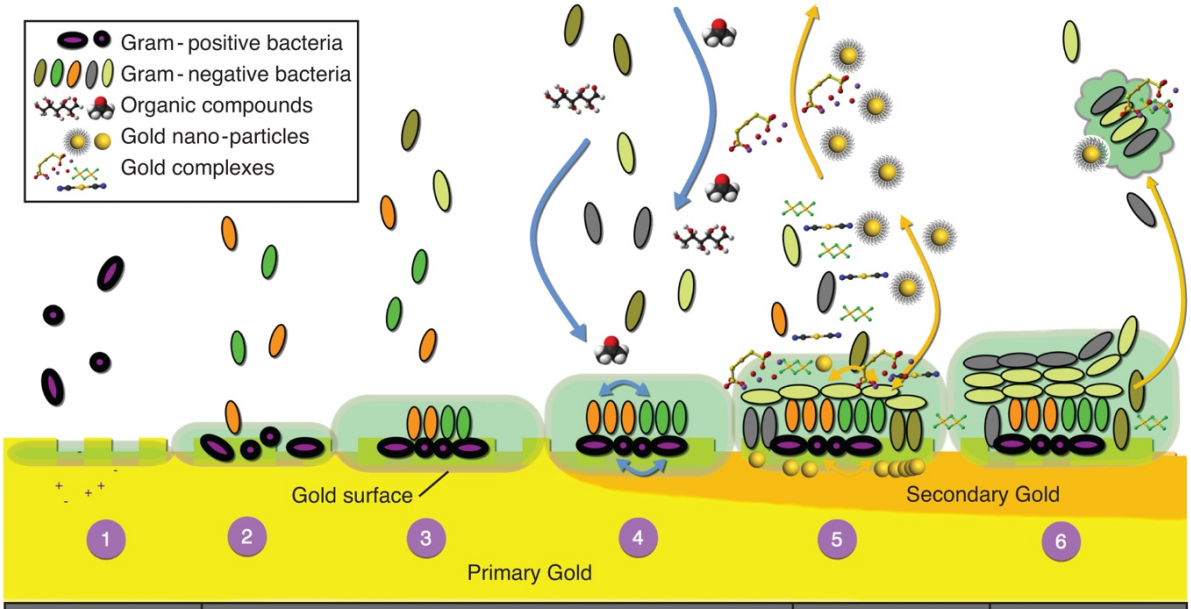

1. Surface Conditioning	Biofilm growth and recruitment			5. Gold mobility	6. Dispersal cells
	2. EPS production (E) Auto-aggregation (A)	3. Nutrient cycling C-fixation (C) N_2-fixation (N) Nitrification (NI) Denitrification (D)	4. Metabolic turnover of complex organics (O); xenobiotic (X), toxins (T)	Gold solubilisation (S) Gold detoxification (G) Metal resistance (M)	
Arthrobacter spp. *Corynebacterium* sp. *Deinococcus* sp. *Kocuria* sp. *Microbacterium* spp. *Micrococcus* spp. *Propionibacterium* spp. *Staphylococcus* spp.	*Pseudomonas* spp. (E) *Burkholderia* spp. (E) *Methylobacterium* sp. (E) *Acinetobacter* spp. (E) *Sediminibacterium* spp. (A) *Rhodobacter* sp. (A)	*Rhodobacter* sp. (C) *Beijerinckia* sp. (N) *Rhizobium* spp. (N) *Herbaspirillum* sp. (N) *Pelomonas* sp. (N) *Nitrobacter* sp. (NI) *Diaphorobacter* sp. (NI,D) *Acidovorax* sp. (D) *Achromobacter* sp. (D) *C. metallidurans* (D) *S. maltophilia* (D) *Pseudomonas* spp. (D)	*Acinetobacter* spp. (O) *Burkholderia* spp. (O) *Pelomonas* sp. (O) *Pseudomonas* spp. (O) *Sphingobium* sp. (O) *Sphingomonas* spp. (O) *Arthrobacter* sp. (X) *Diaphorobacter* sp. (X) *Phenylobacterium* sp. (X) *Xanthomonas* sp. (X) *Methylobacterium* sp. (T)	*Diaphorobacter* sp. (S) *Sphingomonas* spp. (S,M) *Methylobacterium* sp. (S) *C. metallidurans* (G) *D. acidovorans* (G) *S. maltophilia* (G) *Achromobacter* spp. (M) *Halomonas* sp. (M) *Herbaspirillum* sp. (M) *Burkholderia* spp. (M) *Shewanella* sp. (M) *Acinetobacter* spp. (M) *Pseudomonas* spp. (M) *Ideonella* sp. (M)	*Acinetobacter* spp. *Lysobacter* sp. *Duganella* sp.

Figure 1.6 Schematic model showing the development and effect of Au-cycling biofilm on Au particle surfaces: (1) the conditioning of surfaces to their attachment; (2) the recruitment of phototrophic and heterotrophic gram-negative bacteria; (3–5) the proliferation and growth of biofilm community including heterotrophic and metallophilic species; (5) the mobilisation, detoxification and re-precipitation of secondary Au; and (6) the seeding of dispersal cells with release of nanoparticle and Au-complexes. Adapted from "Bacterial biofilms on gold grains – Implications for geomicrobial transformations of gold," by MA. Rea, C. Zammit and F. Reith, 2014, *FEMS Microbiol. Ecol.*, fiw082.

This 'second wave' of colonisers includes bacteria such as *Pseudomonas* spp., *Burkholderia* spp., *Methylobacterium* sp. and *Acinetobacter* spp. capable of EPS production that further stabilises the biofilm (Fig. 1.6; Cérantola et al. 2000; Pal and Paul 2008). *Pseudomonas* spp. produce bio-surfactants known to initiate the formation of micro-colonies and water channels in biofilms as well as to start off the dispersal of cells from the existing biofilm layer (Pamp and Tolker-Nielsen 2007). *Sediminibacterium* spp. and *Rhodobacter* sp. may contribute to the

establishment/stability of biofilms by inducing auto-aggregation (Fig. 1.6; Ayarza et al. 2014). For example, *Rhodobacter* sp. possess a unique quorum sensing molecule that induces the clumping of bacterial cells (Puskas et al. 1997).

When gold is exposed to the surface during turnover, flooding, weathering and erosion, phototrophic *Rhodobacter* sp. may provide the forming biofilm with reduced organic substrates, thereby fuelling heterotrophic organisms (Fig. 1.6; Roeselers et al. 2008). Some resident bacteria also have the ability to fix N_2 (*e.g.*, *Beijerinckia* sp., *Rhizobium* spp., *Pelomonas* sp. *and Herbaspirillum* sp.). Nitrogen is further cycled by resident nitrifying bacteria, *e.g.*, *Nitrobacter* sp. and the simultaneous denitrifying and nitrifying bacteria *Diaphorobacter* sp., and denitrifiers, *e.g.*, *Acidovorax* sp., *Achromobacter* sp., *C. metallidurans, Pseudomonas* spp. and *Stenotrophomonas maltophilia* (Fig. 1.6). Their presence may help to ensure a continuous supply of usable N to other biofilm organisms. Overall, this initial population of C- and N_2-fixers and cyclers may produce intermediate compounds, which provide metabolic resources for colonisation by heterotrophs. Resident organotrophs are likely to metabolise a wide range of complex organic compounds commonly found in placer environments, *e.g.*, low and high molecular weight organic acids (Fig. 1.6). Especially, *Acinetobacter* spp., *Burkholderia* spp., *Pelomonas* sp. *Pseudomonas* spp., *Sphingobium* sp. and *Sphingomonas* spp., as well as *Arthrobacter* spp., *Diaphorobacter* sp., *Phenylobacterium* sp. *and Xanthomonas* sp. to degrade complex organics and xenobiotic compounds (Fig. 1.6; Table 1.2; Xie and Yokota 2005; Liou et al. 2008; Mrozik and Piotrowska-Seget 2010). In addition, *Methylobacterium* sp. can oxidise toxic organic compounds, *e.g.*, methyl chloride, ethylated S-containing compounds, cyanate and thiocyanate to gain metabolic energy (Green 2006). This may contribute to the biomineralisation of Au by utilising Au-complexing ligands thereby destabilising Au-complexes (Korobushkina et al. 1974; Ubaldini et al. 2000; Lengke and Southam 2006).

Bacteria capable of mediating Au solubilisation may now occur in the community and include S-oxidising or cyanide-producing bacteria, *e.g.*, *Diaphorobacter* sp., *Sphingomonas* spp. and *Methylobacterium* sp. (Fig. 1.6; Rother et al. 2001; Tabrez Khan et al. 2002; Green 2006). *Sphingomonas* spp. have a complete *Sox* gene cluster, which permits an S-oxidising enzyme system to convert elemental sulphur to thiosulphate (Rother et al. 2001). Thiosulphate is known to contribute to Au mobility by forming stable, water-soluble complexes with Au (Ta et al. 2014). This would initiate the release of highly toxic Au-complexes into the biofilm environment.

Table 1.2 – Summary of OTUs detected in biofilm on Au particles; shown are classification accession numbers, closest relative(s) in GenBank, sites detected and a summary of metabolic capabilities.

Clone	GenBank Accession No.	Closest relative in NCBI hit/accession nr.	%ID	Gram stain	Sites	Putative metabolic capabilities	Metallo-phile
Firmicutes							
AuOTU1	KX033861–KX033870; KX078227–KX078228	*Staphylococcus epidermidis* GD9 [KF928765.1]; *Staphylococcus aureus* [KC928093.1]	98–100	+	C; L; Pr	N; FAA; COT	
AuOTU2	KX033871–KX033878	*Streptococcus* sp. 10aVMg3 [EF151147.1]	99	+	C	FAA; COT	
AuOTU3	KX033879	*Dialister* sp. C18 [GU429801.1]	98	+	F	OAA	
AuOTU4	KX033880	*Finegoldia magna* ATCC 29328 [NR074677.1]	99	+	C	OAA	
Actinobacteria							
Corynebacteriales							
AuOTU5	KX033881	*Corynebacterium pseudogenitalium* CIP106714 [AJ439348.1]	99	+	F	FAA; COT	
Micrococcales							
AuOTU6	KX033882–KX033889	*Arthrobacter arilaitensis [LN774488.1], Arthrobacter nicotinovorans* THWCSN6 [GQ284335.1]; *Arthrobacter oxydans* [JQ684244.1]	98–100	+	Ar; C; L	Mo; OA; S; X	+
AuOTU7	KX033890	*Kocuria rosea* Mali 173 [AY211171.1]	97	+	F	A; COT	+
AuOTU8	KX033891	*Microbacterium oxydans* JI 2 [KJ627769.1]	99	+	F	Mo; A; COT	+
AuOTU9	KX033892–KX033893	*Micrococcus luteus* N50 [LK020754.1], *M. lylae* BPD-5 [JN377810.1]	99	+	L; S	A; COT	
Propionibacteriales							
AuOTU10	KX033894–KX033903; KX078230–KX078233	*Propionibacterium acnes* hdn-1 [CP006032.1]; *Propionibacterium* sp. KPL1849 [KF906602.1]	97–100	+	Ad; C; F; Pr; L	ATAA; COT	
Bacteroidetes							
Au-OTU11	KX078234–KX078235	*Chryseobacterium hominis* CCUG 15261 [AM423087.1]	99	-	Pr	OA; COT	
Au-OTU12	Shuster *et al.* 2015	*Sediminibacterium* sp. B2-10-2, *Sediminibacterium* sp. I-32	99	-	R	Mo; A	
Deinococcus-Thermus							
AuOTU13	KX033909	*Deinococcus* sp. 3B1 *[EU308577.1]*	99	+	F	A; COT	
α-Proteobacteria							
Caulobacteriales							
Au-OTU14	GU013674.1	*Phenylobacterium* sp. BUT-10 [KJ008916.1]	97–99	-	Pr	A; COT; X	
Rhizobiales							
AuOTU15	KX033910	*Beijerinckia fluminensis* UQM [NR116306.1]	99	-	C	Mo; A; N2	
Au-OTU16	DQ294758.1–DQ294757.1	*Methylobacterium radiotolerans* TH35 [LC026010.1];	99	-	H	Mo; A; COT	
Au-OTU17	Shuster *et al.* 2015	*Nitrobacter* sp. 263		-	R	Mo; FA; NI	
AuOTU18	KX033911–KX033914	*Rhizobium* sp. RP-1 [KF906141.1]; *Rhizobium* sp. Pant-1 [KF906138.1]; *Rhizobium huautlense* OS-49.b[KF906138.1]	99	-	C; F	Mo; A; COT; N2	

Rhodobacteriales							
AuOTU19	KX033915	*Rhodobacter* sp. WS22 [KF309179.1]	99	-	F	Mo; PT; D	
AuOTU20	KX033916	*Rubellimicrobium mesophilum* MSL-20 [NR044275.1]	95	-	F	Mo; A; COT; S/P	
Sphingomonadales							
AuOTU21	KX033917	*Altererythrobacter* sp. AMV9 [FN397680.1]	98	-	Ad	A; CHT	
AuOTU22	KX033918	*Sphingobium limneticum* 301 [NR109484.1]	99	-	F	Mo; A; COT; S	
AuOTU23	KX033919–KX033920; KX078236–KX078237	*Sphingomonas rhizogenes* BW59UT1570 [JF276901.1]; *Sphingomonas* sp. KAR7 [EF451637.1]	98–99	-	Ad; Pr; L	Mo; A; COT; S; Ar	
β-Proteobacteria							
Burkholderiales							
AuOTU24	KX033921–KX033925	*Acidovorax ebreus* TPSY [NR074591.1]	95–99	-	S; L	Mo; A; COT; P/S; D	
AuOTU25	GU013676.1, KX033926–KX033937	*Achromobacter spanius* JN52 [KF150361.1], *A. xylosoxidans* TPL14 [EU373389.1]	98–99	-	Ad; Ar; Pr; L	Mo; A; LAT; P; D	+
Au-OTU26	GU013675.1	*Burkholderia cenocepacia* PSB3 [JX310700.1], *B. lata* 383 [NR102890.1]	99	-	Pr	Mo; OA; Ar	
AuOTU27	GU013680.1	*Cupriavidus metallidurans* CH34 [NR074704.1]	98–100	-	Pr; H; T	Mo; A; CLAT; D	+
Au-OTU28	GU013673.1	*Delftia acidovorans* SPH-1 [NR074691.1]	99–100	-	Pr	Mo; A; COT; P	+
AuOTU29	KX033938	*Diaphorobacter* sp. DS3 [JX272921.1]	99	-	L	Mo; A; COT; D/NI; X	
AuOTU30	KX033939–KX033940	*Duganella* sp. BD-a14 [EF575562.1]	94–97	-	F	Mo; A; COT; P	
AuOTU31	KX033941	*Herbaspirillum* sp. Y1 [FJ811966.1]	99	-	L	Mo; A; N2	+
AuOTU32	KX033942–KX033945, GU013677.1	*Hydrogenophaga atypica* BSB 41.8 [NR029023.1]; *Hydrogenophaga* sp. NL121 [AB636293.1]	98–99	-	F; Pr	Mo; A; CLOT; P	
AuOTU33	KX033946–KX033947	*Ideonella* sp. IMCC1722 [DQ664241.1]	97–99	-	F	Mo; A; COT; D	
AuOTU34	KX033948–KX033951	*Pelomonas* sp. AKB2008HA2 [AM989107.1]	98–99	-	C	Mo; A; N2	
γ-Proteobacteria							
Alteromonadales							
Au-OTU35	Shuster *et al.* 2015	*Shewanella* sp. YM-8	99	-	R	Mo; FAA; CHT: P/C	
Oceanospirillales							
Au-OTU36	KX078238	*Halomonas* sp. *BSi20384 [EF673296.1]*	96	-	Pr	Mo; FAA; COT; NR	
Pseudomonadales							
AuOTU37	KX033952–KX033962	*Acinetobacter calcoaceticus* MCMB881 [EU330417.1], *A. johnsonii* EW7[AY880194.1]	97–99	-	Ar; C	A; Ar	
AuOTU38	KX033963	*Enhydrobacter aerosaccus [KF732812.1]*	99	-	C	FAA; CHT	

AuOTU39	KX033965–KX033985	*Pseudomonas aeruginosa* VRF5362 [JX970978.1], *P. baetica* BD34 [LK021072.1], *P. extremaustralis BND*-YA7 [HQ832854.1], *P. putida* Cal [AY962603.1]	97–99	-	C; F; L	Mo; A; COT; D; Ar	+
Xanthomonadales							
Au-OTU40	KX078239	*Lysobacter* sp. YJ15 [JN848797.1]	95	-	Pr	Mo; A	
AuOTU41	KX033986–KX033988, GU013678.1	*Stenotrophomonas maltophilia* DN1.1 [EU034540.1]	96–100	-	Pr; L; C; Ar	Mo; A; COT; S/C; D	+
AuOTU42	KX033989	*Xanthomonas* sp. S21 [EU747699.1]	97	-	F	Mo; OA; COT; S; X	
Unclassified/unknown bacteria showing closest hit in NCBI							
AuOTU43	KX033990	*Aciditerrimonas ferrireducens* IC-180 *[NR_112972]*	88	+	F		
AuOTU44	KX033991	*Acidobacteriaceae bacterium* A2-4c [HQ995662.1]	77–89	+	Ar; L; F		
AuOTU45	KX033992	*Anaeromyxobacter dehalogenans* 2CP-1 [CP001359.1]	82	-	F		
AuOTU46	KX033993	*Chitinophaga* sp. *MJM 38 [KF534707.1]*	92	-	L		
AuOTU49	KX033994–KX033997	*Ferrovum myxofaciens EHS6 [KC155321.1]*	90	-	C		
AuOTU50	KX033998	*Gemmatimonas aurantiaca* H9-0AF4E_11038 [KF228166.1]	86	-	F		
AuOTU52	KX033999–KX034002	*Neisseria* sp. *93S1 [EU370420.1]*	88-89	-	C		
AuOTU56	KX034003–KX034004	*Thermomonas hydrothermalis* O4 [KM596789.1]	85	-	S		
AuOTU57	KX078240–KX078244	*Thiohalobacter thiocyanaticus HRh1* [NR_116699.1]	90–91		Pr		
AuOTU58	KX034005	*Tistrella bauzanensis* strain BZ78 [NR117256.1]	87	-	S		
AuOTU59	KX034006	Micrococcus lylae partial 16S rRNA gene, strain ES-3089h [FN393784.1]	90	-	L		
AuOTU61	KX034007–KX034011	*Betaproteobacterium* TH-N15 [AJ785978.1]	99	-	C; F; T		
AuOTU62	KX034012	*Hydrogenophaga* sp. p3(2011) [HQ652595.1]	92–93	-	F		
AuOTU63	DQ294754.1	Uncultured bacterium clone TG4	87		T		

a Pr – Prophet Mine; H – Hit or Miss Mine; C – Corrego Bom Successo; R – Rio Saldana; T – Tomakin; S – Shantytown; Ar – Arrowtown; F – Platina Deep Lead System; Ad – Adelaide Hills Facer; L – Lively's Find
b (Motility) Mo – motile; (Respiration) A– aerobic, AA– Anaerobic, OA– Obligate Aerobe, OAA– Obligate Anaerobe, FAA– Facultative Anaerobic, ATAA– Aerotolerant anaerobe; (Metabolism), COT– Chemoorganotrophic, PT– Phototrophic, LAT– Lithoautotrophic, CLOT– Chemolithoorganotrophic, CHT– Chemoheterotrophic, CLT– Chemolithotrophic, AT– Autotrophic; (Polyamines) C– Cadaverine, P– Putrescine, S– Spermidine; (N cycle) N2– Nitrogen fixation; NI– Nitrification, D– denitrification

Note: Reprinted from "Bacterial biofilms on gold grains – Implications for geomicrobial transformations of gold," by MA. Rea, C. Zammit and F. Reith, 2014, *FEMS Microbiol. Ecol.*, fiw082.

Rising Au concentrations would select for metal-resistant bacteria with the ability to detoxify Au-complexes. These include *C. metallidurans, D. acidovorans, Stenotrophomonas* sp., *Achromobacter* sp., *Halomonas* sp. and *Herbaspirillum* sp. (Fig. 1.6, Table 1.2). In *C. metallidurans*, Au sorption and uptake leads to the up-regulation and co-utilisation of a range of metal resistance systems involved in Au efflux, precipitation and possible methylation of Au-complexes, ultimately leading to the

biomineralisation of cell-associated nanoparticulate Au (Reith et al. 2009; Wiesemann et al. 2013). Upon contact with mobile Au, *D. acidovorans* produces and excretes Au-specific siderophore, *delftibactin*, which has a metal binding site enabling the detoxification of the Au-complexes extracellularly via Au reduction and formation of Au nanoparticles (Johnston et al. 2013; Wyatt et al. 2014). Thereby larger secondary Au crystals with distinct size distribution patterns are produced (Wyatt et al. 2014). While the defence mechanism against Au-complexes varies between these species, they are highly complementary and enhance the ability of both species and the entire biofilm when they occur together to tolerate/detoxify toxic Au-complexes (Reith et al. 2009; Van Houdt et al. 2009; Johnston et al. 2013; Wiesemann et al. 2013).

Stenotrophomonas maltophilia forms nanoparticulate Au through charge capping by a phosphate group derived from a cofactor NADH and NADH-dependent enzyme (*e.g.*, nitrate reductase; Nangia et al. 2009a, 2009b). The Au-complex is then converted to metallic Au(0) through electron shuttle enzymatic reduction thereby forming Au nanoparticles along the cytoplasmic membrane (Nangia et al. 2009b). The NADH co-factor and nitrate reductase act as a framework to convert toxic Au-complexes to nanoparticulate metallic Au (Nangia et al. 2009b). Gold complexes are transported in *S. maltophilia* cells by membrane-bound ion channels and subject to enzymatic reduction in the cytoplasm (Sastry et al. 2003).

Other bacteria potentially involved in Au-detoxification include α-, β- and γ-Proteobacteria, such as *Sphingomonas* spp. and *Methylobacterium* sp., *Herbaspirillum* sp., *Burkholderia* spp. and *Ideonella* sp., *Acinetobacter* spp., *Pseudomonas* spp. and *Shewanella* sp. (Fig. 1.6; Table 1.2). *Acinetobacter* spp., *Burkholderia* spp. and *Methylobacterium* sp. can degrade a range of cyano-metal complexes using nitrile-degrading enzymes present in extracellular lipid complexes, acting to destabilise/re-precipitate Au/Ag-cyanide complexes (Finnegan et al. 1991; Vu et al. 2013). *Pseudomonas* spp. which thrive in many harsh environments, contain a range of metal-resistance system and can therefore tolerate high concentrations of heavy metal, *e.g.*, As, Cr, Cu, Cd, Hg, Pb and Ni (Teitzel and Parsek 2003). They have the ability to degrade a range of toxic chemicals, *e.g.*, cyanide-containing compounds (Hancock and Brinkman 2002) and have been shown to form Au nanoparticles by extracellular reduction (Husseiny et al. 2007). Metallophilic *Shewanella* sp. are known to reduce toxic heavy metals, metalloids and radionuclides (Bretschger et al. 2007). Bio-flocculants, which bind heavy metals including Au may also be produced by resident bacteria, *e.g.*, *Herbaspirillum* sp. (Lodewyckx et al. 2001).

Finally, some microorganisms may detach from the biofilm into surrounding environments. Production of quorum sensing molecules by *Acinetobacter* spp. (Sarkar and Chakraborty 2008) and the lytic action of *Lysobacter* sp. and *Duganella* sp. (Hiraishi et al. 1997) may aid in the release of these cells (Stoodley et al. 2002) (Fig. 1.6, Table 1.2). At this stage, nano-sized Au from intracellular bio-precipitation may be carried away thereby increasing the mobility of Au in the environment. Gold-complexes and nano/micro-particulate Au are then available for further chemical/physical dispersion, *e.g.*, by solution transport and ingestion by soil macro-organisms grazing on biofilms (Reith et al. 2010). In a recent study on Finnish Au particles, the composition of the biofilm communities resident on the particles was assessed using the 16S rRNA genes (Reith et al. 2018). After processing, >3.9 million reads, 519 different OTUs were recorded. Results on the study on Finnish Au particles demonstrate that placer Au particle transformation and Au dispersion occur in cold, arctic environments and corroborates the existence of biogeochemical Au cycling in present-day cold environments. Similar to sites studied earlier, biofilm communities were dominated by Actinobacteria, Firmicutes and especially Proteobacteria, with β- and γ-Proteobacteria being most abundant (Rea et al. 2016). Among these the *Oxalobacteraceae* and *Comamonadaceae*, which contain a range of known metal-resistant and metallophilic taxa, *e.g.*, *C. metallidurans* and *Ralstonia* spp. as well as *Delftia* sp. and *Variovorax* spp. were highly abundant. These results suggest that highly specialised biofilm communities adapted to Au-toxicity perform key roles in driving the biogeochemical cycling of Au and the biogeochemical transformation of Au particles. Organisms living in Au-rich environments are constantly exposed to harsh environmental conditions, *e.g.*, heavy metal toxicity conferred from mobile Au(I/III)-complexes and Au-deposit associated pathfinder metals, *e.g.*, Ag, Cu, Ni, Cr, As, Pb, Se, Te and W (Reith et al. 2012b). Concentrations of mobile Au and Ag co-occur, and because of their mobility and high toxicity, need to be detoxified; the co-occurrence of a wide range of heavy metal detoxifying organisms and abilities in the biofilms are required to confer protection to the entire biofilm (Reith et al. 2012b; Wiesemann et al. 2017)

Overall, the action of biofilms not only leads to the dispersion of Au in the environment but also to the progressive transformation of primary Au-Ag particles (Fig. 1.5). While Au particles that have only 'recently' been subjected to Earth surface conditions, *e.g.*, Au particles from the Adelaide Hills in South Australia (Fig. 1.5A), are largely composed of primary Au-Ag, increased time and/or intensity of biogeochemical cycling leads to increased transformation, *i.e.*, formation of secondary

'pure' Au rims (Fig. 1.5B–G) and may result in almost entirely transformed Au particles (Fig. 1.5H).

1.5. Effects on biogeochemical gold cycling

The composition of biofilm communities on Au particles from Australia, New Zealand, Colombia and Brazil and more recently Finland Au particles provides insights into the functional abilities (described or putative) of resident bacteria, which may directly or indirectly affect Au (trans)formation and Au mobility in Earth surface environments. Given the mobility of both Au and Ag in these systems, the composition of biofilms on particles is likely driven by metal toxicity. Bacterial consortia living on Au particles from a range of environments have the ability to deal with Au toxicity to gain a selective advantage and thereby actively perpetuate Au particle transformation and environmental Au-cycling. The β-Proteobacteria dominate microbial communities and the aurophilic β-Proteobacterium, *C. metallidurans*, was detected on particles. Sites around the world show that *C. metallidurans* likely plays a key role for Au detoxification and biomineralisation. Overall, biogeochemical Au transformations lead to similar secondary morphotypes observed on particles in different climatic environments.

1.6. Aims, hypotheses and objectives

Understanding the link between microbial communities and Au transformation is essential to further understand the underlying mechanisms in the biogeochemical cycling of Au. The evidence summarised above strongly suggests the influence of microorganisms on Au transformation and ultimately the biogeochemical cycle of Au. However, studies on natural Au particles have not clearly shown the correlation between the biofilm composition and the stages of progressive transformation of placer Au particles. In addition, no comprehensive study has been done to show the links between the stages of Au transformation and the biogeochemical and physical processes. Thus, to address this knowledge gap, this PhD thesis aims to link Au transformation and microbial community composition to biogeochemical influence, physical factors and mineralisation, and assess the influence of microorganisms to the 'kinetics' of Au mobility. To address this aim, specific hypothesis and objectives were formulated as follows.

Hypotheses

1. Transformation of Au particles occurs in temperate environments of the UK, Switzerland and Germany.
2. The progressive transformation of Au influences the changes in microbial community composition.
3. Microbial communities progressively transform Au particles.
4. The distance of Au transport and biogeochemical processes affect the stages of Au transformation.
5. The deposit or mineralisation system influences Au transformation processes.
6. Biofilm communities increase the mobility of gold by biomineralisation combined with biofilm disintegration.
7. Microbial-assisted mobility in the form of Au-nanoparticle and Au-complexes occur in natural Au particles.

To test these hypotheses, the following objectives were set:

1. Examine Au particles from Germany, Switzerland and the UK using microscopy and spectrometry techniques.
2. Evaluate the presence of secondary Au morphotypes and transformation stages on placer Au particles indicative of biogeochemical Au cycling from different sites and assess if biofilms are present on placer Au particles.
3. To utilise next generation sequencing (NGS) technology to assess microbial diversity and biofilm community composition on Au particles from Switzerland, Germany and the UK.
4. To analyse the phylogenetic composition and characterise putative functional capabilities of biofilm communities that are involved in Au transformation.
5. To link biofilm community compositions to transformation stages and assess the transformation stages of placer Au based on physical and (bio)geochemical factors.
6. To compare and contrast the physical and biogeochemical transformations of placer Au particles from epithermal systems *vs.* classical hydrothermal system.
7. To devise a column experiment that uses varying soil material from Australia, microorganisms (*Cupriavidus metallidurans, Corynebacterium glutamicum and Chromobacterium violaceum*) and fine Au particles to study microbial-mediated Au mobility.

8. To investigate the mobility of Au in the column experiment for up to 18 months and assess the contribution and influence of microbial biofilms in the mobility and transformation of Au.
9. To measure the size distribution of Au nanoparticles released from natural Au particles and assess modes of transport of mobile Au through different soil materials.
10. To assess the dispersion of Au in the soil matrix and identify microbial contributions affecting the mobility of Au.
11. To assess the contribution of microorganisms in the mobility of Au in terms of nanoparticle size and concentration, biofilm formation and surface transformations on Au particles using various microscopy and microanalytical techniques.

1.7. Thesis style and layout

This thesis is presented in the form of individual manuscripts that links Au transformation and microbial community composition to biogeochemical influence, physical factors and mineralisation style, and assess the influence of microorganisms on the 'kinetics' of Au mobility using natural Au particles. The manuscripts constituting each chapter are at present published, accepted, or in preparation for publication in peer-reviewed scientific journals. Each manuscript contains the following sections: abstract, introduction, materials and methods, results, discussion and is self-contained work on its own and may be read individually.

Chapter 1 introduces biogeochemical Au cycling and a review of the current research on the transformation of Au particles. It presents current pieces of literature on microbial-mediated transformations of Au in supergene environments and includes details of transformation features together with mobilisation and precipitation processes involved in Au cycle. Parts of this chapter are derived from the published review paper in *FEMS Microbiology Ecology* on biofilms living on Au particles. The review paper assesses the biofilm consortia on natural Au particles/nuggets. It provides insights into functional abilities (described/putative) of microbial communities, especially on the ability of resident bacteria to contribute to the environmental cycling of Au. It also (1) presents a model of Au-biofilm interactions; (2) assesses the link between community composition and site-specific community association; and (3) shows the progressive transformation of Au particles possibly by

bacterial consortia living on Au. This model lays down the framework of the biofilm community composition in Chapters 2–4.

Chapters 2 to 4 present the geomicrobial transformation of Au in Switzerland, Germany and the UK. It presents a detailed description of field sites, analysis of Au particles using scanning electron microscope (SEM) and electron microprobe (EMP) as well as the biomolecular techniques and statistical analyses. Description of Au particle morphology, surface coatings, secondary Au and progressive transformation of Au were linked to microbial communities based on distance of transport, deposit/formation systems, landscape and climate variations and ultimately show the links between the stages of Au transformation to microbial community structure on Au particles. Finally, functional characterisation of biofilm communities on Au particles and its implications to Au particle transformation and Au cycling were discussed. Results of NGS were further analysed for preliminary metagenomic prediction of biofilm communities on Au particles using PICRUSt. This showed the direction of future research on whole genome metagenomic reconstruction of biofilms on Au particles for a complete understanding of the biogeochemical cycling of Au mediated by microorganisms.

Chapter 5 details the contribution of biofilm communities in the mobility of Au in a wide range of soil types inoculated with microorganisms linked to the biomineralisation and biomobilisation of Au (*e.g., C. metallidurans, C. glutamicum and C. violaceum*). This 18-month column experiment provides a close approximation of the uptake and/or mobilisation of Au in natural systems to which a more detailed model may be derived to elucidate the 'kinetics' of Au cycling. This will improve the use of geochemical models to predict Au transport for applications in Au exploration and to advance the understanding of the biogeochemical cycle of Au.

Chapter 6 consolidates the major findings from the chapters, argues how the data aligns with the current models, and discusses how the findings address the overall aims of this thesis. It also provides a perspective on future research direction and applications in Au bioprospecting and biomining technologies.

Note that in all chapters of this thesis, Phylum Proteobacteria and Phylum Firmicutes are mentioned as Class α- β- δ- ε- γ- Proteobacteria and Class Bacilli and Clostridia, respectively. The abbreviation 'sp.' is used for OTUs with singular identified species

and ‘spp.’ for multiple identified species under the same genus level based on the 16S rRNA sequencing result.

Chapter II

Biogeochemical transformation of gold: Progressive biogeochemical transformation of placer gold particles drives compositional changes in associated biofilm communities

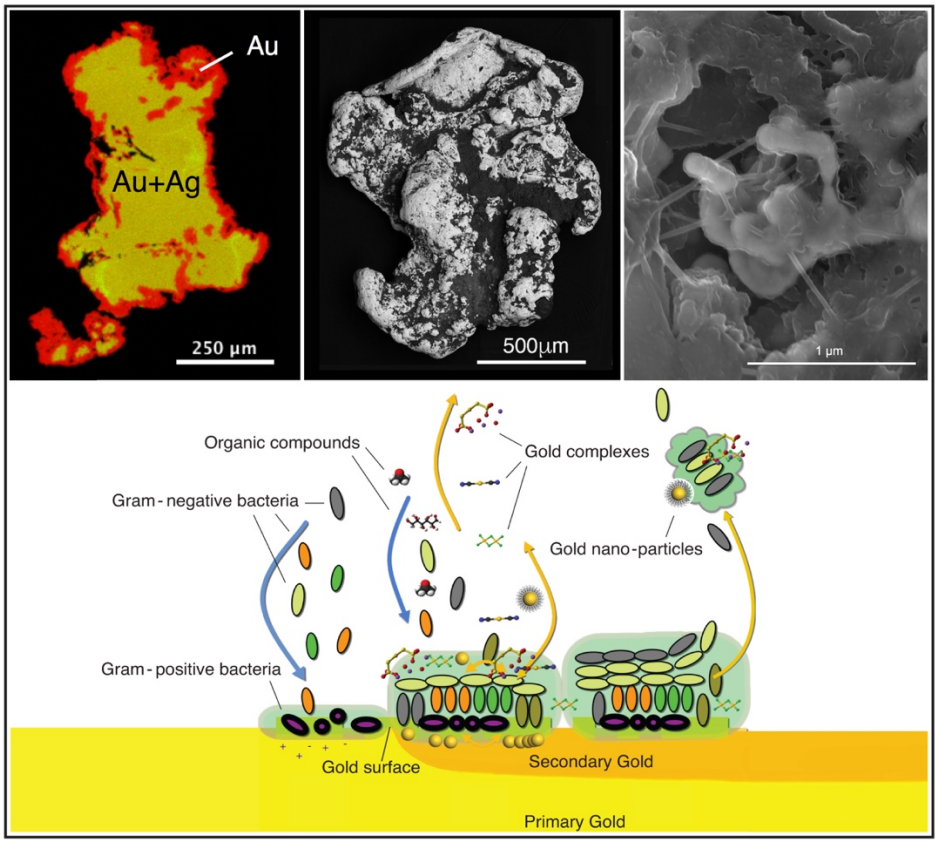

The content of this chapter is the published paper: **Rea MA***, Standish CD, Shuster J, Bissett A, Reith F* (2018) Progressive biogeochemical transformation of placer gold particles drives compositional changes in associated biofilm communities. *FEMS Microbiol. Ecol.* fiy080

Statement of Authorship

Title of Paper	Progressive biogeochemical transformation of placer gold particles drives compositional changes in associated biofilm communities
Publication Status	☑ Published ☐ Accepted for Publication ☐ Submitted for Publication ☐ Unpublished and Unsubmitted w ork w ritten in manuscript style
Publication Details	Rea MA, Standish CD, Shuster J, Bissett A, Reith F (2018) Progressive biogeochemical transformation of placer gold particles drives compositional changes in associated biofilm communities. FEMS Microbiol. Ecol., fiy080

Principal Author

Name of Principal Author (Candidate)	Maria Angelica Rea
Contribution to the Paper	Performed PCR amplification for Illumina Sequencing. Performed final bioinformatic data reprocessing and phylogenetic analysis. Interpreted results. Wrote the manuscript and created the figures. Acted as corresponding author.
Overall percentage (%)	60
Certification:	This paper reports on original research I conducted during the period of my Higher Degree by Research candidature and is not subject to any obligations or contractual agreements with a third party that would constrain its inclusion in this thesis. I am the primary author of this paper.
Signature	Date 15.05.18

Co-Author Contributions

By signing the Statement of Authorship, each author certifies that:

i. the candidate's stated contribution to the publication is accurate (as detailed above);

ii. permission is granted for the candidate in include the publication in the thesis; and

iii. the sum of all co-author contributions is equal to 100% less the candidate's stated contribution.

Name of Co-Author	Dr. Christopher D. Standish
Contribution to the Paper	Collected the samples. Helped in editing the manuscript.
Signature	Date 11/05/2018

Name of Co-Author	Dr. Jeremiah Shuster
Contribution to the Paper	Assisted in data interpretation and analysis. Manuscript evaluation and final editing.
Signature	Date 15/05/2018

Name of Co-Author	Dr. Andrew Bissett		
Contribution to the Paper	Performed bioinformatics data processing. Helped in evaluating and editing the manuscript.		
Signature		Date	14/05/2018

Name of Co-Author	A/Prof. Frank Reith		
Contribution to the Paper	Collected the samples and conceived the study design. Supervised the development of work. Constructed figures. Manuscript evaluation and editing and acted as corresponding author.		
Signature		Date	17/05/2018

Chapter 2: Biogeochemical transformation of gold in the UK

PROGRESSIVE BIOGEOCHEMICAL TRANSFORMATION OF PLACER GOLD PARTICLES DRIVES COMPOSITIONAL CHANGES IN ASSOCIATED BIOFILM COMMUNITIES

In Chapter I, the published review paper summarised the current knowledge concerning the composition and functional capabilities of biofilm communities on Au particles and identified putative contributions of key species involved in Au-cycling. In this chapter, we explore the links between Au particle transformation and (bio)geochemical processes to microbial community composition.

Research highlights

- Biogeochemical transformation of gold occurs on gold particles from the UK
- Microbial communities with putative traits that aids in Au transformation are present on placer gold particles
- The stages of gold transformation impose selective pressure on the microbial community composition
- A more specialised biofilm community involved in overcoming metal-toxicity develops as the degree of Au transformation increases

2.1. Abstract

Biofilms on placer gold (Au)-particle surfaces drive Au solubilisation and reconcentration thereby progressively transforming the particles. Gold solubilisation induces Au-toxicity; however, Au-detoxifying community members ameliorates Au-toxicity by precipitating soluble Au to metallic Au. We hypothesise that Au-dissolution and reconcentration (precipitation) places selective pressures on associated microbial communities, leading to compositional changes and subsequent Au particle transformation. We analysed Au particles from nine United Kingdom sites using next generation sequencing, electron microscopy and micro-analyses. Gold particles contained biofilms composed of prokaryotic cells and extracellular polymeric substances intermixed with (bio)minerals. Across all sites communities were dominated by Proteobacteria (689, 97 % Operational Taxonomic Units, 59.3 % of

total reads), with β-Proteobacteria being the most abundant. A wide range of Au-morphotypes including nanoparticles, microcrystals, sheet-like Au and secondary rims, indicated that dissolution and re-precipitation occurred, and from this transformation indices were calculated. Multivariate statistical analyses showed a significant relationship between the extent of Au particle transformation and biofilm community composition, with putative metal-resistant Au-cycling taxa linked to progressive Au transformation. These included the genera *Pseudomonas, Leptothrix* and *Acinetobacter.* Additionally, putative exoelectrogenic genera *Rhodoferax* and *Geobacter* were highly abundant. In conclusion, biogeochemical Au-cycling and Au particle transformation occurred at all sites and exerted a strong influence on biofilm community composition.

2.2. Introduction

Gold (Au) biogeochemical cycling involves Au solubilisation and re-concentration/precipitation processes which contribute to the transformation of placer Au particles (commonly known as Au grains and nuggets). These processes are mediated, in part, by biofilms occurring on the surface of Au particles (Southam et al. 2009; Reith et al. 2013). It has been demonstrated that Au solubilisation can occur in the presence of reactive Mn-oxide minerals such as birnessite. This mineral, in the presence of a Au-complexing ligand, is capable of oxidizing Au(0) and Au(I) to Au(III)-complexes (Ta et al. 2014, 2015). Many microbes produce Au-complexing ligands, *e.g.*, organic acids, thiosulphate and cyanide, that stabilise Au in solution (Reith et al. 2007; Fairbrother et al. 2009; Shuster et al. 2014). These Au(I/III) complexes are highly cytotoxic as they exert oxidative stress in a similar manner as Ag(I)- and Hg(II)-compounds (Nies 1999). Some bacteria, from biofilms on placer Au particle surfaces, have developed biochemical responses to cope with Au toxicity by reducing Au(I/III) complexes resulting in the formation of Au(0) nanoparticles (Checa et al. 2007; Reith et al. 2009; Johnston et al. 2013; Wiesemann et al. 2013, 2017). These Au nanoparticles exhibit a range of morphologies including triangular, spherical, hexagonal and octahedral crystals, and structures that are bacteriomorphic, sheet-like and wire-like. Primary Au particles often contain cores comprised of both Au and Ag; this Au-Ag alloy composition is indicative of the particles' (high temperature) origin. Accumulation of secondary Au structures on the outer surface of primary Au particles can lead to the formation of pure, *i.e.*, >99 wt. %, Au rims (Reith et al. 2010, 2013; Shuster et al. 2015). The Au-enriched rims can range from a few micrometres to several hundred micrometres in thickness. Typically, they contain a nano- and

microcrystalline fabric and are attributed, in part, to biogeochemical Au/Ag dissolution and Au re-precipitation processes that occur under near-surface conditions (*e.g.*, Fairbrother et al. 2012; Reith et al. 2012a; Shuster et al. 2017a; Stewart et al. 2017). The extent to which these processes influence the formation of these rims depends on environmental conditions since accretionary and detrital processes can produce similar morphotypes (Groen et al. 1990; McCready et al. 2003; Fairbrother et al. 2012; Reith et al. 2012a; Craw and Lilly 2016; Stewart et al. 2017).

Biofilms are known to adapt when exposed to elevated concentrations of heavy metals (*e.g.*, Golby et al. 2014; Koechler et al. 2015). In the context of metal resistance adaptation on a field scale, microbial communities within soils overlying Au-bearing deposits have been shown to have assemblages that are significantly different to that of communities from soils that are distal from deposits (Reith et al. 2012b, 2015; Wakelin et al. 2012). Microbial communities above deposits were enriched in functional genes that enabled heavy metal detoxification; furthermore, the greater enrichment of these genes corresponded with Au deposits that experienced prolonged periods of weathering (Reith et al. 2012b, 2015). Changes in biofilm compositions have also been observed on a localised scale, *i.e.*, on Au particle surfaces. In the study by Rea et al. (2016), microorganisms directly occurring on the surface of Australian, New Zealand and Brazilian placer Au particles were classified into six functional groups based on a range of operational taxonomic units (OTUs). Group one includes organisms such as *Arthrobacter* spp. and *Staphylococcus* spp. that are important for Au particle surface conditioning, microbial attachment and biofilm establishment. Group two taxa contribute to the production of extracellular polymeric substances (EPS) and auto-aggregation and include *Pseudomonas* spp. and *Rhodobacter* spp. Group three microbes affect nutrient cycling, *i.e.*, C and N cycling, and include *Sphingobium* sp., *Corynebacterium* sp. *and Acidovorax* spp. Microorganisms capable of metabolizing complex and xenobiotic organics and toxins, *e.g.*, *Acinetobacter* spp., *Burkholderia* spp. and *Phenylobacterium* spp., were assigned to group four. In group five, microorganisms capable of directly affecting Au biogeochemical cycling were identified. These include putative Au mobilisers, *e.g.*, the sulphur-oxidizing bacterium *Diaphorobacter sp.* and *Methylobacterium* spp. Other species, such as *Pseudomonas* spp., *C. metallidurans, D. acidovorans, Stenotrophomonas* sp. and *Achromobacter* spp., have the ability to actively detoxify Au-complexes *via* biomineralisation (Rea et al. 2016; Reith et al. 2018). Dispersal cells are formed by species that comprise group six, including *Lysobacter* sp. and *Duganella* sp.

Studies by Brugger et al. (2013) and Etschmann et al. (2016) have demonstrated a biogeochemical link between bacterial community composition from Au and Pt particles and the mobility of these metals in natural environments. However, a study assessing biofilm composition and development in relation to Au particle transformation has not yet been conducted and is the aim of this study. In doing so, this study uses Au particles to: (i) characterise secondary Au structures, (ii) evaluate the degree of Au particle transformation, (iii) determine the presence of biofilms, and (iv) analyse the phylogenetic composition and functional capabilities of biofilm communities.

2.3. Materials and methods

2.3.1. Description of field sites and sampling

Primary Au deposits are widespread across the United Kingdom (UK) and Au mining activity predates Roman arrival on the British Isles. Peak exploitation of Au deposits occurred between *ca.* 1860 and 1910, where >3.5 t of Au was recovered (Colman 2010). Most primary deposits in the UK are hosted in Proterozoic to Permian aged rocks. Of the primary Au deposits, orogenic deposit-types are most abundant; however, porphyry, epithermal and unconformity-related redox deposit-types also exist (Gunn and Styles 2002). Physical weathering of these primary deposits results in the formation of secondary deposits such as eluvial and alluvial placer deposits containing primary Au particles that have been transformed by a range of physical and (bio)geochemical processes (Fairbrother et al. 2012; Reith et al. 2012a, 2013).

For this study, Au particles were collected from eight placer sites that were proximal, *i.e.*, within 300 m, to primary deposits located in southern England and Scotland (Table 2.1; Colman 2010). Samples of Au particles were obtained using a field sterile method described by Reith et al. (2010) to minimise contamination and to preserve the integrity of the biofilm communities. See Table 2.1 for detailed descriptions of site location, deposit-style and environmental settings.

2.3.2. Electron microscopy and microanalyses

Samples were washed with a sterile saline solution (0.9 wt. % NaCl) and placed in fixative (4 wt. % paraformaldehyde, 1.25 wt. % glutaraldehyde in PBS, 4 wt. % sucrose, pH 7.2) for at least 24 hours. These fixed Au particles were dehydrated using series of ethanol washes (70, 90 and 2 x 100 vol. %; 10 min each concentration), placed in 100 wt. % hexamethyldisilazane and air dried in the method described by Fratesi et al. (2004). The samples were carbon-coated and analysed using an FEI Quanta™

Table 2.1 – Summary of geological and environmental conditions at sampling localities in the United Kingdom.

Sample name/site	Coordinates	Annual Rainfall [mm]	Mean Annual Temperature [° C] (MetOffice, 2015)	Host geology and primary mineralisation (Colman, 2000; Gunn and Styles, 2002)	Placer type and distance of transport (from nearest primary mineralisation)
Northern Scotland					
Ghanmain (GH; 1), Connonish	N56° 29.372' W4° 47 687'	402	10.9	Orogenic, hypogene source; quartz-sulphide vein Dalradian mudstone	Colluvial/ Alluvial <300m
Eastern Scotland					
Ochill Hills (OHS/OHB; 2)	N56° 14.362' W3° 37 608'	976	10.9	Low sulphidation epithermal mineralisation; andesitic lavas and pyroclastic rocks intruded by dioritic body and phorphyry dikes.	Eluvial/Alluvial <300m
Snails Cleuch, Bothwell Hill (LMH; 3), near Duns, Scotland	N55° 51.804' W2° 32 280'	707	10.4	Unconformity-related; conglomeratic intermontane basin-fill overlane by red sandstones; Silurian turbiditic greywackes;	Alluvial >300m*
Western Scotland					
Glengonnar (GDO; 4), Leadhills	N55° 28.870' W3° 42.101'	900	10.9	Slate belt hosted orogenic vein deposit in the Lower Paleozoic bedrocks, mainly late Ordovician sandstones of the Portpatrick Formation	Alluvial <300m
Mannock Water (MW; 6), Leadhills	N55° 21.452' W3° 51.963'	1721	10.9		Alluvial <300m
Snarwater (SN; 5), Leadhills	N55° 24.883' W3° 45 655'	1311	10.4	Sedimentary breccia; sampling locality is within glacial debris	Alluvial <300m
South Western England					
Brownstone (BS; 7), Devon	N50° 19.551' W3° 58 693'	1007	10.4	Unconformity-related, overlying Permian rocks that had been removed by erosion; zone of carbonate veining, brecciation and oxidation within a sequence of Lower Devonian slates.	Alluvial <300m*
Whympston (WY; 8), Devon	N50° 20.386' W3° 52 873'	1007	10.4	Unconformity related; oxidised Lower Devonian mafic volcanic horizon;	Alluvial <300m*

Reference:
MetOffice (2015) UK climate Summaries 2014 Annual, accessed at http://www.metoffice.gov.uk/climate/uk/summaries/2014/annual.

450 Field Emission Gun Scanning Electron Microscope (FEG-SEM) with Energy Dispersive Spectrometers (EDS) (FEI, Netherlands). Images were taken in Secondary Electron (SE) and Backscattered Electron (BSE) modes using 5 kV and 20 kV, respectively. Selected Au particles were further analysed using an FEI Helios NanoLab DualBeam Focus Ion Beam (FIB)-SEM (FEI, Netherlands). Surface features were characterised in SE and BSE mode using 2 and 20 kV, respectively. An ion beam of 20 kV and 9.7 pA was used for FIB-milling micrometre-size cross-sections made on the surface of Au particles. The FIB-SEM is equipped with energy dispersive X-ray (EDX) spectrometry that was used to collect spectra/maps across the particles surfaces and FIB-milled sections. Elements that were mapped included Au, Ag, Fe, C, N, O, Si, Ti, Al, Ga, Mg, Na, K and Pt.

A total of 28 Au particles were embedded in epoxy resin and polished with 1 μm-size diamond paste to make cross-sections of entire Au particles. These polished cross-sections were analysed using a Cameca™ SXFive Electron Microprobe, operating at 20 kV and 200 nA, (Cameca, France) was equipped with five wavelength dispersive X-Ray detectors. The Au particles were analysed for the following elements with detection limits given in wt. %: Au (0.24 wt. %), Ag (0.09 wt. %), S (0.025 wt. %), Fe (0.06 wt. %) and Cu (0.11 wt. %). These elements were calibrated using chalcopyrite (Cu, Fe and S), telluride (Ag) and pure Au metal standards purchased from Astimex or P&H. The software produces a full quantitative pixel by pixel calculation by using the Mean Atomic Number background correction (Donovan and Tingle, 1996) in CalcImage, and false colorisation and formatting in Surfer10™ to produce net intensity, detection limit and totals image maps.

To estimate the extent of Au particle transformation, electron microprobe analysis (EMPA) maps were processed using Image J v.1.50g (National Institutes of Health, USA; Abràmoff et al. 2004; Rasband 2012). This analysis was performed by converting Au-Ag EMPA maps into binary images and calculating pixel by pixel ratios, *i.e.*, a ratio of transformed secondary Au to untransformed primary Au. This transformation factor (TF) was calculated for each Au particle and the following TF stages were assigned: A (≤ 10 %), B (11–20 %), C (21–30 %), D (31–40 %). These four TF stages were used as a basis for the statistical analyses described below.

2.3.3. Biomolecular and statistical analyses

Additional Au particles were collected and used for microanalyses and DNA analyses. Biofilm communities from Au particles were assessed using nested 16S rRNA polymerase chain reaction (PCR) combined with next generation sequencing (NGS) using the Illumina MiSeq platform – TruSeq SBS v.3 600 cycle using 300 bp paired end sequencing (Reith et al. 2010; Bissett et al. 2016). The universal primers 27F (Lane 1991) and 1492R (Osborn et al. 2000) were used for initial PCR amplification of 16s rRNA genes (Reith et al. 2010). Further amplification using primers 27F and 519R (Lane et al. 1985; Lane 1991) and sequencing at the Australian Genome Research Facility (AGRF, Melbourne, Australia) was performed. DNA amplifications were performed in an Applied Biosystems Veriti™ Thermal Cycler (Applied Biosystems, California, USA). Amplicons were checked in 1.5 % agarose gel with Gel Red (Biotium Inc., Hayward, CA, USA) 1:10,000 (v/v) and run at a constant voltage of 80 V for 1 h. Procedures for sequencing, open OTU picking and assignment are detailed in Bissett et al. (2016). Briefly, sequence read quality was visually assessed using FastQC

(Andrews 2010). Sequences were trimmed to remove poor quality bases and merged using FLASH (Magoč and Salzberg, 2011). Sequences <400 bp or containing N or homopolymer runs of >8 bp were removed (MOTHUR v1.34.1; Schloss et al. 2009). Remaining sequences were submitted to open reference OTU picking at 97 % sequence similarity using UPARSE (Edgar 2013) and OTU abundance tables constructed by mapping all reads to the OTUs (usearch_global, 97 %). Sequences were deposited in GenBank with accession numbers MG373505–MG373528.

Multivariate statistical analyses were conducted using the PRIMER-6 software package with the PERMANOVA+ add-on (Clarke and Warwick 2001; Anderson et al. 2008). Similarity matrices were established on the fourth root transformed abundance data using the Bray-Curtis method (Bray and Curtis 1957). PERMANOVA analyses were conducted using partial sums of squares on 9999 permutations of residuals under a full model. Non-metrical multidimensional scaling (nMDS) and canonical analysis of principal coordinates (CAP) was used to assess the community differences between progressively transformed Au particles. Vector overlays, based on Pearson correlations, were used to explore relationships between significant individual variables and taxa and the ordination axes. CAP analyses were conducted based on the respective resemblance matrices with the significance of test effects determined against null distributions based on 9999 permutations (random allocations) of samples. SIMPER analysis was used to assess groups/phyla that discriminate between transformation stages. Maximum-likelihood (1000 bootstrap replicates) phylogenetic trees were constructed using GENEIOUS 11.0.2 (Biomatters Ltd., New Zealand). Functional assignment of OTUs to the six groups representing the different stages of biofilm development was conducted based on the classification developed by Rea et al. (2016), wherein groupings are based on the dominant functional abilities of each organism.

2.4. Results

2.4.1. Morphology and composition of gold particles and particle surfaces

All Au particles ranged from 0.1 to 2 mm in size (Fig. 2.1; Table 2.1) and demonstrated a range of morphologies including angular, hackly, slightly rounded and wiry shapes. Some sites contained Au particles that were elongated and refolded (Fig. 2.1D–H; Table 2.1). The surface of Au particles demonstrated a range of articulation, *e.g.*, rounded to sub-rounded, scratched and abraded surfaces, which can

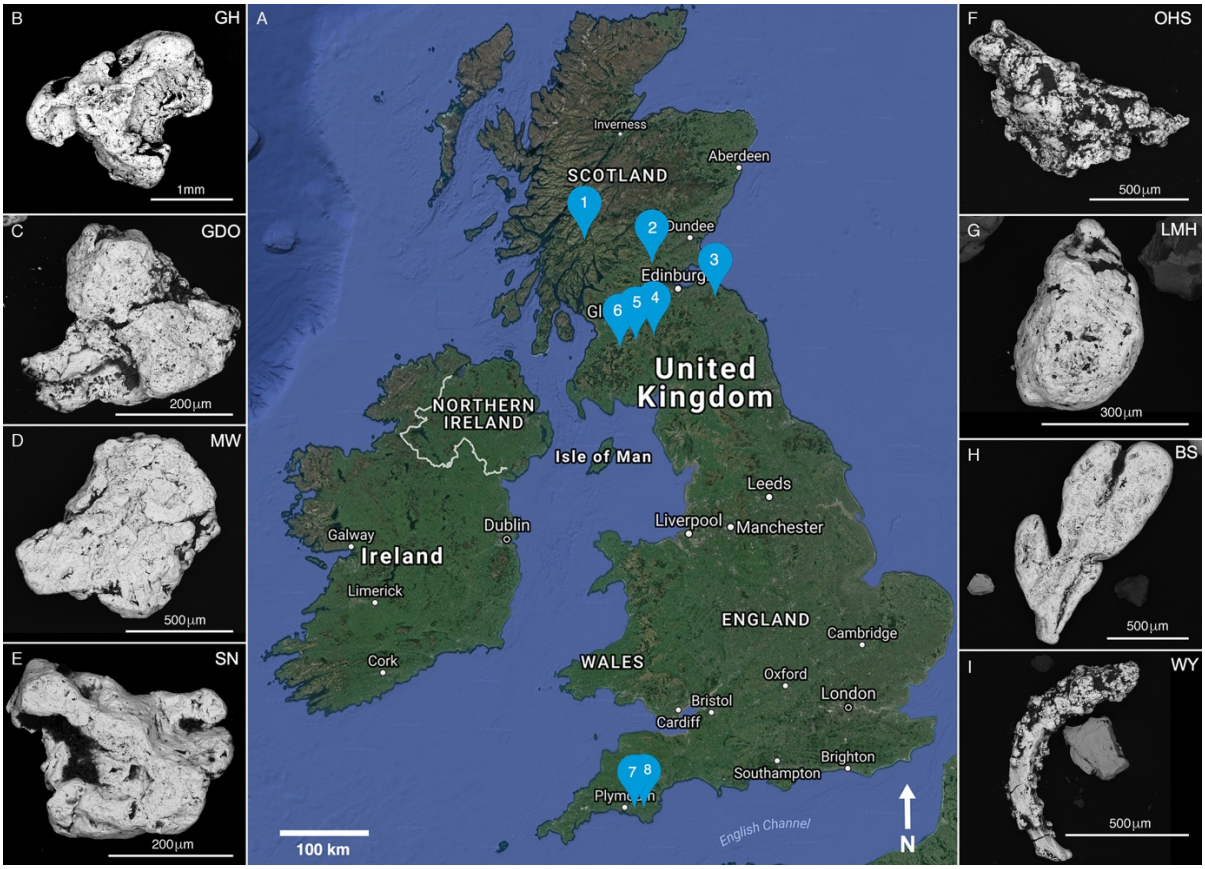

Figure 2.1 **(A)** Sampling locations in the United Kingdom and **(B–I)** Backscattered Electron (BSE) micrographs of representative Au particle morphologies. Gold particles appeared angular (*i.e.*, B from 1–GH), slightly rounded (*i.e.*, C from 4–GDO, E from SN–5), irregular (*i.e.*, F from 2–OHS, H from 7–BS and I from 8–WY), well rounded (*i.e.*, G from 3–LMH) and flattened (*i.e.*, D from 6–MW).

be attributed to physical processes of Au particles during transport from the primary source (Townley et al. 2003). The surface of Au particles contained crevices (Fig. 2.2A) that contained polymorphic layers primarily composed of bacterial cells (Fig. 2.2B), EPS (Fig. 2.2C) and Fe-oxides, clays, silicate minerals inferred from EDS analysis (Fig. 2.2D). These polymorphic layers were more than 20 μm thick. In some regions, EPS appeared to be in direct contact with Au particle surfaces (Fig. 2.2E). Individual prokaryotic cells appeared attached directly on the Au particle surface (Fig. 2.2F). Evidence of biogeochemical transformations were common on all Au particles. This included features of irregular pitting on the Au particle surface and is attributed to Ag and Au dissolution (Fig. 2.3). These dissolution features were often in close proximity to secondary Au structures (Fig. 2.4A) as well as appearing embedded within Fe-oxides, clays and silicate minerals (Fig. 2.4B). Gold nanoparticles occurred as triangular, hexagonal and polygonal shapes (Fig. 2.4C).

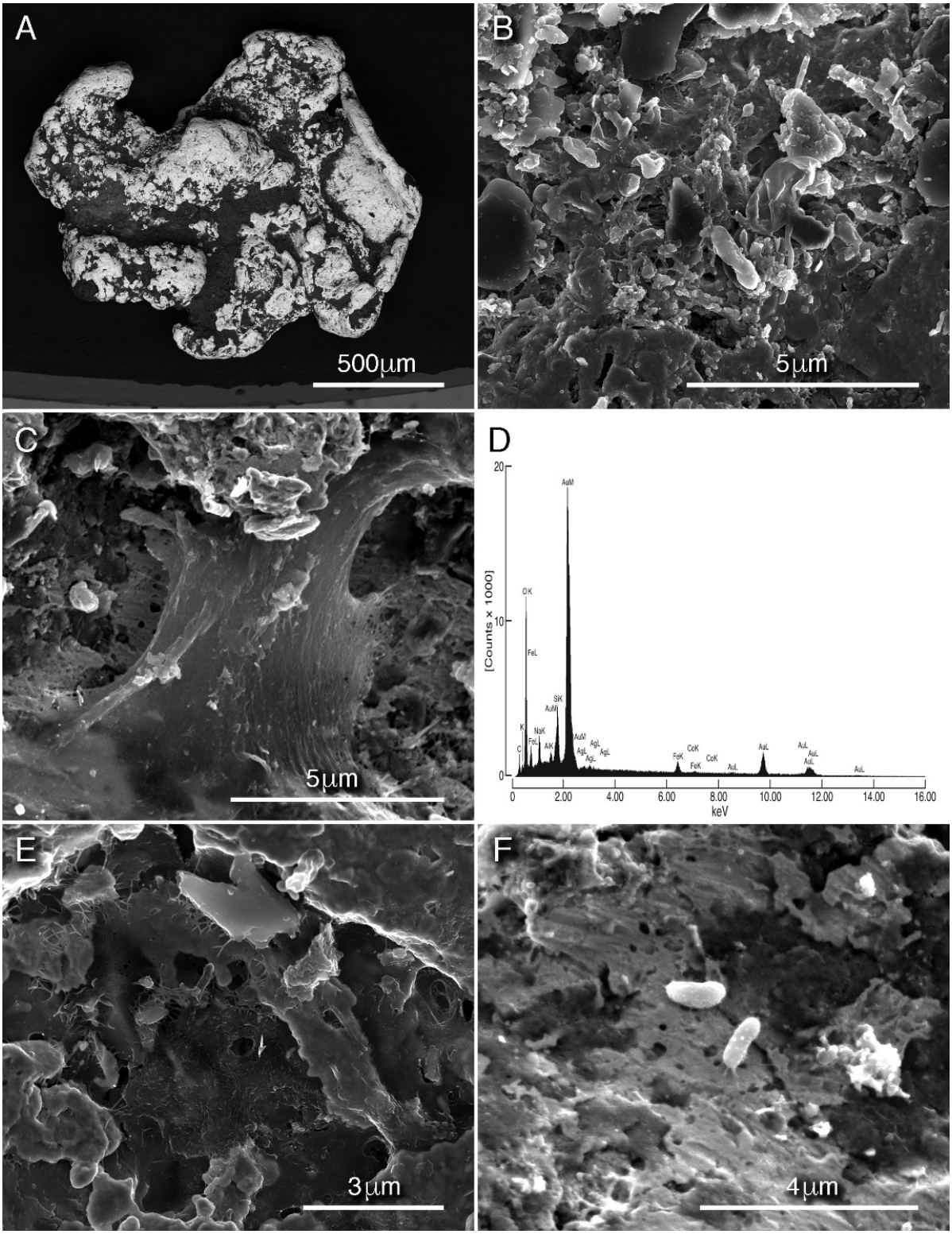

Figure 2.2 Electron micrographs of polymorphic layers on Au particle surfaces. (**A**) A Backscattered Electron (BSE) micrograph of a representative Au particle containing crevices filled with a polymorphic layer. (**B–F**) Secondary Electron (SE) micrographs of remnant cells and EPS. (**D**) A representative spectrum of the elemental composition of Fe-oxide and silicate minerals. (**E, F**) SE micrograph of EPS and microbial cells in direct contact with the Au surface.

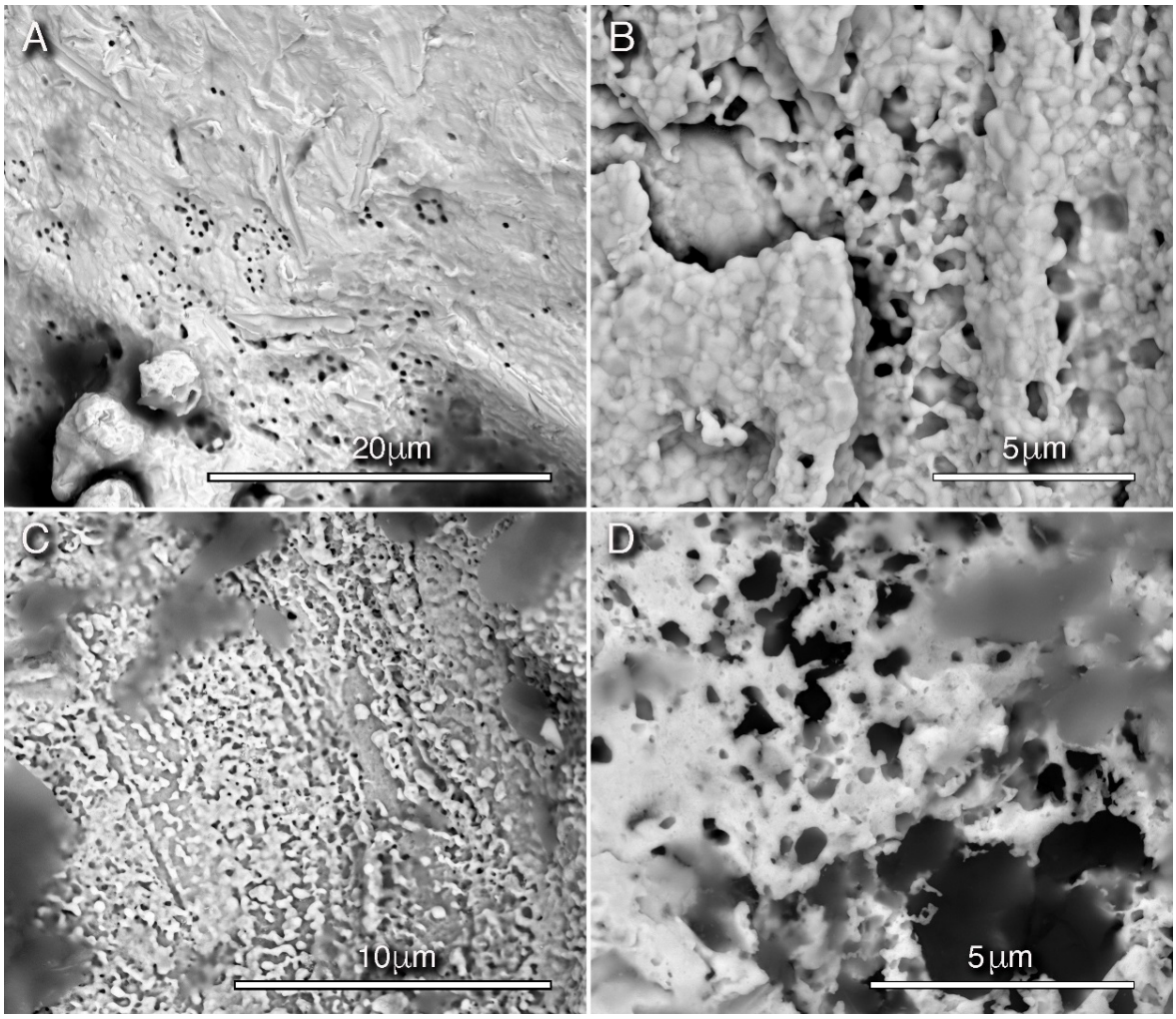

Figure 2.3 **(A)** A BSE micrograph of a Au particle surface. The pitted surface represents initial stages of Au/Ag dissolution. **(B–D)** BSE micrographs demonstrating progressive Au/Ag dissolution of Au particle surfaces leading to more irregular-size pitting and increased roughness of the Au particle surface; during this process Au and Ag are mobilised and released into the environment.

Aggregates of these Au nanoparticles and other secondary Au structures, *i.e.*, bacteriform Au and crystals, appeared to form bridging-like structures that covered the Au particle surface (Fig. 2.4D). Regions of polymorphic layers contained abundant EPS and an abundance of aggregated Au nanoparticles as well as micrometre-size Au structures (Fig. 2.5A–D).

Microprobe analysis confirmed that Au particles contained Au-Ag alloy in the core and Au-rich rim on the outer edge of the Au particle. These rims were up to 100 μm in thickness and show progressive transformation of a typical Au-Ag alloy (Fig. 2.6A) to Au-rich rim (99.9 wt. % Au) (Fig. 2.6). The extent of particle transformation that was assigned based on the binary image of the Au-Ag maps generally shows that Au particles from the same site displayed similar transformation stages.

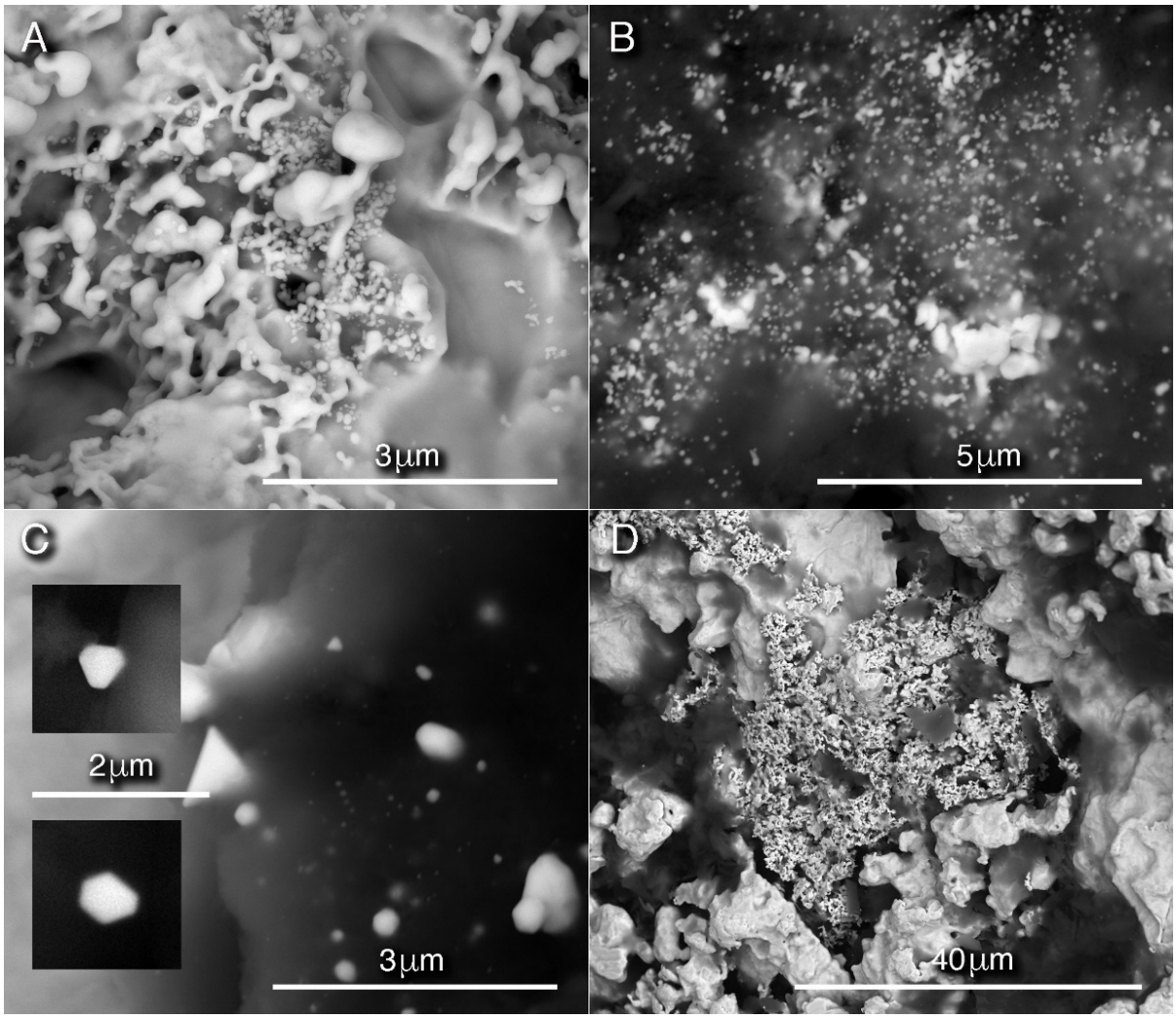

Figure 2.4 (**A, B**) BSE micrographs of Au nanoparticles in close association with Au/Ag dissolution features and embedded within clay minerals, respectively. (**C** and **inset**) BSE micrographs of Au nanoparticles associated with a polymorphic layer. These Au nanoparticles appeared triangular, hexagonal and polygonal in shape. (**D**) A BSE micrograph of aggregated Au nanoparticles covering the surface of a primary Au particle.

The assigned transformation for Au particles from sampling location Ghanmain (GH), Ochill Hills (OHB/OHS), Mannock (MW) and Brownstone (BS) is TF group A, Snarwater (SN) is group B, Whympston (WY) and Glengonnar (GDO) is group C and Snails Cleuch Lammermuir Hills (LMH) is group D (Table 2.2).

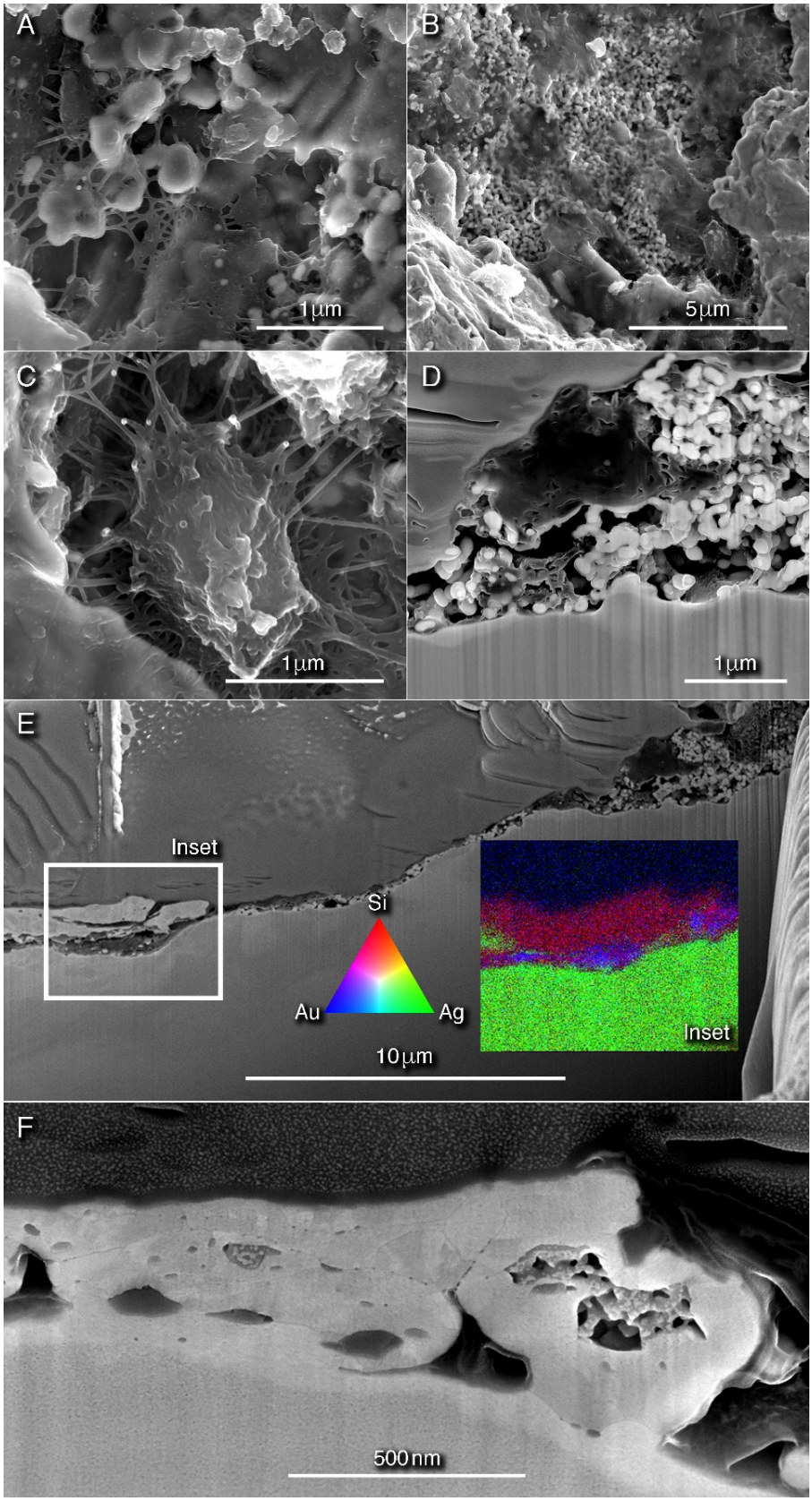

Figure 2.5 Micrographs of Au nano and μ-crystals (**A–C**) SE micrographs of Au nanoparticles and other secondary Au structure in close association with EPS. **(D)** An SE micrograph of a FIB-milled cross-section showing Au aggregates of Au nanoparticles covered by a polymorphic layer. **(E, F)** An SE micrograph of a FIB-milled cross-section demonstrating a Au-enriched structure on the surface of a primary Au-Ag particle. This structure contains a nano-crystalline fabric.

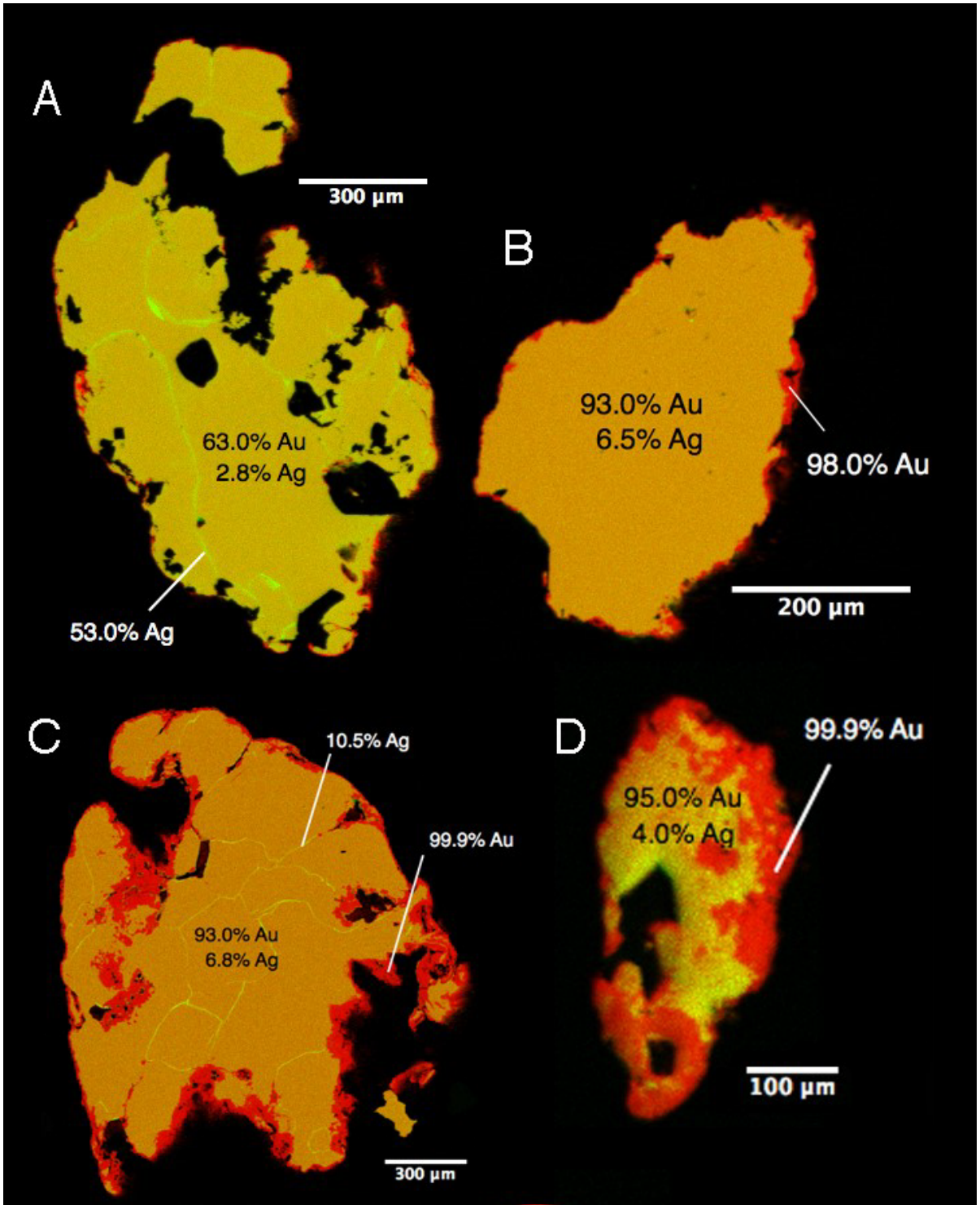

Figure 2.6 A series of representative EMPA maps of cross sections through Au particles demonstrating progressive transformation of Au particles. Gold is represented by the colour red while Ag represented by the colour green. (**A**) A Au particle from TF stage A (*i.e.*, ≤10 % transformation), (**B**) A Au particle from TF stage B (*i.e.*, 11–20 % transformation), (**C**) A Au particle from TF stage C (*i.e.*, 21–30 % transformation) and (**D**) A Au particle from TF stage D (*i.e.*, 31–40 % transformation).

Table 2.2 - Results of quantitative electron microprobe analyses (EMPA) showing the pixel by pixel counts of Au particles rims and cores and their corresponding transformation factor assignment.

Label	Whole Area Counts	Rim Counts	% Transformed	Mean of % Transformed	Degree of Transformation*
GH Grain1	70650	7490	10.6	7.3	A
GH Grain2	113460	4299	3.8		
GH Grain3	62393	5769	9.2		
GHn Grain4	65192	3650	5.6		
OHB Grain1	12908	1213	9.4	8.4	A
OHB Grain2	37441	2396	6.4		
OHB Grain3	13009	1528	11.7		
OHB Grain4	5124	309	6.0		
MW Grain1	75827	5906	7.8	8.4	A
MW Grain2	29124	2646	9.1		
BS Grain1	31802	1685	5.3	8.7	A
BS Grain2	26009	3165	12.2		
OHS Grain1	135314	10926	8.1	8.8	A
OHS Grain2	121341	20474	16.9		
OHS Grain3	107941	5706	5.3		
OHS Grain4	74045	3822	5.2		
SN Grain1	38459	5238	13.6	13.4	B
SN Grain2	115393	20108	17.4		
SN Grain3	53345	8979	16.8		
SN Grain4	116075	6847	5.9		
WY2 Grain1	15381	3644	23.7	21.8	C
WY2 Grain2	7668	1530	20.0		
GDO Grain1	94794	16131	17.0	23.9	C
GDO Grain2	101671	22348	22.0		
GDO Grain3	85334	19930	23.4		
GDO Grain4	80839	26907	33.3		
LMH Grain1	11786	4207	35.7	39.9	D
LMH Grain2	23384	11563	44.0		

Legend:
***A ≤10.0 %; B 11.0 – 20.0 %; C 21.0 % – 30.0 %; D 31.0 40.0 %**

2.4.2. Assessment of biofilm communities

The 16S rRNA gene was amplified to assess the composition of biofilm communities on the particles. More than 90 % of Au particles were positive for target amplicons with greater than 2.3 million reads from 55 selected Au particles. Across all sites, 1610 different OTUs were detected, ranging from 85 at GH to 486 at LMH (Table 2.3). At the phylum level, Proteobacteria comprised the highest number of detected OTUs (39.9 %; Fig. 2.7A) and more than half of the total sequence reads (59.3 %; Fig. 2.7B). Within the Proteobacteria, β-Proteobacteria dominated with 270 OTUs and 29.6 % of total reads. δ-Proteobacteria were numerous with 166 detected OTUs, which made up 11.0 % of total reads; α- and γ-Proteobacteria with 124 and 104 detected OTUs, respectively, made up 3.2 % and 7.6 % of total reads and ε-Proteobacteria with 11 OTUs, made up of 7.6 % of total reads (Fig. 2.7; Table 2.3). The phyla Acidobacteria and Bacteroidetes were also abundant with 246 and 255 OTUs, making up 7.9 % and 9.9 % of total reads, respectively. Other detected phyla included: Planctomycetes (7.9 and 3.0 %, OTUs and reads), Verrucomicrobia (7.9 and 1.1 %,) and 1.0–6.8 % for Firmicutes, Cyanobacteria, Nitrospirae and 22 other rarer phyla (Table 2.3). Across all sites, six OTUs classified from three genera were detected on all particles; these were *Rhodoferax* spp., *Geobacter* spp. and *Pseudomonas* spp., respectively (Fig. 2.8A). Eighteen OTUs were detected on 70 % of the site (Fig. 2.8A; Table 2.4). CAP analyses of *Rhodoferax* spp. and *Geobacter* spp., (Fig. 2.8B, C) in relation to transformation factors shows no significant grouping for *Rhodoferax* with transformation grade; with *Geobacter* spp. forming distinct clusters with transformation grade. Non-metric MDS ordination of community assemblages showed a wide variety of communities associated with grains from TF A sites, with more distinct clustering in TF C and D.

PERMANOVA showed that community composition varied with site ($\sqrt{CV} = 33.77$; $P < 0.001$) and degree of transformation ($\sqrt{CV} = 21.92$; $P < 0.001$). CAP analyses of community data illustrate the significant links of bacterial communities from Au particles with the transformation stages and biofilm group classification ($P < 0.001$; Fig. 2.9). Based on their assigned biofilm groups, organism known as surface coloniser under group one is *Terribacillus* sp., also has the highest reads on Au particles from the UK. OTUs assigned to group two can produce abundant EPS such as *Aeromonas* sp. and *Arcobacter* sp. In group three are organisms known to take part in nutrient cycling including *Geothrix* sp., *Nitrospira* sp. and *Sulfuricurvum* sp.

Table 2.3 – Composition of bacterial communities associated with Au particles from the nine study sites in the United Kingdom.

Classification (Phylum/Class)	BS 7	GDO 4	GH 1	LMH 3	MW 6	OHB 2	OHS 2	SN 5	WY 8	Total (different OTUs)
Proteobacteria										
α-Proteobacteria	16	22	3	33	17	9	34	21	25	124
β-Proteobacteria	47	118	25	96	52	38	57	74	95	270
δ-Proteobacteria	26	54	24	39	35	11	18	33	27	166
ε-Proteobacteria	5	4	1	1	2	3	n.d.	n.d.	3	11
γ-Proteobacteria	24	16	7	28	17	8	30	14	42	104
TA18	2	n.d.	n.d.	1	n.d.	n.d.	2	n.d.	2	7
Proteobacteria_UC	3	n.d.	n.d.	1	n.d.	n.d.	2	1	2	7
Firmicutes										
Bacilli	3	1	n.d.	2	n.d.	n.d.	2	n.d.	2	8
Clostridia	10	7	3	1	4	n.d.	2	n.d.	10	28
Erysipelotrichi	1	n.d.	n.d.	n.d.	n.d.	n.d.	n.d.	n.d.	n.d.	1
[Thermi]	n.d.	n.d.	n.d.	n.d.	n.d.	n.d.	n.d.	n.d.	1	1
Acidobacteria	16	73	13	89	22	15	69	63	40	246
Actinobacteria	2	4	n.d.	4	n.d.	n.d.	2	4	1	14
Armatimonadetes	n.d.	1	n.d.	2	2	1	n.d.	1	2	9
Bacteroidetes	21	42	n.d.	83	23	16	60	38	83	255
BRC1	n.d.	n.d.	n.d.	1	n.d.	n.d.	n.d.	n.d.	1	2
Chlorobi	1	8	1	9	1	n.d.	6	6	2	24
Chloroflexi	2	1	2	7	1	n.d.	8	5	4	22
Cyanobacteria	n.d.	1	n.d.	11	n.d.	n.d.	1	n.d.	5	15
Elusimicrobia	n.d.	2	n.d.	3	n.d.	n.d.	n.d.	1	n.d.	5
FBP	n.d.	n.d.	n.d.	1	n.d.	n.d.	n.d.	n.d.	n.d.	1
FCPU426	n.d.	1	n.d.	n.d.	2	n.d.	n.d.	n.d.	n.d.	2
Fibrobacteres	n.d.	n.d.	n.d.	n.d.	2	n.d.	n.d.	n.d.	n.d.	2
Gemmatimonadetes	1	3	n.d.	2	2	n.d.	5	6	3	19
GN02	4	2	n.d.	1	n.d.	n.d.	n.d.	n.d.	n.d.	6
GOUTA4	n.d.	n.d.	n.d.	2	n.d.	n.d.	n.d.	n.d.	1	3
NC10	n.d.	n.d.	1	n.d.	n.d.	n.d.	n.d.	n.d.	1	2
Nitrospirae	3	5	1	6	1	1	8	8	4	21
NKB19	n.d.	n.d.	n.d.	1	n.d.	n.d.	n.d.	n.d.	n.d.	1
OP11	1	n.d.	n.d.	n.d.	n.d.	n.d.	n.d.	n.d.	2	3
OP3	n.d.	n.d.	n.d.	2	1	n.d.	n.d.	1	1	5
Planctomycetes	7	13	n.d.	33	13	4	37	24	28	127
SBR1093	n.d.	n.d.	1	n.d.	n.d.	n.d.	n.d.	n.d.	n.d.	1
Spirochaetes	n.d.	n.d.	n.d.	2	2	n.d.	n.d.	n.d.	n.d.	4
TM6	1	4	n.d.	n.d.	n.d.	1	n.d.	n.d.	3	9
TM7	n.d.	3	n.d.	1	n.d.	n.d.	n.d.	1	3	8
Verrucomicrobia	4	7	2	23	4	4	15	11	10	64
WPS-2	n.d.	n.d.	n.d.	n.d.	n.d.	n.d.	n.d.	n.d.	1	1
WS3	2	1	n.d.	1	n.d.	n.d.	2	3	1	10
WS5	n.d.	1	1	n.d.	n.d.	n.d.	n.d.	n.d.	n.d.	2
Total	202	394	85	486	203	111	360	315	405	1610

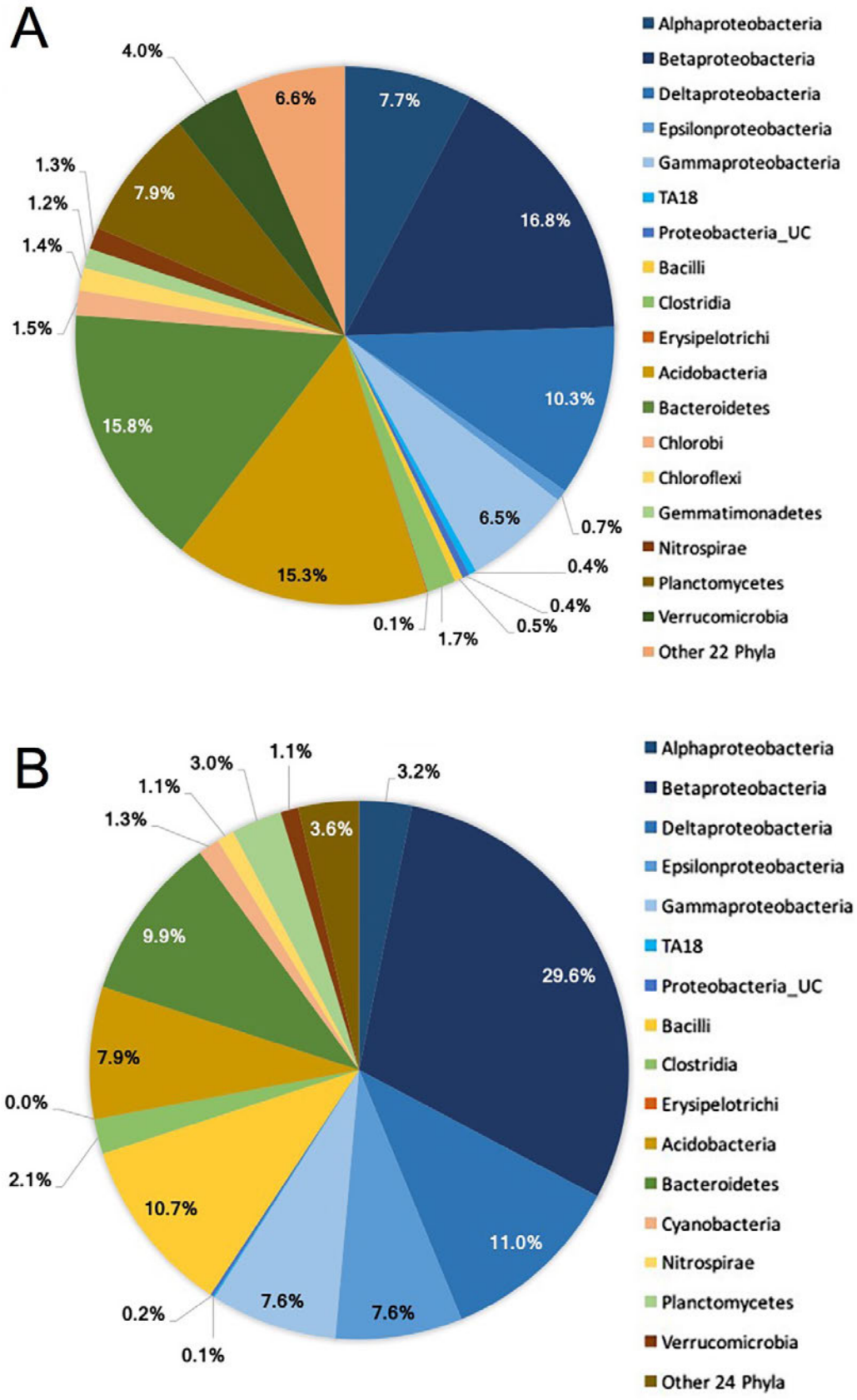

Figure 2.7 Composition of bacterial communities from Au particles. Distribution of dominant bacterial phyla/classes based on **(A)** number of OTUs (1610) and **(B)** OTU reads (>2.3 million). Note: classes are shown for Proteobacteria and Firmicutes.

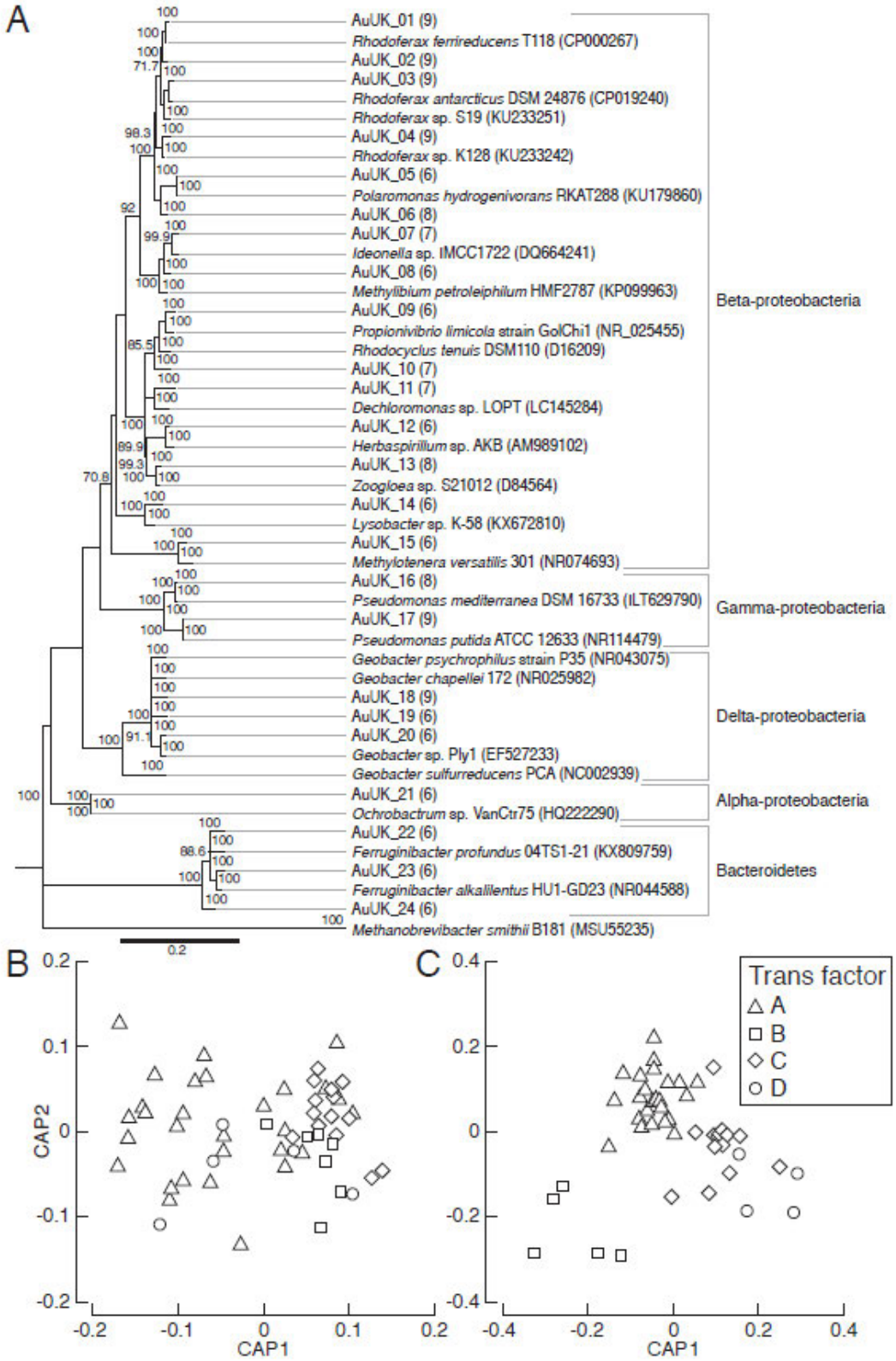

Figure 2.8 **(A)** A neighbour-joining phylogenetic tree of representative 16S rRNA sequences taxa present on particles from 70 % of the sites. Percentages of 1000 bootstrap values < 70 % are not shown. *Methanobrevibacter smithii* was used as the out-group. The first two canonical axes produced by CAP analyses of **(B)** OTUs in the genus *Rhodoferax* and **(C)** *Geobacter* taxa analysed for differences in community assemblages in relation to the grade of transformation (TF A to TF D).

Table 2.4 – Description of OTUs detected on particles from 70 % of the sites.

Clone	GenBank AccessionNo.	Specimen Voucher	Closest relative in NCBI hit/accession nr.	%ID
AuUK_01	MG373505	AuUK11296d	*Rhodoferax ferrireducens* T118 (CP000267)	99.2
AuUK_02	MG373506	AuUK603d	*Rhodoferax ferrireducens* T118 (CP000267)	99.2
AuUK_03	MG373507	AuUK24709a	*Rhodoferax antarcticus* DSM 24876 (CP019240)	99.0
AuUK_04	MG373508	AuUK149140a	*Rhodoferax* sp. K128 (KU233242)	98.4
AuUK_05	MG373509	AuUK1484b	Polaromonas hydrogenivorans	99.4
AuUK_06	MG373510	AuUK5685a	*Polaromonas hydrogenivorans* RKAT288 (KU179860)	97.0
AuUK_07	MG373511	AuUK1070a	*Ideonella* sp. IMCC1722 (DQ664241)	97.7
AuUK_08	MG373512	AuUK3161d	*Methylibium petroleiphilum* HMF2787 (KP099963)	98.4
AuUK_09	MG373513	AuUK57874a	*Propionivibrio limicola* strain GolChi1 (NR_025455)	98.5
AuUK_10	MG373514	AuUK1001d	*Rhodocyclus tenuis* DSM110 (D16209)	97.3
AuUK_11	MG373515	AuUK814d	*Dechloromonas* sp. LOPT (LC145284)	97.0
AuUK_12	MG373516	AuUK61d	*Herbaspirillum* sp. AKB (AM989102)	99.2
AuUK_13	MG373517	AuUK726a	*Zoogloea* sp. S21012 (D84564)	98.8
AuUK_14	MG373518	AuUK14583a	*Lysobacter* sp. K-58 (KX672810)	98.1
AuUK_15	MG373519	AuUK2979a	*Methylotenera versatilis* 301 (NR074693)	98.1
AuUK_16	MG373520	AuUK196a	*Pseudomonas mediterranea* DSM 16733 (ILT629790)	100.0
AuUK_17	MG373521	AuUK366b	*Pseudomonas putida* ATCC 12633 (NR114479)	98.7
AuUK_18	MG373522	AuUK979d	*Geobacter* sp. Ply1 (EF527233)	98.7
AuUK_19	MG373523	AuUK612d	*Geobacter psychrophilus* strain P35 (NR043075)	98.8
AuUK_20	MG373524	AuUK3262d	*Geobacter* sp. Ply1 (EF527233)	98.1
AuUK_21	MG373525	AuUK32958a	*Ochrobactrum* sp. VanCtr75 (HQ222290)	99.8
AuUK_22	MG373526	AuUK5040a	*Ferruginibacter profundus* 04TS1-21 (KX809759)	99.2
AuUK_23	MG373527	AuUK5388d	*Ferruginibacter alkalilentus* HU1-GD23 (NR044588)	98.9
AuUK_24	MG373528	AuUK550a	*Ferruginibacter profundus* 04TS1-21 (KX809759)	98.0

Organisms detected that can perform metabolic turnover of complex and xenobiotic organics and toxins under group 4 included *Flavobacterium* sp., *Paucibacter* sp. and *Polaromonas* sp. Group five contains organisms that are involved in heavy metal cycling and metal detoxification, such as *Geobacter* spp., *Leptothrix* sp., *Pseudomonas* spp. and *Rhodoferax* spp. Organisms forming dispersal cells are included in group six, *e.g.*, *Lysobacter* sp. (Fig. 2.10).

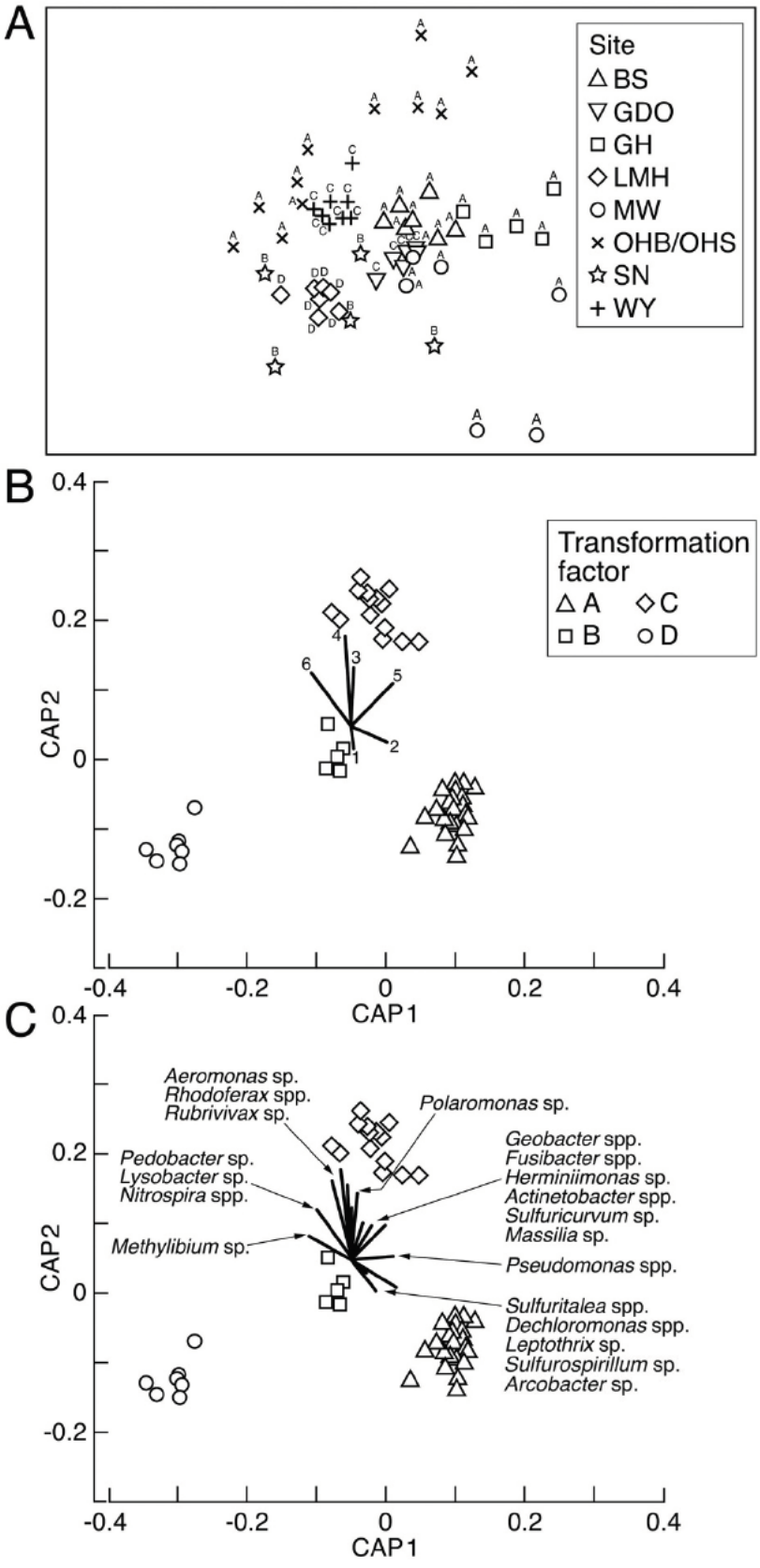

Figure 2.9 **(A)** A non-metric, multidimensional scaling plot displaying increasing similarities of microbial communities with increasing transformation grade. **(B, C)** The first two canonical axes produced by CAP analyses based on individual taxa analysed for differences in community assemblages in relation to the grade of transformation (TF A to TF D); vectors of Pearson's correlations **(B)** of assigned biofilm groups 1–6 and **(C)** of taxa with highest % contribution based on SIMPER analysis overlain.

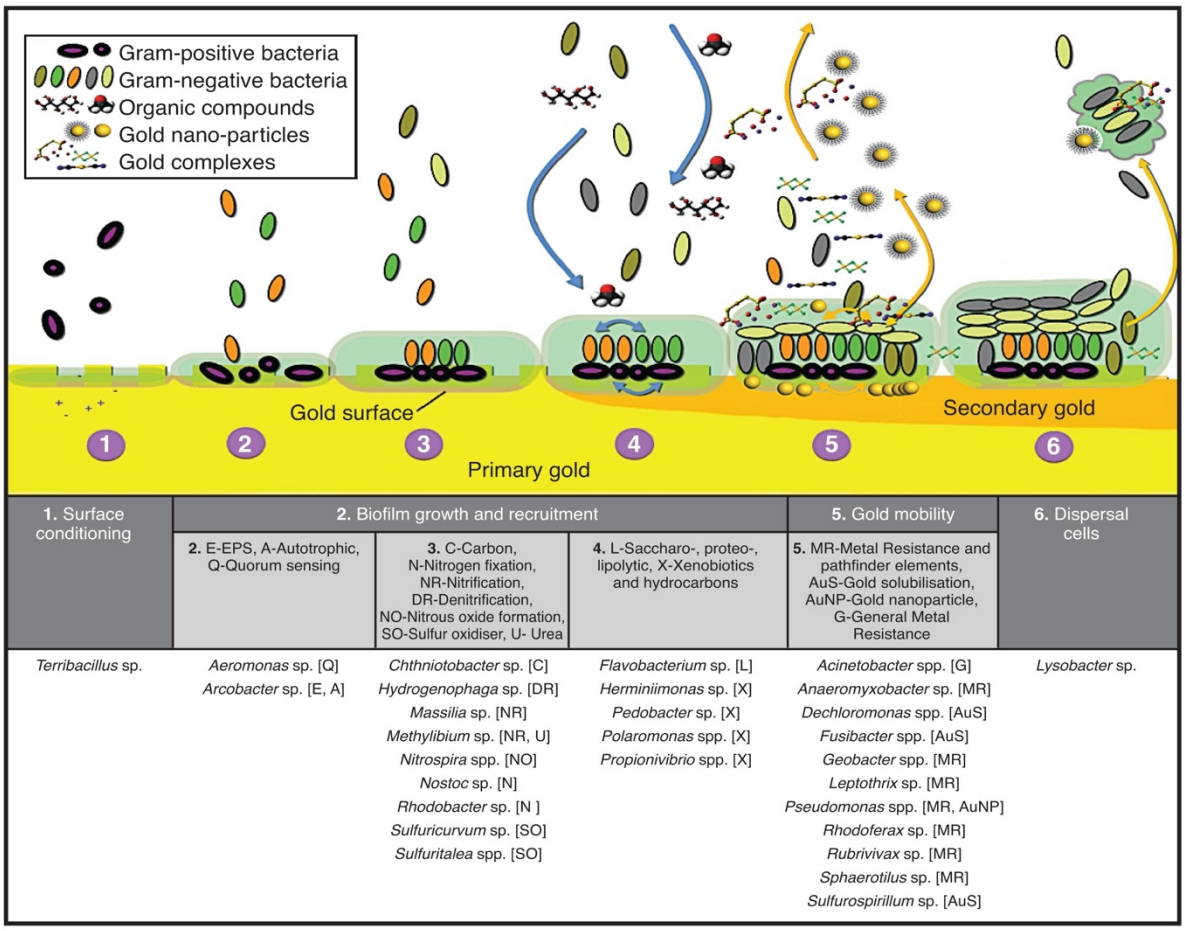

1. Surface conditioning	2. Biofilm growth and recruitment			5. Gold mobility	6. Dispersal cells
	2. E-EPS, A-Autotrophic, Q-Quorum sensing	3. C-Carbon, N-Nitrogen fixation, NR-Nitrification, DR-Denitrification, NO-Nitrous oxide formation, SO-Sulfur oxidiser, U- Urea	4. L-Saccharo-, proteo-, lipolytic, X-Xenobiotics and hydrocarbons	5. MR-Metal Resistance and pathfinder elements, AuS-Gold solubilisation, AuNP-Gold nanoparticle, G-General Metal Resistance	
Terribacillus sp.	*Aeromonas* sp. [Q] *Arcobacter* sp. [E, A]	*Chthniotobacter* sp. [C] *Hydrogenophaga* sp. [DR] *Massilia* sp. [NR] *Methylibium* sp. [NR, U] *Nitrospira* spp. [NO] *Nostoc* sp. [N] *Rhodobacter* sp. [N] *Sulfuricurvum* sp. [SO] *Sulfuritalea* spp. [SO]	*Flavobacterium* sp. [L] *Herminiimonas* sp. [X] *Pedobacter* sp. [X] *Polaromonas* spp. [X] *Propionivibrio* spp. [X]	*Acinetobacter* spp. [G] *Anaeromyxobacter* sp. [MR] *Dechloromonas* spp. [AuS] *Fusibacter* spp. [AuS] *Geobacter* spp. [MR] *Leptothrix* sp. [MR] *Pseudomonas* spp. [MR, AuNP] *Rhodoferax* sp. [MR] *Rubrivivax* sp. [MR] *Sphaerotilus* sp. [MR] *Sulfurospirillum* sp. [AuS]	*Lysobacter* sp.

Figure 2.10 Schematic model and putative functional traits of biofilms on Au particles from the United Kingdom (modified after Rea et al. 2016): (1) conditioning of surfaces to their attachment; (2) the recruitment of photo- and heterotrophic bacteria; (3–4) the proliferation and growth of the biofilm community including heterotrophic species; (5) the mobilisation, detoxification, re-precipitation and utilisation of Au by metallophilic species; and (6) the seeding of dispersal cells with release of nanoparticle and Au-complexes. Functional assignment of OTUs to the six groups are listed in their corresponding columns.

2.5. Discussion

The morphology and extent of transformation of Au particles in this study were similar to those observed on Au particles from different climatic environments from Australia, New Zealand, Finland and South America (Reith and McPhail 2006, 2007; Falconer and Craw 2009; Reith et al. 2010, 2012a, 2018; Shuster et al. 2015, 2017a; Craw and Lilly 2016). These features are the result of mechanical reshaping due to physical factors combined with bio(geo)chemical Au/Ag dissolution and re-precipitation processes occurring under surficial environmental conditions. The presence of polymorphic layers, composed of microbial cells, EPS, clays and other minerals, *e.g.*, Fe-oxides and sulphides, fosters the sorption, embedding and accumulation of Au nano- and micro-particles (Fig. 2.4B, C; Reith et al. 2010; Reith and Cornelis 2017). Aggregations and spongy-form overgrowths of Au nano- and micro-

particles (Fig. 2.4D, 2.5), with their intricate shapes, have likely formed *in situ*, as they would not survive transport as reported in studies from New Zealand (Reith et al. 2012a, 2018; Craw et al. 2017). The presence of EPS, particularly around the spheroidal and chained Au precipitates (Fig 2.5A–C), supports the suggestion of a strong bio-organic influence on secondary Au formation, accumulation and aggregation at the UK sites. Subsequently, nano- and micro-crystalline layers are formed, which are indicative of a link of active dissolution/re-precipitation processes and physical re-crystallisation reactions on grain boundaries (Falconer and Craw 2009). Striated textures within concavities (Fig 2.5A) are possibly relics of Au-Ag dissolution associated with active sulphur cycling (Shuster et al. 2017b). Overall particle shapes, including rounding, folding and scratches are often the results of physical transport in a sedimentary placer environment.

Biofilms are a ubiquitous part of bacterial life and documented on many natural, biological and anthropogenic surfaces (Hall-Stoodley et al. 2004), including placer Au particles from Australia, New Zealand and South America, where commonly 10 to 30 OTUs have been reported to comprise the multispecies biofilms covering the Au particles (Reith et al. 2006, 2010; Shuster et al. 2015; Rea et al. 2016). Far higher numbers of OTUs ranging from 85 at GH to 486 at LMH on each site were detected on Au particles in this study. The difference in the number of detected OTUs is likely a result of the improved resolution of NGS compared to the older PCR-DGGE-Sanger-sequencing technique used in earlier studies. This is supported by the results of another study using NGS with Au particles from 10 adjacent sites from Finland where 519 different OTUs were detected on placer Au (Reith et al. 2018). The higher number of OTUs detected on the UK *vs.* Finnish particles may be linked to the closer spatial relationship of the Finnish sampling sites, which were located within a radius of 50 km, compared to the more widely dispersed UK sites. However, they may also be linked to the presence of extracellular DNA (eDNA) associated with the abundant clay-organic material on the surface of UK Au particles. eDNA can represent a relevant fraction of total DNA and thus a significant portion of the entire soil metagenome (Nielsen and Matz 2006; Carini et al. 2017). Particularly rich in eDNA are clay- and organic matter-rich materials from semi-aquatic environments (Ogram et al. 1988; Cai et al. 2006a; Pietramellara et al. 2009), such as the polymorphic layers of grains collected from active fluvial placers in the UK. The polymorphic layers may serve as eDNA-sinks and thereby provide a record of organisms associated with Au particles throughout their transformation history, given that biofilms are continuously evolving. Indeed, throughout its development different organisms with

diverse metabolic capabilities are recruited to multispecies biofilms, so that the biofilm community can divide the functional traits amongst various groups of organisms (Alvarez et al. 1998; Cai et al. 2006b; Harrison et al. 2007).

Studies of multispecies biofilms have shown that exposure to toxic heavy metals can negatively or positively affect the functional relationships within biofilm communities (Koechler et al. 2015). For example, multispecies biofilms grown from Canadian oil sands were highly resistant to toxic heavy metals, induced biomineralisation of metals and compositionally changed little after exposure to heavy metals compared to unstressed controls (Golby et al. 2014). This suggests that resistance to metals in biofilms is induced in the short term through activation of resistance mechanisms within the existing biofilm species and not by changes to their species composition. Studies of placer Au particles from Australia and Finland have shown that depending on the environmental conditions, transformation stages similar to those observed at UK samples can be achieved within decades to ten millennia of biogeochemical transformation under Earth surface conditions (Shuster et al. 2017a; Reith et al. 2018). Within these time frames, which also may apply to highly transformed particles collected in the UK, changes to community compositions appear to occur. This is confirmed by the results of another Australian study, which showed that in soils formed from Aeolian sediments that had been transported less than 10,000 years ago to a position overlying a polymetallic deposit, microbial communities showed strong species-level differences compared to adjacent background soils (Reith et al. 2015).

The extensive library of detected organisms from present and/or past iterations of biofilms on the particles from the UK allows a more in-depth study of the link between progressive Au particle transformation and the biofilm composition and functional capabilities, compared to earlier studies, where these links were implied based on the presence of multi-metal resistant bacteria (Reith et al. 2006, 2010). Canonical analysis of principal coordinates has shown a significant link of community composition to the grade of secondary Au particle transformation at the UK sites (Fig. 2.9B). Gold particles that were TF stage A, *i.e.*, ≤10 % transformed, are likely at an early stage of recruitment which requires microbial communities capable of establishing a biofilm that is increasingly resilient to metal toxicity from transforming particles, especially Au and Ag toxicity. Both metals are mobilised from the primary Au-Ag alloys of the particle core, but whereas Au is re-precipitated largely *via* biomineralisation, Ag is lost to the environment, where it can form secondary Ag-containing minerals (Shuster et al. 2017b). To establish a biofilm, organisms from the

immediate environment of the Au particle are recruited leading to communities that initially differ strongly between different sites, as shown in this study (Fig. 2.9A). Organisms linked to this stage of transformation are *Arcobacter* sp. and *Sulfurospirillum* sp. of group two and three, as well as *Sulfuritalea* spp., *Leptothrix* sp. and *Dechloromonas* spp., of group five, respectively (Fig. 2.9C). *Arcobacter* sp., a gram-negative ε-Proteobacteria, can set the framework of the biofilm community by hyperproduction of EPS to form polymeric bridges and promote flocculation (Mueller 2015). Polysaccharide-mediated aggregation of EPS and polymers can increase water retention, water being essential to the growing biofilm (Hall-Stoodley et al. 2004). *Sulfurospirillum* sp. contribute to the S cycle and can produce H_2S as ligand that can leach Au by the formation of Au-complexes (Shuster and Southam 2015). Organisms strongly involved in S, P and N cycling are often less resistant to metal stress since microbial energy is primarily used for various enzymatic activities (Azarbad et al. 2016). Thus, we also expected recruitment of biofilm members that can reduce the stress occurring at an early transformation stage of Au particles. These can be achieved by members of the biofilm group five, *Leptothrix* sp., an Fe-oxidizing organism and *Dechloromonas* spp., a facultative anaerobe that uses a heavy metal efflux pump, which can strengthen the biofilm by horizontal gene transfer of inherent genes to other compatible members of the biofilm community (Hall-Stoodley et al. 2004; Harrison et al. 2007).

A more metal-resistant biofilm community evolves as the degree of Au transformation increases and as a result biofilm communities become increasingly similar between sites (Fig. 2.9). This is likely due to an increase in metal toxicity from elevated concentration of mobilised Au and Ag and other pathfinders mobilised from the transforming primary Au particles and Au bearing minerals. Organisms belonging to the metallophilic group five linked to 21–30 % transformation will have the most profound effect on metal detoxification and Au-mobility: *Pseudomonas* spp., *Fusibacter* spp., *Acinetobacter* spp., *Rubrivivax* sp., as well as the exoelectrogens *Rhodoferax* spp. and *Geobacter* spp. *Pseudomonas* spp. are gram-negative, ubiquitous, often heavy metal resistant γ-Proteobacteria, which have now been detected on Au particles from the UK (this study), as well as Brazil and Australia, where they have been shown to dominate communities on particles from some sites (Rea et al. 2016). *Pseudomonas* spp., *e.g.*, *P. aeruginosa*, *P. putida* and *P. plecoglossicida,* are known for their ability to form biofilms and be able to resist up to 600 times higher heavy metal concentrations compared to planktonic cells (Teitzel and Parsek 2003; Meliani and Bensoltane 2016). Gold accumulation in exopolymeric substances played a role in the

detoxification of Au(III)-chloride by *P. aeruginosa*, which displayed a four times higher viability when grown as a biofilm compared to free planktonic cells when subjected to 0.1 mM Au(III)-chloride (Karthikeyan and Beveridge 2002). *Pseudomonas* spp. can produce metabolic products or chelating compounds that may solubilise metals from clays and organic matter minerals (Mueller 2015).

Also detected on Au particles from all sites in the UK were members of the putative exoelectrogenic genera *Geobacter* spp. and *Rhodoferax* spp., which can act as initial colonisers on metallic or solid substrates due to their innate affinity to metals (Dopson et al. 2016). *Geobacter* spp., an anaerobic δ-Proteobacteria, can pass electrons from organic compounds and clays to Fe-oxides and metal surfaces using nanowires to release and harvest electrons (Richter et al. 2008). *Rhodoferax* spp., purple non-sulphur phototrophic β-Proteobacteria, can form persistent biofilm layers on surfaces and oxidise glucose to produce electricity (Chaudhuri and Lovley 2003). Both exoelectrogenic genera can use suitable mineral inclusions, biofilm biomass and most likely Au surfaces to precipitate Au and perform electron "dumping" on the surface for use by other microorganisms (Lloyd et al. 2003; Richter et al. 2008). The process of electron "dumping" is mediated by cytochromes, Fe/S-proteins, by direct electron transfer *via* nanowires or indirect transfer using soluble redox shuttles such as humic acid or inorganic S and H_2S (Reguera et al. 2005; Liu et al. 2014). Microbial-assisted production of electrons directly from organic matter and solid mineral surfaces is beneficial for the microorganisms to extract energy, remove recalcitrant compounds and drive their microbial metabolism and possibly drive the metabolic activity of the whole biofilm community (Nevin et al. 2011; Dopson et al. 2016). Electric signals produced by exoelectrogens mimics the quorum sensing molecule to communicate and attract other organisms (Humphries et al. 2017). The projected electrical signals attract distant cells of similar or an entirely unrelated species, to recruit into the growing biofilm community (Prindle et al. 2015; Humphries et al. 2017; Liu et al. 2017). Apparently, multi-layer biofilms can use this 'electric potential' to communicate more effectively; where inner cells can send electric signals to outer cells of the biofilm more efficiently than using quorum sensing molecules (Liu et al. 2017). This means that recruitment of several other microorganisms that form compounds which react with Au particles can be mediated by these exoelectrogens. For instance, recruitment of SRBs and SOBs, *e.g.*, *Sulfuricurvum* sp. and *Fusibacter* spp., both linked to TF stage C, can produce derivatives of sulphur that contribute to Au mobility, as well as other metallophiles capable of Au detoxification *via* biomineralisation. Recruitment of aerobic organisms such as *Acinetobacter* spp., *Methylibium* sp. and *Nitrospira* spp.

provide the conditions that promote survival of anaerobic members such as *Fusibacter* spp., *Sulfuricurvum* sp. and *Sulfuritalea* spp. The survival of anaerobic bacteria under aerobic conditions is enabled because the aerobes consume the oxygen and thus provide anaerobic conditions in the deeper layers of the biofilm (Elias and Banin 2012). Copper-resistant organisms detected on Au particles from the UK, *e.g.*, the facultative photoheterotrophic β-Proteobacteria *Rubrivivax* sp., may synergistically detoxify Cu-ions and Au-complexes to protect the general population present on the biofilm community (Azzouzi et al. 2013). Resistance to one specific metal may provide cross-resistance or co-tolerance to other metals; the co-tolerance increases the resistance to one stressor as a result of an earlier exposure to a similar stressor, as recently shown for *C. metallidurans* CH34, an aurophilic aerobic β-Proteobacterium detected on Au particles from Australia and Brazil. *Cupriavidus metallidurans* can reduce toxic Au(I/III)-complexes in the periplasm *via* synergistic co-utilisation and regulation of Cu/Au resistance determinants by the metal chaperone *CupC* and the periplasmic Cu-oxidase *CopA* (Wiesemann et al. 2013, 2017; Zammit et al. 2016; Bütof et al. 2018).

However, biofilm mediated Au transformation may not occur effectively without the 'helpers' in the biofilm community other than those under groups two, three and four. These organisms keep the biofilm community functioning and are protected from metal toxicity through the activity of the group five organisms, which can detoxify heavy metals. In the UK samples, these organisms include putative primary colonisers (group one), like the gram-positive bacterium *Terribacillus* sp. Gram-positive bacteria can easily overcome the negatively charged surface of Au particles and associated clay-like minerals (Paget et al. 1992; Rea et al. 2016). This is supported by the strong link of diverse organisms to Au particles that were >20 % transformed, which include biofilm group two *Aeromonas* sp., group three *Massilia* sp., *Methylibium* sp., *Nitrospira* spp. and *Sulfuricurvum* sp., group four *Herminiimonas* sp. and *Polaromonas* spp. Organisms that can produce and recycle biomass in the biofilm under group four includes *Herminiimonas* sp. and *Polaromonas* spp., also reported from a Finnish site, these are more resistant and resilient to environmental stressors because of functional redundancy. This means that the stress response is not focused on these organisms because other microorganisms previously recruited in the biofilm can share a similar function (Azarbad et al. 2016). When biofilms have reached the maximum carrying capacity, it requires the release of cells to decrease microbial load. The killing kinetics of microbial populations may be related to specific cell types that can withstand the action of metal toxicity such as those of persister cells that can form

exponentially to mediate time-dependent tolerance to metal cations and oxyanions (Harrison et al. 2007). In addition, dead cells interspersed with live cells are chemically reactive biomasses that bioabsorb and drive metal precipitation or chelation, preventing the ions from interfering in sensitive metabolic processes (Hall-Stoodley et al. 2004). The formation of this dispersal and dead cells, to decrease microbial load and release particles, is regulated by group six organisms, such as *Lysobacter* sp., present on 70 % of the Au particles and also detected in Australian Au particles. The dead and dispersal cells further increase the mobility of Au and trace metals as they detach from the biofilm community.

2.6. Conclusion

In this study, we show that a highly diverse biofilm community with a wide range of metabolic capabilities is present on Au particles from placer deposits in the United Kingdom. Furthermore, all particles were associated with a variety of secondary Au morphotypes likely resulting from the biomineralisation of Au by resident taxa. These taxa may be able to reductively precipitate toxic mobile Au-complexes as well as act as exoelectrogens which dump excess electrons on Au surfaces, whereas other members produce metabolic products, chelating compounds to solubilise metals and mobilise Au embedded in clay-like minerals. Others can exhibit co-tolerance by co-utilisation and regulation of Cu-Au resistance, similar to the widely reported aurophilic proteobacterium *C. metallidurans*. Overall, this is the first study to confirm a link between the composition and potential functional abilities of biofilm communities and the transformation stages of Au particles. Community assemblages recruited to the biofilm are initially different between sites and evolve to increasingly similar communities of metal-resistant members as the degree of Au transformation increases. This is likely due to increasing the load of toxic mobile Au and Ag experienced by communities during the biogeochemical transformation.

Chapter III

Biogeochemical cycling of gold: Landscape position influences gold transformation and biofilm community composition

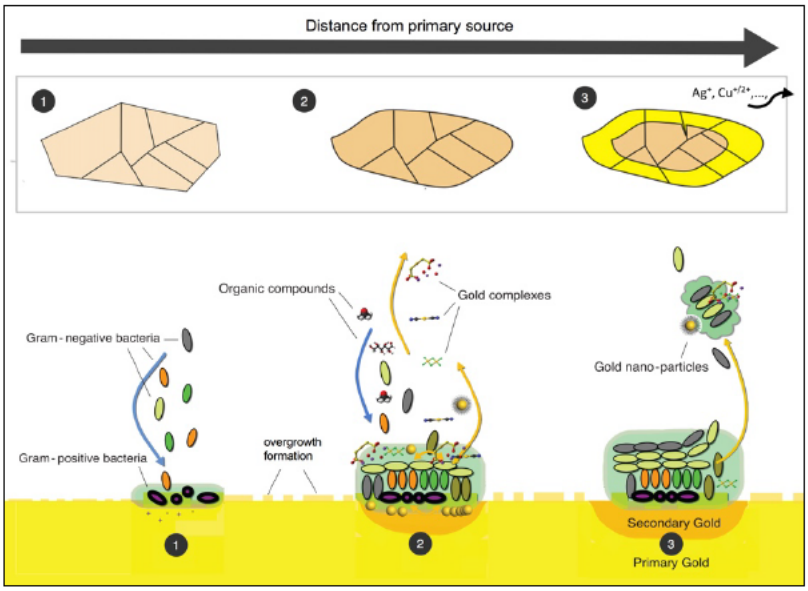

Statement of Authorship

Title of Paper	Landscape position influences gold transformation and biofilm community composition
Publication Status	☐ Published ☐ Accepted for Publication ☐ Submitted for Publication ☑ Unpublished and Unsubmitted w ork w ritten in manuscript style
Publication Details	Rea MA, Brugger J, Etschmann B, Shuster J*, Reith F (in preparation) Landscape position influences gold transformation and biofilm community composition. Gondwana Research.

Principal Author

Name of Principal Author (Candidate)	Maria Angelica Rea
Contribution to the Paper	Run samples in SEM and microprobe and performed PCR amplification for Illumina Sequencing. Performed final bioinformatics data processing and consensus sequence construction. Performed phylogenetic analysis. Interpreted results. Wrote the manuscript and created the figures.
Overall percentage (%)	60
Certification:	This paper reports on original research I conducted during the period of my Higher Degree by Research candidature and is not subject to any obligations or contractual agreements with a third party that would constrain its inclusion in this thesis. I am the primary author of this paper.
Signature	Date 14-05.18

Co-Author Contributions

By signing the Statement of Authorship, each author certifies that:

i. the candidate's stated contribution to the publication is accurate (as detailed above);
ii. permission is granted for the candidate in include the publication in the thesis; and
iii. the sum of all co-author contributions is equal to 100% less the candidate's stated contribution.

Name of Co-Author	Prof. Joël Brugger
Contribution to the Paper	Collected the samples. Advised and edited the manuscript.
Signature	Date 14.05.18

Name of Co-Author	Dr. Barbara Etschmann
Contribution to the Paper	Collected the samples. Advised and edited the manuscript.
Signature	Date 14.05.18

Name of Co-Author	Dr. Jeremiah Shuster		
Contribution to the Paper	Assisted in data interpretation and analysis. Advised and edited the manuscript. Acting corresponding author.		
Signature		Date	15/05/2018

Name of Co-Author	A/Prof. Frank Reith		
Contribution to the Paper	Collected the samples and conceived the study design. Supervised the development of work. Constructed figures. Manuscript evaluation and editing.		
Signature		Date	17.05.2018

Chapter 3: Biogeochemical cycling of gold in Switzerland

LANDSCAPE POSITION INFLUENCES GOLD TRANSFORMATION AND BIOFILM COMMUNITY COMPOSITION

In the previous chapter, findings from the UK Au particles demonstrated that the biofilm community initially recruited to colonise the Au particles are different across sites and develop to a more similar community of metal-resistant members as stages of Au transformation occur. In this chapter, we will discuss the contribution of fluvial transport and bio(geo)chemical factors to Au transformation and community composition.

Research highlights

- Biogeochemical cycle of gold occurs on Au particles from Switzerland situated at proximal, transitional and distal to the primary source.
- Transformation of Au particles in high-energy fluvial systems was primarily attributed to physical factors whereas transformation of Au particles from low-energy systems was attributed to bio(geo)chemical factors.
- A more diverse multi-species biofilm dominates Au particles collected proximal to the primary source whereas specialised multi-species biofilm dominates Au particles collected distal to the source.

3.1. Abstract

Under surface conditions, gold (Au) particles are often (re)shaped through various processes, *e.g.*, mechanical reshaping, uplift, hydrodynamic shear force, as well as gold (Au) biogeochemical processes, *e.g.*, solubilisation, dissolution and re-precipitation. Thus, we suggest that physical and bio(geo)chemical factors contribute to the transformation of Au particles by influencing the composition of biofilms occurring on the surface of Au particles. To test this hypothesis, morphologies, chemical composition and biofilm communities of Au particles sampled from Switzerland were analysed using electron microscopy, micro-analytical techniques and next generation sequencing technology. In terms of morphological and (bio)geochemical characteristics, Au particles from proximal, transitional and distal locations exhibited an increasing amount of transformation. Variable degrees of

rounding from mechanical reshaping due to transport and sedimentation processes is evident from the margins of Au particles. Surface textures displayed dissolution features showing aggregates of spongy-form overgrowths of Au nano- and micro-particles indicative of active Ag/Au mobilisation. The microbial groups with abundant sequence reads and OTUs that were detected from all sites are Proteobacteria (669 OTUs, 49.8 %), Acidobacteria, (172 OTUs, 9.7 %), Bacteroidetes (11.6 %, 222 OTUs), Cyanobacteria (26 OTUs, 13.7 %) and Planctomycetes (125 OTUs, 7.1 %). Metal-resistant organisms *Rubrivivax* spp. and *Rhodoferax* spp., and denitrifying organism *Hydrogenophaga* spp. were present at all sites. Canonical analysis of principal (CAP) coordinates showed a significant correlation between bio(geo)chemical factors and degree of transformation to community composition ($p < 0.01$) as well as physical factors and degree of transformation to landscape position ($p < 0.05$). This study provides a strong link between the stages of Au particle transformation and microbial community composition to physical reshaping and bio(geo)chemical factors.

3.2. Introduction

The biogeochemical cycle of gold, *i.e.*, solubilisation and transport, bioaccumulation, biomineralisation and secondary gold transformation has been studied in a number of ecological and environmental settings (Craw and Lilly 2016; Falconer and Craw 2009; Reith and McPhail 2006, 2007; Reith et al. 2010, 2012a; Shuster et al. 2015, 2017a). In the unified model of Au transformation, primary Au particles, commonly known as gold grains and nuggets, are brought to the surface through weathering and/or mechanical transport, thus, exposing the Au particles to a combination of physical, chemical and biological processes in surface environments (Reith et al. 2013). The Au particle is subjected to biogeochemical transformation involving the solubilisation, dissolution, re-precipitation events assisted by Au-detoxifying members of the biofilm living on the surface of the Au. The Au-Ag particle gets transported and exposed to physical factors including hydrodynamic shear force and mechanical weathering which further transforms/deforms the particle. Often, physical factors that shape the morphology of transported Au-Ag particles is used as a distance-to-source indicator in mineral exploration to pinpoint a primary source (Knight et al. 1999; Hough et al. 2007). These morphological modifications, expressed in terms of degree of roundness and flatness of Au particles, increases with the distance of transport, thus, the separation of Au particles into proximal and distal Au (Knight et al. 1999; Townley et al. 2003).

Under bio(geo)chemical transformation, the composition of the primary gold is altered by Ag mobilisation and depletion, Au mobilisation and re-precipitation as well as aggregation and recrystallisation (Reith et al. 2013). Some of these bio(geo)chemical processes are dependent on the availability of ligands to form soluble gold complexes (Zammit et al. 2015). For example, oxidation of pyrite and arsenopyrite produced temporary thiosulphate ligands that mobilised microparticulate gold encapsulated in the sulphide minerals (Craw and Lilly 2016). (Bio)oxidation by highly reactive manganese (Mn) mobilises Au that is sorbed in the Mn- and Fe- minerals (Ta et al. 2014, 2015). Biofilms invariably contribute to bio(geo)chemical transformation by excretion of these Au-complexing ligands such as organic acids and cyanides, and thiosulphate formed extracellularly, developing a dynamic Au specific bio(geo)chemical response to deal with Au-toxicity and reductively precipitate mobile Au-complexes, all leading to the biomineralisation of secondary Au thus driving the environmental cycle of Au (Reith et al. 2013). The key players among the surface-associated microbiota on Au particles form a distinct group of the microbial community that can collectively form a community with diverse metabolic capabilities such as surface conditioning, production of EPS and autoaggregation, nutrient cycling and metabolic turnover of materials and more importantly in detoxification and mobilisation of Au (Rea et al. 2016). This includes *Delftia acidovorans* which produces a metallophore delftibactin to convert toxic Au(I/III) to metallic Au(0) (Johnston et al. 2013) and the metallophilic *C. metallidurans* which reduces the toxic Au-complex in the periplasm by co-utilisation of metal resistance against copper through genes *copABCD* to form metallic Au (Reith et al. 2009). Other bacteria can form Au nanoparticles by charge capping, extracellular reduction, or formation of bioflocullants as well as degrade a range of cyano-metal complexes using nitrile-degrading enzymes and may hence destabilise/re-precipitate Au/Ag-cyanide complexes (Rea et al. 2016). This eventually leads to the mobility of gold by release of the nanoparticles via formation of dispersal cells. These reported bacteria-gold interactions highlight the contributions of microorganisms in the gold transformation which strongly supports the well-established biogeochemical cycle of gold (Reith and McPhail 2007; Fairbrother et al. 2012).

A study that links the influence of physical reworkings and bio(geo)chemical factors to stages of Au transformation and biofilm formation has not been reported. Most placer Au particles observed display a Au-Ag core indicative of primary origin and contain a rim of high purity secondary Au which was said to be formed from a combination of physical and/or biogeochemical processes under surface conditions

(*e.g.*, Fairbrother et al. 2012; Reith et al. 2012a; Shuster et al. 2017a; Stewart et al. 2017). On the surface of these Au-Ag particles are a range of secondary gold morphologies including triangular, spherical, hexagonal and octahedral nanoparticles and μ-crystals, bacteriomorphic Au and sheet-like and wire Au of high purity (>99 wt. % Au) that is compressed and/or transformed as Au particle moves (Reith et al. 2010, 2013; Shuster et al. 2015). These morphologies make up the Au-rich rims formed by different processes depending on existing environmental conditions. We hypothesise in this study that Au transformation is influenced by a complex interplay of both physical and bio(geo)chemical factors depending on its position from a likely source, *e.g.*, proximal, transitional zone and distal. Thus, this study aims to (i) evaluate secondary Au transformation on Au particles, (ii) assess the transformation stages of placer Au based on physical and (bio)geochemical factors; (iii) assess the biofilm community present on placer Au particles; (iv) and link physical and bio(geo)chemical factors to transformation stages and biofilm community composition.

3.3. Materials and methods

3.3.1. Description of field sites and sampling

The climate in Switzerland is generally temperate, based on the Koppen climate classification system, with mean temperature approximating 8°C and average annual precipitation of 1685 mm in 2014 (Kottek et al. 2006). The natural vegetation varies depending on the location where scrub, pines and chestnut dominates the south, whereas deciduous and coniferous trees like oak beech, maple, spruce pine and fir are present in the north. Valley areas are present mostly in the southern part of Switzerland. The high valleys of the Alps are covered with glaciers where headwaters of major rivers originate; lakes and glaciers cover about 6 % of the territory. The central Swiss Plateau has open and hilly landscapes, partly forested with open pastures containing grazing herds, as well as fruits and vegetable fields.

Gold found its way into the Midlands through erosion in the Alps and transportation in glaciers. From these placer deposits, gold is washed out by creeks and small rivers and deposited in their sediments or transported to bigger rivers such as Kleine Emme, Reuss and Aare and finally into the upper Rhine river (Kirchheimer 1965; Ramdohr 1965). Historic gold workings of placer deposits are known from the upper Rhine valley inside the Alpine mountain chain and in the vicinity of Basel (Oberthür et al. 2015). A detailed description of each sampling site can be found in Table 3.1.

Table 3.1 – Summary of geological and environmental conditions at the sampling localities in Switzerland.

Sample name/site	Coordinates	Placer type, host geology and primary mineralization	Distance of transport (from nearest primary mineralisation)
Col de Plannes (CP)	N46° 5' 30" E7° 6' 49"	Eluvial, local surficial transportation Pyrite, quartz and scheelite in alpine vein and fissures through a large granite porphyry vein body. Saprolith above hydrothermal mineralization in the metamorphic basement rocks of the Aiguille Rouge Massif. Presence of skarn Au in region (gold in arsenopyrite at Salanfe & Petoudes).	< 10 m
Gondo (GO)	N46° 11' 27" E8° 8' 28"	Alluvial in steep river slopes, underneath cliffs hosting pyrite-bearing quartz veins host Au, Ag and Bi. The veins were exploited in the 19th century.	< 1 km
Iselle (IS)	N46° 12' 20" E8° 11' 37"	Alluvial transport in high energy alpine river; material derived from Gondo-style pyrite-bearing quartz veins.	1 to 10 km
Vispa (VI)	N46° 15' 22" E7° 52' 44"	Alluvial in steep river slopes.	0.2 - 15 km
Hübeli (HU)	N47° 4' 2" E7° 57' 10"	Alluvial ante-Pleistocene Fluvial transport in Piedmont rivers (Miocene) and Holocene re-concentration in river; placer Au derived from Tertiary alluvial sediments (conglomerates) of the Molasse Basin	1 to 10 km
Rio de Marnand (RM)	N46° 45' 7" E6° 54' 31"	Moderate alluvial and glacial transport; Au recovered in residual sediments (cobble lag) on bed-rock.	> 10 km
Allondon (AO)	N46° 12' 31" E5° 59' 34"	Alluvial, glacial transport from Valais; multistage placer concentration in alluvial system, preserved from glacial episodes (transverse valley) (~5–30 km); some sedimentary load from the mountain chains of the Alps.	> 10 km
Geneva Kieskwerk (GK)	N46° 12' 6" E6° 3' 50"	Glacial transport from Valais, short alluvial transport (max 3–10 km: "Kieswerk" Satigny (GE) / partial reworking of ancient fluvioglacial (previous interglacials); alluvial Au deposits in fine sediments in Rhone river.	> 10 km

In this study, placer gold was obtained from eight sites in Switzerland with proximal Au particles, *i.e.*, collected within 10 m, transitional Au particles between 1 km to 10 km from source, to distal Au, *i.e.*, greater than 10 km (Table 3.1; Fig. 3.1). Gold particle samples were collected and preserved following the field sterile method described by Reith et al. (2010) to minimise contamination and preserve the integrity of the biofilm.

3.3.2. Electron microscopy and microanalyses

Samples of gold particles for electron microscopy (EM) were processed and dehydrated using series of ethanol (70 vol. %, 90 vol. % and 100 vol. %; 2 x 10 min each) washes and placed in 100 wt. % hexamethyldisilazane (HDMS) to preserve the microbial cells and biofilms (Fratesi et al. 2004). Samples were coated with a thin layer (10 nm) of carbon and analysed using FEG-SEM in secondary electron (SE) and backscattered electron (BSE) imaging modes at 5 kV and 20 kV, (Quanta™ 450 FEG Environmental SEM with EDS detectors, FEI, Netherlands). Selected Au particles

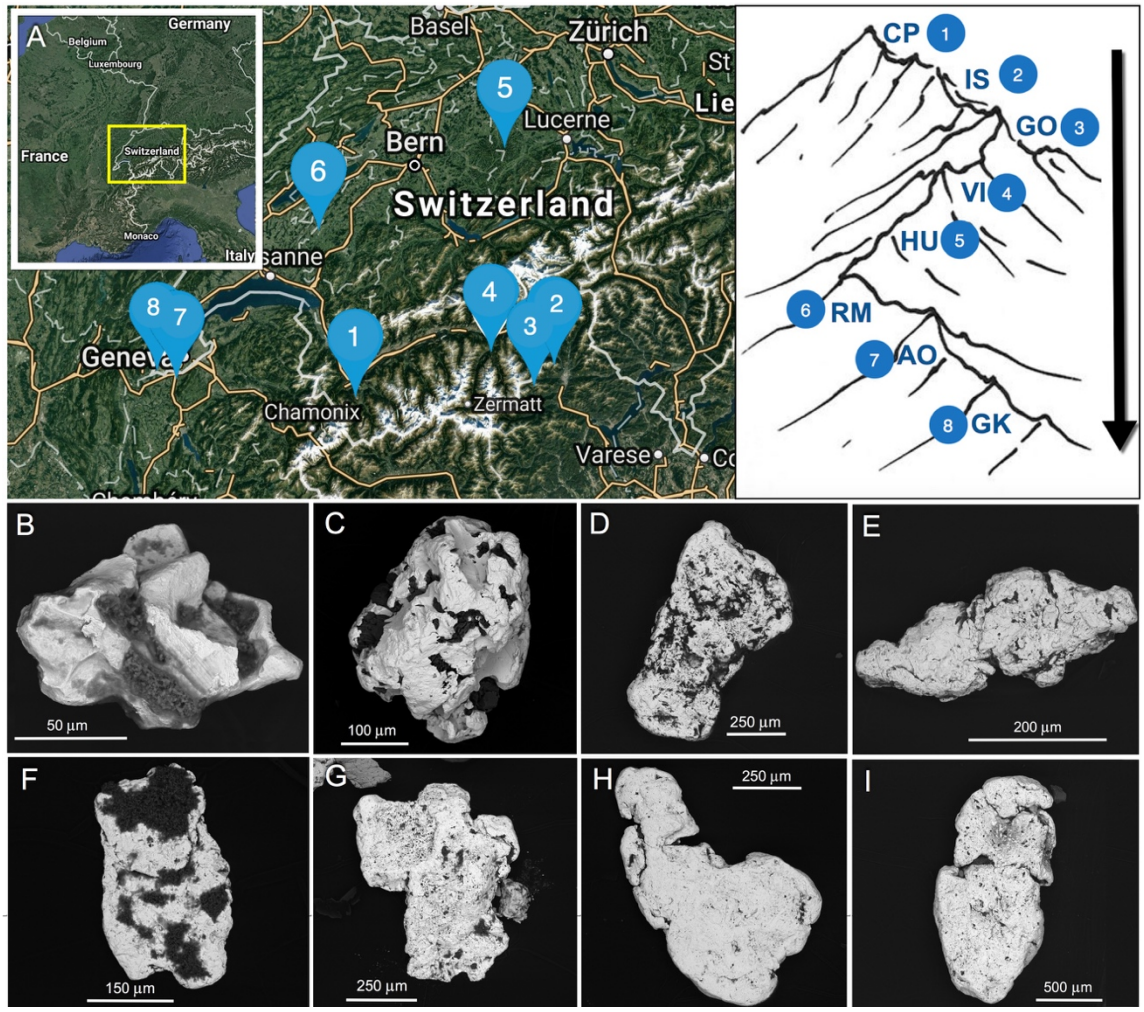

Figure 3.1 (**A**) Sampling locations; (**B-I**) typical morphologies of Au particles from Switzerland. Shown are backscattered electron (BSE) micrographs of particles that are angular (**B** from CP, **C** from GO) to slightly rounded (**D**, from IS; **E** from VI; **F** from HU), irregular (**G** from RM), rounded (**I** from GK) and flattened Au (**H** from AO) particles.

were analysed further using a FIB-SEM (Helios NanoLab DualBeam, FEI, Netherlands). FIB-milling was made on the surface of the Au particles using an ion beam of 20 kV and 9.7 pA. Images of the surface features were collected at 2 to 20 kV and 86 pA. The instrument is equipped with energy dispersive X-ray (EDX) spectrometry and used to collect spectra/maps across the particles surface and milled sections. The elements that were mapped are Au, Ag, Fe, C, N, O, Si, Ti, Al, Ga, Mg, Na, K and Pt.

A total of 24 Au particles were quantitatively mapped using an electron microprobe (EMPA; Cameca™ SXFive Electron Microprobe, France). Samples were set in epoxy resin and polished with 1 μm-size diamond paste. The Cameca™ SXFive Microprobe, equipped with five wavelength dispersive (WLD) X-Ray detectors, with PeakSite software for instrument control and Probe for EPMA™ for data acquisition and processing was used to produce quantitative maps of Au particles. Mapping was

conducted at 20 kV and 200 nA. The Au particles were analysed for (detection limits in parenthesis in wt. %): Au (0.24 wt. %), Ag (0.09 wt. %), S (0.025 wt. %), Fe (0.06 wt. %) and Cu (0.11 wt. %). These elements were calibrated using minerals and pure metal standards from Astimex and P&H. Cu, Fe and S were calibrated on chalcopyrite; Ag on telluride; and Au on a pure metal standard. The EPMA™ software produces a full quantitative pixel by pixel calculation by using the Mean Atomic Number background correction (Donovan and Tingle, 1996) in CalcImage and false colorisation and formatting in Surfer10™ to produce net intensity, detection limit map and totals image. To estimate the amount of particle transformation EMP micrographs were further analysed following the procedure of Rea et al. (2018) by performing a pixel by pixel ratio using Image J v.1.50 g (National Institutes of Health, USA; Abràmoff et al. 2004; Rasband 2012). This is performed by converting Au-Ag EMPA maps into binary images and calculating pixel by pixel ratios, *i.e.*, a ratio of transformed secondary Au to untransformed primary Au (Rea et al. 2018). This transformation factor (TF) was calculated for each Au particle and the following categories were assigned: A (TF ≤10 %), B (TF 10–20 %), C (TF >20 %); these TF categories were used as a basis for the statistical analyses for transformation based on bio(geo)chemical factors. A transformation factor attributed to physical factors were calculated based on surface morphologies, *e.g.*, general shape, outline and surface, of 63 individual Au particles following the procedure of Townley et al. (2003). The following categories were assigned: P if the TM score is ≥9 points; M if TM score is >10 but ≤15; D if TM score is >15. The assigned TM scores were used as basis for physical factor transformation in the statistical analysis.

3.3.3. Biomolecular and statistical analyses

An additional 78 Au particles were assessed for resident biofilm communities using nested 16S rRNA polymerase chain reaction (PCR) combined with next generation sequencing (NGS) using the Illumina MiSeq platform – TruSeq SBS v.3 600 cycle using 300 bp paired end sequencing (Reith et al. 2010; Bissett et al. 2016). The universal primers 27F and 1492R (Lane 1991; Osborn et al. 2000) were used for initial PCR amplification of 16S rRNA genes (Reith et al. 2010) and further amplified using primers 27F and 519R (Lane 1991; Lane et al. 1985) and sequenced at the Australian Genome Research Facility (AGRF, Melbourne, Australia). DNA amplifications were performed in an Applied Biosystems Veriti™ Thermal Cycler (Applied Biosystems, California, USA) and amplicons were checked in 1.5 % agarose gel with Gel Red (Biotium Inc., Hayward, CA, USA) 1:10,000 (v/v). The agarose gel was run at a

constant voltage of 80 V for 1 h. Procedures for sequencing, open OTU picking and assignment are detailed in Bissett et al. (2016). An OTU abundance tables were constructed by mapping all reads to the OTUs (usearch_global, 97 %).

The PRIMER-6 software package with the PERMANOVA+ add-on (Clarke and Warwick 2001; Anderson et al. 2008) were used to conduct multivariate statistical analyses. Similarity matrices were established on the fourth root transformed abundance data using the Bray-Curtis method (Bray and Curtis 1957). Non-metrical multidimensional scaling (nMDS) and canonical analysis of principal coordinates (CAP) was used to assess the community differences between progressively transformed Au particles. Vector overlays, based on Pearson correlations, were used to explore relationships between significant particle transformation and taxa and the ordination axes. SIMPER analysis was used to assess groups/phyla showing differences between transformation stages. The OTUs were assigned to the six functional groups representing the different stages of biofilm development based on the classification developed by Rea et al. (2016).

3.4. Results

3.4.1. Characterisation of gold particle shape and overall outline

The Au particles collected from eight sites in Switzerland ranged from 100 μm up to 4.0 mm. Proximal Au from Col de Plannes (CP) displays an irregular and angular morphology with sharply defined edges (Fig. 3.1B), whereas variable degrees of rounding and a series of irregular protrusions were observed in Gondo (GO). The edges of the GO particles appear to be at an initial stage of rounding with flattening of the margins that are not well-defined (Fig. 3.1C). Gold particles that are situated in the transitional zone, *i.e.*, greater than 1 km but less than 10 km, show varying degrees of rounding, with thick folded edges and has not been significantly flattened while other Au particles show irregular outline (Fig. 3.1D–G). Mechanical reshaping from transport and sedimentation processes is evident as the margins appear smoothed and rounded but with surface textures that are rougher and coarser (Fig. 3.1E, G). Distal Au particles from Allondon (AO) and Geneva Kieskwerk (GK) show flat to rounded and/or elongated morphology typical of Au particles obtained from distal sources. The surface has numerous deep cavities found between refolded and bent limbs (Fig. 3.1H, I).

To quantify the degree of transformation based on physical factors, a total of 63 individual Au particles were assessed and classified based on Townley et al. (2003). Scores were assigned based on general shape, outline, surface and presence of

primary crystal imprints. Different sites exhibit different transformation score, with Au particles from CP and GO grouped to transformation matrix (TM) P. Hübeli (HU), Vispa (VI) and Iselle (IS) grouped to TM D, and AO, GK and Riau de Marnand (RM) under TF D (Table 3.2).

Table 3.2 – Results of Au particle morphological analyses showing transformation matrix scores for general shape, outline, surface and primary crystal imprint for individual Au particles.

Site	Grain	Shape1	Shape2	Outline1	Outline2	Surface1	Surface2	Crystal	Total score	Average	TF
A01	A01_G1	3	2	3	3	3	2	2	18	20	D
	A01_G2	3	3	3	3	3	3	3	21		
	A01_G3	3	2	3	3	3	3	2	19		
	A01_G4	3	3	3	3	3	3	2	20		
	A01_G5	3	3	3	3	3	3	2	20		
	A01_G6	3	2	3	3	3	3	1	18		
	A01_G7	3	3	3	3	3	3	3	21		
A02	A02_G1	3	3	3	3	3	3	3	21	19	D
	A02_G2	3	3	3	3	3	3	3	21		
	A02_G3	3	3	2	3	3	3	2	19		
	A02_G4	3	3	3	3	3	3	3	21		
	A02_G5	2	3	3	3	3	3	2	19		
	A02_G6	2	3	2	2	3	3	2	17		
	A02_G7	3	3	2	3	3	3	2	19		
	A02_G8	3	3	3	2	3	3	3	20		
	A02_G9	3	2	2	2	3	3	2	17		
	A02_G10	3	3	3	3	3	3	2	20		
CP	CP_G1	1	1	1	1	1	1	1	7	7	P
	CP_G2	1	1	1	1	1	1	2	8		
	CP_G3	1	1	1	1	1	1	1	7		
	CP_G4	1	1	1	1	1	1	1	7		
GK	GK_G1	3	3	3	2	3	2	2	18	18	D
	GK_G2	3	3	3	2	2	2	2	17		
	GK_G3	2	2	2	3	3	3	2	17		
	GK_G4	3	3	2	3	3	3	3	20		
	GK_G5	3	3	3	3	3	3	2	20		
	GK_G6	3	3	3	2	3	3	2	19		
	GK_G7	3	3	3	2	3	3	2	19		
	GK_G8	3	2	2	3	2	3	2	17		
	GK_G9	3	3	3	3	3	2	1	18		
	GK_G10	3	3	3	2	3	3	2	19		
GO	GO_G1	1	1	2	2	1	2	1	10	9	P
	GO_G2	1	2	2	2	1	2	1	11		
	GO_G3	1	1	1	2	1	2	1	9		
	GO_G4	1	1	1	2	1	1	1	8		
	GO_G5	1	1	1	2	1	1	1	8		
	GO_G6	1	1	1	1	1	1	1	7		
HU	HU_G1	3	2	2	3	2	2	1	15	16	M
	HU_G2	2	2	2	2	2	2	1	13		
	HU_G3	3	3	3	3	2	3	1	18		
	HU_G4	2	2	2	2	2	3	1	14		
	HU_G5	3	3	3	3	3	2	2	19		
	HU_G6	3	2	3	3	3	2	2	18		
IS	IS_G1	3	2	2	3	2	2	1	15	16	M
	IS_G2	3	2	2	3	2	3	2	17		
RM	RM_G1	3	2	2	2	2	3	2	16	17	D
	RM_G2	3	2	3	2	3	2	3	18		
	RM_G3	3	3	3	3	3	2	2	19		
	RM_G4	2	2	2	2	3	2	3	16		
VI	VI_G1	3	2	2	3	2	2	2	16	15	M
	VI_G2	2	2	2	2	2	2	2	14		
	VI_G3	3	2	2	3	2	2	2	16		
	VI_G4	2	2	2	3	1	2	2	14		

3.4.2. Characterisation of progressive transformation of gold particles

Microprobe maps of Au particles show progressive transformation of the proximal to distal Au particles. Representative maps of proximal particles show a typical homogenous Au-Ag alloy together with the presence of Ag-rich bands up to 23.0 wt. % Ag (Fig. 3.2A, B). The formation of Au-rich rims in transitional to distal Au particle becomes more evident and forms a continuous rim (Fig. 3.2C–F). To quantify the degree of the transformation of Au particles based on bio(geo)chemical factors, the pixel ratio of transformed rim *vs* untransformed rim is calculated from three to four Au particles for each site. Particles from the same site generally exhibit similar transformation stages, with Au particles from CP, GO, IS and RM grouped to Transformation Factor (TF) A, AO and VI in TF B, and GK and HU in TF C (Table 3.3).

Table 3.3 – Results of quantitative electron microprobe analyses (EMPA) showing the pixel by pixel counts of Au particle rims and cores and their corresponding transformation factors.

Label	Whole Area Counts	Rim Counts	% Transformed	Mean of % Transformed	Degree of transformation
A02_Grain1	60250	6715	11.1	17.4	B
A02_Grain2	54219	12547	23.1		
A02_Grain3	88189	15709	17.8		
CP_Grain1	3290	409	12.4	7.8	A
CP_Grain2	8861	61	0.7		
CP_Grain3	15375	1579	10.3		
CP_Grain4	3976	317	8.0		
GK_Grain1	41218	10810	26.2	34.2	C
GK_Grain2	9328	4024	43.1		
GK_Grain3	20279	7622	37.6		
GK_Grain4	22511	6739	29.9		
GO_Grain1	42669	1635	3.8	5.1	A
GO_Grain2	38698	2107	5.4		
GO_Grain3	18884	1259	6.7		
GO_Grain4	23515	1027	4.4		
HU_Grain1	4683	1576	33.7	45.1	C
HU_Grain2	11125	6261	56.3		
HU_Grain3	8665	3927	45.3		
Isr_Grain1	20641	556	2.7	1.9	A
Isr_Grain2	3447	40	1.2		
RM_Grain1	118619	10683	9.0	9.0	A
VI_Grain1	45581	6688	14.7	15.3	B
VI_Grain2	17093	3728	21.8		
VI_Grain3	11233	1050	9.3		

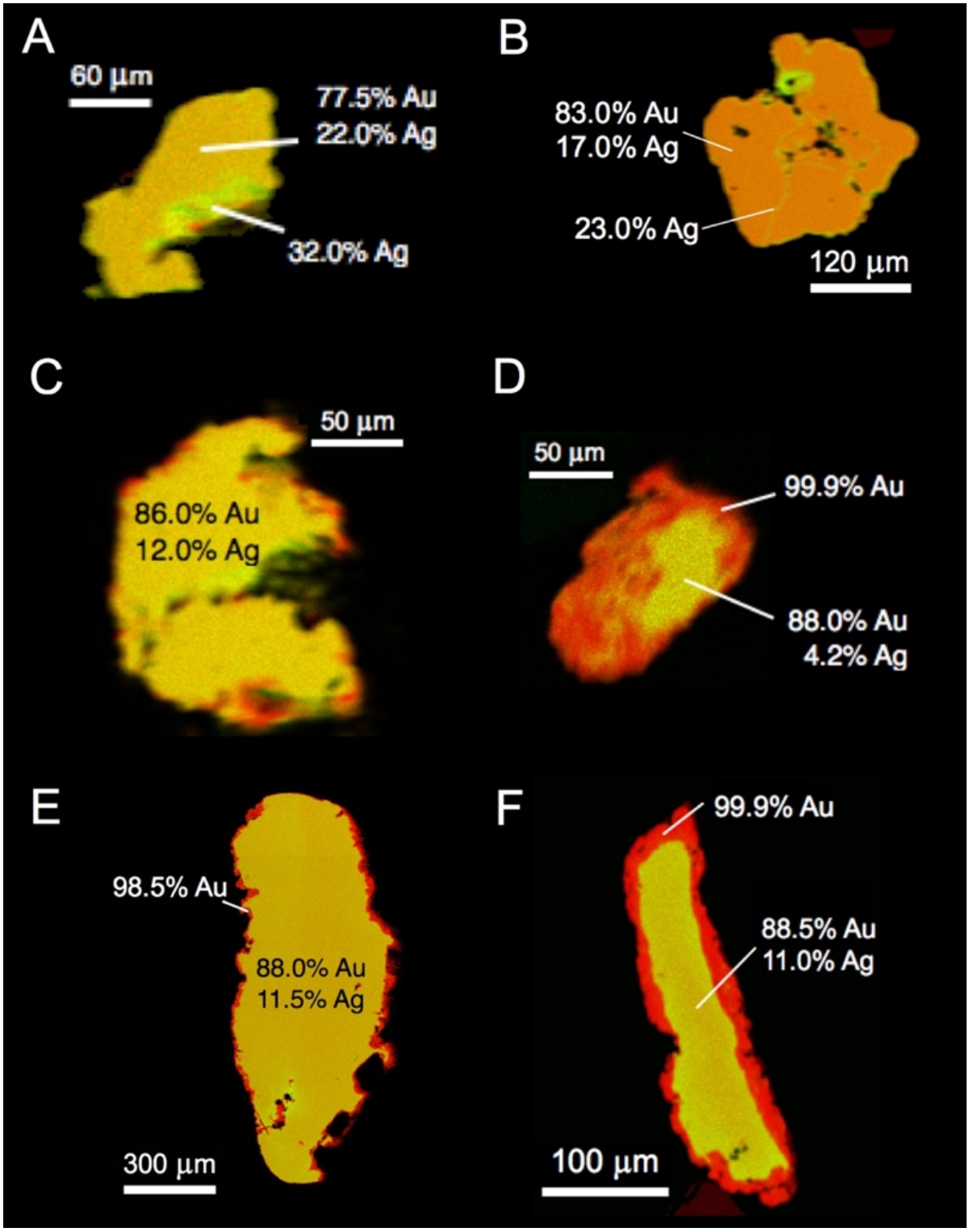

Figure 3.2 Electron microprobe maps, Au (red) and Ag (green), showing the progressive transformation of Au particles. (**A**) Au particles composed of a homogenous Au–Ag alloy; (**B**) Au-Ag alloy with Ag-rich bands indicative of Ag dissolution and **(C–F)** Au-Ag with a partial layer of secondary high purity Au.

3.4.3. Characterisation of gold particle surface and secondary gold morphotypes

The surface of proximal Au particles shows a few impact marks and cavities and contains numerous coarse crystal imprints (Fig. 3.3A–B). Initial signs of pitting were also observed on the surface of these primary Au particles (Fig. 3.3A). In addition, these primary Au were also covered with high purity Au overgrowths (99.9 %). FIB-milled section of the surface of proximal Au particles with Au overgrowths revealed a large solid crystalline core where the Au overgrowths are attached (Fig. 3.3D). For transitional Au particles, the surface contains irregular pitting and dissolution textures (Fig. 3.4A, B) while some areas contain extensive polymorphic layers that hold abundant nanometre- and micrometre-sized secondary Au aggregates (Fig. 3.4C). The FIB-milled section revealed a polymorphic layer covering Au micro- crystals and Au sheets that are oriented diagonally in relation to the surface of the Au particle (Fig. 3.4D, E) and abundant nanophase Au embedded in the EPS cover (Fig. 3.4F).

Micrographs of distal Au particles in high energy fluvial system show prominent striations and scratches consistent in their orientations and spacing with the presence of fine Au and branched wire Au covering crevices (Fig. 3.5A–C). FIB-milled sections of distal Au particles reveal the successive replacement of Au crystals by high purity μ-crystalline Au from the core to rim of the particle (Fig. 3.5D–F, map inset). The crystallinity at the core of the Au particle shows indistinct boundaries whereas rims show porous nano-crystalline Au (Fig. 3.5E, F). Remnants of biological materials (*e.g.,* microbial aggregates) that form microbial mats were visible and abundant on the Au surface, which progressively increase as the Au particles have travelled further from the source (Fig. 3.6). Individual prokaryotic cells and mineralised fabrics were also observed in proximal and transitional Au particles (Fig. 3.6B, C) and some cells were observed to be closely associated with the ferruginous material found in distal Au particles (Fig. 3.6B–D)

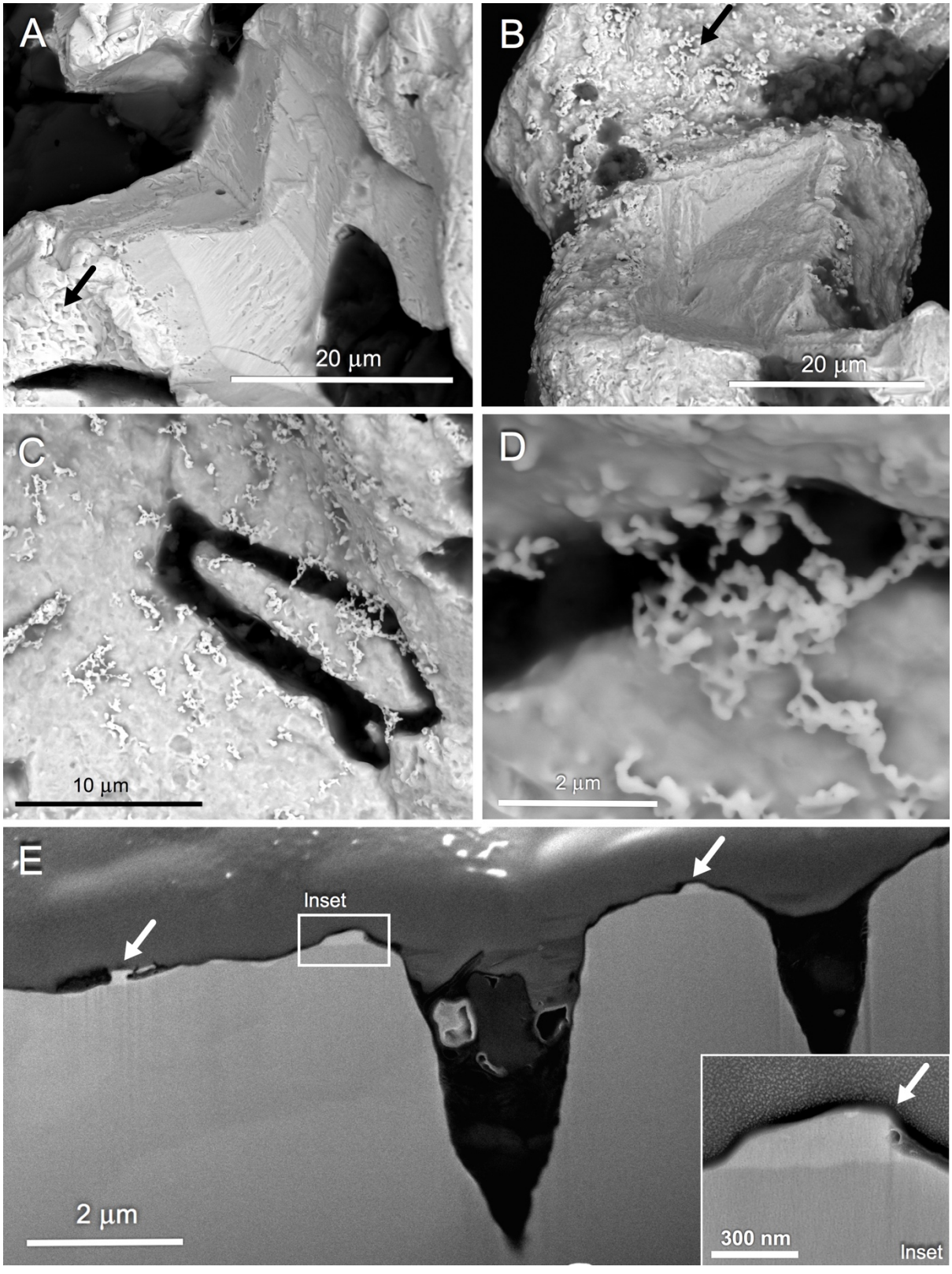

Figure 3.3 BSE micrograph of a characteristic proximal Au particle surface showing **(A)** initial pitting and **(A, B)** large crystal imprint and **(C–D)** the presence of scattered microphase Au overgrowths on the surface spongy-form overgrowths. **(E)** A FIB-milled section of primary Au surface with initial formation of spongy-form overgrowths, revealing the open crevices filled with polymorphic materials and the presence of a high purity overgrowth cemented on the primary crystal surface **(E inset).**

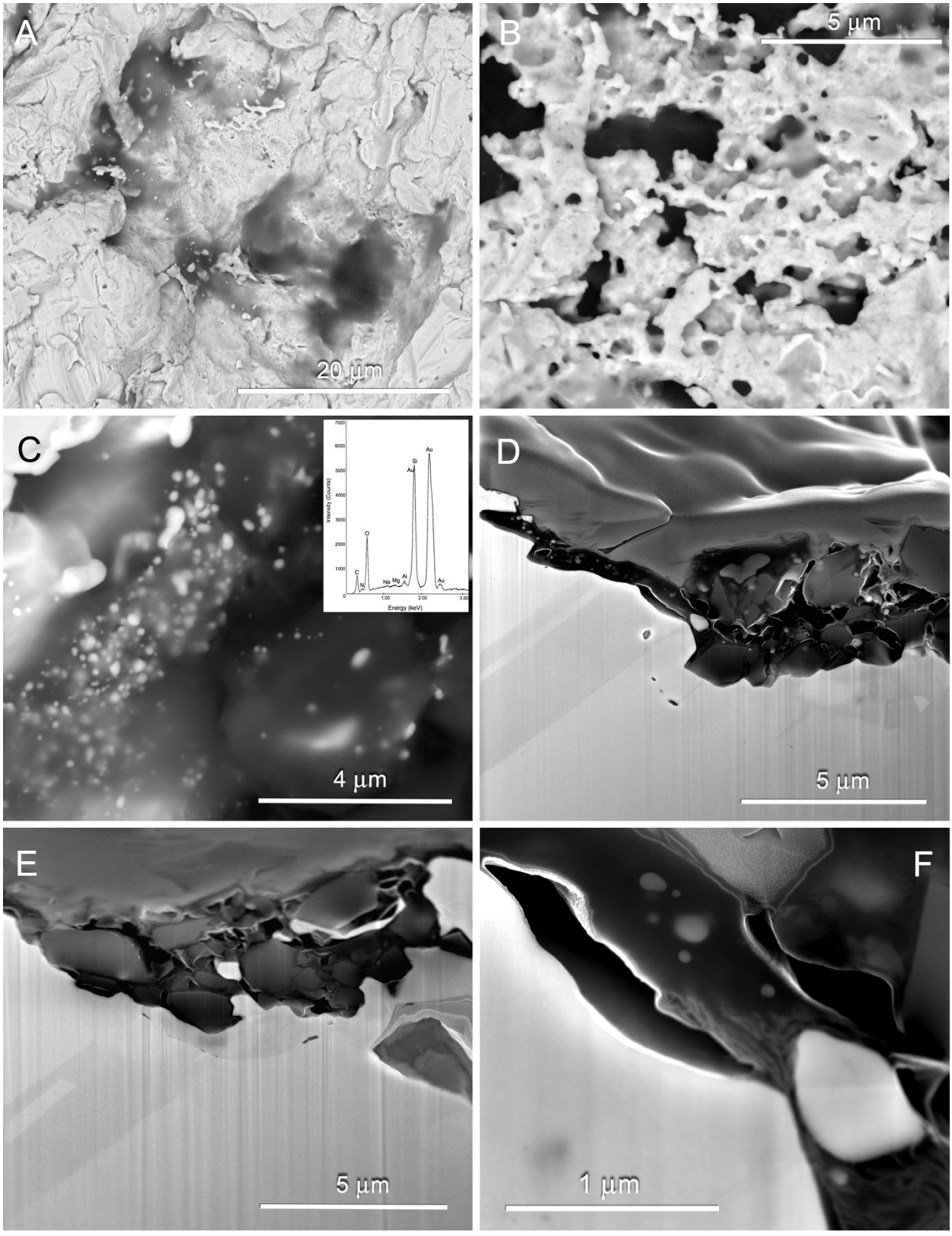

Figure 3.4 BSE micrograph of mid-range transitional Au particles showing **(A–B)** irregular pitting and roughening of the surface, **(C)** nanophase Au associated with the polymorphic layer. **(D–F)** FIB-milled section of microcrystals and nanophase Au embedded in the EPS layer underlying μ-crystalline Au made up of distinct crystals.

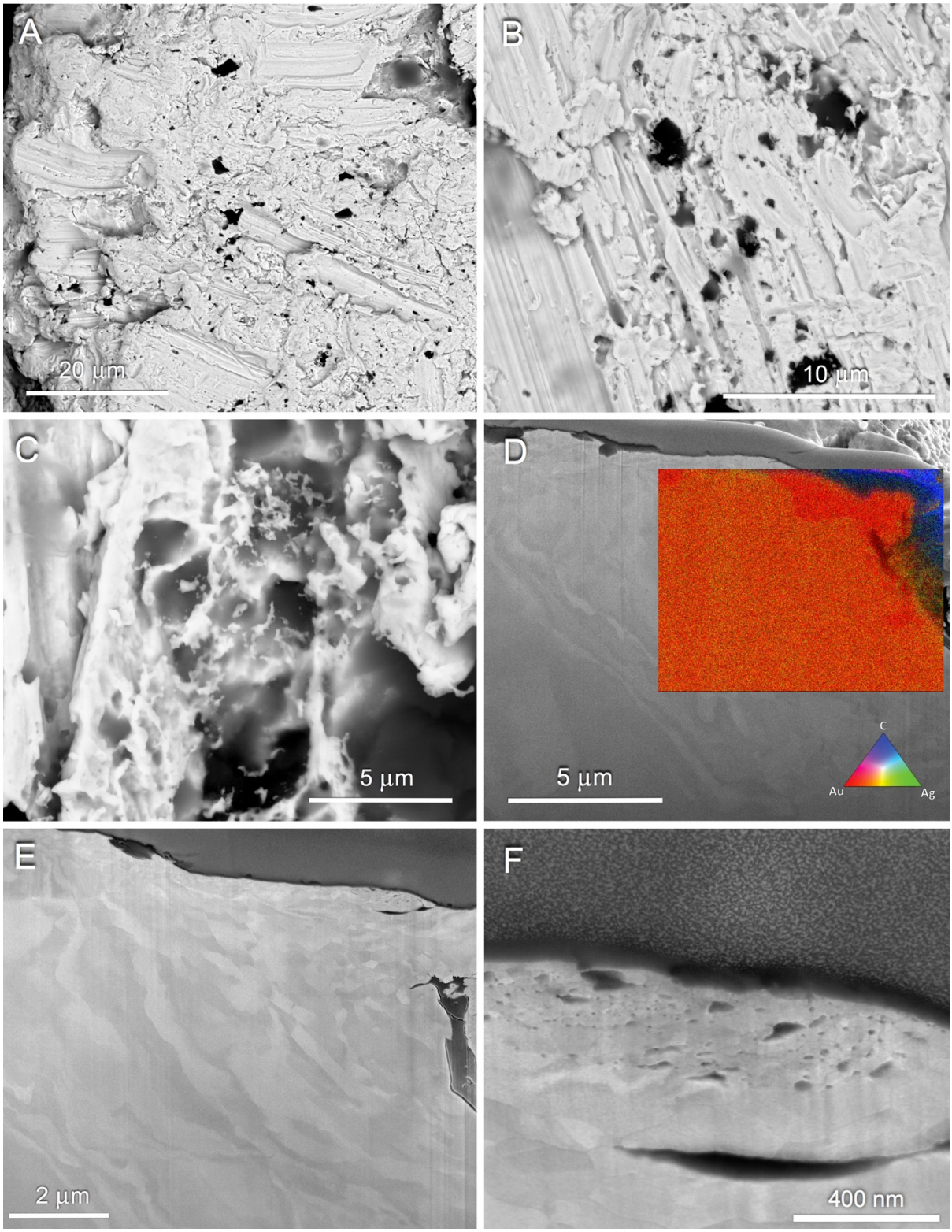

Figure 3.5 **(A–B)** BSE of secondary Au morphologies associated with the numerous striations and scratches on the surface; (**C**) fine-branched wire-like and nanophase Au over open crevices and **(D)** a FIB-milled section and Au-Ag-C map of Au surface with distinct Au rims and (**E–F**) polymorphic carbonaceous layer and aggregates of nanoporous Au over μ-crystals with indistinct boundaries.

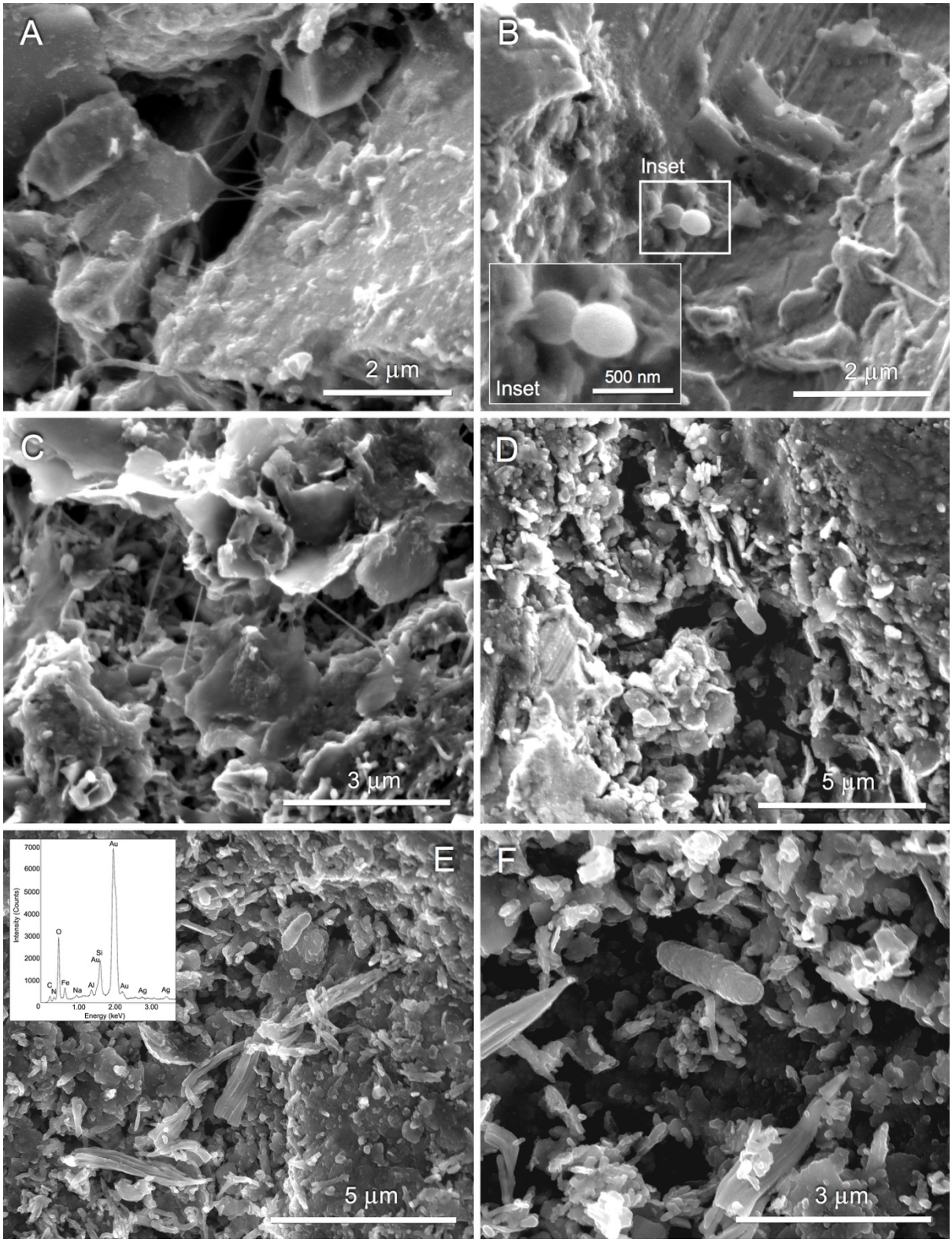

Figure 3.6 SE micrographs of polymorphic layers on Au particle surfaces from proximal to distal Au particles (**A, B**) EPS and a microbial cell on the surface of proximal Au particles (**C, D**) secondary electron (SE) micrographs of EPS cover on mid-range transitional Au particles and (**E**) micrographs with representative EDS spectrum of polymorphic layers composed of nano- and micro-crystal minerals, cells and EPS; (**F**) and a prokaryotic cell with associated ferruginous material.

3.4.4. Microbial communities on gold particles

The majority (93.0 %) of Au particles were positive for target amplicons with greater than 3.3 million reads. Across all sites, 1463 OTUs was detected where individual sites had 194 up to 617 OTUs (Table 3.4). At the phylum level, Proteobacteria comprised 49.8 % of the total sequencing reads and the highest detected OTU (45.7 %). Of the Proteobacteria phylum, β-Proteobacteria has 254 OTUs and 23.7 % of total reads followed by α-Proteobacteria (153 OTUs, 10.47 %). Also numerous are the γ-Proteobacteria with 136 detected OTUs comprising 12.8 % of the total reads. Others include δ-Proteobacteria (99 OTUs, 1.3 %) as well as ε-Proteobacteria (14 OTUs, 1.0 %). In terms of individual sites, GK and AO has the highest number of OTUs classified under Proteobacteria, 71.9 % and 52.7 %, respectively, followed by RM (52.6 %) and IS (50.4 %) then GO and HU (48.1 % and 45.1 %) (Fig. 3.7). Also abundant on all of the sites are the phylum Acidobacteria (172 OTUs, 9.7 %), Bacteroidetes (222 OTUs, 11.6 %), Cyanobacteria (26 OTUs, 13.7 %) and Planctomycetes (125 OTUs, 7.1 %). Other detected phyla comprise 1.0–2.9 % for Bacilli, Clostridia, Cyanobacteria, Verrucomicrobia and 19 other rarer phyla. Across all sites, the genera *Rubrivivax* spp., *Rhodoferax* spp. and *Hydrogenophaga* spp. were present. The top10/top20 most numerous OTUs (by number of reads) contributed between 30.9 to 69.6 and 45.8 to 82.3 % of total reads detected, respectively, with values increasing from proximal to distal site (Table 3.4). Non-metric MDS ordination of community assemblages showed a significant link between the microbial assemblage and transformation factor based on bio(geo)chemical factors ($\sqrt{CV} = 22.6$; $P < 0.001$) and a significant link between microbial assemblage and transformation from physical factors ($\sqrt{CV} = 21.7$; $P < 0.001$). CAP analyses showed a wide variety of communities associated with TF A sites, with more distinct clustering in TF B and TF C as the degree of bio(geo)chemical transformation increases (Fig. 3.8A).

Table 3.4 – Total reads, OTUs and percentage of total reads covered by the most abundant OTUs for the gold particles from Switzerland.

Sample name/ site	Total number of reads	Number of OTUs	Percentage of total reads covered by the 10 most abundant OTUs	Percentage of total reads covered by the 20 most abundant OTUs
GO	356557	372	30.9	45.8
IS	153762	617	34.6	46.1
HU	406192	455	36.6	45.9
A02	532941	275	49.3	62.5
RM	1454077	194	54.9	70.6
GK	430731	224	69.6	82.3

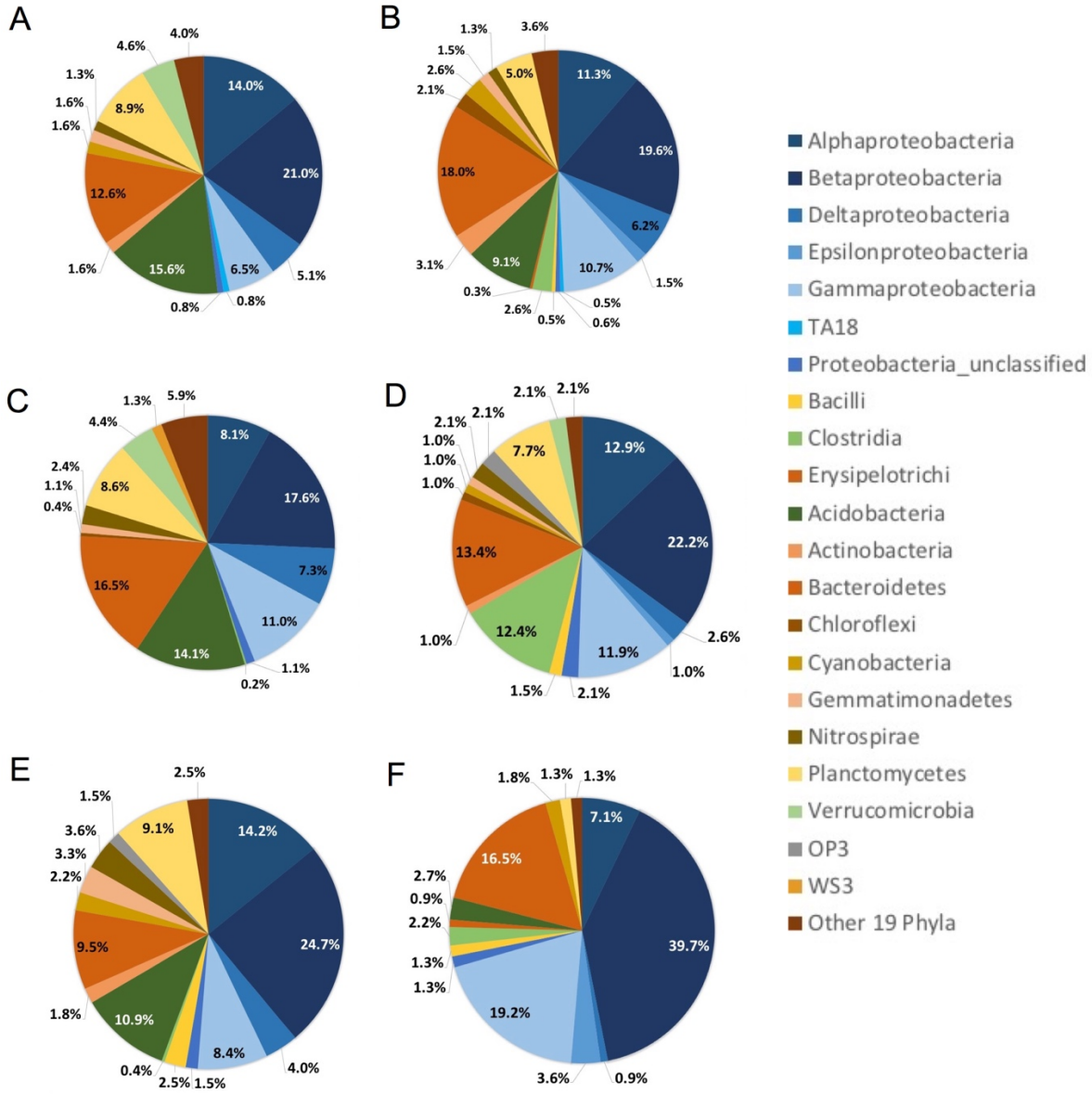

Figure 3.7 Composition of bacterial communities associated with individual Swiss Au particles. Distribution of dominant bacteria phyla/classes shown for the following sites: **(A)** Gondo **(B)** Iselle **(C)** Hübeli **(D)** Riau de Marnand **(E)** Allondon and **(F)** Geneva Kieskwerk; note: classes are shown for Proteobacteria and Firmicutes.

Distinct clustering was also observed in communities associated with groupings for transformation related to physical factors, *i.e.*, TM P, TM M and TM D (Fig. 3.8C). Based on the assigned biofilm groups, organisms known as surface colonisers are *Streptococcus* spp., *Staphylococcus* spp. and *Terribacillus* sp. OTUs assigned to group two were linked to autotrophic growth and autoaggregation such as *Arcobacter* spp. and *Curvibacter* sp. Group three biofilms are involved in nutrient cycling include *Hydrogenophaga* spp., *Methylibium* spp., *Nitrospira* spp. and *Rhodobacter* spp. Group four microorganisms such as *Flavobacterium* spp., *Polaromonas* spp. and *Rheinheimera* spp. are involved in the metabolic turnover of nutrients. Group five

microorganisms include *Acinetobacter* spp., *Micrococcus* sp., *Pseudomonas* spp., *Rhodoferax* spp. and *Rubrivivax* spp. which are involved in metal resistance and gold mobility and the formation of dispersal cells by group six organisms such as *Lysobacter* spp. and *Cystobacter* spp. (Fig. 3.9).

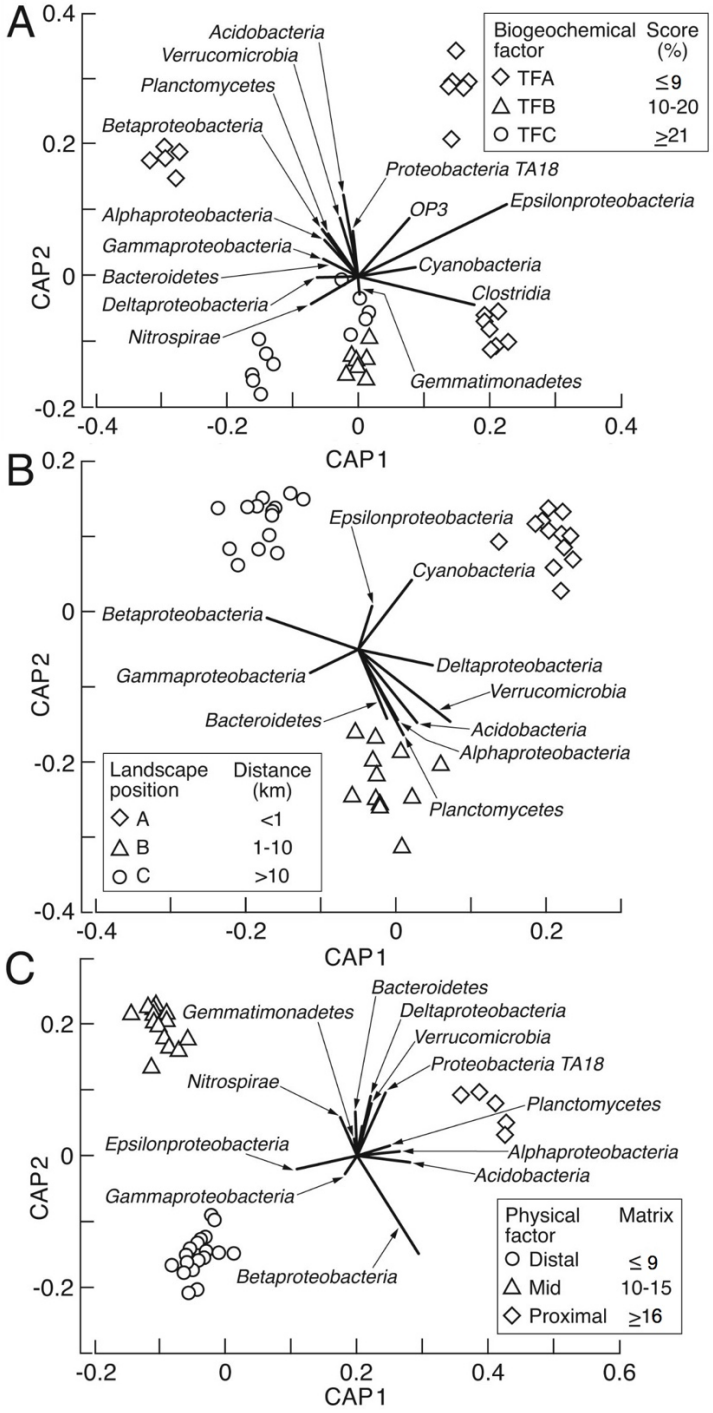

Figure 3.8 **(A)** Ordination plot of the first two canonical axes produced by CAP of MiSeq data analysed for differences in community assemblages in relation to **(A)** assigned bio(geo)chemical transformation factor developed by Rea et al. (2018), **(B)** the distance of transport based on landscape position and **(C)** assigned physical transformation modified after Townley et al. (2003); note: vectors of Spearman correlations of classes/phyla from OTUs with highest % contribution based on SIMPER analysis are overlain.

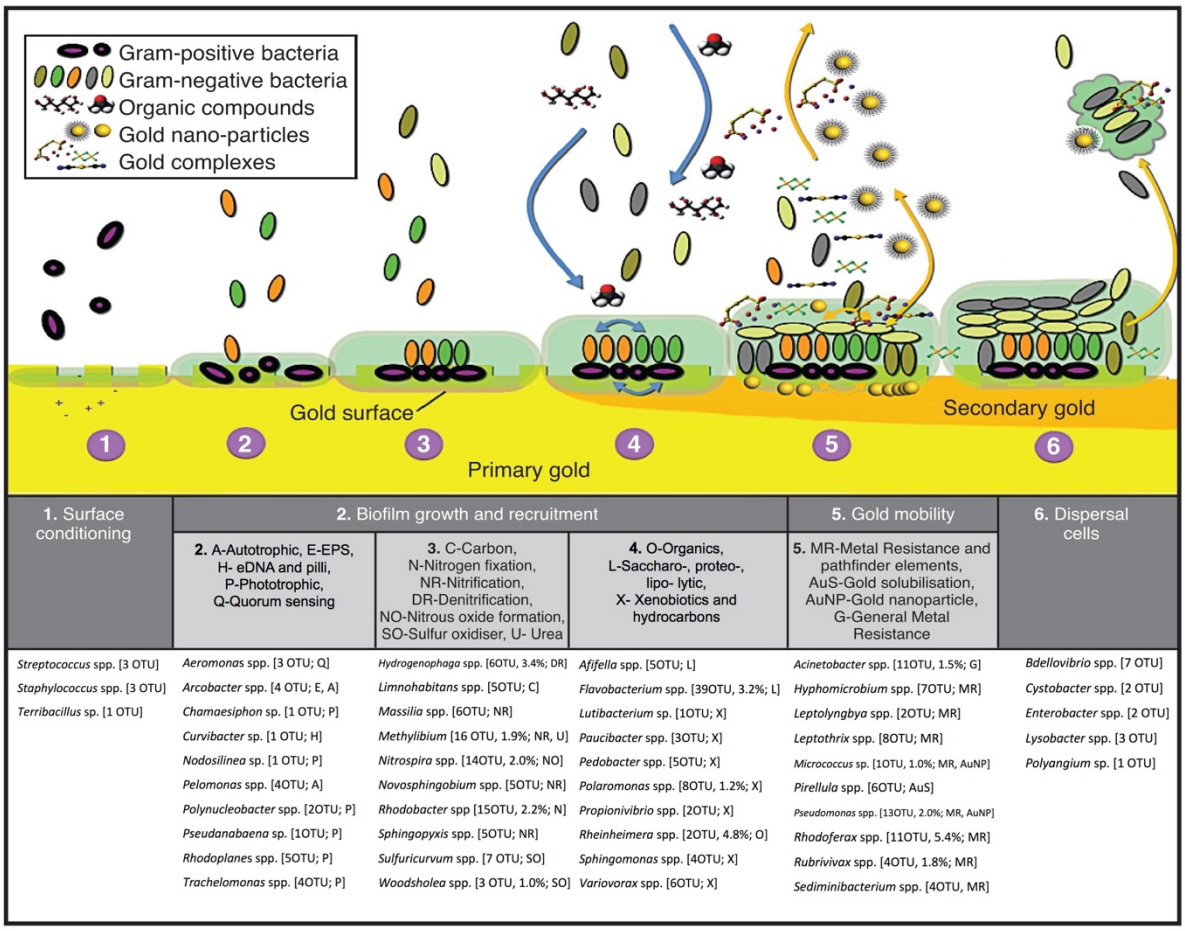

Figure 3.9 Schematic model and putative functional traits of biofilms on Au particles from Switzerland (modified after Rea et al. 2016): (1) conditioning of surfaces to their attachment; (2) the recruitment of autotrophic bacteria; (3–5) the proliferation and growth of the biofilm community including heterotrophic and metallophilic species; (5) the mobilisation, detoxification and re-precipitation of Au; and (6) the seeding of dispersal cells with release of nanoparticle and Au-complexes.

3.5. Discussion

The secondary morphotypes observed in Swiss Au exhibited similarities to those from Australia, New Zealand, South America, UK (Chapter 2) and Finland which were many times attributed to a combined bio(geo)chemical factor and physical transport (Reith and McPhail 2006, 2007; Falconer and Craw 2009; Reith et al. 2010, 2012a, 2018; Shuster et al. 2015, 2017a; Craw and Lilly 2016; Rea et al. 2018). Though it is well-established that the bio(geo)chemical transformation of Au-Ag particles has an impact on the degree of Au transformation and that physical transformation mostly from fluvial transport is correlated to overall morphology of the Au-Ag particles (Youngson and Craw 1993; Rea et al. 2018), the link supported by statistical analysis between the bio(geo)chemical and physical factors that contributes to the overall Au transformation and biofilm composition has not been delineated in

previous works. Therefore, in this study, we assessed these as individual factors to link physical reshaping and biogeochemical factors to transformation stages.

Results from this study showed that the influence of fluvial physical transport is evident in the overall shape, outline and margins of the Au, which progresses from angular to rounded margins as Au particles become transported hundred metres to kilometres from the primary source (Fig. 3.1B–I; Fairbrother et al. 2012; Reith et al. 2012a). Gold transported in fluvial systems decrease in particle size and possibly becomes reconcentrated by interglacial downcutting events and major floods before it becomes more flattened and folded (Youngson and Craw 1993). Progressive bio(geo)chemical transformation, supported by Au-Ag maps of Swiss Au showed an increase in the width of Au-rich rims with increase in distance from the source similar to what was observed in Au particles from Australia, New Zealand, UK and Finland (Fig. 3.2; Falconer and Craw 2009; Reith et al. 2010, 2012a, 2018; Fairbrother et al. 2012; Rea et al. 2018). The formation of high purity rims occurs when Ag is increasingly mobilised out of the Au-Ag alloy and Au re-precipitates back by biomineralisation (Reith et al. 2013; Rea et al. 2018).

In addition, the difference in the contribution of fluvial transport and bio(geo)chemical factors is demonstrated in Au particles collected proximal and distal to the primary source, specifically, the presence of large crystal imprints on the surface as a feature typically observed in primary Au particles (Fig. 3.3A). The presence of high purity Au overgrowths on the surface of these proximal Au particles further supports initial bio(geo)chemical transformation from the mobilisation of Ag out of the Au-Ag alloy and re-precipitation of Au back to the Au-matrix (Fig. 3.3C–D). Since these Au particles were not yet exposed to harsh hydrodynamic forces, these overgrowths were preserved and intact (Reith et al. 2012a; Craw et al. 2017).

From this study, we have also shown that transitional Au particles were either dominated by biogeochemical or by physical factors and their transformation is highly dependent on the landscape setting where the placer gold was collected (Fig. 3.4, 3.5). For instance, a high energy river system where transitional Au particles were collected were subjected to higher shear force leading to transformation-deformation of the surface textures (Fig. 3.5A, B). Distal Au particles collected in a more static environment undergo less physical deformation but more biogeochemical transformation (Fig. 3.5D–F). Furthermore, numerous physical abrasions in Au particles from transitional zones indicate that physical transformation overcomes the biogeochemical transformation in these fast-flowing river system (Fig. 3.5). The degree of physical and chemical transformation corroborates to the amount of EPS

and biological remnants documented on the surface of proximal and distal Au particles. Proximal Au particles that were exposed to minimal physical and biogeochemical transformation contained fewer microbial remnants and EPS on the Au particles (Fig. 3.6A–B). Distal Au exposed to physical and longer biogeochemical transformation contained more EPS materials covering the majority of the Au particles (Fig. 3.6C–F). These polymorphic layers composed of microbial cells, EPS and clays made up of Al, Fe and Si are known to assist in the formation and accumulation of nanophase and microphase Au particles (Reith et al. 2012a, 2013; Shuster et al. 2015; Rea et al. 2016). Together with extensive cover of the polymorphic layer, we observed in this study that a more diverse biofilm community, in terms of the number of OTUs and sequencing reads are present in Au particles in Switzerland that were transported to >300 m from the primary source than those transported to >10 km from the primary source. The contribution of the top10/top20 most numerous OTUs (by number of reads) for each site increases from proximal to distal sites (Table 3.4), suggesting that communities recruit a diverse group of organisms at proximal sites with <10 % transformation and becomes more specialised and more resistant to Au toxicity as the degree of transformation increases (Rea et al. 2018). The strong link between community assemblage and progressive transformation of Au from biogeochemical influence supports the findings from Au in the UK wherein the biofilm composition is attributed to the recruitment of more metal-resistant organisms as transformation progresses (Chapter 2; Rea et al. 2018). Furthermore, there is also a strong link observed between the stages of physical transformation and biofilm community composition in this study, which confirms the influence of physical factors on Au transformation (Fig. 3.8B). This observed link is likely due to an increase in physical reshaping which is known to have a significant influence on the production of EPS and the metabolic behaviour of biofilms (Liu and Tay 2001). Higher hydrodynamic shear force induces a compact, stable biofilm structure by regulating metabolic pathways (Trevors 1984). Thus, the bacterial community channels energy to enhance catabolic activity and reduce growth. High shear stress influences the electron transport system and proton translocation system in bacteria that directs catabolism (Trevors 1984). Higher proton diffusion across the cell membrane is linked to a better hydrophobic interaction of cells and induce protonation and membrane fusion of cells thus maintaining the structural integrity of the biofilm (Tay et al. 2000). The hydrodynamic shear force was also experimentally linked to genetic transformation on the monoculture biofilm of *Acinetobacter* spp., exhibiting the

highest transformation frequency in cells situated on the outer layer of the biofilm exposed to shear stress (Hendrickx et al. 2003).

A complex multi-species biofilm that forms similar functional abilities in the 6-stage biofilm groups developed by Rea et al. (2016) was captured from the 16S 'molecular snapshots' of the microbial community living on Au particles. *Rhodoferax* spp., a group five biofilm, is among the most important component of this community due to its ability to form persistent biofilm layers and exhibit exoelectrogenic capabilities (Chaudhuri and Lovley 2003). The microbial-assisted production of electrons from organic matter and solid mineral surfaces is beneficial for the microorganisms to support energy, nutrients and microbial metabolism, thus, driving the metabolic activity of the whole biofilm community (Nevin et al. 2011; Dopson et al. 2016; Rea et al. 2018). *Pseudomonas* spp. detected from the Swiss Au particles are known to produce metabolic products or chelating compounds to solubilise metals such as Fe and Al from clay-like minerals as well as form Ag and Au nanoparticles from metal complexes (Klaus-Joerger et al. 2001). The presence of microorganisms that form Ag-nanoparticle may possibly aid in the cumulative Ag dissolution event that leads to the formation of high purity Au (Reith et al. 2013). The reduction of trace elements incorporated in the clays and uptake of trace elements from this matrix by siderophores and metal chelators produced by the microorganisms can mediate the release of trace elements to the surrounding environment, thus increasing mobility not only of Au but also of other metals (Mueller 2015). Other organisms under group five are the metal-detoxifying and ligand-producing *Acinetobacter* spp. which can produce gluconic acid that was reported as an organic complexant with Fe; iron being present on clay-like minerals on the surface of Au particles. Copper-resistant organisms detected on Au particles from the UK like *Rubrivivax* spp., can further handle toxic transition metal cations to protect the general population present in the biofilm community (Azzouzi et al. 2013; Rea et al. 2018).

The 'helper' community in the process of Au transformation include group one, or the primary colonisers like the gram-positive *Terribacillus* sp., *Staphylococcus* spp. and *Streptococcus* spp. These organisms can easily overcome the negatively charged surface of Au particles and associated clay-like minerals to colonise the Au surface (Paget 1992; Rea et al. 2016). It is also important to include group two organisms such as *Aeromonas* spp. and *Arcobacter* spp., which can set the framework of the biofilm community by EPS production to regulate water retention (Mueller 2015). The biofilm also requires key organisms that can drive the C, N and S production under group three. These include *Methylibium* spp., a facultative

methylotroph, present also in Finland and the UK Au particles (Rea et al. 2018; Reith et al. 2018). The progression of multi-species biofilm recruitment leads to the formation of larger polymeric groups as more complex components are produced (Alimova et al. 2009; Flemming and Wingender 2010). Organisms detected that could produce and recycle biomass in the biofilm under group four include *Polaromonas* spp. which was also detected in Au particles from the UK and Finnish sites. New usable carbon sources and organics are formed with the help of *Acinetobacter* spp., which are involved in the degradation of aromatic and organic compounds. Lastly, dispersal cells are released into a biofilm with the help of antagonistic microorganisms such as *Cystobacter* spp. and *Lysobacter* spp., under group six. These dispersal cells further increase the mobility of Au and trace metals as it detaches from the biofilm community.

3.6. Conclusion

Gold particles from Switzerland showed a progressive transformation of Au from proximal to distal sites in terms of physical and biogeochemical factors. Variable degrees of rounding from mechanical reshaping due to transport and sedimentation processes is evident from the margins of the Au-Ag particles. This study confirmed that the biogeochemical and physical transformation of the Au collectively dictates the overall Au transformation and biofilm composition. The contribution of fluvial transport and biogeochemical factors are highly dependent on the landscape scenario wherein a high-energy fluvial system is dominated by physical transformation whereas low-energy fluvial environments will undergo less physical (de)formations but more bio(geo)chemical transformation. A strong link between microbial assemblage on Au particles and the degree of transformation from biogeochemical and physical factors is established. An increase in bio(geo)chemical transformation leads to specialization of the biofilm community capable of overcoming metal toxicity. The increase in physical reshaping could encourage the formation of compact, stable biofilm by altering metabolic behaviour and possibly inducing genetic transformations.

Chapter IV

Transformation of gold: Regional mineralisation directs the stage of (bio)geochemical and physical transformations of placer gold

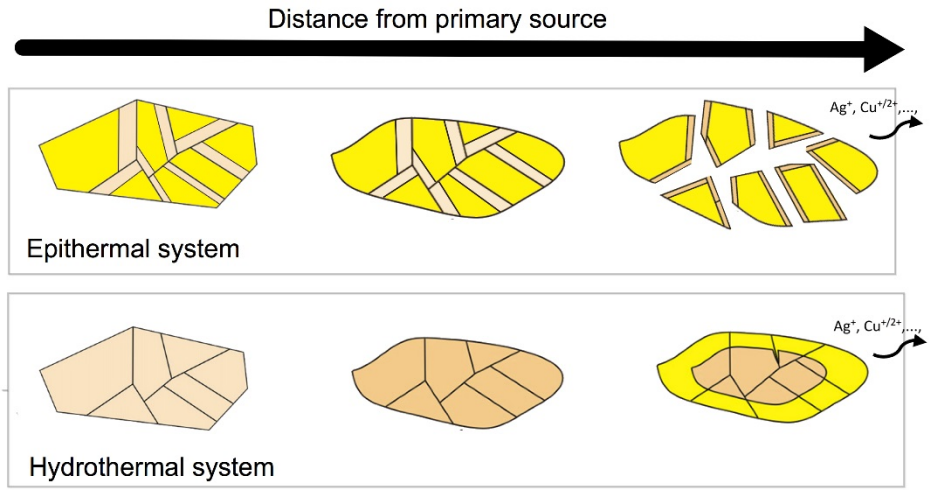

Statement of Authorship

Title of Paper	Regional mineralization directs the stage of (bio)geochemical and physical transformations of placer gold
Publication Status	☐ Published ☐ Accepted for Publication ☐ Submitted for Publication ☑ Unpublished and Unsubmitted work written in manuscript style
Publication Details	Rea MA, Shuster J*, Reith F (in preparation) Regional mineralization directs the stage of (bio)geochemical and physical transformations of placer gold. Science of the Total Environment.

Principal Author

Name of Principal Author (Candidate)	Maria Angelica Rea
Contribution to the Paper	Run samples in SEM and microprobe and performed PCR amplification for Illumina Sequencing. Performed final bioinformatic data processing. Interpreted results. Wrote the manuscript and created the figures and tables
Overall percentage (%)	70
Certification:	This paper reports on original research I conducted during the period of my Higher Degree by Research candidature and is not subject to any obligations or contractual agreements with a third party that would constrain its inclusion in this thesis. I am the primary author of this paper.
Signature	Date 15.05.18

Co-Author Contributions

By signing the Statement of Authorship, each author certifies that:

i. the candidate's stated contribution to the publication is accurate (as detailed above);

ii. permission is granted for the candidate in include the publication in the thesis; and

iii. the sum of all co-author contributions is equal to 100% less the candidate's stated contribution.

Name of Co-Author	Dr. Jeremiah Shuster
Contribution to the Paper	Assisted in data interpretation and analysis. Advised and edited the manuscript. Acting corresponding author.
Signature	Date 15/05/2018

Name of Co-Author	A/Prof. Frank Reith
Contribution to the Paper	Collected the samples and conceived the study design. Supervised the development of work. Manuscript evaluation and editing.
Signature	Date 17/05/2018

REGIONAL MINERALISATION DIRECTS THE STAGE OF BIOGEOCHEMICAL AND PHYSICAL TRANSFORMATIONS OF PLACER GOLD

In the previous chapters, the transformation of Au particles and its effect on the biofilm community composition (Chapter 2) and the influence of physical transport to transformation (Chapter 3) were shown. In this chapter, we highlight the link of regional mineralisation and deposit style to the fate of gold in the transformation process.

Research highlights

- Gold particles from German placers are physically and biogeochemically transformed.
- Biogeochemical gold cycling occurs in epithermal and hydrothermal systems
- Biofilms with putative traits that aids in Au mobility exist on placer gold particles from epithermal systems.
- The direction of the biogeochemical transformation of placer gold is driven by the mineralisation of the primary source.
- (Bio)geochemical signature is distinct for epithermal systems whereas physical signatures are preserved in hydrothermal systems.

4.1. Abstract

Epithermal gold deposits are a common type of primary source for gold (Au) where 2.8×10^4 kg of annual gold is produced from epithermal deposits in the Asia Pacific region. This type of deposit is becoming increasingly important due to their contribution to global Au mining production. Our current understanding of Au biogeochemical cycling and the stages of Au particle transformation is largely based on placer Au particles weathered from hydrothermal deposits, another type of primary source. To date, no study has compared physical, chemical and biological factors that contribute to the transformation of Au particles derived from epithermal and hydrothermal deposits. We hypothesise that the mineralisation system of the

primary source is the overarching factor that dictates the "next step" in the physical and (bio)geochemical transformation processes and ultimately the transformation stages and biofilm community composition. For this study, Au samples were collected from a placer deposit sourced from sites with an otherwise comparable environmental setting from an epithermal system (Eisenberg, Germany) and from a placer deposit sourced from a hydrothermal system (Thuringia and Black Forest, Germany). There were no distinctions in the physical morphologies and textures attributed to mechanical reshaping and sedimentation processes suggesting that Au derived from epithermal sources behaved in a similar way to Au derived from hydrothermal sources. Microprobe analysis confirmed that (bio)geochemical conditions of epithermal and hydrothermal deposits produce different Au:Ag mineralisation resulting in a different Au-Ag 'fabric'. This supports the concept that the mineralisation of the primary deposit determines the Au:Ag ratios of the Au particles as well as the internal fabric, *i.e.,* crystallographic orientation within the Au particle. The process of Au/Ag dissolution and Au re-precipitation evident on Au particles accentuates the Ag-fabrics and Au-rich clusters on Au particles from epithermal systems and increases the depth of Au-rims formed on Au particles from classical hydrothermal systems. These textures are often associated with polymorphic coatings and remnants of biofilm material, with some extracellular polymeric substances (EPS) containing nanoparticles. Microbial communities were dominated by Proteobacteria (763 OTUs, 49.7 % of the total sequencing reads), wherein Au from epithermal systems has 531 OTUs and 67.8 % of total reads and classical hydrothermal system has 435 OTUs with 29.3 % reads. Canonical analysis of principal coordinates (CAP) showed a significant separation between mineralisation of primary source and microbial community composition ($P < 0.01$). This suggests that the biofilm community "senses" the difference in Au particle fabric and therefore directs Au transformation differently. Thus, the mineralisation fabric showed a strong influence on the microbial community composition, biofilm development and ultimately the transformation of Au in the placer environment.

4.2. Introduction

Gold mined throughout history amounts to over 150,000 tonnes, of which over 2.8 X 10^4 kg of gold (Au) is produced annually from epithermal deposits in the Asia Pacific region (World Gold Council 2018). Despite the significant growth of mine production over the last decade and the tapping of different deposit styles, new substantial discoveries are increasingly rare. Additionally, production levels are

increasingly constrained since accessible ore deposits have already been exploited (Konopa et al. 2015). Epithermal deposits are a significant component of the global Au mining production and are characterised as having high-grade variability, relatively low tonnages and narrow vein geometry often extending over large lateral areas (White and Hedenquist 1995; Konopa et al. 2015). Epithermal deposits are formed from fluids that accumulated by depressurisation and associated processes such as boiling, fluid mixing, cooling and wall rock interaction in low temperature 150–300°C at a shallow depth (<1500 m). Epithermal deposits are characterised based on the sulphidation state of mineralisation where low-sulphidation systems involve mineralising fluids connected to active geothermal systems mixed in a near-neutral pH and reduced fluids whereas high-sulphidation systems are associated with acidic and oxidised fluids formed adjacent to young volcanoes with the oxidised fluid leaching the host rocks (Rye 1993). Examples of known epithermal deposits are the Emperor Mine in Fiji, the Pajingo in Australia, Exciban Au mine in the Philippines, Aginskoe Deposit in Central Kamchatka and the Eisenberg Korbach in Germany (Lehrberger 1995; White and Hedenquist 1995). Hydrothermal deposits are formed from magmatic circulating fluids at maximum depth and high temperature (300 – 500 °C) that undergo physicochemical reactions to reduce the fluid. This leads to gold deposition between the veins and other transcrustal contractional structures to form hydrothermal vein deposits.

Gold accumulates progressively in sedimentary settings through transport by river, gravity and weathered material near the point of formation and often becomes concentrated within depressions such as river bends which forms secondary deposits in placer settings (Knight et al. 1999; Hough et al. 2007; Townley et al. 2003; Craw et al. 2017). In these placer settings, Au is exposed to episodes of deformation and metamorphosis that remobilised the materials either by physical or chemical means. Physical modification of Au particles by hydrodynamic shear force and mechanical weathering deforms particles leading to Ag depletion via deformation-induced recrystallisation as particles are transported away from the source. Therefore, the morphology and chemistry of particles can be used as indicators of distance travelled and determination of the primary sources (Knight et al. 1999; Townley et al. 2003; Hough et al. 2007; Kerr et al. 2016; Craw 2017). Primary physical surface features include the presence of primary cavities, growth hillocks, microlaminations and deformation textures, *e.g.*, striated surfaces and rare pulled filaments (Kinnunen 1996). Secondary surface features are formed on Au when in contact with mineral and rock edges such as corners of quartz fragments and pebbles or soft minerals forming

mechanical markings such as shaving scratches, rimmed pits, rippled grooves and impact pits. These morphological transformations are easily abraded and destroyed during sedimentological and erosional processes (DiLabio 1991; Kinnunen 1996).

Biogeochemical transformation involves the dissolution and re-precipitation of Ag and Au. These processes, along with re-mobilisation, can occur under various environmental conditions. Therefore, Au particles from placer deposits could have a varying composition and chemical signature as they could be derived from different primary sources. The difference in the biogeochemical signatures can be used as a tool for identifying the deposit type, erosion level and ultimately as a vector for pointing towards undiscovered Au deposits in basement rocks (Knight et al. 1999; Chapman et al. 2011; Chapman and Mortensen 2016). These biogeochemical processes are ligand-dependent to merit the formation of soluble Au-complexes (Zammit et al. 2015). Gold-thiosulphate complexation involves oxidation of pyrite and arsenopyrite to produce thiosulphate that can mobilise micro-particulate Au (Craw and Lilly 2016). The process involves the initial dissolution of micro-particulate Au from oxidizing pyrite followed by re-precipitation of mobilised Au as the thiosulphate ions undergo further oxidation. Gold is also soluble as bisulphide complex ($Au(HS)_2^-$) occurring in a weakly reducing condition which when destabilised by minor pH or redox state leads to deposition of Au. The ongoing turnover of pH from acidic to ambient circumneutral gradient can facilitate periodic destabilisation and reformation of Au-complexing ligands and remobilisation of Au (Craw 2017). This process may occur via inorganic reactions or mediated and rate-enhanced by microbial processes. (Bio)oxidation of highly reactive manganese (Mn) oxides mobilises Au that is sorbed in the Mn- and Fe-minerals (Ta et al. 2014, 2015). Microorganisms can excrete Au-complexing ligands (*e.g.*, organic acids, thiosulphate and cyanide) and develop Au-specific biogeochemical response to reductively precipitate mobile Au-complexes (Reith et al. 2013). Furthermore, microbes can form an acidic microenvironment in an oxidizing mineral surface to create a micro-scale formation of ions and secondary minerals (Chen et al. 2014; Dockrey et al. 2014). Indeed, the microbial community on the surface of Au particles forms a dynamic biofilm assemblage with diverse metabolic capabilities which were described and grouped into six bacterial groups based on their putative contribution in biofilm development (Rea et al. 2016). A range of detected OTUs was classified based on biofilm establishment involving abilities for surface conditioning and attachment, production of EPS and autoaggregation, nutrient cycling and metabolic turnover of materials, as well as reduction of bacterial load by dispersal cells and most importantly, Au mobilisation (Rea et al. 2016).

Sulphate-reducing bacteria (SRB) may drive the micro-formation of Au-bearing sedimentary pyrite (Reith et al. 2007) and metabolically degrade thiosulphate as well as Au-thiosulphate complexes (Kaji and McElroy 1959). Destabilised Au-thiosulphate complexes can be directly incorporated into the pyrite lattices as well as be ab/adsorbed by the bacterial cells (Lengke and Southam 2006) that liberate Au from Au-hosting minerals. Other microbial mechanisms that are directly involved in metal detoxification are the production of a metallophore to convert toxic Au(I/III) to metallic Au(0) by *Delftia acidovorans* (Johnston et al. 2013) and the reductive precipitation of toxic Au-complex by co-utilisation of metal resistance against copper to form metallic Au by metallophilic *Cupriavidus metallidurans* (Reith et al. 2009; Wiesemann et al. 2013, 2017). Other mechanisms include Au nanoparticles by charge capping, extracellular reduction, or formation of biopolymers that bind to metal ions by *Stenotrophomonas* sp., *Pseudomonas* spp. and *Herbaspirillum* sp., respectively (Lodewyckx et al. 2001; Husseiny et al. 2007; Nangia et al. 2009). In addition, microorganisms can initiate degradation of cyano-metal complexes using a nitrile-degrading enzyme present in extracellular lipid complexes of *Acinetobacter* spp., *Burkholderia* spp. and *Methylobacterium* sp., to destabilise/re-precipitate Au/Ag-cyanide complexes (Finnegan et al. 1991; Vu et al. 2013). Increasing evidence in bacteria-Au interactions supports the role of microorganisms in Au transformation which strongly supports the well-established biogeochemical cycle of Au (Reith and McPhail 2007; Fairbrother et al. 2012).

Studying Au particles from sites with a comparable environmental setting which originated from different primary deposit style addresses the concept of whether the source of primary deposit or the environment influences the transformation. The complex interplay between physical reshaping and (bio)geochemical factors was previously linked to stages of Au transformation (Chapter 3) and biofilm formation focusing on placer particles that originated from the hydrothermal systems, providing more insights into the biogeochemical cycling of Au (Chapter 2; Reith et al. 2010, 2012a, 2018; Shuster et al. 2015, 2017a; Rea et al. 2016, 2018). However, no study at present has linked the morphology and composition of the Au particles and microbial community composition to the influence of the primary deposit style, *i.e.*, epithermal system *vs.* classical hydrothermal system. Thus, our study hypothesised that Au from epithermal deposit styles will have a distinct Au composition, physical transformation and biofilm community from the strong influence of mineralisation system. For the purpose of this study, we define placer Au derived from hydrothermal deposits as the classical

system and placer Au derived from epithermal deposits as non-classical system. Therefore, the aims of this study are to: (i) differentiate the biogeochemical transformation of placer Au particles from epithermal systems and compare it to hydrothermal system under similar climatic and environmental conditions; (ii) evaluate the presence of secondary Au morphotypes indicative of biogeochemical Au cycling; (iii) assess the transformation stages of placer Au in Germany based on biogeochemical and physical processes; and (iv) assess the presence of biofilms on Au particles. To achieve this, Au particles were collected from placer deposits derived from an epithermal source and compared to placer Au derived from classical hydrothermal sources in Germany.

4.3. Field Sites

Germany's climate is temperate, with cold, cloudy, wet winters and moderately warm summers (Kottek et al. 2006). The majority of the country is covered with arable land or forestry and woodlands dominated by beeches, oaks and other deciduous trees. Spruce and fir trees predominate in the upper mountains, while pine and larch are found in sandy soil. Germany stretches from the Alps in the south, to the North Sea in the northwest and Baltic Sea in the northeast. The majority of south-central Germany is composed of hilly and mountainous landscapes formed by ancient volcanic activities (Oberthür et al. 2016). A description of each site is summarised in Table 4.1.

4.3.1. Eisenberg, Iron Mountain, Korbach

The Eisenberg or Korbach gold deposit is located in the Eastern part of the Rhenish Schist mountains (Ramdohr 1932). The most important rivers in Eisenberg are the Fulda and Eder Rivers in the north, the Lahn in the central part, and the Main and Rhine in the south. The Rhine borders Eisenberg on the southwest and the Alt-Rhein runs through Eisenberg. The bedrock geology of the Eisenberg Iron Mountains is characterised by low-grade metamorphic rocks of sedimentary origin altered in the course of low-grade to high-grade regional metamorphism and by the subsequent replacement of acidic igneous rocks (Dill 2008). The geology of the surroundings of Korbach is derived from the rocks of the Lower Carboniferous of the Rhenish Slate Mountains and the Permian and Mesozoic rocks of the Hessen valley. Korbach is located on the western edge of the Hessen Valley built up by rocks of the Zechstein and the Lower Red Sandstone. In the west of Eisenberg are the Lower Carboniferous shales and greywacke in Kulm facies of the Rhenish Mountains and in the east are the

Table 4.1 – Summary of geological and environmental conditions at the sampling localities in Germany.

Sample name/site	Coordinates	Host geology and primary mineralisation
Eisenberg (EI)[a]	N51° 14.575' E8° 49.764'	Low-epithermal deposit; eastern Rhenish Schist mountain; bedrock geology is characterised by low-grade metamorphic rocks altered by regional metamorphism and by the subsequent replacement of acidic igneous rocks, gold appears as irregular, dendritic or in isometric form.
Eisenberg_Alte Wiese1 (MA1)	N51° 14.170' E8° 53.016'	
Eisenberg_Alte Wiese2 (MA2)	N51° 15.728' E8° 49.722'	
Silberkuhle (SK)[a,b]	N51° 16.749' E8° 48.575'	Low-epithermal deposit; Rhenish Schist mountain; gold mineralisation in the Zechstein conglomerate
Rhena(RH)	N51° 16.672' E8° 47.394'	Low-epithermal deposit; Au is associated with pyrite and arsenopyrite, Low Ag and low mineral intergrown with gold, heavy minerals are derived from high-grade metamorphic rocks and from erosion of granites and pegatites
Anraff (AN) [a,b]	N51° 08.898, E009° 09.058	
Itter (I1)	N51° 11.706, E008° 53.316	
Tannenhöhe (TN)[a,b]	N51°05'28.0" E9°19'19.6"	
Niedermoehlen (NM) [a,b]	N51° 06.760, E009° 21.352	
Fritzlar 3 (EN) [a,b]	N51° 06.565, E009° 15.604	
Sulzburg (SB)	N47°49'32.2"E 7°44'12.0"	Hydrothermal vein deposit; western slope of the Black Forest; predominantly made up of metamorphic rocks and granites, gold-bearing conglomerates carry barite and sphalerite as well as pyrite
Rheinzabern (RZ)	N49°05'50.8" E8°18'28.1"	
Grumpenbach (GR)	N50° 26.670' E11° 03.812'	Hydrothermal vein deposit; Thuringia forest; polymetallic ore comes in clay shales and quartzite with low-grade gold quartz vein as well as gold sulphide mineralisation
Schwarza (SW)	N50° 38.544' E11° 11.702'	

[a] in addition to placer Au particles, soil samples were obtained

[b] in addition to placer Au particles, water samples were obtained

Meineringhausen rocks of Lower Red Sandstone at the Westheimer. The rocks that border Ense in the Rhenish Mountains is characterised by the Saxon fracture tectonics. The lithology of Ense covers the Zechstein sequences above the subsurface of Variscan rocks of the Lower Carboniferous surrounded by the sandstone in the higher Zechstein and parts of the Lower Red Sandstone in the form of the Korbach or Calvörde sequence. The rocks of the Zechstein are formed from the carbonates with layers of predominantly reddish silt and claystone as well as rare anhydrite layers. The fossil deposit of Korbach is associated with fossil formation seen today as shell prints associated with pyrite. Towards the end of the Carboniferous period, lateral force and uplift acted on the layers of shale rocks as the seawater drained out of the reservoirs. This orogeny is an essential prerequisite for the formation of the Eisenberg Au deposit. The magmatic fluid of up to 300°C permeated Eisenberg and neighbouring mountains causing changes in the rocks and minerals especially pyrite, calcite and lead-selenium ore. In the primary deposits of Eisenberg, Au appears as an

irregular, dendritic or in isometric form. Another primary Au mineralisation around Eisenberg is the Zechstein conglomerate of the north Silberkuhle (SK). Around 1.5 tonnes of Au were mined from the Eisenberg which started in the 11th Century and continued to the 12th to 14th Century seen today as old workings, trial pits and large open cuts. Traces of this mining operation is still evident on the mountain from collapsed and filled shafts and extensive Au panning areas out of the weathered rocks of the mountain slopes. From the 11th to 16th Centuries, the eluvial Au on the eastern slope of Eisenberg was panned and continually harvested from deposits in tributaries. The long fluvial transport of up to 50 km transformed the larger Au particles by mechanical action, appearing to be hammered and deformed flat. Some placer Au seen today at the Eder river also suggest that they represent a derivative of the primary deposit from the Eisenberg system.

4.3.2. Thuringia Forest, Southern Germany

In the southern parts of Germany, placer deposits have been worked mainly in Thuringia forest along the major rivers. Forested hills and mountains extend in an irregular line from the neighbourhood of Eisenach in west-central Thuringia south-eastward to the Bavarian frontier, where it merges with the Franconian Forest. This range encloses valleys and glens, as well as forests, chiefly of pines and firs. The area is composed of uplifted and deformed metamorphic and igneous rocks that divide the flat sedimentary plains to the northeast. It consists of a large fault block in Hercynian orientation, which is made up of sandstones and conglomerates of Permian age in the Eisenach trough located in the western part, followed by granites and gneisses of the Ruhlaer Kristallin formation during early Paleozoic. These were uplifted in the Permian era, with the conglomerates, sandstones and abundant volcanic rocks such as rhyolites and andesites of the Oberhof trough. The Ordovician units of the Phycodes and Frauenbach series show stratiform deposits and former magnetite placer in the form of clearly demarcated bands within quartzite. A variety of low-grade Au quartz vein, as well as Au sulphide mineralisation, occurs in the Thuringian forest (Morávek 1992). The ore comes in clay shales and quartzite of the Ordovician series and contains Au of up to 100 ppb (Meinel 1993). The release of placer Au from anomalous Au-containing metasediments is suspected to originate from this polymetallic ore in Thuringia. Several Au mineralisation and related old workings were also previously reported where deposits often occur in close association with Paleozoic volcanics of basaltic composition (Lehrberger 1995).

4.3.3. Black Forest, Southwest Germany

Sulzburg site (SB) is situated in the Black forest, southwest of Germany, a large forested mountain range bound by the Rhine valley to the west and south. The variety of geological features and strong tectonic stresses such as intrusion of the edge granite, the collision of two tectonic units and Permian volcanism in Paleozoic time as well as the formation of the Rhine trench in the Tertiary Period have developed the present landscape setting. The bedrock geology is composed of pre-variscic gneiss, deformed granite and red porphyry in the north, and conglomerates and slate of the Kulm (Upper Devonian-Lower Carboniferous) of the so-called Badenweiler-Lenzkirch zone in the south. Heavy minerals such as Au, monazite, zircon and almandine are found in the area, some of which come from the conglomerates and the acidic magmatite composed of marginal granite and porphyries. Gold in the carbon conglomerate contains as much as 18–20 g Au per ton. The observation that Au-bearing conglomerates carry barite and sphalerite, as well as pyrite, supports a hydrothermal origin of the Au.

Rheinzabern (RZ) is located about 180 km from Sulzburg in a hydrothermal system. The geological development of the Rhine River drainage system is complex with a number of changes in paleocurrent directions related to tectonic movements in the Earth's crust since the late Pliocene and the older Pleistocene (Hagedorn and Boenigk 2008). The northern part of the Alpine mountain range is characterised by limestones and folded molasse sediments, mantling a crystalline core zone (Dill et al. 2009). A derivation of much of the sedimentary load and heavy minerals of the Rhine River from the mountain chains of the Alps is apparent, as are additional sources from the surrounding areas (for the upper Rhine, especially the Black Forest and the Vosges mountains). The Rhine River sediments have at least 25 different heavy minerals including, garnet, hematite, zircon, rutile, monazite as well as rarer platinum, cinnabar, galena, arsenopyrite and both detrital, partly corroded pyrite and authigenic pyrite (Ramdohr 1965). The majority of the heavy minerals in the Rhine River appears to originate from rock successions of Variscan age. The fluvial gravels and terrace sediments along the Rhine valley from Basel to Mainz have been worked since prehistoric times with >300 kg of Au recovered in the 18th to 19th century; however, no extensive mining was done due to low Au contents of the gravels (Oberthür et al. 2016). Primary Au sources most probably originated in the Swiss Alps and some contributions from tertiary sediments in the Molasse zone along the northern Alps (Lehrberger 1995) and were supplied by the subsidiary rivers Emme and Aare. The Aare River, entering into the Rhine after Lake Constance may have

transported heavy minerals into the upper Rhine especially the Black Forest and the Vosges mountains including material from ultramafic zones within the pre-Alpine Aar and Gotthard massifs.

4.4. Materials and methods

4.4.1. Description of field sites and sampling

To assess the biogeochemical and physical transformation of Au, particles were collected near old mine workings and active modern streams from 14 sites in Germany: 10 from the Eisenberg system and representative proximal and distal Au particles from two sites in Thuringia and two in the Black forest (Fig. 4.1; Table 4.1). Sites were chosen based on the contrasting source of deposit style, *e.g.,* low-epithermal deposits and hydrothermal deposit at increasing distance from primary mineralisation (Fig. 4.1). The Au particles were collected and preserved following the field sterile method described by Reith et al. (2010) to minimise contamination and preserve the integrity of the biofilm communities. Samples were stored in sterile saline solution and transported on ice (micro-analysis) or frozen (DNA-analysis) to the laboratory.

4.4.2. Electron microscopy and microanalyses

Samples of Au particles for electron microscopy (EM) were washed with sterile 0.9 wt. % NaCl solution and kept in EM fixative (4 wt.% paraformaldehyde, 1.25 wt.% glutaraldehyde in PBS, 4 wt.% sucrose, pH 7.2). Gold particles were processed and dehydrated using a series of ethanol washes (70 vol. %, 90 vol. % and 100 vol. %; 2 x 10 min each) and placed in 100 wt. % hexamethyldisilazane (HDMS) to preserve microbial cells and biofilms (Fratesi et al. 2004). Samples were analysed using FEG-SEM in secondary electron (SE) and backscattered electron (BSE) modes at 5 kV and 20 kV (Quanta™ 450 FEG Environmental SEM with EDS detectors, FEI, Netherlands). Selected Au particles were analysed further using a FIB-SEM (Helios NanoLab DualBeam, FEI, Netherlands). The surface of selected Au particles was FIB-milled using 20 kV and 9.7 pA and images of the surface features and sections were collected at 2 to 20 kV and 86 pA. Spectra and maps of the Au surface were collected using energy dispersive X-ray (EDX) spectrometry; elements mapped were Au, Ag, Fe, C, N, O, Si, Ti, Al, Ga, Mg, Na, K and Pt.

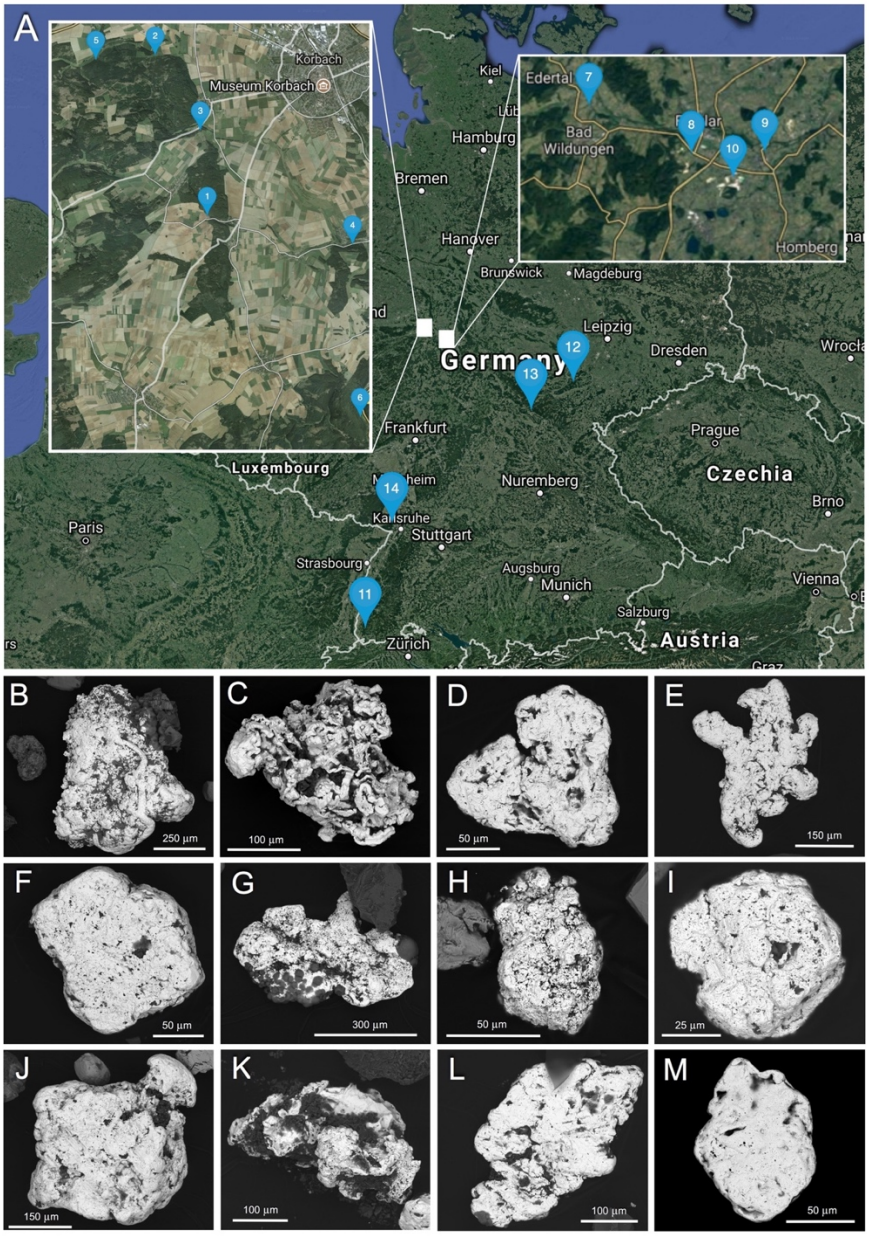

Figure 4.1 **(A)** Sampling locations; **(B–M)** typical morphologies of Au particles from the Germany. Shown are backscattered electron (BSE) micrographs of Au particles that are irregular (**B** from EI, **C** from SK, **E** from RH, **G** from I1, **J** from SB, **L** from GR and **K** from SW) to slightly rounded (**D** from MA1; **F** from AN, **H** from NM), well-rounded (**I** from EN) and flattened Au (**M** from RZ) Au particles. Gold particles are derived from placer systems where Au may have originated from epithermal deposit style **(B–I)** and hydrothermal deposit styles **(J–M)**.

Quantitative maps of element compositions of particles were collected using an electron microprobe, with a total of 72 samples quantitatively mapped. Samples were set in epoxy resin and polished with 1 μm diamond paste. The Cameca™ SXFive Microprobe is equipped with five wavelength dispersive (WLD) X-Ray detectors, with PeakSite software for instrument control and Probe for EPMA™ software for data acquisition and processing. The Au particles were mapped at 20 kV and 200 nA and analysed for (detection limits in parenthesis in wt. %): Au (0.24). Ag (0.09), S

(0.025), Fe (0.06), Cu (0.11). These elements were calibrated using minerals and pure metal standards from Astimex and P&H. Copper (Cu), iron (Fe), sulphur (S), silver (Ag) and Au were calibrated using pure chalcopyrite ($CuFeS_2$), telluride (Ag_2Te) and pure Au foil, respectively. EPMA™ produces a full quantitative, pixel by pixel calculation by using the Mean Atomic Number background correction (Donovan and Tingle 1996) in CalcImage, and false colorisation and formatting in Surfer10™ to produce net intensity, detection limit map and totals image.

4.4.3. Chemical analyses of soil and water samples

To further assess physicochemical parameters from the epithermal system, soil and water samples from the Eisenberg system were analysed following methods published in Reith et al. (2012b) and Brugger et al. (2013). Soil samples were homogenised in a ring mill and water samples were filtered through 0.45 μm sterile syringe filters. Waters and soil analysis (1:5 soil : H_2O) was conducted for pH, electrical conductivity and alkalinity. The total carbon (C) and nitrogen (N) in soils were determined using a Leco CNS-2000. Dissolved carbon (DC) in waters was determined by Skalar Formacs HT TOC/TN Analyser. Inorganic carbon was acidified to form CO_2 prior to detection and dissolved organic carbon (DOC) was determined by the difference between total and inorganic C. Flow analysis and spectrometric detection was used to determine ammonia-nitrogen (NH_4-N) according to ISO 11732. Nitrate- and nitrite-N were determined using the automated segmented flow analyser (Alpkem Flow Solution 3) at 540 nm. A Dionex ICS-2500 ion chromatography system with 2 mm AS16 anion separation column was used to measure anions in waters (F^-, Cl^-, NO_2^-, Br^-, NO_3^-, SO_4^{2-} and PO_4^{3-}). Soils were microwave-digested in concentrated *aqua regia* before analysis for elemental concentrations. Element concentrations of microwave-digested soils and water samples were determined using inductively coupled plasma – optical emission spectrometry (ICP–OES) on a Spectro ARCOS analyser (Spectro Analytical Instruments, Kleve, Germany). Trace and ultratrace elements were analysed by inductively coupled plasma – mass spectrometry (ICP–MS; Agilent 7700, Japan).

4.4.4. Biomolecular and statistical analyses

Microbial communities resident on 45 Au particles were assessed using nested 16S rRNA polymerase chain reaction (PCR) combined with next generation sequencing (NGS) using the Illumina MiSeq platform (Reith et al. 2010; Bissett et al. 2016). The universal primers 27F (Lane 1991) and 1492R (Osborn et al. 2000) were used for initial PCR amplification of 16S rRNA genes (Reith et al. 2010), further amplified using primers 27F and 519R (Lane 1991; Lane et al. 1985) and sequenced at the Australian Genome Research Facility (AGRF, Melbourne, Australia). DNA amplifications were performed in an Applied Biosystems Veriti™ Thermal Cycler (Applied Biosystems, California, USA). Amplicons were checked in 1.5 % agarose gel with Gel Red (Biotium Inc., Hayward, CA, USA) 1:10,000 (v/v) and run at a constant voltage of 80 V for 1 h. Procedures for sequencing, open OTU picking and assignment are detailed in Bissett et al. (2016).

Statistical analysis was conducted using the PRIMER-6 software package with the PERMANOVA+ add-on (Clarke and Warwick 2001; Anderson et al. 2008). Similarity matrices using the Bray-Curtis method were established on the fourth root transformed abundance data (Bray and Curtis 1957). Canonical analysis of principal coordinates (CAP) was used to assess the community differences between progressively transformed placer Au particles from the epithermal and hydrothermal system. CAP analyses were conducted based on the respective resemblance matrices with the significance of test effects determined against null distributions based on 9999 permutations (random allocations) of samples.

Functional analysis of 16S amplicons was performed using the default settings of Phylogenetic Investigation of Communities by Reconstruction of Unobserved States (PICRUSt) genome prediction software [http://picrust.github.io/picrust/] version 1.1.0 (Langille et al. 2013). PICRUSt allows metagenome functional predictions by multiplying each normalised OTU abundance by the predicted functional trait abundance to produce a table of functions analysed for Kyoto Encyclopaedia of Genes and Genomes (KEGG) orthologues. PICRUSt predictions were carried out on closed OTUs at the 97% similarity level and were mapped to the Greengenes ver. 13.5 database for functional prediction. Functional predictions were assigned up to Tier 3 for all genes. Organismal system and human disease pathway were deleted as it is poorly relevant to the environmental samples in this study.

4.5. Results

4.5.1. Morphology and composition of gold particles and particle surfaces

The Au particles collected from 14 sites in Germany measured 50 μm up to 1 mm. Samples from Eisenberg (EI) and Silberkuhle (SK) displayed an irregular and angular morphology with sharp irregular outline and topography (Fig. 4.1B, C). Gold from majority of the sites, both in the classical hydrothermal and non-classical epithermal systems are slightly elongated with variable degrees of rounding, some with thick folded edges while others have irregular protrusions (Fig. 4.1). Mechanical reshaping from transport and sedimentation processes is visible on all placer Au particles as the Au particle margins appear smoothed but with rougher and coarser surface textures. The surface of proximal Au particles on both the epithermal and classical hydrothermal system has numerous deep cavities, some with the presence of silicates and associated minerals. Most of the Au particles, particularly from sites along the Eisenberg system have not been significantly flattened (Fig. 4.1D–G). Flattened Au particles were only observed from Rheinzabern (RZ) of the classical system. These Au particles that were collected >10 km from the source occurred as disks with bent corners as well as roundish particles with smooth folded margins typical of Au particles obtained from distal sources. There were no distinguishing physical features between placer Au derived from epithermal and classical hydrothermal system.

Microprobe maps of Au particles show a prominent difference in the overall elemental composition of Au particles. Representative maps of Au derived from epithermal systems display Au core of >99.0 wt. % with Ag fabrics traversing irregularly shaped Au-cluster (Fig. 4.2). This is different compared to the microprobe maps in classical systems showing a typical homogenous Au-Ag alloy in the core of the Au particles and progressive formation of a Au-rich high-purity rim (>99.0 wt. %) (Fig. 4.3). There is an absence of Au-rim formation on Au particles from the epithermal system whereas Au-rich rim formation is particularly distinct in Au particles from the classical system (Fig. 4.2, 4.3). Particle maps from the same site in the classical system exhibit little variations in Au-Ag ratio whereas particles from the Eisenberg system has Au particles with <2 wt. % Ag, a large population of Au particles with some variation between 5 up to 15 % Ag and a distinct high-Ag group with greater than 20 % Ag (Fig. 4.2, 4.3).

Proximal Au particles from the epithermal system have thick belts (Fig. 4.4A–B) that run in different directions across the Au particle; the belts have minimal signs

of physical damage from transport (Fig. 4.4). FIB-milled sections of a thick belt overlying the bulk of the Au particle shows polycrystalline textures of the belt (Fig. 4.4C–E) with a long strip of Au crystal cutting diagonally across the belt's core (Fig. 4.4C). Successive replacement of Au crystals is observed here as high purity μ-crystalline Au traverses from core to rim of the Au particle (Fig 4.4D–E). Crystallinity at the core of the Au particle shows indistinct boundaries covered by a porous polycrystalline Au crystal (Fig. 4.4E). A common texture in the proximal epithermal

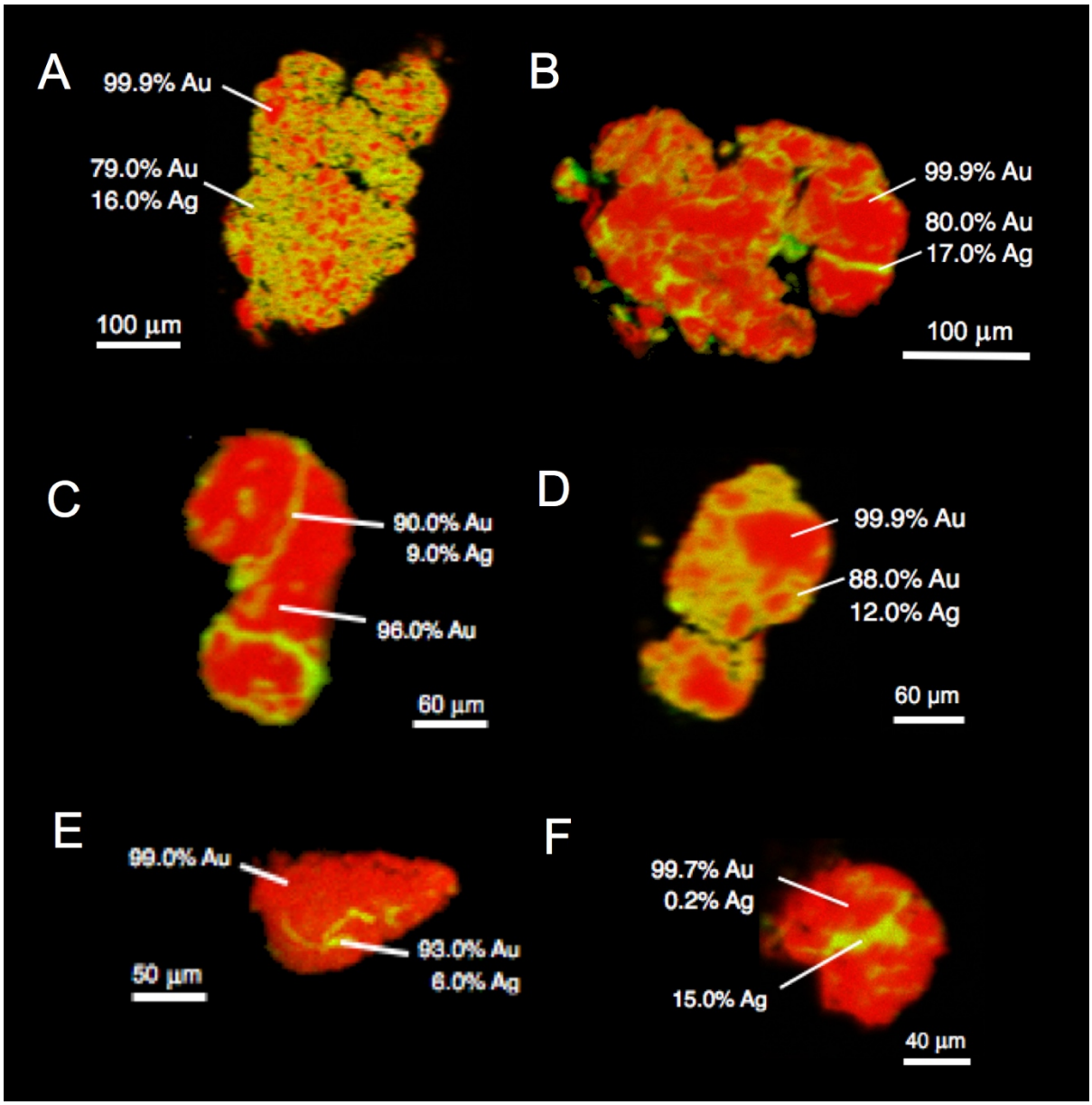

Figure 4.2 Electron microprobe maps, Au (red) and Ag (green), showing placer Au particles from epithermal deposit style. (**A–B**) Au particles composed of distinct Ag-rich fabrics an indicative of Ag dissolution; **(C–F)** increasingly transported Au particles leading to pinching off of smaller Au particles from the parent primary particle.

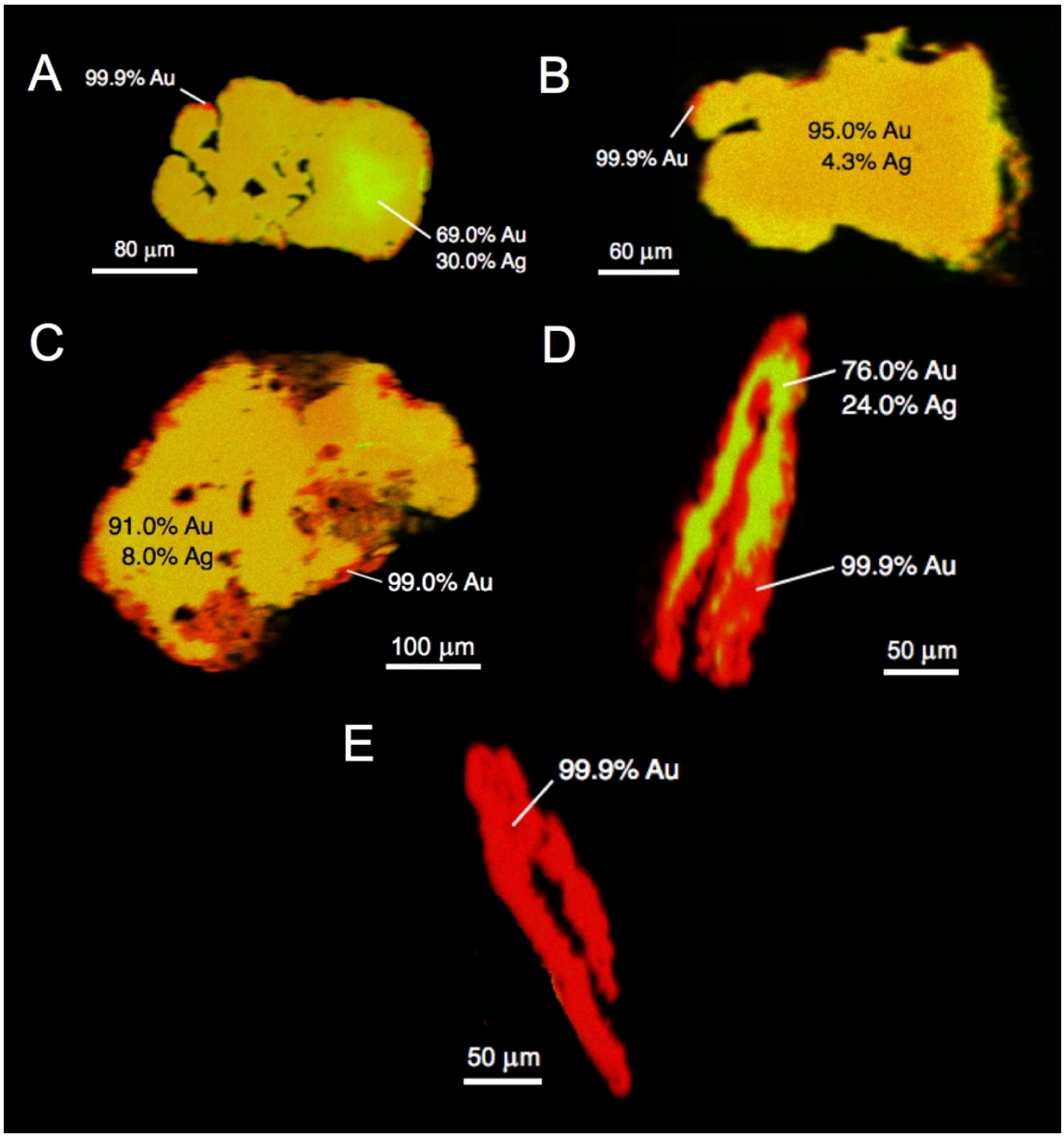

Figure 4.3 Electron microprobe maps, Au (red) and Ag (green), showing the classical progressive transformation of Au particles in placer settings. (**A–C**) Placer Au composed of a homogenous Au–Ag alloy with a partial layer of secondary high purity Au; **(D)** increasingly transformed Au particle with a continuous ring of Au-rich rim and **(E)** an entirely transformed Au particle from RZ**.**

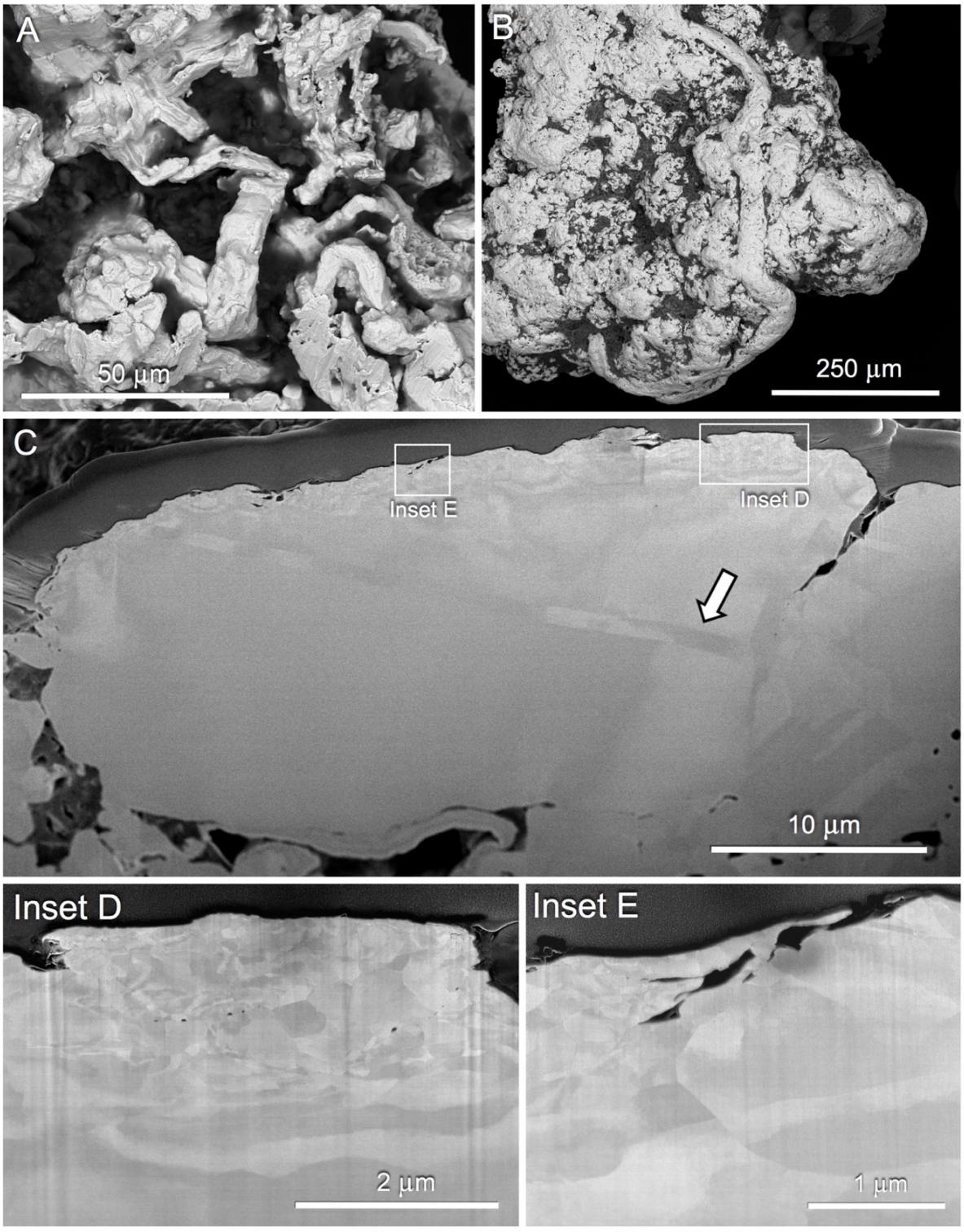

Figure 4.4 BSE micrographs showing **(A–B)** a belt-like band that appears to be fusing to the bulk of the Au particle and **(C–E)** a FIB-milled section of the belt-like band merging with the microcrystalline Au core; indistinct crystal boundaries at the core and distinct coarse crystals towards the surface.

Au particles are the terracing textures where Au sheets appear to stack on top of each other showing layered and stepped crystal formation (Fig. 4.5A–B). Rough surface

textures and overgrowth formation are prominent on Au surfaces. A section through the rough texture on a distal Au particle from epithermal system shows Au and Ag bands that are randomly oriented with respect to the Au particle surface with large gaps/spaces between a Au-rich crystal and a Au-Ag crystal (Fig. 4.5C–F, map inset). Towards the core of the Au particle, indistinct crystal boundaries with light and dark contrast of Au particles is observed with the difference in contrast based on the backscattering coefficient (Fig. 4.5GF–G). Gold particles with light contrast are Ag-poor and dark contrast are Ag-rich. Surface texture with multiple overgrowths was present on Au particles from both systems showing active chemical solubilisation on the 3D lattice of dissolution/re-precipitation overgrowth textures (Fig. 4.6A). The spongy-form lattice is covered/associated with polymorphic layers and remnants of biofilm material as well as EPS (Fig. 4.6B). FIB-milled cross-section revealed that the 3D lattice has overlain the polycrystalline core with distinct crystal boundaries; wherein the lattice is composed mostly of Au and the solid core made of Au-Ag (Fig. 4.6C-F, map inset). The spongy-form Au overgrowths showed interspersed EPS and remnants of carbonaceous materials (Fig. 4.6F). Other (bio)geochemical transformations observed in Au are precipitation textures wherein pitting and branching networks of Au are evident on the surface (Fig. 4.7A–C). FIB-milled sections showed cracks and pitting on the surface of the Au particle embedded in polymorphic layers with associated minerals (Fig. 4.7C, inset D, E). The observed pitting is possible cementation or compaction of the spongy form 3D Au overgrowth lattice deformed by mechanical transport.

Gold particles from both deposit styles have Au nanoparticles embedded on the polymorphic layer, and triangular plates of Au are covered entirely by a polymorphic layer (Fig. 4.8). Evidence of remnants of biofilm materials on the surface of the Au particles as well as individual prokaryotic cells attached to the surface of the Au and associated minerals were observed (Fig. 4.9).

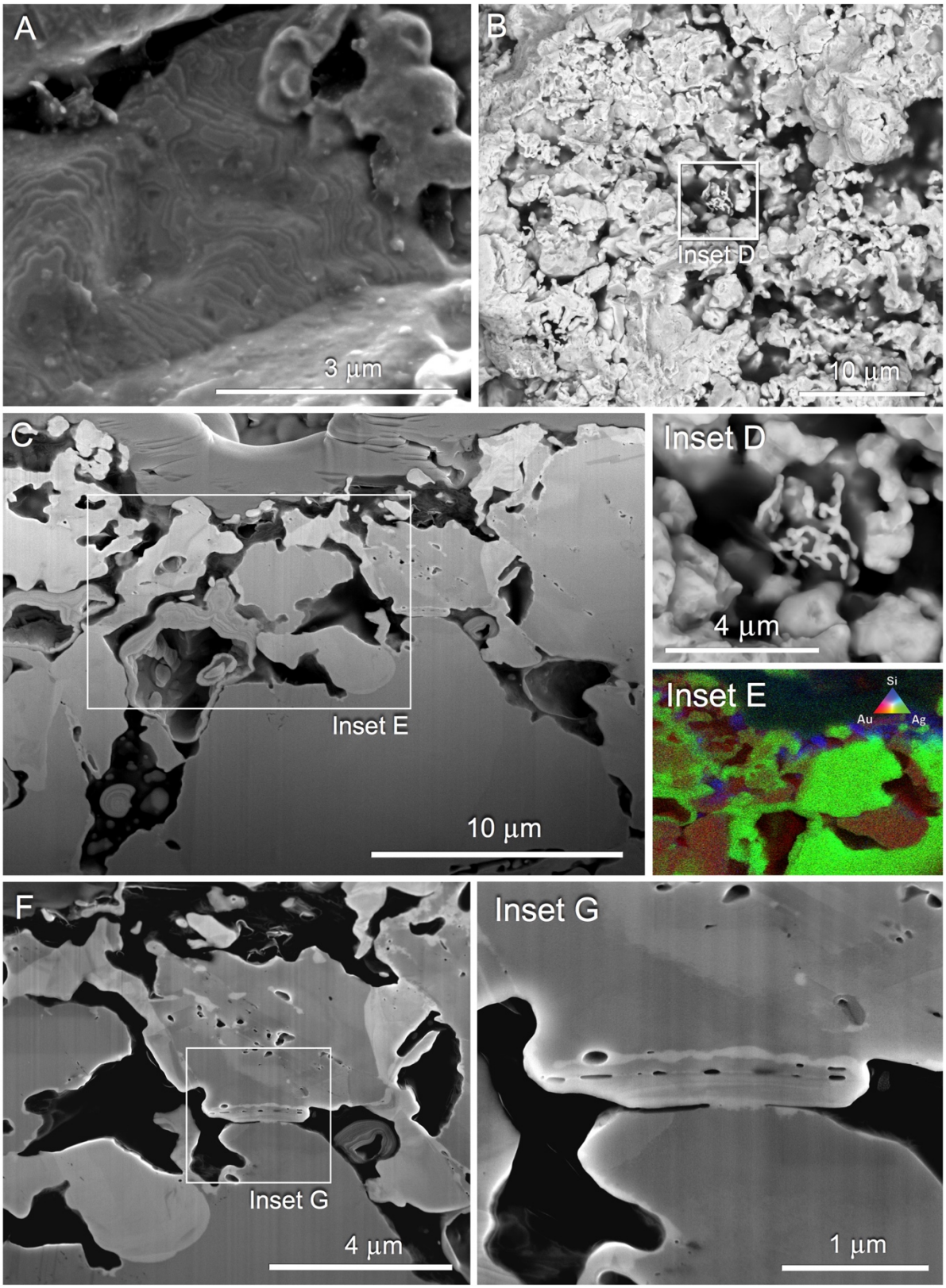

Figure 4.5 BSE and Secondary Electron (SE) micrographs of **(A)** terrace-like texture on Au particles. (**B**) Typical surface texture of epithermal Au particles with overgrowths **(C)** FIB-milled section of the internal crystal textures, **(inset D)** high magnification of the overgrowth texture that was FIB-milled in C, **(inset E)** Au-Ag-Si map of the internal crystal textures. **(F, inset G)** A microcrystalline texture of Au where dark contrast generally contains high Ag:Au ratio and light contrast for low Ag:Au ratio.

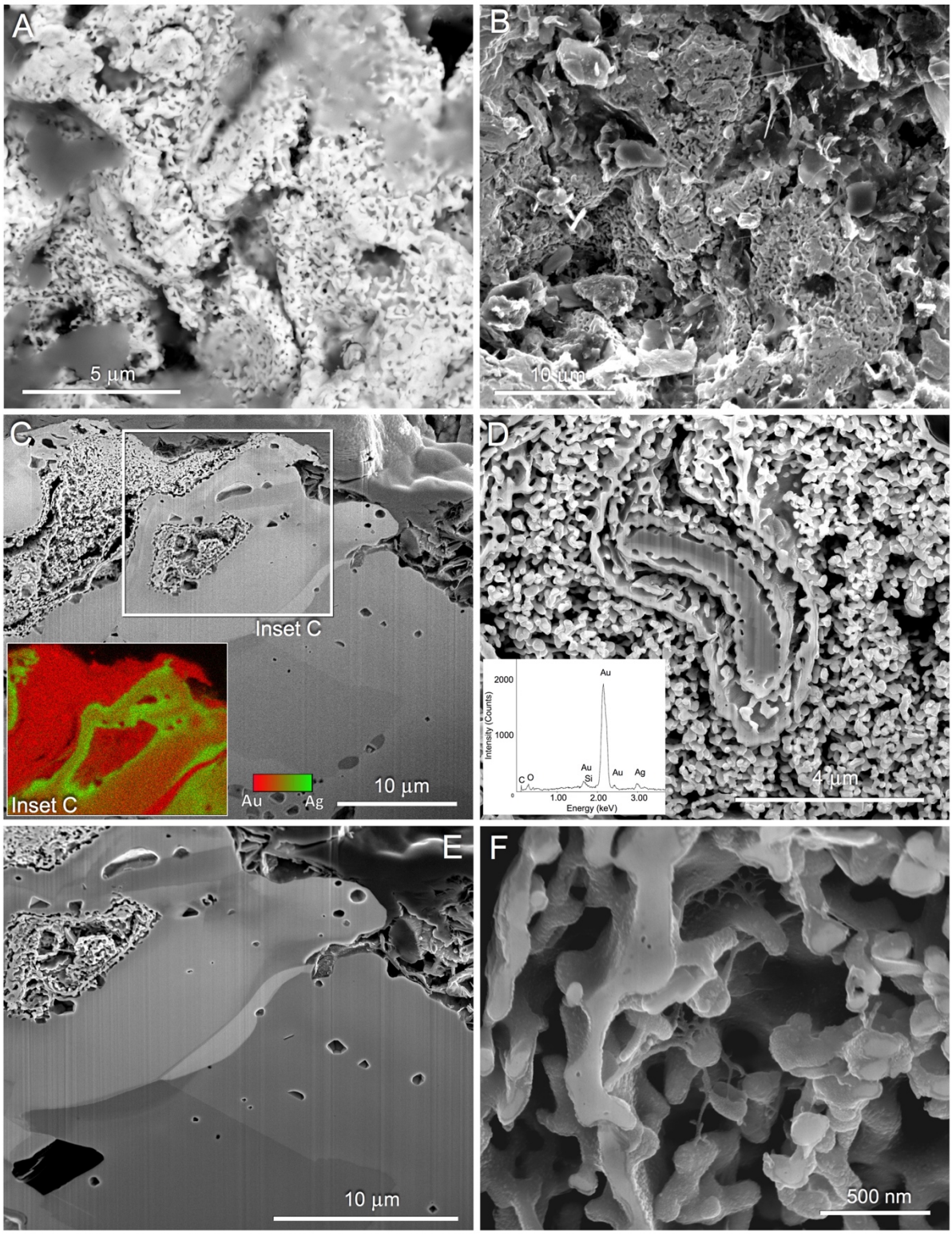

Figure 4.6 **(A)** A BSE micrograph and **(B)** SE micrograph of a characteristic Au particle surface showing dissolution/re-precipitation and of the surface feature covered with EPS layer; **(C)** FIB-milled section showing open crevices between microcrystalline overgrowths and **(inset C)** map of Au (red) and Ag (green) of spongy-form overgrowths; **(D–F)** high magnification view of the micron-scale overgrowths and the microcrystalline core of the Au particle.

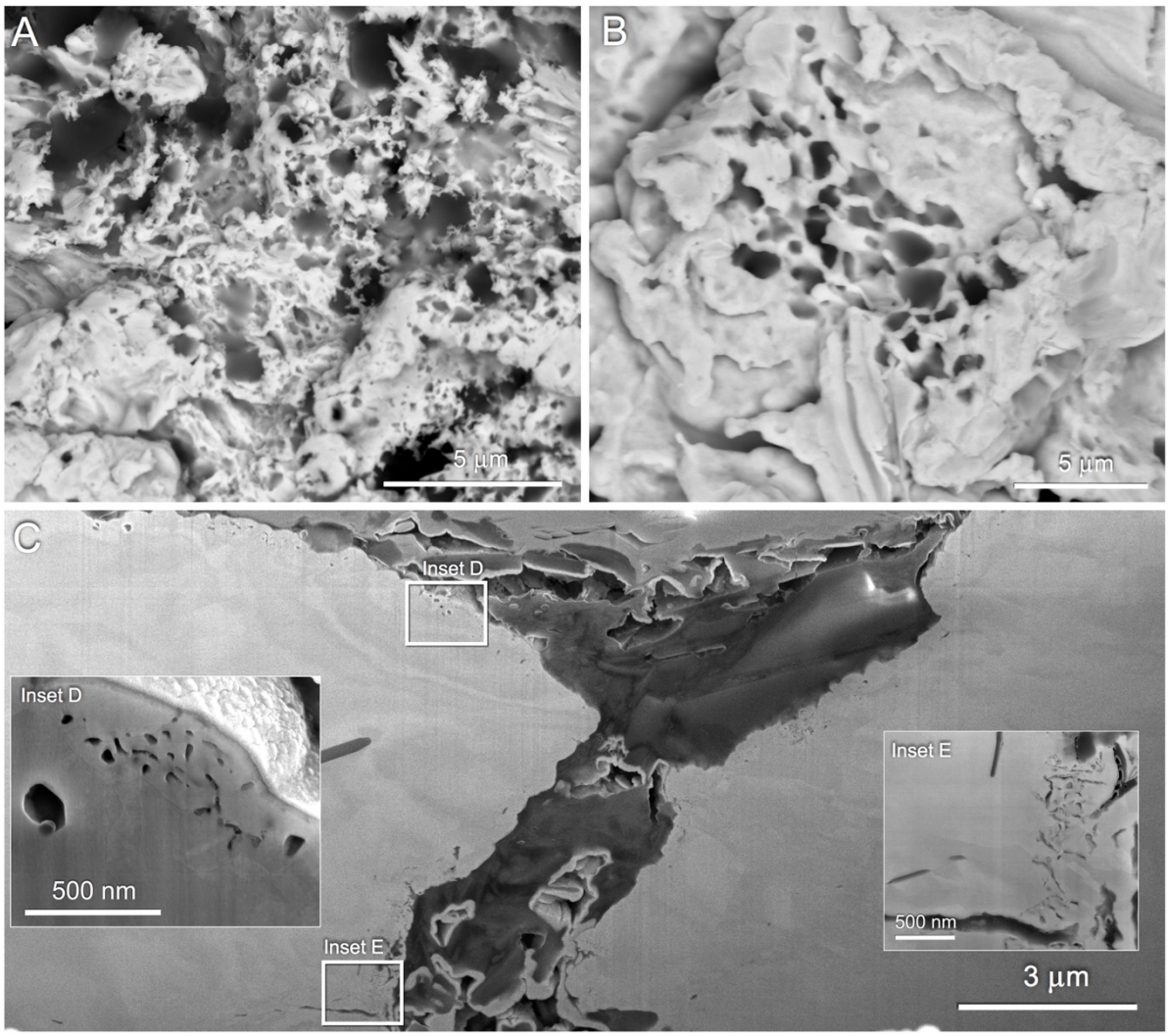

Figure 4.7 BSE micrographs of **(A–B)** Au feather-like bridges on the surface forming thin wires and **(C)** FIB-milled section and EPS layer showing open crevices, pits and cracks on the surface and **(Inset D, E)** smeared spongy-form overgrowths.

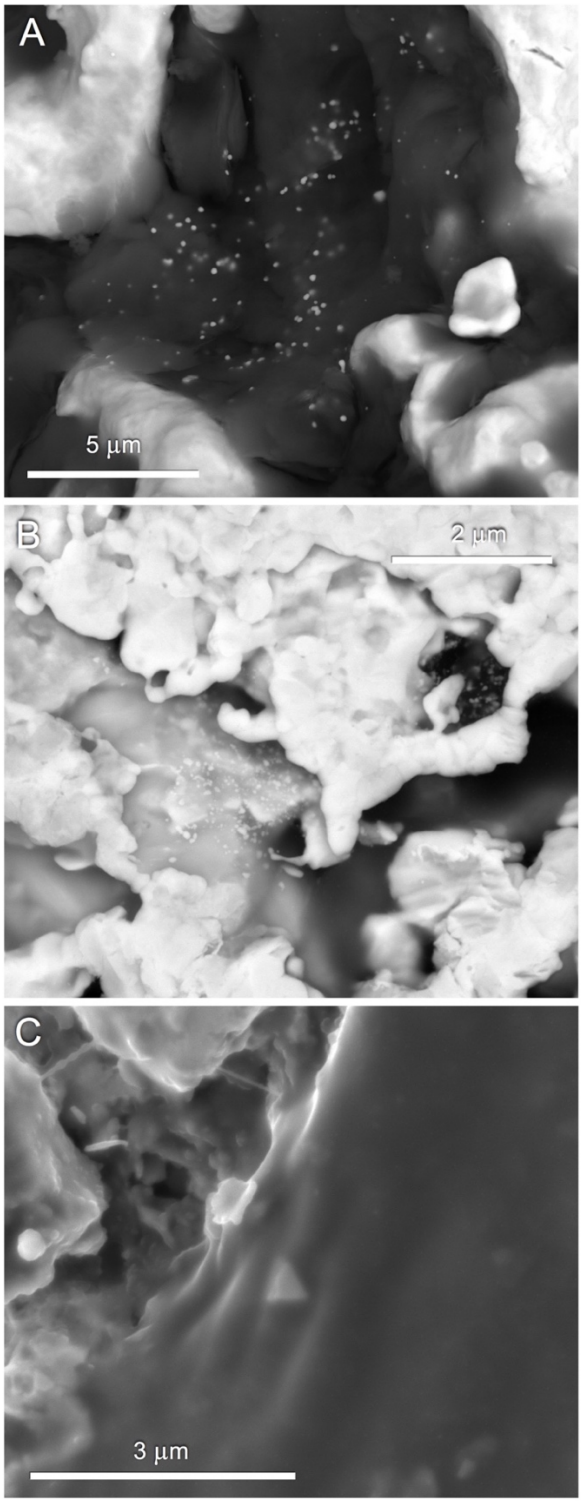

Figure 4.8 BSE and SE micrographs of secondary Au morphologies **(A–B)** nanophase Au and EPS cover associated with polymorphic layers and **(C)** triangular platy phase Au covered with EPS.

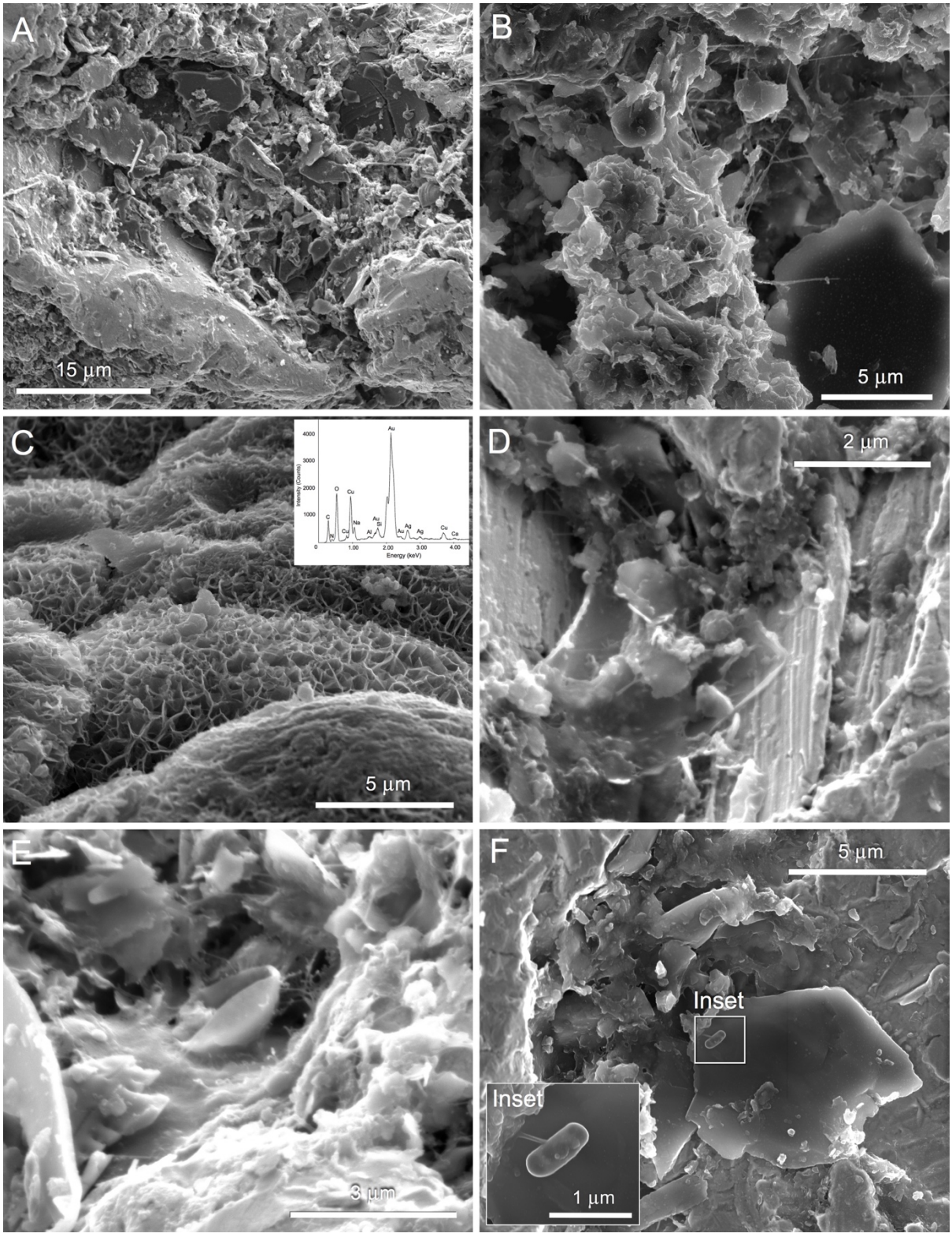

Figure 4.9 **(A–B)** SE micrographs of polymorphic layers on Au particle surfaces composed of nano- and micro-crystal minerals, cells and EPS; **(C)** SE micrograph and EDS of Au particle surface covered with copper globules associated with microbial remnants and (**D–F, inset**) SE micrograph of EPS and microbial cells.

4.5.2. Assessment of water and soil geochemistry

To provide a framework of physicochemical conditions in which Au mobility occurred in the Eisenberg system, five water and four soil samples from key sites were analysed for more than 50 parameters (Table 4.2). The water sample in the Eisenberg system contained 1.3–2.0 $\mu g.L^{-1}$ mobile Au and <0.05 $\mu g.L^{-1}$ of Ag, with S, V, As, Cu, Ni and Zn were also detected (Table 4.2). Surface waters had a pH range of 6.6–7.65 (Table 4.2). NPOC TOC in waters range from 0.1 and 14.0 $mg.L^{-1}$, whereas TN is between 0.6 to 4.0 $mg.L^{-1}$ up to 16 $mg.L^{-1}$ of chloride and 61 $mg.L^{-1}$ of sulphate were detected (Table 4.2). Soil samples contained Au and Ag concentrations of up to 450 and 360 $\mu g.kg^{-1}$ of soil, respectively. The highest concentration of Au (*i.e.*, 450.0 $\mu g/kg$) was detected in SK (Table 4.3). Other elements such as As, Sb, Zn, Pb, Se, K and Cu were also detected (Table 4.3). Soil-pH does not vary greatly with a range of 6.3 up to 6.8. Sulphur content was highest in the proximal site SK with 2231 $mg.kg^{-1}$ and much lower concentrations were detected in all other samples ranging from 60 up to 93 $mg.kg^{-1}$ samples. TOC is highest in SK with 14.0 % while other sites have <0.7 % TOC. TN was below 0.8 wt. % (Table 4.3).

4.5.3. Microbial communities on gold particles

To assess the composition of the biofilm communities on the surface of the particles, 16S RNA genes were amplified yielding 95.0 % of Au particles positive for target amplicons with more than 5.9 million reads from 45 selected Au particles. Across all sites, 1616 OTUs was detected with 48 to 737 OTUs for individual sites (Table 4.4; Fig. 4.10). Sites comprising the Eisenberg epithermal system has 1045 OTUs with >3.1 million reads, whereas sites in the classical hydrothermal system have 941 OTUs with >2.8 million sequencing reads.

The two mineralisation systems are both dominated by Proteobacteria, wherein the epithermal system has 531 OTUs with 67.8 % total reads and the classical system has 435 OTUs with 29.3 %. Particularly abundant are β-Proteobacteria for epithermal systems (186 OTUs, 28.6 %) and the classical hydrothermal system (182 OTUs, 14.3 %). Community composition in terms of OTU distribution is similar in both the epithermal and classical system; however, an abundance of the OTUs showed a difference most especially for α-, β-, γ-Proteobacteria as well as Acidobacteria and Actinobacteria (Fig. 4.10B).

Table 4.2 – Physicochemical conditions and element concentrations in Eisenberg water samples.

Parameter	Unit	EI	SK	AN	EN/TN/NM1 (Wehr Fritzlar)	EN/TN/NM2 (Affoldern)	Quantification Limit
Sample depth	n.a.[b]	Surface water	Surface water	Surface water	Surface water	Groundwater	n.a.
pH	n.a.	7.7	6.6	6.9	7.3	7.0	n.a.
Electrical conductivity	$dS.m^{-1}$	419.0	185.3	212.2	212.0	260.0	0.01
TOC	$mg.L^{-1}$	2.6	14.1	7.7	0.1	5.3	0.01
TN	$mg.L^{-1}$	2.1	2.8	4.0	0.6	4.0	0.01
NH_x-N	$mg.L^{-1}$	<0.005	0.5	0.3	0.3	0.2	0.005
NO_x-N	$mg.L^{-1}$	1.5	0.4	2.3	0.1	2.1	0.005
Total Alkalinity	$meq.L^{-1}$	1.6	0.9	0.7	1.3	0.8	0.01
Cl^-	$mg.L^{-1}$	12.0	2.6	16.3	13.7	15.8	2
NO_3^-	$mg.L^{-1}$	4.9	0.8	9.0	0.1	8.2	2
SO_4^{2-}	$mg.L^{-1}$	61.2	9.5	15.6	7.1	14.4	2
Ca	$mg.L^{-1}$	21.3	13.6	17.8	19.7	18.1	0.5
Fe	$mg.L^{-1}$	<0.1	<0.1	<0.1	<0.1	<0.1	0.1
K	$mg.L^{-1}$	2.3	2.3	2.3	1.9	2.1	0.5
Mg	$mg.L^{-1}$	30.9	5.5	6.1	6.7	5.9	0.5
Mn	$mg.L^{-1}$	<0.05	0.6	<0.05	1.1	<0.05	0.05
Na	$mg.L^{-1}$	5.8	3.4	10.1	10.0	10.0	0.5
S	$mg.L^{-1}$	24.1	4.0	6.2	2.9	5.9	0.5
As	$\mu g.L^{-1}$	0.4	0.8	0.5	0.8	0.7	0.05
Au	$\mu g.L^{-1}$	<0.5	<0.5	0.7	1.3	2.0	0.05
Cd	$\mu g.L^{-1}$	<0.05	<0.05	<0.05	2.6	<0.05	0.05
Sb	$\mu g.L^{-1}$	0.2	<0.1	<0.1	<0.1	<0.1	0.1
Co	$\mu g.L^{-1}$	0.2	0.2	<0.05	0.2	0.1	0.05
Ni	$\mu g.L^{-1}$	2.0	0.6	0.7	1.4	0.8	0.2
Cu	$\mu g.L^{-1}$	<1	<1	4.0	<1	4.0	1
Mo	$\mu g.L^{-1}$	1.9	0.2	<0.2	0.7	<0.2	0.2
Pb	$\mu g.L^{-1}$	<0.05	<0.05	<0.05	0.4	<0.05	0.05
Se	$\mu g.L^{-1}$	14.5	<0.2	0.3	<0.2	0.3	0.2
V	$\mu g.L^{-1}$	<0.05	0.1	0.1	0.1	0.1	0.05
Zn	$\mu g.L^{-1}$	0.9	2.0	1.2	40.6	2.7	0.2

[a]Notes: The fo ow ng e ements were ana ysed and data s ava ab e on request: Sc, Y, Pd, Ga, Ge, Ru, Re, Ta, Ce, Pr, Nd, Eu, Gd, Tb, Dy, Ho, Er, Tm, Yb, Lu, Re, Rh, Ir, Pt, Th.
[b] n.a., not app cab e
[c] A , Fe, Ag, Sn, Cr are be ow detect on m t

Table 4.3 – Physicochemical parameters, major element contents and concentration of Au and its pathfinder elements in soil samples from Eisenberg system.

Parameter	Unit	SK	AN	EN/TN/NM1 (Wehr Fritzlar)	EN/TN/NM2 (Affoldern)	Quantification Limit
pH	n.a.	6.9	7.4	7.1	7.7	n.a.
Electrical conductivity	$dS.m^{-1}$	50.4	26.1	14.2	19.6	0.01
Total C	%	14.1	0.7	0.2	0.3	0.01
Total N	%	0.8	0.1	0.0	0.0	0.01
Al	$mg.kg^{-1}$	36698.8	28038.2	17806.1	24717.6	100
Ca	$mg.kg^{-1}$	5874.0	4302.0	3131.9	2552.3	100
Fe	$mg.kg^{-1}$	36586.9	39366.5	25948.7	42357.5	100
K	$mg.kg^{-1}$	11070.9	8199.0	4878.3	6782.8	100
Mg	$mg.kg^{-1}$	6648.6	7150.5	5378.9	5392.2	100
Mn	$mg.kg^{-1}$	863.6	920.7	7591.4	1094.4	50
Na	$mg.kg^{-1}$	787.5	616.1	805.9	458.9	50
P	$mg.kg^{-1}$	1606.3	984.6	1277.5	738.7	100
S	$mg.kg^{-1}$	2231.3	93.1	61.1	60.5	40
Ag	$\mu g.kg^{-1}$	0.4	0.2	0.04	0.1	0.01
As	$mg.kg^{-1}$	11.5	14.2	10.1	15.2	0.1
Au	$\mu g.kg^{-1}$	0.5	<0.08	<0.08	<0.08	0.08
Cd	$mg.kg^{-1}$	1.4	0.2	0.1	0.2	0.1
Co	$mg.kg^{-1}$	11.0	12.7	10.6	20.8	0.2
Ni	$mg.kg^{-1}$	53.1	52.6	42.9	43.9	0.2
Cu	$mg.kg^{-1}$	39.3	33.6	15.8	27.4	0.2
Mo	$mg.kg^{-1}$	1.2	1.8	2.0	1.0	0.1
Pb	$mg.kg^{-1}$	32.3	19.9	10.5	15.6	0.1
Se	$mg.kg^{-1}$	2.4	0.5	<0.2	<0.2	0.2
Sn	$mg.kg^{-1}$	1.7	1.4	1.5	0.9	0.1
Sb	$mg.kg^{-1}$	0.8	1.1	0.5	1.0	0.1
V	$mg.kg^{-1}$	67.0	60.5	42.9	52.5	0.1
U	$mg.kg^{-1}$	1.3	0.4	1.1	1.2	0.1
Zn	$mg.kg^{-1}$	188.0	89.0	63.4	70.3	0.2

[a] Notes: The following elements were analysed, and data is available on request: Sc, Y, Pd, Ga, Ge, Ru, Re, Ta, La, Pr, Nd, Eu, Gd, Tb, Dy, Ho, Er, Tm, Yb, Lu, Re, Rh, Ir, Pt, Th.

[b] n.a., not applicable

Table 4.4 – Total reads, OTUs and characteristic features of gold particle from Germany collection sites.

	OTU Counts								
Phylum / Class	**G10 RZ**	**G11 SB**	**G13 SW**	**G4 GR**	**G14 TN**	**G15 EN**	**G1 AN**	**G5 I1**	**Total (different OTUs)**
Proteobacteria									
α-Proteobacteria	8	58	36	18	15	89	16	77	193
β-Proteobacteria	14	89	119	27	21	62	19	142	272
δ-Proteobacteria	n.d.	49	28	6	7	5	4	49	126
ε-Proteobacteria	1	n.d.	11	1	n.d.	5	n.d.	3	15
γ-Proteobacteria	10	31	38	7	5	46	8	68	136
TA18	n.d.	n.d.	n.d.	n.d.	n.d.	1	1	4	6
Proteobacteria_UC	9	9	10	9	9	10	9	13	15
Firmicutes									
Bacilli	1	2	2	1	1	7	n.d.	1	10
Clostridia	n.d.	n.d.	7	n.d.	n.d.	5	n.d.	3	15
[Thermi]	n.d.	1	2	1	n.d.	1	n.d.	1	6
AC1	n.d.	1	1	n.d.	1	n.d.	n.d.	n.d.	1
Acidobacteria	1	106	68	14	4	16	13	129	230
Actinobacteria	2	6	9	6	4	23	5	10	51
Armatimonadetes	n.d.	2	n.d.	1	n.d.	1	1	1	6
Bacteroidetes	n.d.	79	53	10	7	20	9	90	198
BRC1	n.d.	2	n.d.	n.d.	n.d.	n.d.	n.d.	n.d.	2
Chlorobi	n.d.	6	6	1	n.d.	n.d.	n.d.	11	17
Chloroflexi	n.d.	3	2	2	n.d.	6	4	16	30
Cyanobacteria	2	6	7	1	n.d.	2	2	8	15
Elusimicrobia	n.d.	n.d.	2	n.d.	n.d.	n.d.	n.d.	3	5
Fibrobacteres	n.d.	1	2	n.d.	n.d.	n.d.	n.d.	n.d.	3
Fusobacteria	n.d.	n.d.	1	n.d.	n.d.	n.d.	n.d.	n.d.	1
GAL15	n.d.	n.d.	n.d.	n.d.	n.d.	n.d.	n.d.	1	1
Gemmatimonadetes	n.d.	5	5	2	n.d.	1	n.d.	14	22
GN04	n.d.	1	n.d.	n.d.	n.d.	n.d.	n.d.	2	3
NC10	n.d.	n.d.	1	1	n.d.	n.d.	n.d.	2	3
Nitrospirae	n.d.	11	5	4	2	5	4	11	21
OD1	n.d.	n.d.	n.d.	n.d.	n.d.	1	1	1	3
OP11	n.d.	n.d.	2	n.d.	n.d.	1	n.d.	n.d.	3
OP3	n.d.	1	1	1	1	1	n.d.	1	5
Planctomycetes	n.d.	45	18	17	1	7	4	50	116
Spirochaetes	n.d.	1	n.d.	n.d.	n.d.	n.d.	n.d.	1	2
TM6	n.d.	1	3	1	n.d.	3	n.d.	5	13
TM7	n.d.	n.d.	4	1	n.d.	4	n.d.	3	10
Verrucomicrobia	n.d.	19	9	5	1	5	9	14	52
WPS-2	n.d.	n.d.	n.d.	n.d.	n.d.	1	n.d.	n.d.	1
WS3	n.d.	4	1	1	n.d.	n.d.	n.d.	3	8
Total OTUs	48	539	453	138	79	328	109	737	1616

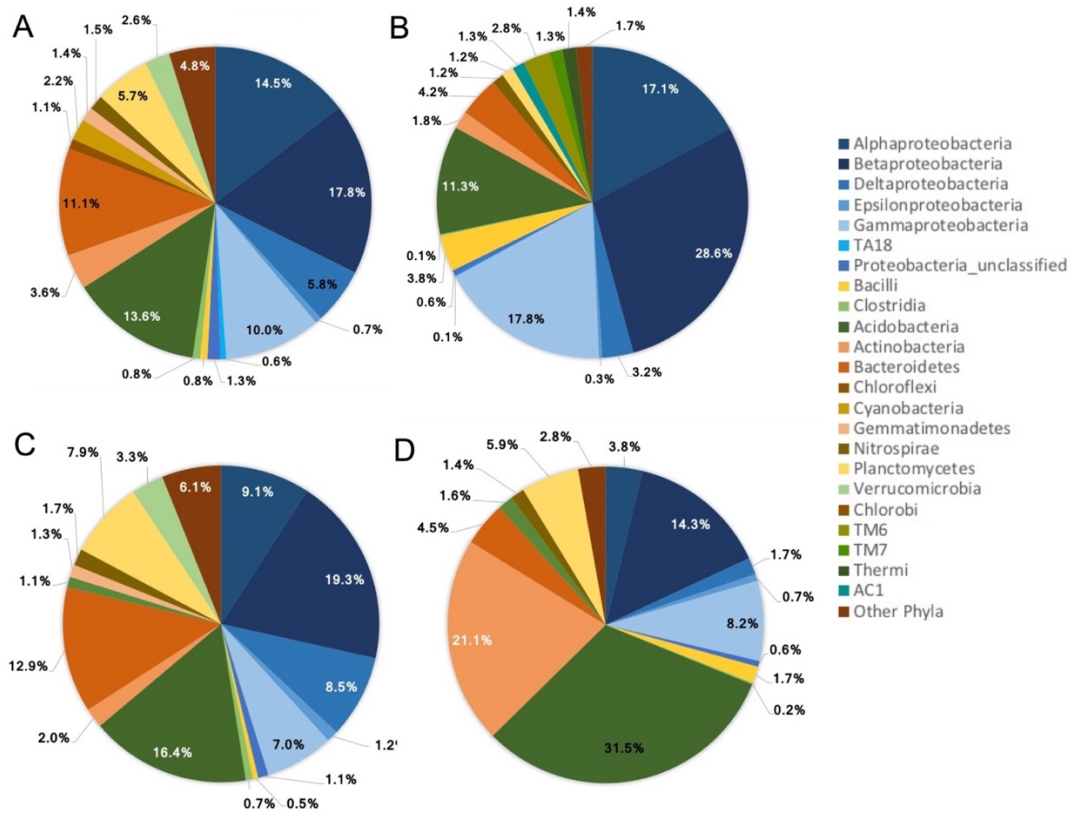

Figure 4.10 Composition of bacterial communities associated with Germany Au particles from **(A–B)** epithermal system in Eisenberg shown as % of OTUs and % of sequencing reads and **(C–D)** hydrothermal vein deposit system in the Thuringia and Black forest shown as % of OTUs and % of sequencing reads. Distribution of dominant bacteria phyla/classes based on the number of OTUs (1616) and >5 million sequencing reads; note: classes are shown for Proteobacteria and Firmicutes.

Across the Eisenberg system, the top 10 and top 20 most numerous OTUs (by number of reads) contributed between 51.7 to 76.8 % and 74.6 to 92.6 % of total reads detected, respectively. In the classical hydrothermal system, the top 10 and top 20 contributed between 25.1 to 98.1 % and 36.7 to 99.6 %, respectively, with values increasing from proximal to distal sites on both systems (Table 4.5). CAP analyses of community data illustrate a significant separation between microbial communities in the two deposit styles (Fig. 4.11A) and a strong separation between communities on proximal and distal epithermal sites (Fig. 4.11B).

In both epithermal and hydrothermal system, the greatest number of genes (>45 %) were assigned a function involved in metabolism among Tier 1 KO categories followed by genetic- and environmental information processing in the PICRUSt dataset (Fig. 4.11). Among Tier 3 KO categories, the greatest number of genes were assigned to transporters (5.3 % for Epithermal, 4.8 % for Hydrothermal) and ABC transporters (3.4 % Epithermal, 3.0 % Hydrothermal) followed by bacterial two-component systems, DNA repair and recombination proteins and bacterial motility proteins.

Table 4.5 – Total reads, OTUs and percentage of total reads covered by the most abundant OTUs for the gold particle from Germany.

Sample name/site	Total number of reads	Number of OTUs	Percentage of total reads covered by the 10 most abundant OTUs	Percentage of total reads covered by the 20 most abundant OTUs
Anraff (AN)	309715	109	56.9	77.4
Itter (I1)	636810	737	70.0	74.6
Tannenhöhe (TN)	307826	79	76.8	92.6
Fritzlar 3 (EN)	1924495	328	51.7	69.7
Sulzburg (SB)	331976	539	25.1	36.7
Rheinzabern (RZ)	940006	48	98.1	99.6
Schwarza (SW)	682970	453	58.4	70.4
Grumpenbach (GR)	865946	138	80.6	91.2

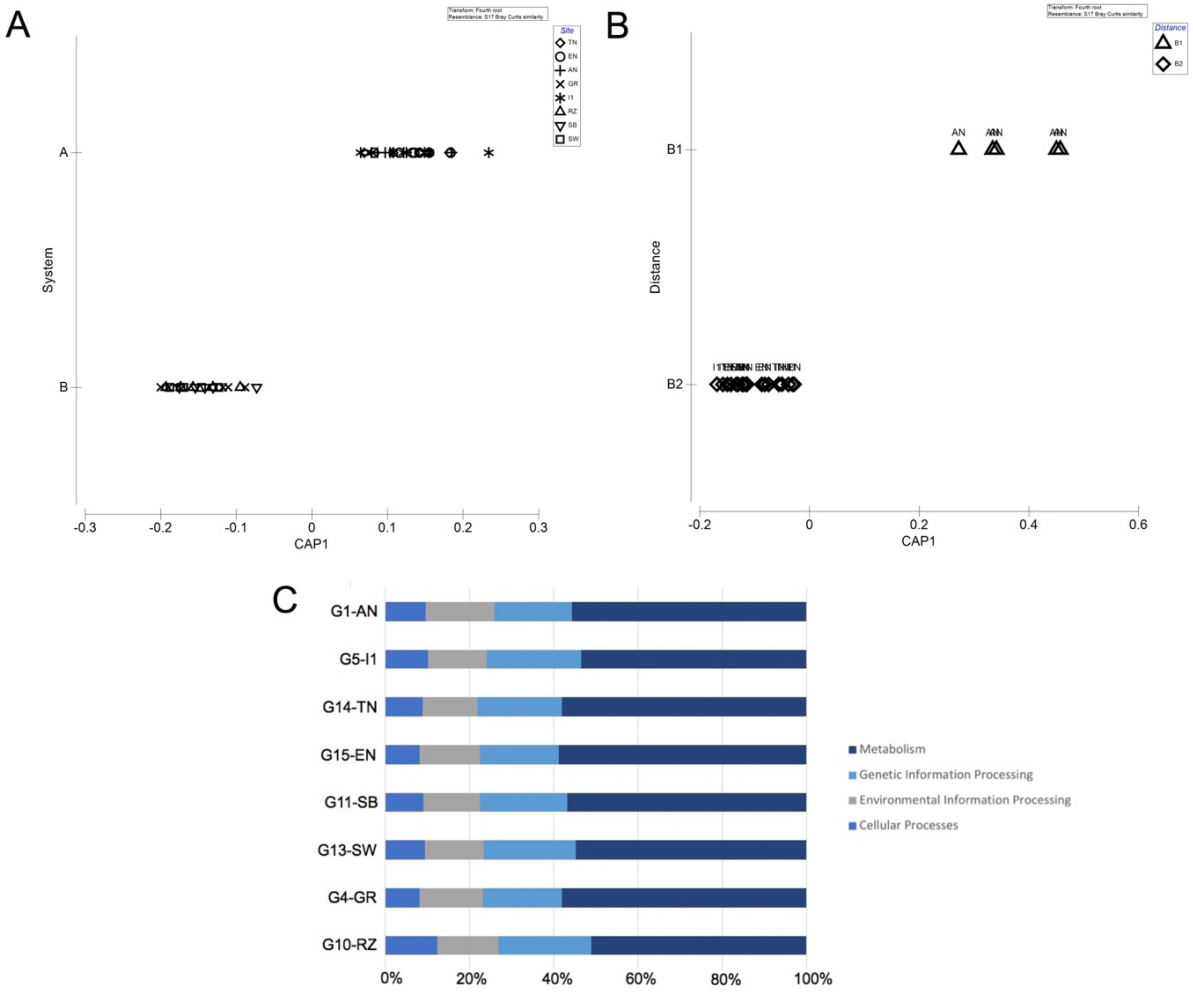

Figure 4.11 Ordination plot of the first two canonical axes produced by canonical analyses of principal coordinates (CAP) of MiSeq data analysed for differences in community assemblages in relation to **(A)** deposit styles and **(B)** distance of transport in the epithermal environment. **(C)** Percentages of tier1 PICRUSt functional predictions of identified OTUs. Note: Functional categories for organismal systems and human diseases were omitted.

4.6. Discussion

The progressive transformation and ultimately the biogeochemical cycle of Au has been demonstrated on numerous studies on Au that originated from the classical hydrothermal systems in different environmental and climatic settings (Fairbrother et al. 2012; Reith et al. 2010, 2018; Craw and Lilly 2016; Rea et al. 2016; Shuster et al. 2016). The main aim of the present study was to differentiate particle transformation of placer Au particles in terms of physical and (bio)geochemical transformation originating from an epithermal deposit style and compare it with the widely studied hydrothermal deposit style. The rim formation of distal Au particles from epithermal source showed Ag-rich rims instead of the pure-Au rim. This is a different (bio)geochemical signature that is not observed on Au from classical hydrothermal source. The Ag-rich fabrics cutting the Au-rich clusters in the epithermal system (Fig. 4.2) is formed based on the conditions of the primary source. In low-epithermal systems, fluid boiling occurs due to the drop in the confining pressures pushing the solution above the boiling zone where Au will drop out of the solution (White and Hedenquist 1995). Since the change in depth, pressure, temperature and pH is drastic in low-epithermal systems, very little time lapses before phase equilibrium is reached thus preserving the transition phase, *i.e.*, phase separation texture. In classical hydrothermal systems, materials are composed of undiluted acidic hydrothermal fluid circulating at alteration zones (Shanks and Thurston 2012). These alteration zones possibly allow longer phase transition, thereby achieving phase equilibrium before Au drops out of the solution, thus, leading to the observed homogenous Au-Ag alloy (Fig. 4.3).

Dendrite spikes and protrusions are minimal/absent on proximal Au particles from the Eisenberg epithermal system suggesting that the spikes have folded around the core of the Au particle resulting to the observed belt/bands indicative of transport (Fig 4.1A–B). Exposure of the primary Au particles to strong mechanical transport possibly detaches multiple small <150 μm diameter of Au-globule along the Ag fabric boundaries (Fig. 4.2). This explains the resulting texture and size of the collected Au particles distal to an epithermal source (Fig. 4.2.E, F). The release of small Au particles from whole Au particles was previously documented on Au from an epithermal deposit in Zimbabwe where multiple crystal impinged-faces were present as a result of recent detachment from another Au particle undergoing deformation/transport (Styles et al. 1995). The Ag-rich boundaries of the distal Au particles in the epithermal system and the presence of several populations of Au particles with varying Ag content that coexists in the same placer deposit further supports this impingement-

detachment occurrence, thus, implying that the Ag-rimmed distal Au particles were not transformed *in situ* but were freshly liberated Au particles with Ag-rims open for chemical attack (Webster 1986; Craw et al. 2017; Stewart et al. 2017). This leads to remobilisation of Ag and re-concentration of Au particles in placer deposits in favour of Ag expulsion and Au retention (Craw and Lilly 2016; Craw et al. 2017).

This recrystallisation processes occurring at the Ag-rich fabrics on the epithermal system and at the Au-rich particle margins on classical hydrothermal system is supported by the presence of overgrowth formation observed on both systems. This implies that similar chemical processes act on the Au particles resulting in deformation, chemical recycling and preferential expulsion of Ag; however, the observable effect of this chemical transformation varies depending on the primary mineralisation system. To elaborate on this, the gaps on FIB sections of a distal epithermal Au particle (Fig. 4.5C-G) is a possible result of the remobilisation of Ag with the gaps representing the area previously occupied by Ag-fabrics. This can also remobilise the Au back to the sedimentary system (Craw et al. 2017). The increase in the exposed surface area from the gaps may also aid in speeding the remobilisation of metals in an epithermal system. In the hydrothermal system, active chemical solubilisation, represented by the 3D lattice of dissolution/re-precipitation overgrowth textures in Au particles represents the lattice previously occupied by the remobilised Ag, preserved by the spongy form texture of the pure Au matrix (Fig. 4.6D). This is then followed by the smearing of the overgrowths back on to the nugget surface (Fig. 4.7C, inset D, E) by mechanical transport to enhance the nugget mass leading to increase in Au-rich rims in hydrothermal systems (Craw et al. 2017; Stewart et al. 2017).

The mobility and recycling of Au particles in the epithermal system in this study showed that the process is enhanced by the high concentrations of ligands and organic acids for Au complexation, nanoparticle formation and Ag dissolution (Zipperian et al. 1988). In this study, the high Au to Ag ratio in soils corresponds to the high Au and Ag composition of Au particles which signify mobilisation and dispersion of Au and Ag in the landscape where complexing ligands are available (Mann 1984; Shuster et al. 2017b; Reith et al. 2018). Furthermore, the high concentration of chloride detected in the water samples (Table 4.3), provides an abundant inorganic ligand for Au complexation (Usher et al. 2009), *e.g.*, formation of Au(III)-chloride complexes in surface water under circumneutral reducing conditions (Ta et al. 2014). The high sulphur content in soils and waters near the primary source of the epithermal system suggests an active dissolution, *e.g.*, pyrite and arsenopyrite,

often from host-rock fluid interaction during oxidation that contributes to the dissolved sulphate and sulphur-derivatives in surface waters and rocks. Temporary formation of intermediate metastable thiosulphate from oxidised pyrite leads to thiosulphate complexation that can mobilise Ag and Au (Webster and Mann 1984, Craw et al. 2015). Furthermore, thiosulphate can decompose during interaction with dissolved Fe(III) or oxidised progressively to sulphate. Both thiosulphate and bisulphide ion complexation in neutral to alkaline pH can mobilise Au and Ag (Webster 1986; Craw and Lilly 2016). Mobile Ag nanoparticles are labile under a range of soil conditions, further contributing to the dissolution and the formation of mobile ionic complexes (Levard et al. 2012).

Microorganisms were previously reported to contribute to the mobilisation of Au and Ag to some extent, via ligand coupled oxidation with inorganic or bioorganic ligands. The most numerous OTUs (by number of reads) for Eisenberg epithermal and classical hydrothermal systems increase from proximal to distal site suggesting that Au particles proximal to the site were at an early stage of Au transformation. This suggests that the Au particles harbour a diverse group of microorganisms from initial microbial recruitment, whereas distal Au particles are more transformed and have recruited a more specialised community in terms of metal resistance (Chapter 2; Rea et al. 2018). A higher percentage of Proteobacteria was observed on Au particles from an epithermal source compared to the hydrothermal system. This relates back to the higher Ag to Au ratio in epithermal systems, thereby showing a strong association to the recruitment of microbial groups adapted to overcome Ag toxicity. This is further supported by the PICRUSt assignment of bacterial two-component systems, transporter and ABC transporters as dominant predicted genes under the Tier 1 environmental and information processing category (Fig. 4.11). The bacterial two-component system is involved in the stimulus-response system from environmental factors such as redox state, quorum signals and regulation of heavy metal resistance (Nies and Brown 1998). Transporters and ABC transporters are responsible for the regulation of the supply of external nutrients, removal and sequestration of toxic compounds and essential in metal ion transport (Wilkens 2015). Furthermore, Mn(II) uptake in bacteria may be mainly catalysed by transporters (Nies 1999). The high Mn measured in the soils and detection of an abundant OTU identified as *Leptothrix* spp., an Mn- and Fe- oxidizing sheathed filamentous bacterium, may be important for the dissolution and mobilisation process for oxidation/complexation of Au by Mn-oxide biominerals under these micro-environments (Ta et al. 2014, 2015). *Leptothrix* can produce biogenic Mn oxides (Nelson et al. 1998) that sometimes coat the sheaths of

the bacteria from the by-product of metal chelation and biological iron oxidation process (Dickinson et al. 1997; Florea et al. 2011).

The formation of Au nanoparticles and triangular nanoplates commonly occurring within clay minerals (Fig. 4.8) is attributed to the abiogenic or bioorganic reduction of Au-complexes due to changing physicochemical conditions, reduction on mineral surfaces or by organic acids, or during active or passive microbial biomineralisation which further exemplifies the key role that microbes play in mediating the mobility of Au in surface environments (Craw et al. 2017; Reith et al. 2010; Hough et al. 2011). Indeed, studies point to biofilms on Au surfaces as an important source of mobile Au nanoparticles (AuNPs), from active extracellular AuNPs production, stabilisation by charge capping and release to soils and groundwater during episodes of environmental stress (Reith et al. 2010; Hough et al. 2011; Johnston et al. 2013; Shuster et al. 2017a). Organic acids, *e.g.*, citrate, acetate, oxalate, humic and fulvic acids, present in biofilms may not only act as ligands for Au complexation but also stabilise metallic AuNPs (Vlassopoulos et al. 1990; Hough et al. 2011; Reith and Cornelis 2017). Mobile Au-complexes have been shown to be preferentially associated with organic matter, clays and Fe-oxides indicative of continuous microscale solubilisation and re-adsorption of mobile Au by the organic matter (Gray et al. 1998; Reith et al. 2005; Reith and McPhail 2006). *Deinococcus* sp., detected on Au particles, can reduce humic acid and transfer electrons to Fe(III) oxides hydrous ferric oxide and goethite by an electron shuttle mechanism as well as reduce Au(III) and biosynthesise AuNPs distributed in the cell envelope and in the extracellular space (Li et al. 2016). Other means to increase Au mobility are the micron-scale H_2S production by *Herbaspirillum* spp., *Microbacterium* spp. and *Pirerulla* spp., present in Eisenberg Au particles that can aid in thiosulphate and bisulphide complexation. Complexes and nanoparticles are re-precipitated and thereby immobilised when the complexing ligands or stabilizing agents are decomposed and when they are sorbed by minerals, organics or microbiota and subsequently aggregated (Hough et al. 2011; Craw and Kerr, 2017; Reith and Cornelis, 2017). Furthermore, biofilm communities can create a suitable pH gradient wherein microbes may form microenvironments on the oxidizing mineral surfaces (Dockrey et al. 2014; Chen et al. 2014) to provide a conducive microenvironment for the formation of Au-complexes, assumed to occur as an indirect effect of the metabolic processes (Reith et al. 2018).

Overall, physical processes lead to similar secondary morphotypes as observed on particles from epithermal and classical hydrothermal system, but it appears that

(bio)geochemical transformation is highly influenced by the primary mineralisation system driven by the total metal budget of the system, *e.g.,* Au to Ag ratio and composition of associated minerals, thereby, indirectly shaping the microbial footprint.

4.7. Conclusion

Particle transformation of placer Au particles originating from an epithermal source showed a difference to transformed particles derived from a hydrothermal source where the resulting Au:Ag ratio is highly affected by the primary mineralisation. Spongy-form overgrowths documented on Au particles are an outcome of preferential Ag expulsion and the recrystallisation processes from a combination of inorganic chemical reactions and microbial activity (Craw et al. 2017; Stewart et al. 2017). The release of Ag from the Au-Ag alloy, especially of Au particles derived from the epithermal system liberates fresh surface along the particle margins remobilising the Ag and re-concentrating the Au. (Bio)geochemical interaction with labile minerals and dissolved chemical load further increase (trans)formation of the Au particle. Resident communities on Au particles sense the difference in the Au:Ag ratio resulting in the observed separation of microbial community composition. Organisms detected in Au particles in this study that are adapted to metal toxicity are *Leptothrix* spp. and *Deinococcus* spp., similar to *C. metallidurans,* involved in the active formation of Au-complexing ligands and organic acids thus, driving the biogeochemical transformation of Au in Germany

Chapter V

Microbial-mediated mobility of gold: Assessing the mode of transport of gold from natural gold particles

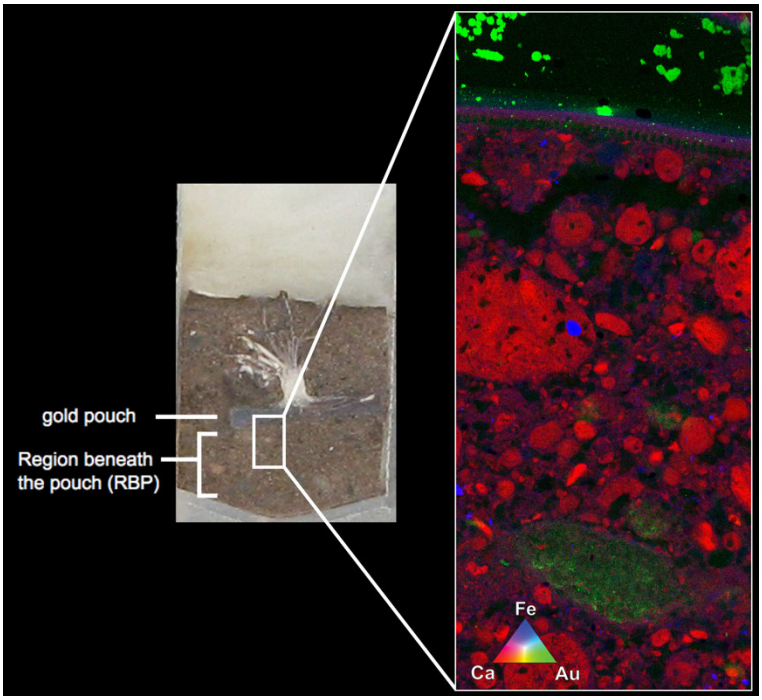

The content of this chapter is part of a journal article for submission to *Nature Communications*.

Statement of Authorship

Title of Paper	Microbial-mediated mobility of gold: Assessing the mode of transport of Au from natural gold particles
Publication Status	☐ Published ☐ Accepted for Publication ☐ Submitted for Publication ☑ Unpublished and Unsubmitted w ork w ritten in manuscript style
Publication Details	**(this is part of the manuscript for submission to Nature Communications)** Rea MA, Brugger J, Etschmann B, Shuster J*, Reith F (in preparation) Microbial-mediated mobility of gold: Assessing the mode of transport of Au from natural gold particles. Nature Communications.

Principal Author

Name of Principal Author (Candidate)	Maria Angelica Rea
Contribution to the Paper	Planned the study design. Performed column experiment set-up. Run samples in SP-ICP-MS, Standard solution ICP-MS. Helped in the synchrotron experiment. Interpreted results. Wrote the manuscript and created the figures and tables.
Overall percentage (%)	70
Certification:	This paper reports on original research I conducted during the period of my Higher Degree by Research candidature and is not subject to any obligations or contractual agreements with a third party that would constrain its inclusion in this thesis. I am the primary author of this paper.
Signature	Date 15.05.18

Co-Author Contributions

By signing the Statement of Authorship, each author certifies that:

i. the candidate's stated contribution to the publication is accurate (as detailed above);

ii. permission is granted for the candidate in include the publication in the thesis; and

iii. the sum of all co-author contributions is equal to 100% less the candidate's stated contribution.

Name of Co-Author	Prof. Joël Brugger
Contribution to the Paper	Performed the synchrotron experiment.
Signature	Date 14.05.18

Name of Co-Author	Dr. Barbara Etschmann
Contribution to the Paper	Performed the synchrotron experiment.
Signature	Date 14.05.18

Name of Co-Author	Dr. Jeremiah Shuster
Contribution to the Paper	Run samples in SP-ICP-MS. Performed the synchrotron experiment. Assisted in data interpretation and analysis. Advised and edited the manuscript. Acting corresponding author
Signature	Date 15/05/2018

Name of Co-Author	A/Prof. Frank Reith
Contribution to the Paper	Conceived and planned the study design. Supervised development of work. Run samples in SP-ICP-MS. Performed the synchrotron experiment. Manuscript evaluation and editing.
Signature	Date 17.05.2018

ASSESSING THE MODE OF TRANSPORT OF GOLD FROM NATURAL GOLD PARTICLES

In Chapters 2 to 4, biofilm community compositions of gold particles were analysed to understand better the biogeochemical cycling of gold. This chapter is an experimental study of the contribution of microorganisms in the mobility and immobility of gold in natural systems and serves as baseline information to predict gold transport for applications in gold exploration.

Research highlights

- Soils rich in iron (Fe), calcium (Ca) and organic matter (OM) aids in the mobility/immobility of gold.
- Microbial-assisted mobility of gold occurs on natural gold nanoparticles in Fe-rich, Ca-rich and OM-rich soils.
- Ligand-formation by *Chromobacterium violaceum* and *Corynebacterium glutamicum* leads to gold-complexation reactions and reductive precipitation by *Cupriavidus metallidurans* leads to gold nanoparticle formation.
- Biofilm disintegration contributes to the mobility of gold nanoparticles.

5.1. Abstract

The underlying mechanisms involving gold (Au) mobility and eventual precipitation forming secondary enrichment zones in gold deposits is complex and involves (hydro)geological and (bio)geochemical processes, which have not been quantitatively investigated. This study addresses this knowledge gap by quantifying gold transport from natural Au particles and minerals that have undergone secondary transformation leading to the formation of nano- and micro- phase gold. Gold particles obtained from Prophet gold mine, Queensland were characterised using scanning electron microscopy. Soil columns with Au particles placed in pouches were prepared using iron (Fe)-rich, organic matter (OM)-rich and calcium (Ca)-rich soils and sand as control. Soil columns were inoculated with active Au mobilisers *Chromobacterium violaceum* and *Corynebacterium glutamicum*, and precipitating organism *Cupriavidus metallidurans.* Results showed that gold particles were mobilised

on all soils either as nanoparticles or complexes. Outlet solution and soil suspension of columns amended with *C. metallidurans*, measured in single particle - inductively coupled plasma - mass spectrometry (SP-ICP-MS), demonstrated that gold was mobilised as AuNPs particularly in the region below the gold pouch (RBP) (~27–38 nm) from the gold source indicative of mobility. Columns amended with microbial consortia *C. metallidurans, C. violaceum and C. glutamicum* had no AuNPs detected in SP-ICP-MS and up to 320 $mg.L^{-1}$ of Au in the solution detected in standard ICP-MS. This supports the process of reductive precipitation of toxic Au(I/III)-complexes to form AuNPs in columns containing metallophilic bacterium *C. metallidurans*, a key species in Au cycling, whereas columns with *C. violaceum* and *C. glutamicum* implied amino acid- and cyanide complexation leading to mobility as Au-complex. This provides a fundamental understanding of Au dispersion from natural Au to develop a numerical model for Au mobility beneficial to mining explorations.

5.2. Introduction

Gold nanoparticles (AuNPs) are widely used in industrial and medical applications, in automotive, as a chemical catalyst, surface coatings, for biological imaging and for diagnosis of cancers and infectious agents (Alex and Tiwari 2015). These nanoparticles are commonly produced in mass quantities by reducing soluble Au-complexes, *e.g.,* Au(III)-chloride. Organic acids such as citric, tannic and oxalic acid as well as sulphur, phosphine-, amine- and carboxylate-ligands are often used to stabilise AuNPs and prevent them from agglomerating (Reith et al. 2014; Ahmed et al. 2016). Other methods for producing AuNPs are by seeding, microemulsion, use of surfactants and UV irradiation including AuNP biosynthesis using microorganisms to organise pre-synthesised nanoscale components (Daniel and Astruc 2004). Gold nanoparticles up to 500 nm in diameter are known to form in natural environments during the weathering of Au-bearing mineral deposits as well as the transformation of Au nuggets and particles (Fairbrother et al. 2012; Melchiorre et al. 2018; Rea et al. 2018; Reith et al. 2012a, 2018; Shuster et al. 2017a). Indeed, Au cycling in Earth's surficial environments is largely driven by biogeochemical processes resulting in Au dispersion and re-concentration in soils and other regolith materials. Microbial weathering is a possible mechanism that releases the trapped AuNPs within minerals and solubilise it via oxidation-promoting complexation from Au particles (Southam et al. 2009; Reith et al. 2013).

Biofilms may stabilise these AuNPs by the production of organic acids, *e.g.,* acetate, citrate and oxalate as well as peptides and proteins (Vlassopoulus et al. 1990;

Wood 2002; Rea et al. 2016). For example, *Corynebacterium glutamicum*, an aerobic, gram-positive soil bacterium, has been shown to perform a large-scale fermentative production of l-amino acids such as glutamate (Kalinowski et al. 2003). Glutamate is an acidic anion that can cap the AuNP surfaces similar to conventional methods of stabilisation by citrate and oxalate. Glutamate ions are adsorbed on the AuNPs thereby inducing electrostatic repulsion among the nanoparticles keeping them from agglomerating. In addition, the metallophilic bacterium *Cupriavidus metallidurans* CH34, one of the key-species involved in Au cycling from Australian, Brazilian and Finnish sites, reduces toxic Au(I/III)-complexes in the periplasm, which leads to the formation of AuNPs (Reith et al. 2009, 2018; Wiesemann et al. 2013, 2017; Rea et al. 2018). This biochemical response to deal with Au toxicity leads to upregulation of metal resistance systems ultimately leading to the biomineralisation of cell-associated AuNPs and drives the environmental cycle of Au (Reith et al. 2009; Wiesemann et al. 2013). The cyanide-producing bacterium *Chromobacterium violaceum* has been shown to solubilise Au from metallic Au surfaces by Au cyanidation contributing to Au mobilisation (Fairbrother et al. 2009). Humic and fulvic acids contribute to the mobilisation of Au by forming complexes with Au(I/III)-ions and the formation of stabilised AuNPs (Freise, 1931; Ong and Swanson 1969; Boyle, 1979). The mobilised Au is eventually released and transported as dissolved mobile Au-complexes and/or nanoparticles on the surface, soils and groundwater systems and exposed to further biogeochemical transformations leading to the formation of secondary enrichment zones (Southam et al. 2009; Reith et al. 2010; Hough et al. 2011). The underlying mechanisms of Au solubilisation, dispersion and eventual precipitation in secondary enrichment zones are complex and have not been quantitatively investigated. As a result of this knowledge gap, the absence of a geochemical halo over a deposit, or of false positives, is impossible to assess, which greatly limits the effectiveness of geochemical exploration. To achieve a quantitative understanding of these mechanisms, Au transport and sorption needs to be quantified to understand the mobility of Au. Gold is highly mobile in the regolith which can lead to the formation of the secondary enrichment zones, thus, extending the footprint of buried Au deposits and guide mineral explorers towards new deposits. Yet, the mode of Au transport (nanoparticle and/or Au-complex) and the time scales of Au mobility in determining the formation of these 'halos' remain unknown. Though a recent study has reported on the stability of AuNPs in solid and aqueous soil phase using citrate-capped AuNPs (Reith and Cornelis 2017), no study has used natural Au particles to examine the mobility of AuNPs in soils. Thus, this study aims to (i) assess the release

of AuNPs and transport of mobile Au through different soil materials, (ii) characterise size distribution of AuNPs released from natural Au particles, (iii) assess dispersion and distribution of Au in the soil matrix and identify microbial contributions affecting the mobility of Au. To achieve this, a range of soils were incubated in the dark for up to 18 months to assess the dispersion and distribution of mobilised Au and examine microbial-mediated Au transport under controlled conditions.

5.3. Materials and methods

5.3.1. Microbial culture preparation

Microbial cultures of *C. metallidurans, C. violaceum* and *C. glutamicum* in glycerol stocks were cultured in agar plates with either peptone meat extract (PME, BD Difco™ Nutrient Broth, U.S.A.) and tris-buffered minimal medium (MME). The MME was prepared by the methods described by Mergeay et al. (1985) supplemented with sodium gluconate (2 $g.L^{-1}$) to provide a carbon source. *Cupriavidus metallidurans* was grown in both PME and MME plates and *C. violaceum* and *C. glutamicum* were cultured in PME only. A colony was selected and placed in 100 mL PME (8 $g.L^{-1}$) broth at pH 6.5, 25° C, 100 rpm on a shaker plate for 24 hours, or MME at 30° C for 48 hours. These differing incubations ensure the stationary growth phase was reached before inoculation in the columns (Reith et al. 2009). Cells were harvested by centrifugation at 3,000 x *g* for 5 minutes, the supernatant was removed and discarded, and the cells were washed twice using a vortex and sterile saline solution (0.9 wt. %). After the final wash, the supernatant was removed and discarded and replaced with a fresh saline solution before storing at 4° C. This served as the working stock for the inoculation of mobility experiments. Using the working stocks, centrifuge tubes containing 30 mL media (PME or MME) were inoculated with 4.0 X 10^6 $cells.mL^{-1}$ with incubation conditions as indicated above.

5.3.2. Columns set-up

A total of 175 columns was prepared for this experiment to test for microbial-associated mobility of Au in various soil materials. Different types of soil were used to assess Au dispersion as these soils represent typical regolith matrices in which Au could be detected during exploration. These soils included those rich in organic matter (OM), iron oxide and calcium carbonate; quartz sand was used as a control. See Table 5.1 for soil parameters.

Table 5.1 – Soil properties of soils used in the columns.

Soil name	Fe-Cu-soil	Sandy soil	Ca-rich soil	OM-rich soil
Collection site adjacent to exploration/mining site	No	Yes	No	Yes
EC [dS/m]	0.10	0.018	0.197	0.12
pH	6.5	5.8	9.3	4.0
C.E.C. [cmol(+)/kg]	12	10	15	8.3
C org [wt.%]	2.03	4.96	6.82	2.83
Clay [wt.%]	27.76	3.16	36.62	21.43
Clay + Corg [wt.%]	29.78	8.12	43.44	24.25
Silt [wt.%]	7.6	0.6	20.2	22.1
Sand [wt.%]	55.1	44.5	39.0	48.7
Fine sand [wt.%]	9.6	51.7	4.2	7.8
Total sand [wt.%]	64.7	96.3	43.2	56.5
Ca [mg/kg]	1690	910	27500	1190
K [mg/kg]	2220	n.d.	7240	8230
Mg [mg/kg]	959	238	11100	2250
Na [mg/kg]	188	n.d.	833	322
S [mg/kg]	252	230	682	376
Al [mg/kg]	28300	298	30400	38500
Co [mg/kg]	7.65	n.d.	n.d.	n.d.
Cr [mg/kg]	32.5	n.d.	34.7	37.2
Cu [mg/kg]	7.7	n.d.	n.d.	n.d.
Fe [mg/kg]	18300	169	18600	18300
Mn [mg/kg]	317	n.d.	282	23.4
Mo [mg/kg]	n.d.	n.d.	n.d.	n.d.
Ni [mg/kg]	13.6	n.d.	15.7	11.6
P [mg/kg]	258	n.d.	284	122
Pb [mg/kg]	9.44	n.d.	n.d.	11
Zn [mg/kg]	11.5	n.d.	29	23.2

The bioreactor columns were constructed using 30 mL Terumo™ syringes with 20 μm pore-size mesh plug placed at the bottom of each tube to prevent soil loss and allow fluids to permeate. Each column was filled with 10 g of OM, iron oxide or calcium carbonate soil. Natural Au particles were panned from Prophet gold mine in Queensland. Approximately 400 Au particles (100 – 800 μm in size) were placed in a pouch made of 20 μm pore-size nylon mesh and buried in each column. The purpose of the pouch was to keep the Au particles in a localised position within the column. Each column was inoculated with 1 mL of bacterial consortia containing *C. violaceum*, *C. glutamicum* and *C. metallidurans* (ca. 5.5 x 10^6 cells.mL^{-1}). Columns were supplemented with MME and PME growth media at the beginning of each month over the duration of the entire experiment (18 months). Sand columns with fine Au

served as a control. All column containing a different type of soil were performed in triplicate and were incubated at 25° C in the dark.

5.3.3. Single particle - Inductively coupled plasma - Mass spectrometry

Residual PME solutions that percolated through the columns were collected in 2 mL microcentrifuge tubes over the course of each month. Here on, residual PME or MME solutions will be called 'outlet solutions' for simplicity. These outlet solutions were analysed for the presence of AuNPs. Soils immediately surrounding the Au-bearing pouch from the 18-month columns were also analysed since AuNPs can readily adsorb to clay minerals (Reith and Cornelis 2017). To release any AuNPs adsorbed to clay minerals, soils were prepared as slurries by mixing 1 g of soil into 2 mL of milliQ in sterile Falcon™ tubes. The tubes were shaken at 120 rpm for 16 h and placed vertically into a 20 °C water bath for ca. 1 hour to allow clay particles to separate by size fraction through gravitational settling. The slurry solutions containing the fine fraction (<0.45 μm in size) were transferred to separate microcentrifuge tubes (Gimbert et al 2006).

The concentration and size distribution of AuNPs from the outlet solutions and the solutions containing the fine clay fraction were measured using a PerkinElmer NexION™ 350D Single Particle Inductively Coupled Plasma – Mass Spectrometer (SP-ICP-MS) and analysed using the Nano Application Module Syngistix™ software. Soluble 0.5, 1.0 and 2.0 $\mu g.L^{-1}$ Au standards were volumetrically prepared by diluting 1000 mg L^{-1} Au(III)-chloride (NIST SRM 3121, High Purity Standards, United States) into 2 % (v/v) hydrochloric acid. Four different AuNP standards were also used; these solutions contained 20 nm, 40 nm, 60 nm or 80 nm size (diameters) AuNPs suspended in ultrapure water (British Biocell International (BBI), Cardiff, UK). All AuNP standards were sonicated for one minute to prevent AuNP aggregation (Laborda et al. 2013). Samples were analysed using a 20.0 rpm, with 50 μs dwell time and 100 s sampling time, and transport efficiency <10 %. Remaining sample solutions were measured for residual soluble Au using an Agilent 8900x triquad inductively coupled plasma – mass spectrometry (QQQ ICP-MS) (quantification limit 0.4 ppb; Agilent Technologies) connected to a CETAC ASX-500 autosampler with He as collision gas. A two-tailed t-test was performed to calculate the difference between means of the AuNP at cut off values of $p < 0.01$ and $p < 0.05$ as level of significance, as reported in results.

5.3.4. Scanning electron microscopy - Energy dispersive spectrometry

Gold particles harvested at the end of the experiment were processed and dehydrated in a serial 70, 90 and 2 x 100 vol. % ethanol (10 min for each concentration) and placed in 100 wt. % hexamethyldisilazane to ensure the integrity of bacterial cells and biofilms (Fratesi et al. 2004). Samples were carbon coated and analysed using a Quanta™ 450 Field Emission Gun - Scanning Electron Microscope (FEG-SEM) equipped with an Energy Dispersive Spectrometer (EDS) detector (FEI, Netherlands). Images were taken in secondary electron (SE) and backscattered electron (BSE) imaging modes using 5 kV and 20 kV, respectively.

5.3.5. X-ray fluorescence mapping

Columns from the 18-month replicate were prepared for micro synchrotron X-ray Fluorescence (μXRF) Imaging collected at the X-ray Fluorescence Microscopy (XFM) beamline (Australian Synchrotron, Melbourne) to determine how much Au was associated with the solid soil phase, *i.e.*, outside the mesh pouch. The columns were embedded in Polyester Casting resin thinned with Methyl Methacrylate Monomer and set using a very low ratio of MEKP and Cumene hydroperoxide as the catalyst. The embedded columns were cut to produce cross-sections down the length of the column (ca. 5 x 2 cm cross-sectional regions). The XFM beamline is an undulator beamline with a Si (111) monochromator and an energy resolution ($\Delta E / E$) of 2 Å~ 10^{-4} at 10 keV. Kirkpatrick-Baez mirrors were used to focus the beam to a spot size of ~1.5 μm^2 and the 384-element Maia detector system was used for analyses. The detector was placed in front of the sample at a distance of 2 mm, resulting in a solid angle of 1.8 Sr. The incident X-rays travel through a central hole in the detector. The elastic scatter peak was used as a proxy for Si, since the Si–Kα line is below the energy range of the Maia X-ray detector. The cross-sectional regions were mapped with a beam size of ~2x2 μm^2 at an energy of 18.5 keV. Maps of Au, Fe, Pb, Zr, Ca were obtained. These initial maps were used to triage samples and select for smaller regions for higher resolution maps and X-Ray Absorption Near Edge Structure (XANES) mapping which was collected using ~100 monochromator energy points across the Au edge. The spectral data for each pixel were fitted based on a combination of arctangent and voigt functions using GeoPIXE Software (Ryan et al. 2005).

5.4. Results

5.4.1. Characterisation of mobilised gold particles in different soils

Representative size histograms of month 18 sand columns amended with *C. metallidurans* showed the difference in the mean size of AuNPs in the region beneath the Au pouch (RBP) (36.4 nm) and the collected outlet solution (37.7 nm) (Fig. 5.1A–B). A significant difference ($P < 0.01$) was also demonstrated in sand columns using MME from month 6 (36.3 nm) and month 18 (37.7 nm) and using PME from month 6 (26.8 nm) and month 18 (40.6 nm) (Table 5.3). Mean size of AuNPs measured in outlet solution increased with incubation period (Table 5.2). The AuNP size distribution from RBP *vs* outlet solution (R) on sand columns and Ca-rich soil columns inoculated with *C. metallidurans* demonstrated a significant difference ($P < 0.01$) (Fig. 5.2, Table 5.3). Ten Au particles from the original stock which were not used for the soil columns were sonicated to introduce an artificial force yielding larger mean size of measured AuNPs (53.0 nm) compared to the mean size of AuNPs from the soil columns (26.5 up to 37. 7 nm). This demonstrates that only a strong artificial force, *i.e.*, sonication, can dislodge the AuNPs already present on the Au surface.

Table 5.2 – Summary of mean size of AuNPs of sand columns from outlet solutions in month 6 (F) and month 18 (R) and outlet solution of controls in month 6 (Fctrl) and month 18 (Rctrl) without *C. metallidurans*.

	Sand-MME-F	Sand-MME-R	Sand-PME-F	Sand-PME-R	Sand-MME-Fctrl	Sand-MME-Rctrl	Sand-PME-Fctrl	Sand-PME-Rctrl
Sand-MME-F	36.3 nm							
Sand-MME-R	**	37.7 nm						
Sand-PME-F	**		26.8 nm					
Sand-PME-R		**	**	40.6 nm				
Sand-MME-Fctrl	**				28.8 nm			
Sand-MME-Rctrl		**			**	39.5 nm		
Sand-PME-Fctrl			**		**		30.2 nm	
Sand-PME-Rctrl				**		**	**	33.4 nm

Values shown are mean size, ** significant difference at 0.01

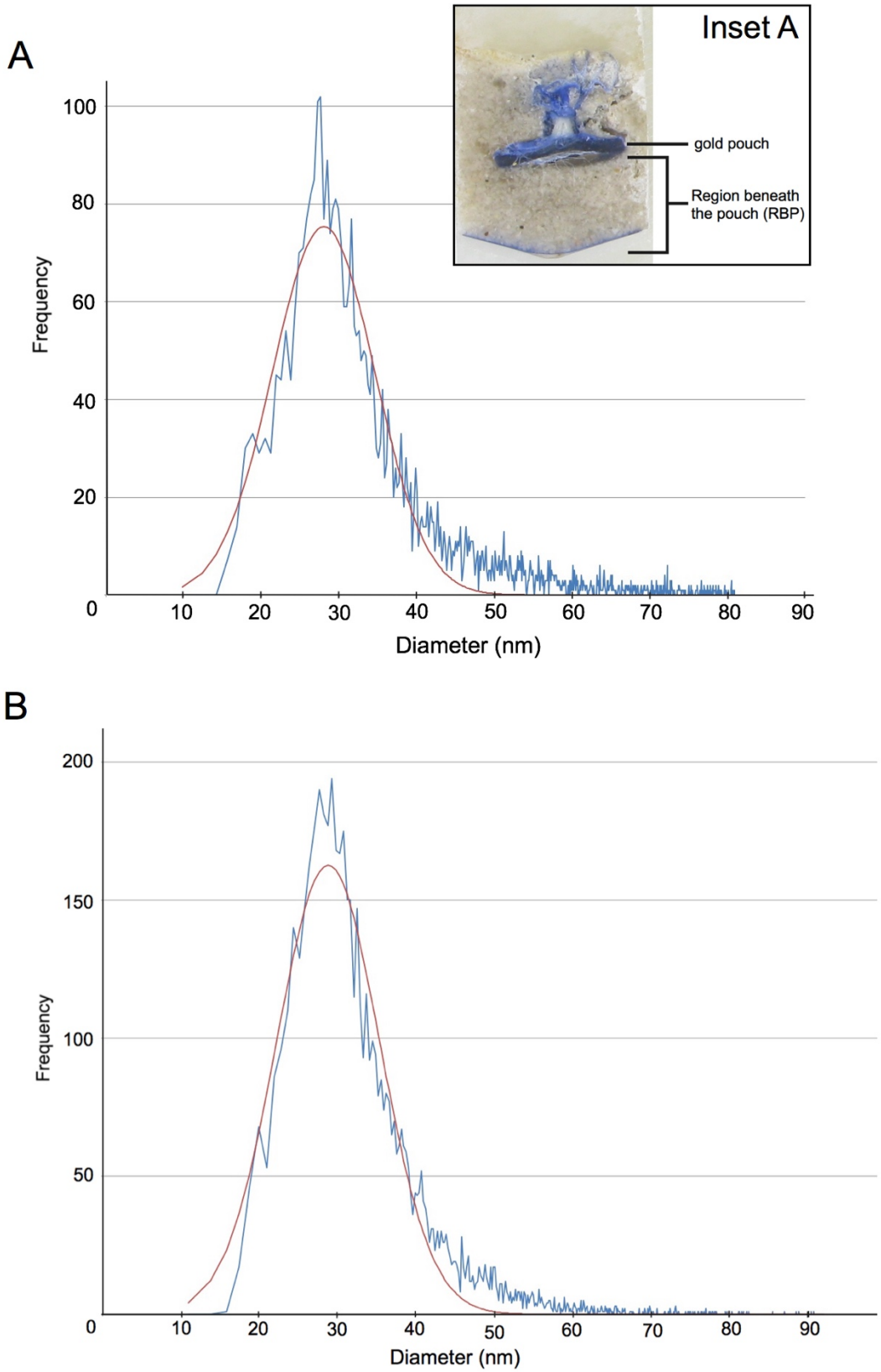

Figure 5.1 (**A**) Representative size histogram with Gaussian fitting of gold nanoparticles (AuNPs) detected in single particle – inductively coupled plasma – mass spectrometry (SP-ICP-MS) for (**inset A**) month 18 columns outlet solution from sand columns and (**B**) size histogram of soil suspension from sand columns in the region below the pouch (RBP).

Table 5.3 – Summary of mean size of AuNPs from the region below the pouch (RBP) and outlet solution (R).

	Ca-RBP	Ca-R	OM-RBP	OM-R	Fe-RBP	Fe-R	Sand-RBP	Sand-R
Ca-RBP	26.9							
Ca-R	**	28.3						
OM-RBP			29.6					
OM-R			none	26.5				
Fe-RBP					26.6			
Fe-R					none	28.1		
Sand-RBP							36.4	
Sand-R							**	37.7

Values shown are mean size, ** significant difference at 0.01, X- no significant difference

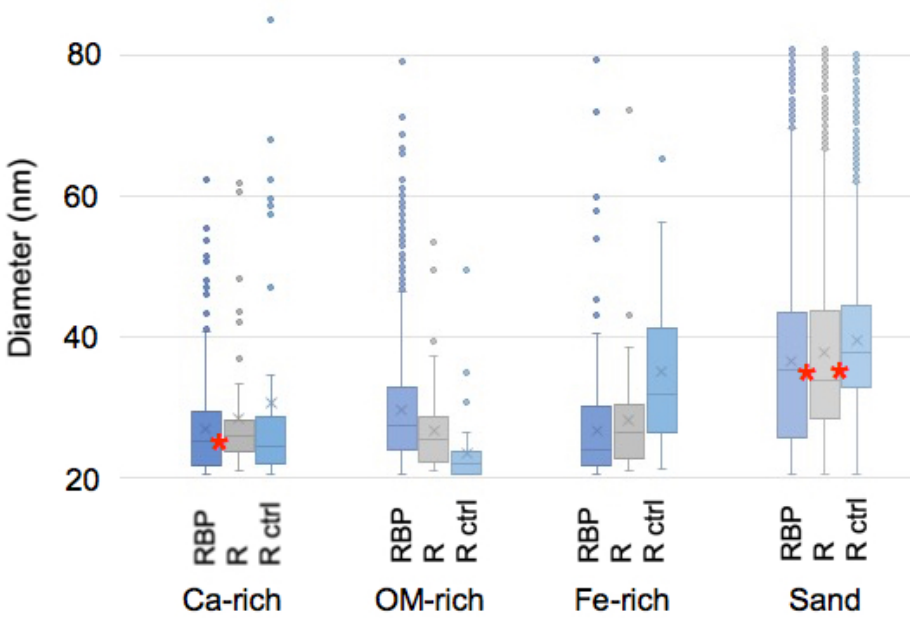

Figure 5.2 A box and whisker plot of measured AuNPs on the region below the pouch (RBP), outlet solutions (R) of soil columns and outlet solution of controls (R ctrl) in different soil matrices. Note: red * shows significant difference at $p < 0.01$.

Nanoparticles were below observable range (<20 nm) on columns amended with *C. metallidurans*, *C. violaceum* and *C. glutamicum*; however, up to 320 mg.L^{-1} of dissolved Au was detected from these columns using solutions ICP-MS (Table 5.4). Representative BSE and SE micrographs of Au particles showed minimal biofilm growth on Au surface before the experiment and evidence of biofilm development after the column experiment (Fig. 5.3A–B). Microbial cells forming clusters were observed extensively on Au particles (Fig. 5.3C inset) with microbial extensions attached on the particle surface (Fig. 5.3D). The crevices and cavities of Au particles were also observed to contain microbial aggregates of cells (Fig. 5.3E). Similarly, the associated soil materials in the column experiment hosts abundant microbial cells (Fig. 5.3F).

Table 5.4 – Summary of solution ICP-MS result for outlet solution and the region below the pouch (RBP).

SampleName	Soil material	Au μg.L⁻¹	Ag μg.L⁻¹	Ti μg.L⁻¹	Mn μg.L⁻¹	Fe μg.L⁻¹	Ni μg.L⁻¹	Cu μg.L⁻¹	Zn μg.L⁻¹	As μg.L⁻¹
Ca-RBP	Ca-rich	<0.224	<0.064	3.34 X 10^01	1.87 X 10^03	<1.346	<2.004	1.39 X 10^02	1.00 X 10^03	<1.687
Ca-R	Ca-rich	2.00 X 10^02	2.42	3.86 X 10^01	2.77 X 10^06	1.80 X 10^03	5.82 X 10^01	2.30 X 10^01	3.43 X 10^03	1.08
Ca-RBP ctrl	Ca-rich	<0.224	2.84	4.76 X 10^01	1.22 X 10^04	<1.346	<2.004	1.99 X 10^01	1.65 X 10^04	<1.687
Ca-R ctrl	Ca-rich	1.57 X 10^01	5.75	8.35 X 10^01	6.67 X 10^07	3.60 X 10^02	<2.004	7.58	1.72 X 10^04	2.78
OM-RBP	OM-rich	2.22 X 10^01	1.95 X 10^01	7.14 X 10^03	9.83 X 10^04	1.34 X 10^04	2.61 X 10^01	6.55 X 10^01	1.55 X 10^05	2.55 X 10^01
OM-R	OM-rich	2.43 X 10^01	1.17	8.94	9.01 X 10^04	1.76 X 10^02	<2.004	8.37 X 10^01	3.61 X 10^03	<1.687
OM-RBP ctrl	OM-rich	1.09 X 10^01	1.51 X 10^01	4.51 X 10^03	4.13 X 10^04	4.60 X 10^03	<2.004	1.37 X 10^02	5.95 X 10^04	1.33 X 10^01
OM-R ctrl	OM-rich	9.11	2.90	1.06 X 10^02	5.97 X 10^05	1.37 X 10^03	2.80 X 10^01	7.28	4.46 X 10^05	2.51
Fe-RBP	Fe-rich	6.96	1.96	1.19 X 10^03	1.13 X 10^06	3.70 X 10^02	<2.004	8.20 X 10^01	1.48 X 10^03	2.10E-01
Fe-R	Fe-rich	1.00 X 10^01	<0.064	5.42 X 10^01	9.86 X 10^06	2.21 X 10^02	<2.004	5.96 X 10^01	4.04 X 10^03	<1.687
Fe-RBP ctrl	Fe-rich	<0.224	<0.064	4.36 X 10^02	1.32 X 10^06	<1.346	<2.004	6.11 X 10^01	1.08 X 10^04	<1.687
Fe-R ctrl	Fe-rich	2.50	2.61	2.14 X 10^01	1.73 X 10^07	3.04 X 10^01	<2.004	8.20 X 10^01	7.97 X 10^03	1.00
Sand-MME-F	Sand	1.95 X 10^03	3.00 X 10^01	<1.217	6.17 X 10^05	4.60 X 10^02	<2.004	7.03	1.66 X 10^03	<1.687
Sand-MME-RBP	Sand	1.17 X 10^02	3.78 X 10^01	<1.217	3.34 X 10^03	1.96 X 10^01	<2.004	6.68 X 10^01	4.15 X 10^03	<1.687
Sand-MME-R	Sand	6.12 X 10^02	1.04 X 10^02	9.17 X 10^03	1.52 X 10^06	3.54 X 10^03	7.34 X 10^01	1.05 X 10^02	1.54 X 10^05	2.81
Sand-PME-F	Sand	5.72 X 10^02	<0.064	<1.217	1.24 X 10^04	1.57 X 10^02	<2.004	1.98 X 10^01	2.78 X 10^02	<1.687
Sand-PME-RBP	Sand	4.28 X 10^03	1.18 X 10^01	1.24 X 10^02	6.00 X 10^05	1.25 X 10^04	<2.004	5.95	2.09 X 10^04	<1.687
Sand-PME-R	Sand	5.79 X 10^03	<0.064	<1.217	5.20 X 10^04	1.74 X 10^03	<2.004	<1.079	2.65 X 10^03	<1.687
143F	Sand	1.89 X 10^05	1.09 X 10^03	<1.217	2.73 X 10^06	3.72 X 10^04	<2.004	<1.079	2.96 X 10^05	<1.687
147F	Sand	3.10 X 10^05	8.04 X 10^02	2.48 X 10^02	8.31 X 10^06	7.20 X 10^04	<2.004	7.94	7.82 X 10^04	<1.687
147R	Sand	3.20 X 10^05	7.90 X 10^02	<1.217	8.03 X 10^06	6.13 X 10^04	<2.004	8.14	6.63 X 10^04	<1.687
Sand-MME-Fctrl	Sand	7.82 X 10^02	1.66 X 10^02	<1.217	1.93 X 10^04	3.60 X 10^01	<2.004	1.52 X 10^03	8.51 X 10^04	<1.687
Sand-MME-RBPctrl	Sand	8.35 X 10^01	2.95 X 10^01	7.47 X 10^01	1.27 X 10^04	1.75 X 10^02	<2.004	2.04 X 10^02	1.33 X 10^05	<1.687
Sand-MME-Rctrl	Sand	7.72 X 10^02	8.18 X 10^01	3.26 X 10^01	5.63 X 10^06	7.71 X 10^03	8.58 X 10^01	2.16 X 10^03	1.65 X 10^06	6.28 X 10^01
Sand-PME-Rctrl	Sand	8.33 X 10^02	3.29	2.42 X 10^02	1.06 X 10^07	5.11 X 10^04	7.64 X 10^00	4.72 X 10^01	1.46 X 10^05	4.95

Note: Detection of gold is below background levels
Column # 143 inoculated with *C. violaceum* only; Column # 147 inoculated with *C. metallidurans*, *C. violaceum* and *C. glutamicum*

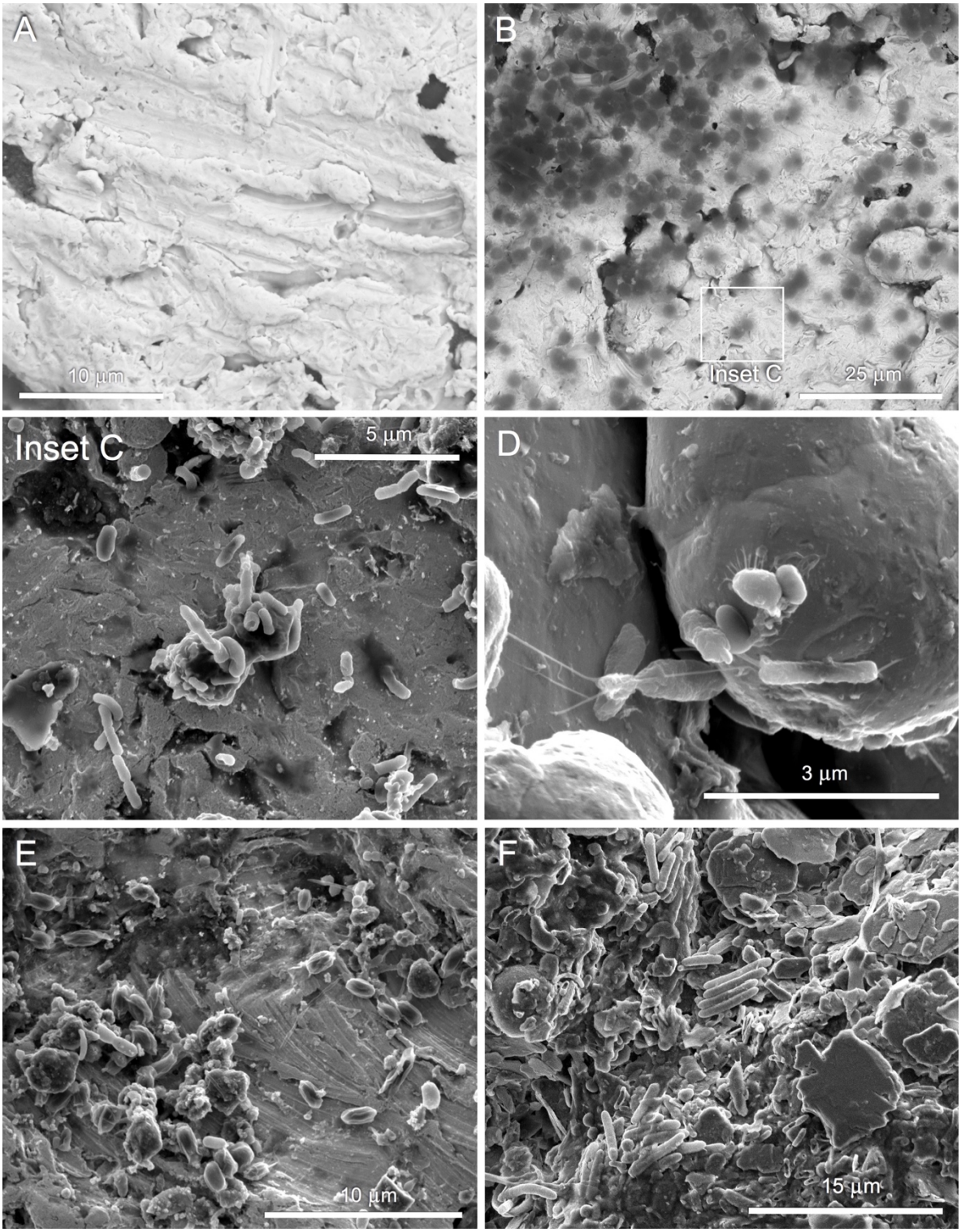

Figure 5.3 Backscattered Electron (BSE) micrograph and Secondary Electron (SE) micrograph of Au particle surface (**A**) before and (**B**) after the column experiment. Gold particles recovered at the end of the experiment show (**C**) extracellular polymeric substances (EPS) and remnants of biofilm (**D**) microbial cells and EPS attached on the Au surface and biofilm colonising crevices of Au particles and (**E**) rod-shaped cells colonising particle surface and abundant EPS materials. (**F**) An SE micrograph of soil recovered from month 18 column in the RBP showing microbial cells.

5.4.2. Assessment of mobility of gold

The transport of AuNP from the Au pouch to the outlet solution is more evident on sand columns than in other soils, *i.e.*, OM-rich, Fe-rich and Ca-rich soils based on the measured AuNP in SP-ICP-MS. The synchrotron-based mapping was used to assess the dispersion and distribution of Au in the soil columns. The SXRF maps demonstrated that Au has moved from the Au pouch to RBP area of sand and Ca-rich soil matrix (Fig. 5.4A, B). A similar trend of dispersion and re-concentration of Au was observed in Fe-rich and OM-rich soil columns. In sand columns, there is an absence of a prominent region of Au re-concentration (Fig. 5.4C inset). In the Ca-rich soil column, the AuNPs were trapped in the RBP soil matrix as demonstrated in the SXRF maps (Fig. 5.4D inset).

5.5. Discussion

The effect of AuNPs and Au-complexes on soil microbiota and soil properties as well as the stability of AuNPs and its association with organics and clays in solid and aqueous soil phases were reported in recent research using synthesised citrate-capped AuNPs (Darlington et al. 2009; Fairbrother et al. 2009; Cornelis et al. 2014; Reith and Cornelis 2017). However, gold mobility and AuNP transport have not been demonstrated using natural Au particles, thus, warrants the quantification of the mode of Au transport either as nanoparticle and/or Au-complex in soils and regolith materials using Au particles to understand mobility of Au and ultimately linked to the biogeochemical cycling of Au. Results showed that the mean size of AuNP increased in soil columns inoculated with *C. metallidurans* as the inoculation period increased implying that AuNPs has agglomerated possibly by bio(geo)chemical precipitation of mobile Au-complex and subsequent aggregation mediated by *C. metallidurans*. The metallophilic bacteria *C. metallidurans* are known to reduce toxic Au(I/III)-complexes in the periplasm via co-utilisation and regulation of Cu/Au resistance determinants using the metal chaperone *CupC* and the periplasmic Cu-oxidase *CopA* for the detoxification of Au-complexes and the formation of AuNPs (Wiesemann et al. 2013, 2017; Zammit et al. 2016; Bütof et al. 2018). This results in the formation of up to 10 nm sized AuNPs in the periplasm (Reith et al. 2009). Over time nano- to micro- size Au aggregates encapsulate and replace cells forming mm-sized Au particles (Fairbrother et al. 2013; Shuster et al. 2015).

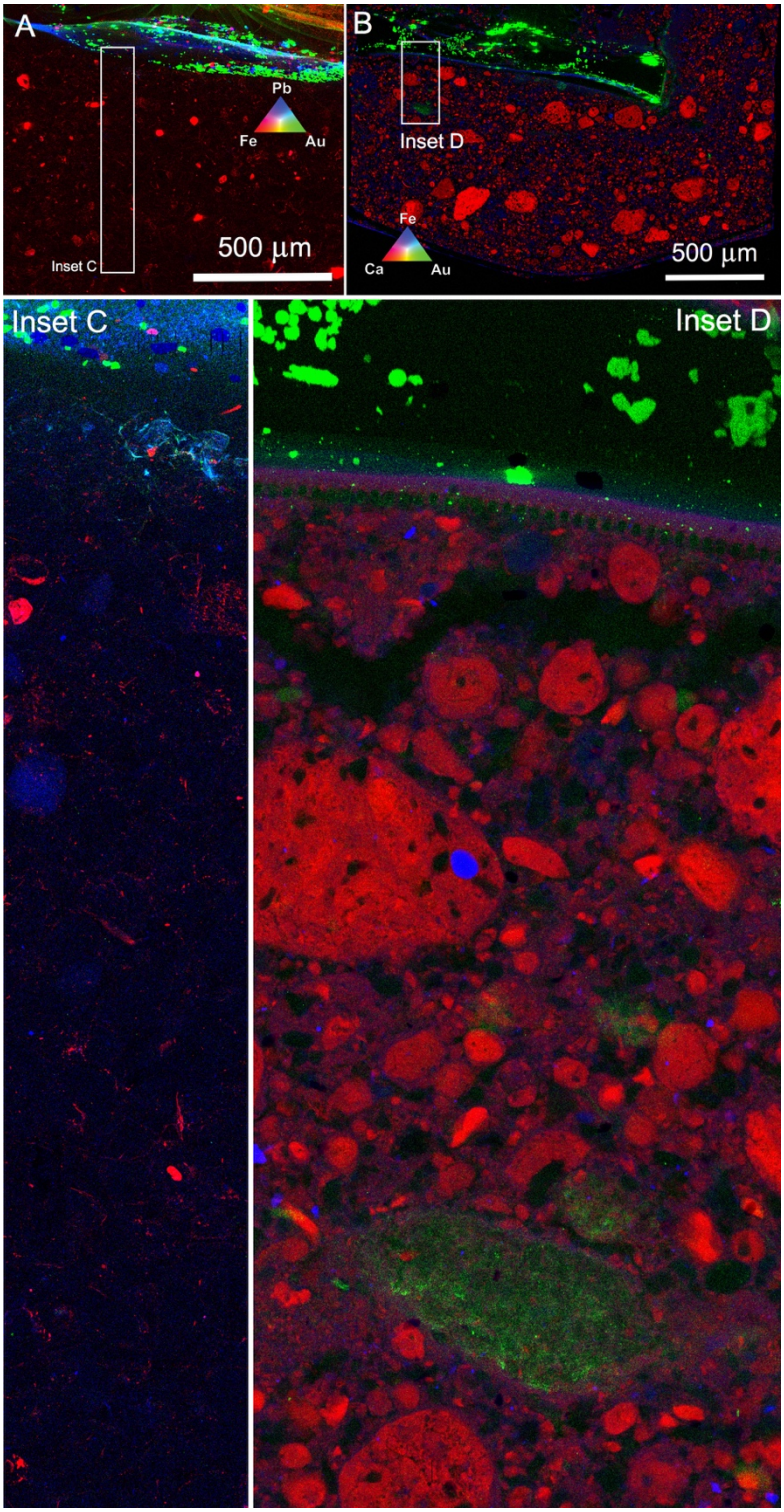

Figure 5.4 Synchrotron micro-Xray fluorescence (SXRF) elemental map of (**A**) an overview map of the section through a sand column showing iron (Fe) in red, gold(Au) in green and lead (Pb) in blue, and (**B**) an overview map of a section through a calcium (Ca)-rich soil column showing Ca in red, Au in green and Fe in blue. Detailed maps of selected regions for (**C**) sand columns and (**D**) Ca-rich column showing evidence of gold mobility/immobility.

In this study, soil columns with microbial consortia of metallophilic *C. metallidurans*, cyanide-producing *C. violaceum* and glutamate-producing *C. glutamicum* resulted in low-detection or absence of measurable AuNPs and the presence of up to 320 mg. L^{-1} of Au in solution. This implies that Au was dominantly re-mobilised by cyanidation and amino acid complexation (Fairbrother et al. 2009). Earlier experimental studies have shown that heterotrophic microbiota can aid in the formation of Au-amino acid complexes (*e.g.,* Korobushkina et al. 1976, 1983). In addition, amino acids are metabolic precursors for cyanide production by microorganisms which have been shown to solubilise Au from metallic Au surfaces (Fairbrother et al. 2009). Cyanide produced by microorganisms such as *C. violaceum* is often not utilised by the organism for metabolic activities but used to set a competitive ground to induce cyanide toxicity in nutrient-limiting conditions. Cyanide production may be continuous in these soil environments since soils are severely growth limiting due to low C and N in soils even in OM-rich soils (Batjes 1996). Furthermore, this can also lead to mobilisation not only of Au but of other metals such as Fe and Mn (Dzombak et al. 2005) explaining the high Fe and Mn measured in solution (Table 5.3). Both dispersed and remobilised AuNPs as well as mobile Au-complexes play a role in the formation of surface and soil anomalies including the (trans)formation of Au particles (Reith et al. 2012b, 2016; Ta et al. 2014, 2015; Anand et al. 2016; Shuster et al. 2016, 2017a). Solubilisation of Au by cyanide and amino acid contributes to the dispersion of Au in natural environments (Reith and McPhail 2006, 2007; Fairbrother et al. 2009). Gold-complexes are easily reduced by living or dead organic matter, resulting in the formation of nanoparticles (*e.g.,* Lengke et al. 2006; Reith et al. 2009; Etschmann et al. 2016).

The high clay and OM content in soils have been shown to be important factors to the mobility/immobility of nanoparticles (Cornelis et al. 2014; Reith and Cornelis 2017). A number of studies have shown that OM strongly affects Au mobility where organic acids, such as humic, fulvic and amino, and biomass readily reduce Au(I/III) complexes, promote the formation of Au colloids, immobilise Au-complexes as well as form stabilised Au nanoparticles (*e.g.,* Freise, 1931; Ong and Swanson 1969; Fisher et al. 1974; Boyle 1979; Gray et al. 1998; Kenney et al. 2012; Etschmann et al. 2016). Up to 80 wt. % of citrate-capped AuNPs remained highly mobile/dispersible in an experimental study on Australian soils and are preferentially associated with organic matter, clays and Fe-oxides (Reith and Cornelis 2017). The strong affinity of Au to organic matter and ligands is further observed in previous experiments on environmental samples where direct associations of OM with secondary nanophase

and microphase Au is hosted in pisolitic ferricrete in Moolart Well, Western Australia (Anand et al. 2016). In addition, AuNPs are highly abundant on the surface of Au particles, where they are associated with remnants of microbial cells, exopolymeric substances, clays and Fe-oxides comprising the polymorphic biofilm layer coating the Au surfaces (Reith et al. 2010, 2012a; Fairbrother et al. 2012; Shuster et al. 2015, 2017a). Furthermore, dissolved natural organic matter (DNOM) including humic substances and proteins can completely or partially coat AuNPs as capping agents for steric and electrostatic stability (Diegoli et al. 2008; Alonso et al. 2009). In the presence of calcium ions, a partially covered DNOM-coated AuNP is stabilised by the mechanism called cation-assisted bridging flocculation where the negatively charged DNOM binds to positively charged Ca(II) ions site (Cornelis et al. 2014). If AuNPs are uncoated/uncapped, similar to the mobilised AuNPs in this study, the electrostatic repulsion decreases, and thereby encourage aggregation and sedimentation with the negatively charged AuNPs sorbed or deposited on soil surfaces. Similarly, some AuNPs are favourably attached to variable charge minerals including Fe- and Mn-oxides present in clay fractions (Cornelis et al. 2012, 2013), thus, explains the absence of measurable AuNP in outlet solution of Fe-rich and OM-rich soil columns.

5.6. Conclusion

This study highlighted microbial-mediated mobility of gold where Au-complexation reactions as well as OM, clays and Fe/Mn-oxides aids in the reduction of Au-complexes leading to nanoparticle mobility/immobility in soils. The detection of AuNPs and dissolved Au in solution further supports the microbial-mediated mobility of Au by active Au mobilisers and precipitating organisms. This provides evidence for the long-held assumption that elevated Au concentration detected in anomalous soils is not only derived from complexes but also a result of mobilised and sorbed nanoparticles in the soil matrix. Nanoparticulate gold is therefore important for Au transport as a common product of (bio)geochemical transformations. Future work is needed to determine the distribution coefficients for Au kinetic rate equations that can be fitted to and integrated into a numerical model. This can be used to estimate the dispersion of Au in the environment and help design effective exploration strategies, leading to innovative, low-impact Au recovery methods.

Chapter VI

Conclusions

CONCLUSIONS – REVISED MODEL OF THE BIOGEOCHEMICAL CYCLE AND TRANSFORMATION OF GOLD IN DIFFERENT ENVIRONMENTAL CONDITIONS

This thesis presented the current knowledge concerning the composition of biofilm communities residing on Au particles and provided greater insight into how functional abilities of bacteria influence Au particle (trans)formation and Au mobility in Earth's surficial environments. This final chapter draws the conclusions of this PhD research by highlighting the microbial contribution to the biogeochemical cycling of gold, *i.e.*, its solubilisation, transport and re-precipitation, leading to the (trans)formation of Au particles. This chapter ends with an outlook into the type of studies that have to be taken to elucidate the underlying mechanisms and kinetics of these processes.

6.1. Introduction

The biogenic (trans)formations of Au particles are driven by (geo)biochemical processes mediated by distinct biofilm consortia living on these particles (Rea et al. 2016, 2018; Reith et al. 2018). The evidence presented in Chapters 2 to 4 on Au particles from a range of environments including UK (eight sites), Switzerland (eight sites) and Germany (14 sites) suggests a stronger influence of microorganisms in the biogeochemical cycling of Au than previously demonstrated. We have shown that Au particles act as selective pressure for the development of biofilms occurring on their surface. The bacterial composition of biofilms has evolved to actively withstand the toxicity of soluble gold thereby influencing the transformation of Au particles. Proteobacteria dominated the community assemblage from all sites in UK, Switzerland and Germany with β-Proteobacteria being the most abundant proteobacterial group (>40 % of total OTUs and sequencing reads). This suggests that highly-specialised biofilm communities, adapted to Au-rich micro-environments, perform key roles in the transformation of Au particles. In Chapter 5, the contribution of biofilm communities on Au mobility was further demonstrated using a wide range

of soil types inoculated with microorganisms linked to Au biomineralisation and biomobilisation.

6.2. Progressive biogeochemical transformation of placer gold particles drives compositional changes in associated biofilm communities

This is the first study to demonstrate a direct relationship between biofilm composition and the progressive transformation, *i.e.*, involving Au/Ag dissolution and Au refinement, of Au particles. The community assemblage was initially different between sites. With increasing degrees of Au particle transformation, the function of the microbial communities increasingly become more specialised in regard to metal-resistance. This trend is likely attributed to the increased concentration of soluble Au and Ag during dissolution processes in the chemical load of toxic mobile Au and Ag experienced by communities during biogeochemical transformation. The resident taxa, detected on the UK Au particles, is comprised of diverse biofilm communities containing a range of metabolic capabilities that are capable of reducing toxic soluble Au into secondary Au morphotypes.

Conclusions in Chapter 2

1. Secondary Au morphotypes and transformation features on placer Au from UK sites showed many similarities to those observed on particles from sites located in different geological and environmental conditions, *i.e.*, Australia, New Zealand, Finland and South America.
2. The higher detection of OTUs from Au particles, compared to earlier studies, is attributed to the improved resolution of NGS and possibly linked to eDNA associated with organic material.
3. The progressive transformation of Au particles influences the composition of the microbial community by placing selective pressure to recruit microorganisms adapted to withstand the toxic effect of ionic gold.
4. During progressive Au particle transformation, biofilm development involves the recruitment of different organisms with diverse metabolic capabilities that are capable of dividing the functional traits amongst the biofilm.
5. As the degree of Au transformation increases, the biofilm evolves to become more metal-resistant and as a result, the microbial community becomes increasingly similar between sites.

6.3. Landscape position influences gold transformation and biofilm composition

In this study, the influence of fluvial transport is correlated to the progressive transformation of Au particles and biofilm composition. This confirmed that fluvial transport and bio(geo)chemical factors are highly dependent on the landscape scenario. High-energy fluvial systems are dominated by physical transformation whereas low-energy fluvial environment will undergo less physical (de)formations but more bio(geo)chemical transformation. Progressive transformation of Au particles from proximal to distal locations shaped the microbial assemblage; increased Au particle transformation led to the recruitment of more diverse members capable of overcoming metal toxicity within a biofilm. Transport distance leads to the physical reworking of Au particles. Simultaneously, it induces the formation of compact, stable biofilm on Au particles.

Conclusions in Chapter 3

1. The distance of transport from a likely source (*e.g.*, proximal, transitional zone and distal) influences the stage of Au transformation and the microbial community composition.
2. The degree of Au transformation and physical reshaping from fluvial transport is correlated to overall morphology of the Au-Ag particles in Switzerland.
3. Higher species diversity in Au particles from the proximal site suggests an early stage of microbial recruitment and becomes more specialised and more resistant to Au toxicity; with lower diversity but a more specialised community as the degree of transformation increases.
4. The physical reshaping of Au by fluvial transport induces a compact, stable biofilm thereby influencing biofilm community composition and its putative capabilities in EPS production and metabolic behaviour.

6.4. Regional mineralisation directs the stage of biogeochemical and physical transformations of placer gold

The progressive transformation of Au particles was further studied to differentiate between the biogeochemical and physical characteristics in relation to the regional mineralisation. Comparison of the microprobe maps of Au particles from the two mineralisation style showed a different chemical signature/pattern observed in an epithermal system compared to a typical placer Au derived from the hydrothermal system. The texture of Au particles from the epithermal system showed

Ag-rich fabrics in between Au-rich clusters. This is possibly influenced by the conditions in epithermal systems involving the rapid change in temperature, pressure and pH of the circulating fluid before gold dropped out of the solution. The presence of a homogenous Au-Ag alloy in a classical hydrothermal system is attributed to a longer phase equilibrium stage along alteration zones before gold dropped out of the solution. Thus, a chemical signature is preserved as Au particles undergo transformation in surface environments. Preferential expulsion on Ag-rich boundaries in Au particles from the epithermal system depletes the electrum of Ag composition and exposes fresh surface along the particle margins for further biogeochemical transformation.

Conclusions in Chapter 4

1. The regional mineralisation influences the next "step" in the physical and biogeochemical transformation processes and ultimately the transformation stages and biofilm composition.
2. Placer Au particles from Germany are physically and biogeochemically transformed with the distinct Au:Ag fabric for epithermal systems compared to a typical Au-Ag alloy of Au particles from classical hydrothermal systems.
3. Biofilms with putative traits that aids in Au mobility exist on placer gold particles from epithermal systems.
4. The difference in the Au:Ag ratio based on the conditions of the mineralisation system results in changes in the microbial community composition as an adaptive response to high Ag-toxicity in Au particles from epithermal systems and high Au-toxicity in classical hydrothermal systems.

6.5. Assessing the mode of transport of gold from natural gold particles

The mobility/immobility of Au nanoparticles is influenced by OM, clays and Fe/Mn-oxides within soils from which placer Au particles would likely occur (Reith and Cornelis 2017). In Chapter 5, natural Au particles were used to experimentally demonstrate the "release" or formation of AuNPs by microorganisms. Microbially-mediated Au mobility by active Au mobilisers, *e.g.*, *C. violaceum* and *C. glutamicum*, precipitating organisms *C. metallidurans,* as well as growth of resident microorganisms from the natural Au particles, provided evidence that elevated Au concentration detected in anomalous soils is a result of mobilised Au and AuNPs

adsorbed to the soil matrix. This study highlighted the importance of nanoparticulate gold and essential contribution of Au transport to (bio)geochemical transformations.

Conclusions in Chapter 5

1. Gold is mobile in the environment with the aid of microbial communities on Au particles. These microbes can reductively precipitate dissolved elemental Au forming Au-complexes or form AuNPs.
2. Mobile AuNP, as well as mobile Au-complexes, plays a role in the formation of surface and soil anomalies including the occurrence of transformed Au particles.
3. Solubilisation of Au by cyanide and amino acid was experimentally verified and contributes to the dispersion of Au in natural environments.
4. Clay and organic matter content contributes to mobility and immobility of natural AuNPs.

6.6. Model for the biogeochemical cycle and transformation of gold particles

This PhD thesis leads to a final conclusion and formation of a revised model as shown in Fig. 6.1. that supports the existing unified model of gold transformation by Reith et al. (2010) and Fairbrother et al. (2012). In this model, the links between Au particle transformation and (bio)geochemical processes including deposit style/regional mineralisation, biofilm development and physical weathering are shown to constitute the biogeochemical cycling of gold.

Final Conclusion

The increase in bio(geo)chemical transformation and physical reworking is associated with the recruitment of more diverse and more stable biofilms capable of overcoming metal toxicity, alter metabolic behaviour and share putative functional traits

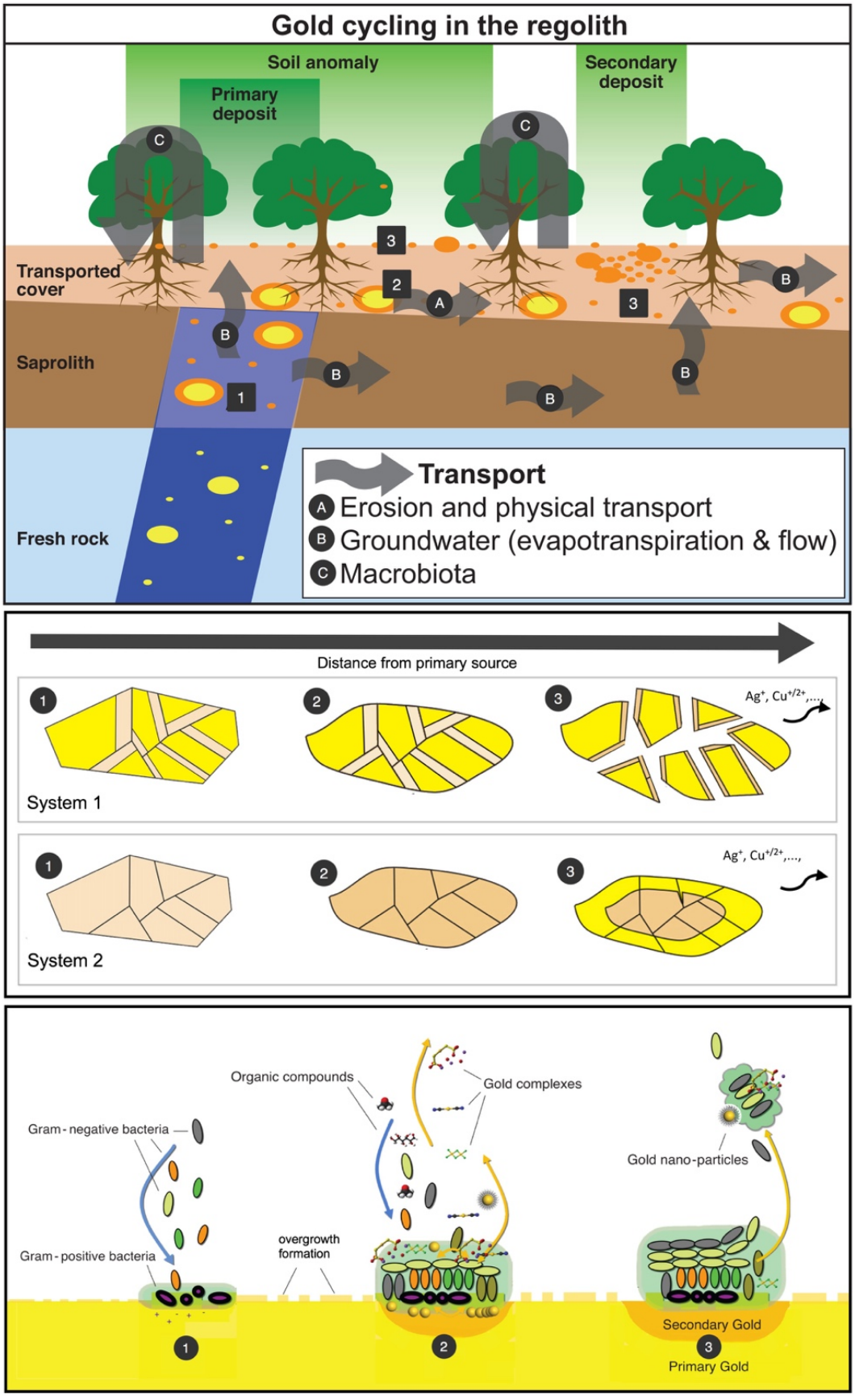

Figure 6.1. Model of gold transformation. Modified after Reith et al. (2010) and Fairbrother et al. (2012). Bright yellow is high purity Au (>99.9 wt. %), orange is Au-Ag alloy.

6.7. Applications and limitations of the revised model and future research directions

The main results of this PhD research show: (i) putative functional ability of resident microorganisms on the surface of Au particles, (ii) stages of Au particle transformation influencing microbial community composition and *vice versa*, and (iii) role of the resident microbial community on Au particles in the mobility of natural Au nanoparticles and/or release of Au-complexes in the formation of surface soil anomalies including secondary enrichment zones and exploration halos. Exploring the relationships between bio(geo)chemical processes, physical reworkings and regional mineralisation to Au particle transformation is essential to fully understand the biogeochemical cycle of Au. These answers address the long held-assumption that biofilms living on the surface of Au particles are the main contributors to the transformation of Au and eventually in the greater scale, aids in the formation of Au dispersion halos. However, more questions concerning the gold cycle remain unanswered and require addressing if further understanding is to be achieved. Among these are:

- How does the revised model apply to other mineralisation/deposit style and extreme environmental conditions?
- What are the physiological, bio(geo)chemical and microbial mechanisms involved in Au particle transformation and Au cycling?
- How long does progressive bacterial surface transformation happen and can the kinetics of these processes be further elucidated?
- What are the changes (up regulation and down regulation) which occur in transcriptomes of these microbial isolates to deal with Au toxicity brought by Au transformation?
- Which functional proteins/enzymes drive the bio(geo)chemical reactions involved in Au transformation?
- How do phylogenetic analysis and assumed functions on microbial community composition from Au particles compare with actual functional analysis?

These studies highlighted the influence of microbial communities on biogeochemical cycling of Au; primarily, Au particle transformation and mobility. However, a number of further studies and additional experiments are needed to address the questions previously raised. The experimental demonstration of Au

mobility in these studies assessed the contribution and influence of microbial biofilms in the mobilisation and transformation of gold. This also provided baseline information on the dispersion, size distribution and mode of transport of mobile Au in the soil matrix. However, the functional traits of the resident microorganisms that contributed to the mobility of gold in terms of nanoparticle dispersion, biofilm development and Au surface transformations on gold particles need to be elucidated in future studies. The results of this study have also demonstrated that microorganisms assist in mobility of Au from natural Au particles; however, calculation of the rate of formation of these natural particles needs to be conducted to resolve the time scale of Au-nanoparticle/complex formation and assess how this equates to the overall Au transformation processes. To elucidate Au speciation, high-performance liquid chromatography-inductively coupled plasma- mass spectrometry (HPLC-ICP-MS; Ta et al. 2014) can be used to measure the speciation of gold under *in situ* conditions in various liquid samples together with the quantified gold nanoparticle dispersion and distribution using single particle (SP)-ICP-MS analysis as we recently demonstrated in this study. This ultimately quantifies the (de)stabilisation of mobile Au and sorption of Au-complexes and Au particles to the formation of secondary zones of gold enrichment. Kinetic rate equations can be fitted to and integrated into a numerical model that can be used to estimate the dispersion of gold in the environment and help design effective exploration strategies when a quantitative understanding of transport, sorption and speciation of gold is achieved.

Furthermore, this study has also evaluated the presence of secondary Au morphotypes and stages of gold transformation indicative of biogeochemical Au cycling in various physical and (bio)geochemical factors from different mineralisation system found in otherwise comparable climatic and environmental conditions. The microbial diversity and biofilm community composition on Au particles was assessed using NGS and led to the analysis of phylogenetic composition and characterisation of putative functional capabilities of biofilm communities that are involved in Au transformation. However, further investigation is needed to address the questions above to obtain a better understanding of multi-species biofilm development and link those compositions directly to functional abilities. Initially, isolation of resident microorganism on Au particles needs to be done to do further work on identifying functional genetic determinants and proteomic responses, *e.g.*, metabolic activities, transcriptional regulation, efflux and especially metal transport for resistance and survival to Au toxicity. It is essential to determine the entire metabolic capabilities of individual species involved in these biofilm communities, which may be achieved by

metagenomic sequencing and high-density functional microarrays, *e.g.*, GeoChip (He et al. 2007; Zhou et al. 2010). This will aid in understanding the roles played by each member of the consortium by shedding light on the principles governing recruitment, maintenance, compartmentalisation and redundancy of metabolic function (Johnson et al. 2012). In addition, directly identifying and characterizing the proteins involved in Au-sensing and detoxification may aid in Au exploration, by providing ultra-sensitive Au biosensors for field measurement of Au in environmental samples.

6.8. Future applications of this research

Gold cycling in Earth surface environments is largely driven by biogeochemical processes leading to gold dispersion and re-concentration in soils and other regolith materials. The decline in discovery rates of Au in Australia and other parts of the world calls for innovative gold exploration and low impact gold recovery method to provide a firm foundation for geochemical mineral exploration. Exploration in buried gold deposit is difficult, expensive and therefore often relies on assessing gold contents in easily obtainable materials, *e.g.*, soils, groundwaters, plants and other regolith materials. The discovery of new gold deposits requires consistent improvement of exploration strategies and technologies. Understanding the significance of geochemical halos is a key step in this process. This is especially important to allocate on exploration budgets for the large international mining companies.

Elucidating the links between the stages of Au transformation and the biogeochemical and physical processes increases our fundamental knowledge of gold biogeochemical cycling and transport in Earth's surface environments. The mobilisation of gold aided by microbial weathering releases gold trapped within minerals to surface, soil and ground waters as dissolved complexes and/or nanoparticles. The development of a numerical model for the movement of gold in the regolith, which can be turned into a practical tool for predicting the formation of secondary enrichment zones and ranking geochemical halos will be a useful tool in gold exploration programs. This study can serve as baseline data on the distribution of mobile gold which can be extended to enhance our ability to track the movement of dissolved and nanoparticulate gold in the regolith. This approach is essential to remove the 'nugget' effect in many gold exploration programs, thereby enabling exploration companies to enhance their ability to target gold anomalies in soils and sediments.

References

Abràmoff MD, Magalhães PJ, Ram SJ (2004) Image processing with ImageJ. *Biophotonics international,* **11**, 36–42.

Ahmed S, Ahmad M, Swami BL, Ikram S (2016) A review on plants extract mediated synthesis of silver nanoparticles for antimicrobial applications: a green expertise. *Journal of advanced research,* **7**, 17–28.

Alex S, Tiwari A (2015) Functionalized gold nanoparticles: synthesis, properties and applications—a review. *Journal of nanoscience and nanotechnology,* **15**, 1869–1894.

Alimova A, Katz A, Steiner N, Rudolph E, Wei H, Steiner JC, Gottlieb P (2009) Bacteria-clay interaction: structural changes in smectite induced during biofilm formation. *Clays and Clay Minerals,* **57**, 205–212.

Alonso U, Missana T, Patelli A, Ceccato D, Albarran N, Garcia-Gutierrez M, Lopez-Torrubia T, Rigato V (2009) Quantification of Au nanoparticles retention on a heterogeneous rock surface. *Colloids and Surfaces A: Physicochemical and Engineering Aspects,* **347**, 230–238.

Alvarez A, Khanna M, Toranzos G, Stotzky G (1998) Amplification of DNA bound on clay minerals. *Mol. Ecol.,* **7**, 775–778.

Anand RR, Aspandiar MF, Noble RR (2016) A review of metal transfer mechanisms through transported cover with emphasis on the vadose zone within the Australian regolith. *Ore Geology Reviews,* **73**, 394–416.

Anderson M, Gorley RN, Clarke RK (2008) *Permanova+ for Primer: Guide to Software and Statistical Methods.* Plymouth, UK: Primer-E Limited.

Andrews S (2010) FastQC: a quality control tool for high throughput sequence data. Babraham Bioinformatics, Babraham Institute, Cambridge, UK, https://www.bioinformatics.babraham.ac.uk/projects/fastqc/

Ayarza JM, Figuerola EL, Erijman L (2014) Draft genome sequences of type strain Sediminibacterium salmoneum NJ-44 and Sediminibacterium sp. strain C3, a novel strain isolated from activated sludge. *Genome announcements,* **2**, e01073–01013.

Azarbad H, Van Gestel CA, Niklińska M, Laskowski R, Röling WF, Van Straalen NM (2016) Resilience of Soil Microbial Communities to Metals and Additional Stressors: DNA-Based Approaches for Assessing "Stress-on-Stress" Responses. *Int. J. Mol. Sci.,* **17**, 933.

Azzouzi A, Steunou AS, Durand A, Khalfaoui-Hassani B, Bourbon ML, Astier C, Bollivar DW, Ouchane S (2013) Coproporphyrin III excretion identifies the anaerobic coproporphyrinogen III oxidase HemN as a copper target in the Cu+-ATPase mutant copA− of Rubrivivax gelatinosus. *Mol. Microbiol.,* **88**, 339–351.

Batjes NH (1996) Total carbon and nitrogen in the soils of the world. *European journal of soil science,* **47**, 151–163.

Bissett A, Fitzgerald A, Meintjes T, Mele PM, Reith F, Dennis PG, Breed MF, Brown B, Brown MV, Brugger J (2016) Introducing BASE: the Biomes of Australian Soil Environments soil microbial diversity database. *GigaScience,* **5**, 1.

References

Boyle RW (1979) The geochemistry of gold and its deposits: together with a chapter on geochemical prospecting for the element, *Geological Survey of Canada* Ottawa.

Boyle RW (1987) *History and Genesis of Deposits,* Springer, Boston, MA.

Brandl H, Lehmann S, Faramarzi MA, Martinelli D (2008) Biomobilization of silver, gold, and platinum from solid waste materials by HCN-forming microorganisms. *Hydrometallurgy,* **94**, 14–17.

Bray JR, Curtis JT (1957) An ordination of the upland forest communities of southern Wisconsin. *Ecol. Monogr.,* **27**, 325–349.

Bretschger O, Obraztsova A, Sturm CA, Chang IS, Gorby YA, Reed SB, Culley DE, Reardon CL, Barua S, Romine MF (2007) Current production and metal oxide reduction by Shewanella oneidensis MR-1 wild type and mutants. *Appl. Environ. Microbiol.,* **73**, 7003–7012.

Brugger J, Etschmann B, Grosse C, Plumridge C, Kaminski J, Paterson D, Shar SS, Ta C, Howard DL, De Jonge MD (2013) Can biological toxicity drive the contrasting behavior of platinum and gold in surface environments? *Chem. Geol.,* **343**, 99–110.

Bütof L, Wiesemann N, Herzberg M, Altzschner M, Holleitner A, Reith F, Nies DH (2018) Synergistic gold–copper detoxification at the core of gold biomineralisation in Cupriavidus metallidurans. *Metallomics*.

Cai P, Huang Q, Zhang X, Chen H (2006a) Adsorption of DNA on clay minerals and various colloidal particles from an Alfisol. *Soil Biology and Biochemistry,* **38**, 471–476.

Cai P, Huang Q-Y, Zhang X-W (2006b) Interactions of DNA with clay minerals and soil colloidal particles and protection against degradation by DNase. *Environ. Sci. Technol.,* **40**, 2971–2976.

Carini P, Marsden PJ, Leff JW, Morgan EE, Strickland MS, Fierer N (2017) Relic DNA is abundant in soil and obscures estimates of soil microbial diversity. *Nature microbiology,* **2**, 16242.

Cérantola S, Bounéry J-D, Segonds C, Marty N, Montrozier H (2000) Exopolysaccharide production by mucoid and non-mucoid strains of Burkholderia cepacia. *FEMS Microbiol. Lett.,* **185**, 243–246.

Chapman R, Mortensen J (2016) Characterization of gold mineralization in the Northern Cariboo Gold District, British Columbia, Canada, through integration of compositional studies of lode and detrital Gold with historical placer production: a template for evaluation of orogenic gold districts. *Economic Geology,* **111**, 1321–1345.

Chapman RJ, Mortensen JK, Lebarge WP (2011) Styles of lode gold mineralization contributing to the placers of the Indian River and Black Hills Creek, Yukon Territory, Canada as deduced from microchemical characterization of placer gold grains. *Mineralium Deposita,* **46**, 881–903.

References

Chaudhuri SK, Lovley DR (2003) Electricity generation by direct oxidation of glucose in mediatorless microbial fuel cells. *Nat. Biotechnol.,* **21**, 1229–1232

Checa SK, Espariz M, Audero MEP, Botta PE, Spinelli SV, Soncini FC (2007) Bacterial sensing of and resistance to gold salts. *Mol. Microbiol.,* **63**, 1307–1318.

Chen Y-T, Li J-T, Chen L-X, Hua Z-S, Huang L-N, Liu J, Xu B-B, Liao B, Shu W-S (2014) Biogeochemical processes governing natural pyrite oxidation and release of acid metalliferous drainage. *Environ. Sci. Technol.,* **48**, 5537–5545.

Clarke KR, Warwick R (2001) Change in marine communities. *An approach to statistical analysis and interpretation*. Primer-E Ltd., Plymouth, United Kingdom 2001.

Colman T (2010) Gold in Britain: past, present and future. *Mercian Geologist,* **17**, 173–180.

Cornelis G, Doolettemadeleine Thomas C, Mclaughlin MJ, Kirby JK, Beak DG, Chittleborough D (2012) Retention and dissolution of engineered silver nanoparticles in natural soils. *Soil Science Society of America Journal,* **76**, 891–902.

Cornelis G, Hund-Rinke K, Kuhlbusch T, Van Den Brink N, Nickel C (2014) Fate and bioavailability of engineered nanoparticles in soils: a review. *Critical Reviews in Environmental Science and Technology,* **44**, 2720–2764.

Cornelis G, Pang L, Doolette C, Kirby JK, Mclaughlin MJ (2013) Transport of silver nanoparticles in saturated columns of natural soils. *Sci. Total Environ.,* **463**, 120–130.

Corti CW, Holliday RJ (2004) Commercial aspects of gold applications: from materials science to chemical science. *Gold Bulletin,* **37**, 20–26.

Costerton JW, Lewandowski Z, Caldwell DE, Korber DR, Lappin-Scott HM (1995) Microbial biofilms. *Annual Reviews in Microbiology,* **49**, 711-745.

Craw D (2017) Placer gold and associated supergene mineralogy at Macraes Flat, East Otago, New Zealand. *New Zealand Journal of Geology and Geophysics,* **60**, 353–367.

Craw D, Hesson M, Kerr G (2017) Morphological evolution of gold nuggets in proximal sedimentary environments, southern New Zealand. *Ore Geology Reviews,* **80**, 784–799.

Craw D, Lilly K (2016) Gold nugget morphology and geochemical environments of nugget formation, southern New Zealand. *Ore Geology Reviews,* **79**, 301–315.

Craw D, Mackenzie D, Grieve P (2015) Supergene gold mobility in orogenic gold deposits, Otago Schist, New Zealand. *New Zealand Journal of Geology and Geophysics,* **58**, 123–136.

Daniel M-C, Astruc D (2004) Gold nanoparticles: assembly, supramolecular chemistry, quantum-size-related properties, and applications toward biology, catalysis, and nanotechnology. *Chem. Rev.,* **104**, 293–346.

References

Darlington TK, Neigh AM, Spencer MT, Guyen OT, Oldenburg SJ (2009) Nanoparticle characteristics affecting environmental fate and transport through soil. *Environ. Toxicol. Chem.,* **28**, 1191–1199.

Dickinson WH, Caccavo F, Olesen B, Lewandowski Z (1997) Ennoblement of Stainless Steel by the Manganese-Depositing Bacterium *Leptothrix discophora*. *Appl. Environ. Microbiol.,* **63**, 2502–2506.

Diegoli S, Manciulea AL, Begum S, Jones IP, Lead JR, Preece JA (2008) Interaction between manufactured gold nanoparticles and naturally occurring organic macromolecules. *Sci. Total Environ.,* **402**, 51–61.

Dilabio R (1991) Classification and interpretation of the shapes and surface textures of gold grains from till. In: *Gisements alluviaux d'or (Alluvial Gold Placers/Yacimientos aluviales de oro)*. ORSTOM Paris, pp. 297–313.

Dill H (2008) Geogene and anthropogenic controls on the mineralogy and geochemistry of modern alluvial–(fluvial) gold placer deposits in man-made landscapes in France, Switzerland and Germany. *Journal of Geochemical Exploration,* **99**, 29–60.

Dill HG, Klosa D, Steyer G (2009) The "Donauplatin": source rock analysis and origin of a distal fluvial Au-PGE placer in Central Europe. *Mineralogy and Petrology,* **96**, 141–161.

Dockrey JW, Lindsay MB, Mayer KU, Beckie RD, Norlund KL, Warren LA, Southam G (2014) Acidic microenvironments in waste rock characterized by neutral drainage: Bacteria–mineral interactions at sulfide surfaces. *Minerals,* **4**, 170–190.

Donlan RM (2002) Biofilms: microbial life on surfaces. *Emerg. Infect. Dis.,* **8**.

Donovan JJ, Tingle TN (1996) An improved mean atomic number background correction for quantitative microanalysis. *Microsc. Microanal.,* **2**, 1–7.

Dopson M, Ni G, Sleutels TH (2016) Possibilities for extremophilic microorganisms in microbial electrochemical systems. *FEMS Microbiol. Rev.,* **40**, 164–181.

Dzombak DA, Ghosh RS, Wong-Chong GM (2005) *Cyanide in water and soil: chemistry, risk, and management,* CRC press.

Edgar RC (2013) UPARSE: highly accurate OTU sequences from microbial amplicon reads. *Nature methods,* **10**, 996–998.

Elias S, Banin E (2012) Multi-species biofilms: living with friendly neighbors. *FEMS Microbiol. Rev.,* **36**, 990–1004.

Etschmann B, Brugger J, Fairbrother L, Grosse C, Nies D, Martinez-Criado G, Reith F (2016) Applying the Midas touch: Differing toxicity of mobile gold and platinum complexes drives biomineralization in the bacterium Cupriavidus metallidurans. *Chem. Geol.,* **438**, 103–111.

Fairbrother L, Brugger J, Shapter J, Laird J, Southam G, Reith F (2012) Supergene gold transformation: Biogenic secondary and nanoparticulate gold from arid Australia. *Chem. Geol.,* **320**, 17–31.

References

Fairbrother L, Etschmann B, Brugger J, Shapter J, Southam G, Reith F (2013) Biomineralization of gold in biofilms of Cupriavidus metallidurans. *Environ. Sci. Technol.*, **47**, 2628–2635.

Fairbrother L, Shapter J, Brugger J, Southam G, Pring A, Reith F (2009) Effect of the cyanide-producing bacterium Chromobacterium violaceum on ultraflat Au surfaces. *Chem. Geol.*, **265**, 313–320.

Falconer D, Craw D (2009) Supergene gold mobility: a textural and geochemical study from gold placers in southern New Zealand. *Economic Geology Special Publication*, **14**, 77–93.

Falconer D, Craw D, Youngson J, Faure K (2006) Gold and sulphide minerals in Tertiary quartz pebble conglomerate gold placers, Southland, New Zealand. *Ore Geology Reviews*, **28**, 525–545.

Faramarzi MA, Stagars M, Pensini E, Krebs W, Brandl H (2004) Metal solubilization from metal-containing solid materials by cyanogenic Chromobacterium violaceum. *J. Biotechnol.*, **113**, 321–326.

Finnegan I, Toerien S, Abbot L, Smit F, Raubenheimer H (1991) Identification and characterisation of an Acinetobacter sp. capable of assimilation of a range of cyano-metal complexes, free cyanide ions and simple organic nitriles. *Appl. Microbiol. Biotechnol.*, **36**, 142–144.

Fisher E, Fisher V, Millar A (1974) Nature of the interaction of natural organic acids with gold. *Sov Geo*, **7**, 142–146.

Flemming H-C, Wingender J (2010) The biofilm matrix. *Nature Reviews Microbiology*, **8**, 623.

Florea LJ, Stinson CL, Brewer J, Fowler R, Kearns BJ, Greco AM (2011) Iron oxide and calcite associated with Leptothrix sp. biofilms within an estavelle in the upper Floridan aquifer. *International Journal of Speleology*, **40**, 11.

Fratesi SE, Lynch FL, Kirkland BL, Brown LR (2004) Effects of SEM preparation techniques on the appearance of bacteria and biofilms in the Carter Sandstone. *Journal of Sedimentary Research*, **74**, 858–867.

Freise FW (1931) The transportation of gold by organic underground solutions. *Economic Geology*, **26**, 421–431.

Frimmel H, Le Roex A, Knight J, Minter W (1993) A case study of the postdepositional alteration of the Witwatersrand Basal Reef gold placer. *Economic Geology*, **88**, 249–265.

Gadd GM (2004) Microbial influence on metal mobility and application for bioremediation. *Geoderma*, **122**, 109-119.

George M (2013) Gold: US Geological Survey Mineral Commodity Summaries.

Geslin C, Llanos J, Prieur D, Jeanthon C (2001) The manganese and iron superoxide dismutases protect Escherichia coli from heavy metal toxicity. *Res. Microbiol.*, **152**, 901–905.

References

Gillan DC (2016) Metal resistance systems in cultivated bacteria: are they found in complex communities? *Curr. Opin. Biotechnol.,* **38**, 123–130.

Golby S, Ceri H, Marques LL, Turner RJ (2014) Mixed-species biofilms cultured from an oil sand tailings pond can biomineralize metals. *Microb. Ecol.,* **68**, 70–80.

Gottenbos B, Grijpma DW, Van Der Mei HC, Feijen J, Busscher HJ (2001) Antimicrobial effects of positively charged surfaces on adhering gram-positive and gram-negative bacteria. *J. Antimicrob. Chemother.,* **48**, 7–13.

Gray D, Lintern M, Longman G (1998) Chemistry of gold-humic interaction CSIRO Division of Exploration Geoscience Report 128R, 1990. *Second impression*.

Green PN (2006) Methylobacterium. In: *The Prokaryotes: Volume 5: Proteobacteria: Alpha and Beta Subclasses* (eds Dworkin M, Falkow S, Rosenberg E, Schleifer K-H, Stackebrandt E). Springer New York, New York, NY, pp. 257–265.

Groen JC, Craig JR, Rimstidt JD (1990) Gold-rich rim formation on electrum grains in placers. *The Canadian Mineralogist,* **28**, 207–228.

Gunn A, Styles M (2002) Platinum-group element occurrences in Britain: magmatic, hydrothermal and supergene. *Applied Earth Science,* **111**, 2–14.

Hagedorn E, Boenigk W (2008) The Pliocene and Quaternary sedimentary and fluvial history in the Upper Rhine Graben based on heavy mineral analyses. *Netherlands Journal of Geosciences-Geologie en Mijnbouw,* **87**, 21.

Hall-Stoodley L, Costerton JW, Stoodley P (2004) Bacterial biofilms: from the natural environment to infectious diseases. *Nature Reviews Microbiology,* **2**, 95–108.

Hancock RE, Brinkman FS (2002) Function of Pseudomonas porins in uptake and efflux. *Annual Reviews in Microbiology,* **56**, 17–38.

Harrison JJ, Ceri H, Turner RJ (2007) Multimetal resistance and tolerance in microbial biofilms. *Nature Reviews Microbiology,* **5**, 928–938.

He Z, Gentry TJ, Schadt CW, Wu L, Liebich J, Chong SC, Huang Z, Wu W, Gu B, Jardine P (2007) GeoChip: a comprehensive microarray for investigating biogeochemical, ecological and environmental processes. *The ISME journal,* **1**, 67–77.

Hendrickx L, Hausner M, Wuertz S (2003) Natural genetic transformation in monoculture Acinetobacter sp. strain BD413 biofilms. *Appl. Environ. Microbiol.,* **69**, 1721–1727.

Hiraishi A, Shin YK, Sugiyama J (1997) Proposal To Reclassify Zoogloea ramigera IAM 12670 (PR Dugan 115) as Duganella zoogloeoides gen. nov., sp. nov. *Int. J. Syst. Bacteriol.,* **47**, 1249–1252.

Hough R, Butt C, Reddy S, Verrall M (2007) Gold nuggets: supergene or hypogene? *Australian Journal of Earth Sciences,* **54**, 959–964.

Hough R, Noble R, Reich M (2011) Natural gold nanoparticles. *Ore Geology Reviews,* **42**, 55–61.

Humphries J, Xiong L, Liu J, Prindle A, Yuan F, Arjes HA, Tsimring L, Süel GM (2017) Species-independent attraction to biofilms through electrical signaling. *Cell,* **168**, 200–209. e212.

Husseiny M, El-Aziz MA, Badr Y, Mahmoud M (2007) Biosynthesis of gold nanoparticles using Pseudomonas aeruginosa. *Spectrochimica Acta Part A: Molecular and Biomolecular Spectroscopy,* **67**, 1003–1006.

Hutchins S, Davidson M, Brierley J, Brierley C (1986) Microorganisms in reclamation of metals. *Annual Reviews in Microbiology,* **40**, 311–336.

Johnson DR, Goldschmidt F, Lilja EE, Ackermann M (2012) Metabolic specialization and the assembly of microbial communities. *The ISME journal,* **6**, 1985–1991.

Johnston CW, Wyatt MA, Li X, Ibrahim A, Shuster J, Southam G, Magarvey NA (2013) Gold biomineralization by a metallophore from a gold-associated microbe. *Nat. Chem. Biol.,* **9**, 241–243.

Kaji A, Mcelroy W (1959) Mechanism of hydrogen sulfide formation from thiosulfate. *J. Bacteriol.,* **77**, 630.

Kalinowski J, Bathe B, Bartels D, Bischoff N, Bott M, Burkovski A, Dusch N, Eggeling L, Eikmanns BJ, Gaigalat L (2003) The complete Corynebacterium glutamicum ATCC 13032 genome sequence and its impact on the production of L-aspartate-derived amino acids and vitamins. *J. Biotechnol.,* **104**, 5–25.

Kamenov GD, Melchiorre EB, Ricker FN, Dewitt E (2013) Insights from Pb isotopes for native gold formation during hypogene and supergene processes at Rich Hill, Arizona. *Economic Geology,* **108**, 1577–1589.

Karthikeyan S, Beveridge T (2002) Pseudomonas aeruginosa biofilms react with and precipitate toxic soluble gold. *Environ. Microbiol.,* **4**, 667–675.

Kenney JP, Song Z, Bunker BA, Fein JB (2012) An experimental study of Au removal from solution by non-metabolizing bacterial cells and their exudates. *Geochim. Cosmochim. Acta,* **87**, 51–60.

Kerr G, Malloch K, Lilly K, Craw D (2017) Diagenetic alteration of a Mesozoic fluvial gold placer deposit, southern New Zealand. *Ore Geology Reviews,* **83**, 14–29.

Kinnunen KA (1996) Classification scheme for surface textures of gold nuggets from Finnish Lapland. *Bulletin-Geological Society of Finland,* **68**, 18–33.

Knight J, Morison S, Mortensen J (1999) The relationship between placer gold particle shape, rimming, and distance of fluvial transport as exemplified by gold from the Klondike District, Yukon Territory, Canada. *Economic Geology,* **94**, 635–648.

Koechler S, Farasin J, Cleiss-Arnold J, Arsène-Ploetze F (2015) Toxic metal resistance in biofilms: diversity of microbial responses and their evolution. *Res. Microbiol.,* **166**, 764–773.

Konopa S, Chesher R, Gleeson E, Allen P, Boakye D (2015) Challenges in maximising the value from epithermal gold deposits. *AusIMM Bulletin*, 70.

References

Korobushkina E, Cherniak A, Mineev G (1974) Dissolution of gold by microorganisms and the products of their metabolism. *Mikrobiologiia,* **43**, 49.

Korobushkina E, Karavaiko G, Korobushkin I (1983) Biochemistry of gold. *Ecological Bulletins*, 325–333.

Korobushkina E, Mineev G, Praded G (1976) Mechanism of microbiological dissolution of gold. *Mikrobiologiia,* **45**, 535–538.

Kottek M, Grieser J, Beck C, Rudolf B, Rubel F (2006) World map of the Köppen-Geiger climate classification updated. *Meteorologische Zeitschrift,* **15**, 259–263.

Laborda F, Jiménez-Lamana J, Bolea E, Castillo JR (2013) Critical considerations for the determination of nanoparticle number concentrations, size and number size distributions by single particle ICP-MS. *Journal of Analytical Atomic Spectrometry,* **28**, 1220–1232.

Lane DJ, Pace B, Olsen GJ, Stahl DA, Sogin ML, Pace NR (1985) Rapid determination of 16S ribosomal RNA sequences for phylogenetic analyses. *Proceedings of the National Academy of Sciences,* **82**, 6955–6959.

Lane, D. (1991). 16S/23S rRNA sequencing. *Nucleic acid techniques in bacterial systematics*. 115–175

Langille MG, Zaneveld J, Caporaso JG, Mcdonald D, Knights D, Reyes JA, Clemente JC, Burkepile DE, Thurber RLV, Knight R (2013) Predictive functional profiling of microbial communities using 16S rRNA marker gene sequences. *Nat. Biotechnol.,* **31**, 814.

Lehrberger G (1995) The Gold Deposits of Europe. In: *Prehistoric Gold in Europe*. Springer, pp. 115–144.

Lengke M, Southam G (2006) Bioaccumulation of gold by sulfate-reducing bacteria cultured in the presence of gold (I)-thiosulfate complex. *Geochim. Cosmochim. Acta,* **70**, 3646–3661.

Lengke MF, Ravel B, Fleet ME, Wanger G, Gordon RA, Southam G (2006) Mechanisms of gold bioaccumulation by filamentous cyanobacteria from gold (III)-chloride complex. *Environ. Sci. Technol.,* **40**, 6304–6309.

Levard C, Hotze EM, Lowry GV, Brown Jr GE (2012) Environmental transformations of silver nanoparticles: impact on stability and toxicity. *Environ. Sci. Technol.,* **46**, 6900–6914.

Li J, Li Q, Ma X, Tian B, Li T, Yu J, Dai S, Weng Y, Hua Y (2016) Biosynthesis of gold nanoparticles by the extreme bacterium Deinococcus radiodurans and an evaluation of their antibacterial properties. *International journal of nanomedicine,* **11**, 5931.

Liou JC, Derito C, Madsen E (2008) Field-based and laboratory stable isotope probing surveys of the identities of both aerobic and anaerobic benzene-metabolizing microorganisms in freshwater sediment. *Environ. Microbiol.,* **10**, 1964–1977.

Liu J, Chakraborty S, Hosseinzadeh P, Yu Y, Tian S, Petrik I, Bhagi A, Lu Y (2014) Metalloproteins containing cytochrome, iron–sulfur, or copper redox centers. *Chem. Rev,* **114**, 4366–4469.

Liu J, Martinez-Corral R, Prindle A, Dong-Yeon DL, Larkin J, Gabalda-Sagarra M, Garcia-Ojalvo J, Süel GM (2017) Coupling between distant biofilms and emergence of nutrient time-sharing. *Science,* **356**, 638–642.

Liu Y, Tay JH (2001) Metabolic response of biofilm to shear stress in fixed-film culture. *J. Appl. Microbiol.,* **90**, 337-342.

Lloyd JR, Leang C, Myerson ALH, Coppi MV, Cuifo S, Methe B, Sandler SJ, Lovley DR (2003) Biochemical and genetic characterization of PpcA, a periplasmic c-type cytochrome in Geobacter sulfurreducens. *Biochem. J.,* **369**, 153–161.

Lodewyckx C, Taghavi S, Mergeay M, Vangronsveld J, Clijsters H, Lelie DVD (2001) The effect of recombinant heavy metal-resistant endophytic bacteria on heavy metal uptake by their host plant. *International journal of phytoremediation,* **3**, 173–187.

Magoč T, Salzberg SL (2011) FLASH: fast length adjustment of short reads to improve genome assemblies. *Bioinformatics,* **27**, 2957–2963.

Mann A (1984) Mobility of gold and silver in lateritic weathering profiles; some observations from Western Australia. *Economic Geology*, **79**, 38–49.

McCready A, Parnell J, Castro L (2003) Crystalline placer gold from the Rio Neuquen, Argentina: Implications for the gold budget in placer gold formation. *Economic Geology,* **98**, 623–633.

Meinel G (1993) *Die Bildung der Gangmineralisation Thüringens,* Thüringer Landesanst. für Bodenforschung.

Melchiorre EB, Orwin PM, Reith F, Rea MaD, Yahn J, Allison R (2018) Biological and Geochemical Development of Placer Gold Deposits at Rich Hill, Arizona, USA. *Minerals,* **8**, 56.

Meliani A, Bensoltane A (2016) Biofilm-mediated heavy metals bioremediation in PGPR Pseudomonas. *J Bioremediat Biodegrad,* **7**, 370.

Michaels R, Corpe W (1965) Cyanide formation by Chromobacterium violaceum. *J. Bacteriol.,* **89**, 106–112.

Mineyev G (1976) Organisms in the gold migration-accumulation cycle. *Geochemistry International,* **13**, 577–582.

Morávek P, Pouba Z, Janatka J, Malec J, Novák F, Litochleb J, Váňa T, Veselý J, Vaněček M, Kalenda Z (1992) Gold in the Bohemian Massif. *Czech Geological Survey. Prague*, 1–245.

Mossman DJ, Dyer BD (1985) The geochemistry of Witwatersrand-type gold deposits and the possible influence of ancient prokaryotic communities on gold dissolution and precipitation. *Precambrian research,* **30**, 303–319.

Mrozik A, Piotrowska-Seget Z (2010) Bioaugmentation as a strategy for cleaning up of soils contaminated with aromatic compounds. *Microbiol. Res.,* **165**, 363–375.

Mueller B (2015) Experimental interactions between clay minerals and bacteria: A review. *Pedosphere,* **25**, 799–810.

Mycroft J, Bancroft G, Mcintyre N, Lorimer J (1995) Spontaneous deposition of gold on pyrite from solutions containing Au (III and Au (I) chlorides. Part I: A surface study. *Geochim. Cosmochim. Acta,* **59**, 3351–3365.

Nangia Y, Wangoo N, Goyal N, Shekhawat G, Suri CR (2009a) A novel bacterial isolate Stenotrophomonas maltophilia as living factory for synthesis of gold nanoparticles. *Microb Cell Fact,* **8**, 39–46.

Nangia Y, Wangoo N, Sharma S, Wu J-S, Dravid V, Shekhawat G, Suri CR (2009b) Facile biosynthesis of phosphate capped gold nanoparticles by a bacterial isolate Stenotrophomonas maltophilia. *Applied Physics Letters,* **94**, 233901.

Nelson Y, Lion L, Ghiorse W, Shuler M (1998) Pb adsorption and surface area of bacterially oxidized Mn. *Mineralogical Magazine A,* **62**, 1073–1074.

Nevin KP, Hensley SA, Franks AE, Summers ZM, Ou J, Woodard TL, Snoeyenbos-West OL, Lovley DR (2011) Electrosynthesis of organic compounds from carbon dioxide is catalyzed by a diversity of acetogenic microorganisms. *Appl. Environ. Microbiol.,* **77**, 2882–2886.

Nielsen R, Matz M (2006) Statistical approaches for DNA barcoding. *Syst. Biol.,* **55**, 162–169.

Nies DH (1999) Microbial heavy-metal resistance. *Appl. Microbiol. Biotechnol.,* **51**, 730–750.

Nies DH (2016) The biological chemistry of the transition metal "transportome" of Cupriavidus metallidurans. *Metallomics*.

Nies DH, Brown NL (1998) Two-component systems in the regulation of heavy metal resistance. In: *Metal ions in gene regulation*. Springer, pp. 77–103.

Oberthür T, Melcher F, Goldmann S, Wotruba H, Gerdes A, Dijkstra A, Dale CW (2016) Mineralogy and mineral chemistry of detrital heavy minerals from the Rhine River in Germany as evidence to their provenance, sedimentary and depositional history: focus on platinum-group minerals and remarks on cassiterite, columbite-group minerals and uraninite. *International Journal of Earth Sciences,* **105**, 637–657.

Ogram A, Sayler GS, Gustin D, Lewis RJ (1988) DNA adsorption to soils and sediments. *Environ. Sci. Technol.,* **22**, 982–984.

Ong HL and Swanson VE (1969). Natural organic acids in the transportation, deposition and concentration of gold. Colo. Sch. Mines Q. **64**, 395–425.

References

Orberger B, Pasava J, Gallien JP, Daudin L, Trocellier P (2003) Se, As, Mo, Ag, Cd, In, Sb, Pt, Au, Tl, Re traces in biogenic and abiogenic sulfides from Black Shales (Selwyn Basin, Yukon territories, Canada): a nuclear microprobe study. *Nuclear Instruments and Methods in Physics Research Section B: Beam Interactions with Materials and Atoms,* **210**, 441–448.

Osborn AM, Moore ER, Timmis KN (2000) An evaluation of terminal-restriction fragment length polymorphism (T-RFLP) analysis for the study of microbial community structure and dynamics. *Environ. Microbiol.,* **2**, 39–50.

Paget E, Monrozier LJ, Simonet P (1992) Adsorption of DNA on clay minerals: protection against DNaseI and influence on gene transfer. *FEMS Microbiol. Lett.,* **97**, 31–39.

Pal A, Paul A (2008) Microbial extracellular polymeric substances: central elements in heavy metal bioremediation. *Indian J. Microbiol.,* **48**, 49–64.

Pamp SJ, Tolker-Nielsen T (2007) Multiple roles of biosurfactants in structural biofilm development by Pseudomonas aeruginosa. *J. Bacteriol.,* **189**, 2531–2539.

Parsek MR, Greenberg E (2005) Sociomicrobiology: the connections between quorum sensing and biofilms. *Trends Microbiol.,* **13**, 27–33.

Peeters E, Nelis HJ, Coenye T (2008) Resistance of planktonic and biofilm-grown Burkholderia cepacia complex isolates to the transition metal gallium. *J. Antimicrob. Chemother.,* **61**, 1062–1065.

Pietramellara G, Ascher J, Borgogni F, Ceccherini M, Guerri G, Nannipieri P (2009) Extracellular DNA in soil and sediment: fate and ecological relevance. *Biol. Fertil. Soils,* **45**, 219–235.

Prindle A, Liu J, Asally M, Ly S, Garcia-Ojalvo J, Süel GM (2015) Ion channels enable electrical communication in bacterial communities. *Nature,* **527**, 59–63.

Puskas A, Greenberg EÁ, Kaplan S, Schaefer AÁ (1997) A quorum-sensing system in the free-living photosynthetic bacterium Rhodobacter sphaeroides. *J. Bacteriol.,* **179**, 7530–7537.

Ramdohr P (1932) Die goldlagerstätte des Eisenbergs bei Corbach. *Geologiska Föreningen i Stockholm Förhandlingar,* **54**, 528–529.

Ramdohr P (1965) Rheingold als Seifenmineral. *Jh Geol Landesamt Baden-Württemberg,* **7**, 87–95.

Rasband W (2012). ImageJ: Image processing and analysis in Java. U.S. National Institutes of Health, Bethesda, Maryland, USA. *Astrophysics Source Code Library*. https://imagej.nih.gov/ij/

Rea MA, Standish CD, Shuster J, Bissett A, Reith F (2018) Progressive biogeochemical transformation of placer gold particles drives compositional changes in associated biofilm communities. *FEMS Microbiol. Ecol.*, fiy080.

Rea MA, Zammit CM, Reith F (2016) Bacterial biofilms on gold grains – Implications for geomicrobial transformations of gold. *FEMS Microbiol. Ecol.*, fiw082.

References

Reguera G, Mccarthy KD, Mehta T, Nicoll JS (2005) Extracellular electron transfer via microbial nanowires. *Nature,* **435**, 1098.

Reith F, Brugger J, Zammit CM, Gregg AL, Goldfarb KC, Andersen GL, Desantis TZ, Piceno YM, Brodie EL, Lu Z (2012) Influence of geogenic factors on microbial communities in metallogenic Australian soils. *The ISME journal,* **6**, 2107–2118.

Reith F, Brugger J, Zammit CM, Nies DH, Southam G (2013) Geobiological cycling of gold: from fundamental process understanding to exploration solutions. *Minerals,* **3**, 367–394.

Reith F, Cornelis G (2017) Effect of soil properties on gold-and platinum nanoparticle mobility. *Chem. Geol.,* **466**, 446–453.

Reith F, Etschmann B, Grosse C, Moors H, Benotmane MA, Monsieurs P, Grass G, Doonan C, Vogt S, Lai B (2009) Mechanisms of gold biomineralization in the bacterium Cupriavidus metallidurans. *Proceedings of the National Academy of Sciences,* **106**, 17757–17762.

Reith F, Fairbrother L, Nolze G, Wilhelmi O, Clode PL, Gregg A, Parsons JE, Wakelin SA, Pring A, Hough R, Southam G, Brugger J (2010) Nanoparticle factories: Biofilms hold the key to gold dispersion and nugget formation. *Geology,* **38**, 843–846.

Reith F, Lengke MF, Falconer D, Craw D, Southam G (2007) The geomicrobiology of gold. *The ISME Journal,* **1**, 567–584.

Reith F, Mcphail D (2006) Effect of resident microbiota on the solubilization of gold in soil from the Tomakin Park Gold Mine, New South Wales, Australia. *Geochim. Cosmochim. Acta,* **70**, 1421–1438.

Reith F, Mcphail D (2007) Mobility and microbially mediated mobilization of gold and arsenic in soils from two gold mines in semi-arid and tropical Australia. *Geochim. Cosmochim. Acta,* **71**, 1183–1196.

Reith F, Mcphail D, Christy A (2005) Bacillus cereus, gold and associated elements in soil and other regolith samples from Tomakin Park Gold Mine in southeastern New South Wales, Australia. *Journal of Geochemical Exploration,* **85**, 81–98.

Reith F, Rea MAD, Sawley P, Zammit CM, Nolze G, Reith T, Rantanen K, Bissett A (2018) Biogeochemical cycling of gold: Transforming gold particles from arctic Finland. *Chem. Geol.*

Reith F, Rogers S (2008) Assessment of bacterial communities in auriferous and non-auriferous soils using genetic and functional fingerprinting. *Geomicrobiology Journal,* **25**, 203–215.

Reith F, Rogers SL, Mcphail D, Webb D (2006) Biomineralization of gold: biofilms on bacterioform gold. *Science,* **313**, 233–236.

Reith F, Stewart L, Wakelin SA (2012) Supergene gold transformation: Secondary and nanoparticulate gold from southern New Zealand. *Chem. Geol.,* **320**, 32–45.

Reith F, Zammit CM, Pohrib R, Gregg AL, Wakelin SA (2015) Geogenic factors as drivers of microbial community diversity in soils overlying polymetallic deposits. *Appl. Environ. Microbiol.,* **81**, 7822–7832.

Richter H, Mccarthy K, Nevin KP, Johnson JP, Rotello VM, Lovley DR (2008) Electricity generation by Geobacter sulfurreducens attached to gold electrodes. *Langmuir,* **24**, 4376–4379.

Roeselers G, Van Loosdrecht M, Muyzer G (2008) Phototrophic biofilms and their potential applications. *Journal of applied phycology,* **20**, 227–235.

Rother D, Henrich H-J, Quentmeier A, Bardischewsky F, Friedrich CG (2001) Novel genes of the sox gene cluster, mutagenesis of the flavoprotein SoxF, and evidence for a general sulfur-oxidizing system in Paracoccus pantotrophusGB17. *J. Bacteriol.,* **183**, 4499–4508.

Ryan C, Etschmann B, Vogt S, Maser J, Harland C, Van Achterbergh E, Legnini D (2005) Nuclear microprobe–synchrotron synergy: towards integrated quantitative real-time elemental imaging using PIXE and SXRF. *Nuclear Instruments and Methods in Physics Research Section B: Beam Interactions with Materials and Atoms,* **231**, 183–188.

Rye RO (1993) The evolution of magmatic fluids in the epithermal environment; the stable isotope perspective. *Economic Geology,* **88**, 733–752.

Sarkar S, Chakraborty R (2008) Quorum sensing in metal tolerance of Acinetobacter junii BB1A is associated with biofilm production. *FEMS Microbiol. Lett.,* **282**, 160–165.

Sastry M, Ahmad A, Islam Khan M, Kumar R (2003) Biosynthesis of metal nanoparticles using fungi and actinomycete. *Curr. Sci.,* **85**, 162–170.

Sbordone L, Bortolaia C (2003) Oral microbial biofilms and plaque-related diseases: microbial communities and their role in the shift from oral health to disease. *Clin. Oral Investig.,* **7**, 181–188.

Schippers A, Sand W (1999) Bacterial leaching of metal sulfides proceeds by two indirect mechanisms via thiosulfate or via polysulfides and sulfur. *Appl. Environ. Microbiol.,* **65**, 319–321.

Schloss PD, Westcott SL, Ryabin T, Hall JR, Hartmann M, Hollister EB, Lesniewski RA, Oakley BB, Parks DH, Robinson CJ (2009) Introducing mothur: open-source, platform-independent, community-supported software for describing and comparing microbial communities. *Appl. Environ. Microbiol.,* **75**, 7537–7541.

Shanks WC, Thurston R (2012) *Volcanogenic massive sulfide occurrence model,* US Department of the Interior, US Geological Survey.

Shuster J, Bolin T, Maclean LC, Southam G (2014) The effect of iron-oxidising bacteria on the stability of gold (I) thiosulphate complex. *Chem. Geol.,* **376**, 52–60.

Shuster J, Johnston CW, Magarvey NA, Gordon RA, Barron K, Banerjee NR, Southam G (2015) Structural and Chemical Characterization of Placer Gold Grains: Implications for Bacterial Contributions to Grain Formation. *Geomicrobiology Journal,* **32**, 158–169.

Shuster J, Lengke M, Márquez-Zavalía MF, Southam G (2016) Floating gold grains and nanophase particles produced from the biogeochemical weathering of a gold-bearing ore. *Economic Geology,* **111**, 1485–1494.

Shuster J, Reith F, Cornelis G, Parsons JE, Parsons JM, Southam G (2017a) Secondary gold structures: Relics of past biogeochemical transformations and implications for colloidal gold dispersion in subtropical environments. *Chem. Geol.,* **450**, 154–164.

Shuster J, Reith F, Izawa MR, Flemming RL, Banerjee NR, Southam G (2017b) Biogeochemical Cycling of Silver in Acidic, Weathering Environments. *Minerals,* **7**, 218.

Shuster J, Southam G (2015) The in-vitro "growth" of gold grains. *Geology,* **43**, 79–82.

Southam G, Beveridge TJ (1996) The occurrence of sulfur and phosphorus within bacterially derived crystalline and pseudocrystalline octahedral gold formed in vitro. *Geochim. Cosmochim. Acta,* **60**, 4369–4376.

Southam G, Lengke MF, Fairbrother L, Reith F (2009) The biogeochemistry of gold. *Elements,* **5**, 303–307.

Stewart J, Kerr G, Prior D, Halfpenny A, Pearce M, Hough R, Craw D (2017) Low temperature recrystallisation of alluvial gold in paleoplacer deposits. *Ore Geology Reviews,* **88**, 43–56.

Stoffregen RE (1987) Genesis of acid-sulfate alteration and Au-Cu-Ag mineralization at Summitville, Colorado. *Economic Geology,* **82**, 1575–1591.

Stoodley P, Sauer K, Davies D, Costerton JW (2002) Biofilms as complex differentiated communities. *Annual Reviews in Microbiology,* **56**, 187–209.

Styles M, Wetton P, Bland D (1995) Characterization of gold from Zimbabwe: Part 2. Alluvial and soil gold. *British Geological Survey*, 21.

Ta C, Brugger J, Pring A, Hocking RK, Lenehan CE, Reith F (2015) Effect of manganese oxide minerals and complexes on gold mobilization and speciation. *Chem. Geol.,* **407**, 10–20.

Ta C, Reith F, Brugger JL, Pring A, Lenehan CE (2014) Analysis of gold (I/III)-complexes by HPLC-ICP-MS demonstrates gold (III) stability in surface waters. *Environ. Sci. Technol.,* **48**, 5737–5744.

Tabrez Khan S, Hiraishi A (2002) Diaphorobacter nitroreducens gen. nov., sp. nov., a poly (3-hydroxybutyrate)-degrading denitrifying bacterium isolated from activated sludge. *The Journal of general and applied microbiology,* **48**, 299–308.

Tay J-H, Xu H-L, Teo K-C (2000) Molecular mechanism of granulation. I: H+ translocation-dehydration theory. *Journal of Environmental Engineering,* **126**, 403–410.

Teitzel GM, Parsek MR (2003) Heavy metal resistance of biofilm and planktonic Pseudomonas aeruginosa. *Appl. Environ. Microbiol.,* **69**, 2313–2320.

Tomkins AG (2013a) On the source of orogenic gold. *Geology,* **41**, 1255–1256.

Tomkins AG (2013b) A biogeochemical influence on the secular distribution of orogenic gold. *Economic Geology*, **108**, 193–197.

Townley BK, Hérail G, Maksaev V, Palacios C, De Parseval P, Sepulveda F, Orellana R, Rivas P, Ulloa C (2003) Gold grain morphology and composition as an exploration tool: application to gold exploration in covered areas. *Geochemistry: Exploration, Environment, Analysis*, **3**, 29–38.

Trevors J, Knowles R (1984) Electron transport system activity in soil, sediment, and pure cultures. *CRC Crit. Rev. Microbiol.*, **11**, 83–100.

Ubaldini S, Veglio F, Beolchini F, Toro L, Abbruzzese C (2000) Gold recovery from a refractory pyrrhotite ore by biooxidation. *International journal of mineral processing*, **60**, 247–262.

Van Houdt R, Monchy S, Leys N, Mergeay M (2009) New mobile genetic elements in Cupriavidus metallidurans CH34, their possible roles and occurrence in other bacteria. *Antonie Van Leeuwenhoek*, **96**, 205–226.

Vlassopoulos D, Wood SA, Mucci A (1990) Gold speciation in natural waters: II. The importance of organic complexing—Experiments with some simple model ligands. *Geochim. Cosmochim. Acta*, **54**, 1575–1586.

Vu H, Mu A, Moreau J (2013) Biodegradation of thiocyanate by a novel strain of Burkholderia phytofirmans from soil contaminated by gold mine tailings. *Lett. Appl. Microbiol.*, **57**, 368–372.

Wakelin S, Anand RR, Macfarlane C, Reith F, Noble R, Rogers S (2012) Assessing microbiological surface expression over an overburden-covered VMS deposit. *Journal of Geochemical Exploration*, **112**, 262–271.

Webster J (1986) The solubility of gold and silver in the system Au Ag S O2 H2O at 25° C and 1 atm. *Geochim. Cosmochim. Acta*, **50**, 1837–1845.

Webster J, Mann A (1984) The influence of climate, geomorphology and primary geology on the supergene migration of gold and silver. *Journal of Geochemical Exploration*, **22**, 21–42.

White NC, Hedenquist JW (1995) Epithermal gold deposits: styles, characteristics and exploration. *SEG newsletter*, **23**, 9–13.

Widler A, Seward T (2002) The adsorption of gold (I) hydrosulphide complexes by iron sulphide surfaces. *Geochim. Cosmochim. Acta*, **66**, 383–402.

Wiesemann N, Bütof L, Herzberg M, Hause G, Berthold L, Etschmann B, Brugger J, Martinez-Criado G, Dobritzsch D, Baginsky S (2017) Synergistic toxicity of copper and gold compounds in Cupriavidus metallidurans. *Appl. Environ. Microbiol.*, AEM. 01679-01617.

Wiesemann N, Mohr J, Grosse C, Herzberg M, Hause G, Reith F, Nies DH (2013) Influence of copper resistance determinants on gold transformation by Cupriavidus metallidurans strain CH34. *J. Bacteriol.*, **195**, 2298–2308.

References

Wilkens S (2015) Structure and mechanism of ABC transporters. *F1000prime reports,* **7**.

Wood S (2002) The aqueous geochemistry of the platinum-group elements with applications to ore deposits. *The geology, geochemistry, mineralogy and mineral beneficiation of platinum-group elements,* **54**, 211–249.

World Gold Council (2018) *How much gold has been mined?*, accessed at https://www.gold.org/about-gold/gold-supply/gold-mining/how-much-gold-has-been-mined (20 February 2018).

Wyatt MA, Johnston CW, Magarvey NA (2014) Gold nanoparticle formation via microbial metallophore chemistries. *Journal of nanoparticle research,* **16**, 1–7.

Xie C–H, Yokota A (2005) Reclassification of Alcaligenes latus strains IAM 12599T and IAM 12664 and Pseudomonas saccharophila as Azohydromonas lata gen. nov., comb. nov., Azohydromonas australica sp. nov. and Pelomonas saccharophila gen. nov., comb. nov., respectively. *Int. J. Syst. Evol. Microbiol.,* **55**, 2419–2425.

Yesares L, Aiglsperger T, Sáez R, Almodóvar GR, Nieto JM, Proenza JA, Gómez C, Escobar JM (2015) Gold Behavior in Supergene Profiles Under Changing Redox Conditions: The Example of the Las Cruces Deposit, Iberian Pyrite Belt. *Economic Geology,* **110**, 2109–2126.

Youngson J, Craw D (1993) Gold nugget growth during tectonically induced sedimentary recycling, Otago, New Zealand. *Sedimentary geology,* **84**, 71–88.

Zammit CM, Shuster JP, Gagen EJ, Southam G (2015) The geomicrobiology of supergene metal deposits. *Elements,* **11**, 337–342.

Zammit CM, Weiland F, Brugger J, Wade B, Winderbaum LJ, Nies DH, Southam G, Hoffmann P, Reith F (2016) Proteomic responses to gold (III)-toxicity in the bacterium Cupriavidus metallidurans CH34. *Metallomics,* **8**, 1204–1216.

Zhou J, He Z, Van Nostrand JD, Wu L, Deng Y (2010) Applying GeoChip analysis to disparate microbial communities. *Issues*.

Zipperian D, Raghavan S, Wilson J (1988) Gold and silver extraction by ammonical thiosulfate leaching from a rhyolite ore. *Hydrometallurgy,* **19**, 361–375.